PhD thesis

Adam Leśniewski

Electrodes modified with imidazolium functionalized materials

Supervisor: prof. dr hab. Marcin Opałło,
Departament of Electrode Processes

This dissertation was prepared within
the International Ph.D. Studies in Chemistry
at the Institute of Physical Chemistry
of the Polish Academy of Sciences
ul. Kasprzaka 44/52, 01-224 Warsaw

Warsaw 2010

I owe my deepest gratitude to prof. dr hab. Marcin Opałło for being my guide through the world of science.

I would like to thank dr Joanna Niedziółka-Jönsson for all help she is always giving to me.

I would like to thank dr hab. Mikołaj Donten, who pointed me the right way.

It is a pleasure to thank those, who made this thesis possible: prof. dr Alain Walcarius, dr Laurent Gaillon, dr Cecile Rizzi, dr Juliette Sirieix-Plenet, dr Barbara Pałys, dr Janusz Malinowski, dr Maciej Paszewski, dr Martin Niedziółka-Jönsson, dr Adam Presz, dr Frank Marken, Monika Więckiewicz and Kamil Paduszyński.

I'm grateful to all my colleagues from the Department of Electrode Processes for many valuable discussions and an unforgettable atmosphere.

I would like to show my gratitude to my mother for being an inexhaustible source of support.

Many grateful thanks to Marta Białobrzeska, who is the one.

This research have been financially supported by:

The Institute of Physical Chemistry, Polish Academy of Sciences

The Ministry of Science and Higher Education (project NN204 3687 33)

The Polonium framework (project No 6497)

The European Union, European Regional Development Fund, grant Innovative Economy (POIG.01.01.02-00-008/08).

Content

Major abbreviations

(+)AuNPs - 1-(11-mercaptoundecyl)-3-methyl-imidazolium chloride modified gold nanoparticles

(-)AuNPs - sodium 11-mercapto-1-undecane sulfonate modified gold nanoparticles

ABTS - 2,2'-azino-bis(3-ethylbenzthiazoline-6-sulphonic acid)

AFM – atomic force microscopy

AuNPs – gold nanoparticles

BET - Brunauer, Emmett, Teller isotherm

BMIMBF4 - 1-butyl-3-methylimidazolium tetrafluoroborate

BMIMNTf2 - 1-butyl-3-methylimidazolium bis(trifluoromethanesulphonyl)imide

BMIMPF6 - 1-butyl-3-methylimidazolium hexafluorophosphate

BOx – bilirubin oxidase

BPyPF6 – Butylpiridinium hexafluorophosphate

CA – chronoamperometry

CCE – carbon ceramic electrode

CCNFE - carbon ceramic nanoparticulate film electrode

CMC - critical micelle concentration

CNPs - carbon nanoparticles

CNT – carbon nanotube

CNTs – carbon nanotubes

CPE – carbon paste electrode

CTAB - Cetyl trimethylammonium bromide

CV – cyclic voltammetry / cyclic voltammogram

DMFc – decamethylferrocene

DPV – differential pulse voltammetry

EMIMBF4 - 1-ethyl-3-methylimidazolium tetrafluoroborate

FA – formic acid

FDM – ferrocenedimethanol

FTIR – Fourier transform infra red spectroscopy

GOx – glucose oxidase

IL – ionic liquid

ILCPE – ionic liquid carbon paste electrode

IR – infra red

ITO – tin-doped indium oxide

LbL – layer by layer

MCM-41 - Mobil Composition of Matter No. 41

MCM-48 - Mobil Composition of Matter No. 48

MCM-50 - Mobil Composition of Matter No. 50

MIUSHCl - 1-(11-mercaptoundecyl)-3-methyl-imidazolium chloride

MWCNTs – multi walled carbon nanotubes

NADH - Nicotinamide adenine dinucleotide

NPs – nanoparticles

NTf2 - bis(trifluoromethanesulphonyl)imide

OPyPF6 - Octylpyridinium hexafluorophosphate

ORR - oxygen reduction reaction

P(TMOS)MIMNTF2 - 1-methyl-3-(3-trimethoxysilylpropyl)imidazolium bis(trifluoromethyl sulfonyl)imide

PAH - Poly(allylamine hydrochloride)

RTIL – room temperature ionic liquid

SCILF – silicate confined ionic liquid film

SDS - Sodium dodecyl sulfate

SEM – scanning electron microscopy

SWCNTs – single walled carbon nanotubes

$TBAPF_6$ - Tetra-n-butylammonium hexafluorophosphate

tBuFc – tertbutylferrocene

TEM – transmission electron microscopy

TEOS – tetraethoxysilane

TMOS – tetramethoxysilane

Introduction

The chemically modified electrodes appeared in the world of electrochemistry in 1970's. They soon became popular and kept this popularity till now. Nowadays, it is impossible to ignore the advantages of designing the new electrodes considering their further application. Ionic liquids have also well deserved status in electrochemistry. The are used as solvents in basic electrochemical experiments, as electrolytes in dye-sensitized photoelectrochemical cells, electrochemical supercapacitors, lithium-ion batteries and many others. However the combination of these two has started to be appreciated only in the middle of the first decade of 21^{th} century. Many papers on ionic liquid modified electrodes already appeared. Among them there are a few on covalently bonded ionic liquid modified electrodes and the topic was not exhaustively investigated.

This thesis is the result of the research on covalently bonded ionic liquid modified electrodes since 2007 till 2010. Its considerable part is devoted to the electrodes modified with ionic liquids covalently bonded to the sol-gel processed materials. Electrodes modified both with thin silicate films and submicroparticles are described. Various methods of ionic liquid modified silicate particles immobilization have been used. Among them their deposition together with carbon nanoparticles by layer by layer method is proposed and employed. Another part of the thesis describes electrodes modified with ionic liquid bearing a thiol moiety. It was used both to modify gold electrodes and to stabilize the gold nanoparticles. These nanoparticles have been further used to modify tin-doped indium oxide electrodes together with carbon or oppositely charged gold nanoparticles by layer by layer method. The ion accumulation, electrocatalytic and bioelectrocatalytic properties of the both classes of electrodes have been investigated.

Literature review

1. Electrodes modified with ionic liquids

Although the surface of electrode becomes modified after its immersion in electrolyte solution, the history of deliberately modified electrodes started not earlier than in 1970's. The first reports described electrode modification with adsorbed molecules, covalently bonded functional groups, polymer films and other non-liquid deposits [1,2]. Later this path became significant part of electrochemical research [3]. Until now thousands of reports on chemically modified electrodes were published and many ways of electrode modification were proposed.

It was in the late 1990's when liquid was for the first time deliberately used for electrode modification. Marken and coworkers [4] reported stable deposition of redox active oil droplets on the electrode surface. This was due to immiscibility of N,N,N',N'-tetrahexylphenylene diamine with water and its adhesion to the surface of wide range of solid electrodes. The voltammetry of redox liquid droplets was found to be strongly affected by the type of the salt present in aqueous solution [4]. Next, reversible electrochemistry of hydrophobic redox probes like ferrocene or metalloporphyrins dissolved in supported nitrobenzene film covering modified edge plane pyrolytic graphite electrode was reported [5]. Later this approach was extended to electrodes modified with single drop of unsupported hydrophobic redox probe solution in water immiscible solvent [6]. The electrochemical properties of this new class of modified electrodes are determined by the presence of well defined liquid|liquid interface and three phase junction electrode|liquid|liquid where in most cases the electrode reaction starts [7,8]. Not surprisingly the report on hydrophobic ionic liquid (IL) modified electrode [9] was among the firsts on liquid modified electrodes and the selective extraction of redox active anions into IL deposit was detected. It has to be emphasized that research on liquid modified electrodes started after 30 years of electrochemical studies of interface between the two immiscible electrolyte solutions (ITIES) [10], recently extended to IL|aqueous electrolyte interface [11].

Here one should not forget about other class of electrodes with much longer history, having hydrophobic liquid as one of the components. Carbon paste electrodes were invented more than 50 years ago and became popular tool in electronalysis [12-14]. Their classic version is composed on carbon particles and highly viscous paraffin oil. Clearly oil|aqueous solution interface and three phase junction electrode|oil|aqueous electrolyte play an important role in the electrochemical properties of CPE. This is especially the case of CPE modified with simple redox active compound like ferrocene [15]. Taking into account high viscosity and

hydrophobicity of significant number of ILs it is not surprising that they were recently selected as a binder for CPE [16] and these electrodes became popular electroanalytical tool.

The application of ILs as electrolytes in electrochemical research enormously increases and many review articles appeared [11,17-21]. In some of them electrodes modified with IL or having IL as one of the components were briefly mentioned [11,19-22]. The reviews covering specific area as ion transfer reactions on IL modified electrodes [23] and bioelectroanalytical application of ionic liquid gel carbon nanotubes modified electrodes [24] came out recently.

In first few years of 21st century only few papers per year on IL modified electrodes were published (Fig. 1). However, starting from 2005 the usefulness of IL for electrode modification was recognized and resulted in rapid increase of the number of reports reaching almost 300 in the middle of 2010 (Fig. 1). In the next chapter the different classes of IL modified electrodes (Fig. 2) will be reviewed.

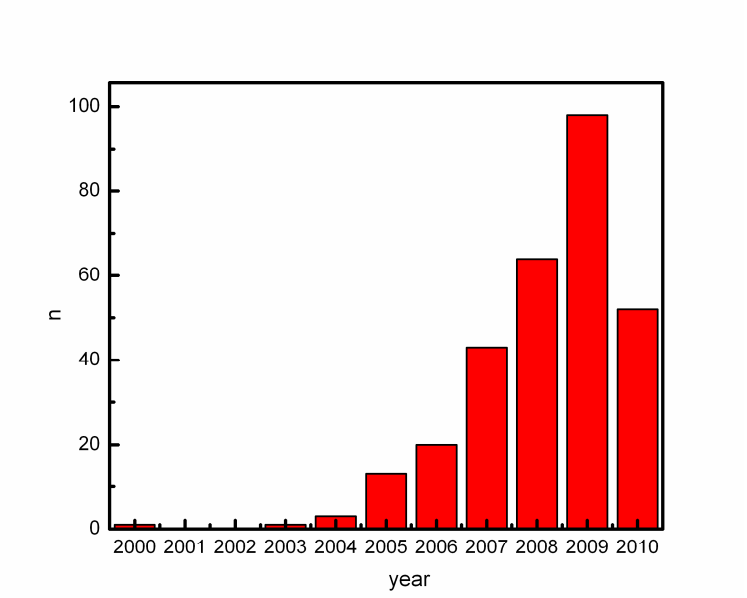

Fig. 1. A bar chart showing the number (n) of papers published on electrodes modified with ionic liquids in individual years according to the Web of Science v4.31, June 2010.

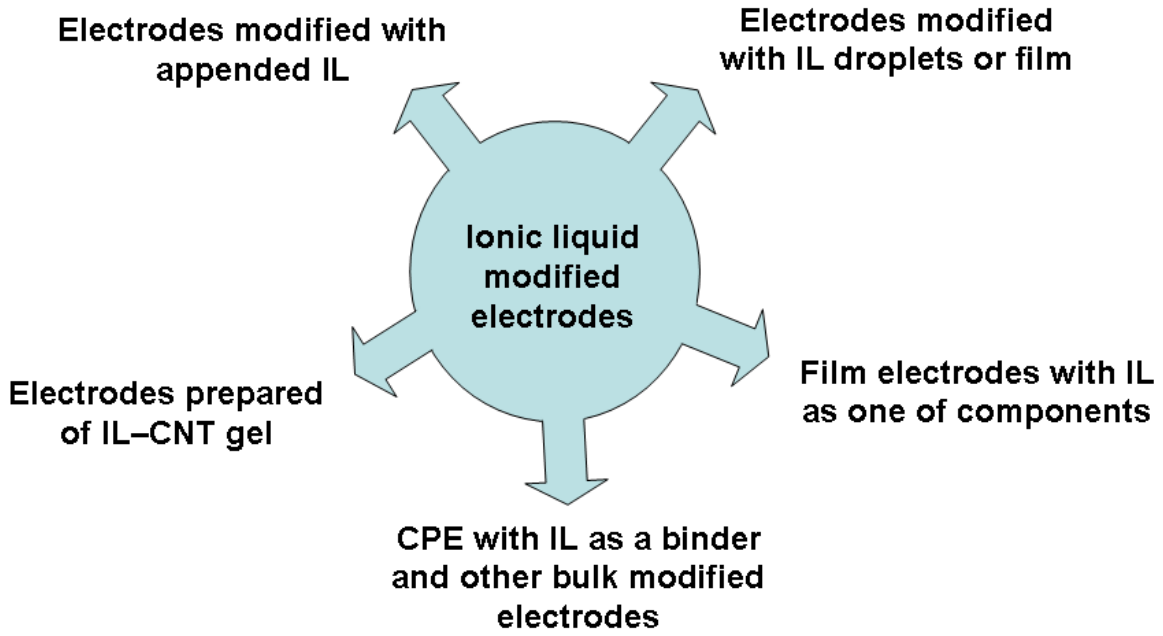

Fig. 2. The different classes of ionic liquids modified electrodes.

1.1. Some properties of ionic liquids related to their use for electrode modification

ILs are entirely composed of anions and cations and melting point of their majority is below room temperature. Operational definition sets limit higher, at 100°C, [25] and indeed ILs with m.p. above 60°C are also applied for electrode modification. Low tendency to crystallization is realized by combination of large, usually asymmetric cation and smaller anion. 1-butyl-3-imidazolium hexafluorophosphate (BMIMPF6) (Fig. 3) perhaps most often used for electrode modification is a typical example. The flexibility of the anion like bis(trifluoromethanesulphonyl)imide (NTf2) (Fig. 3) also contributes to decrease of melting point. Ionic composition of ILs important, when preparation of the electrode material explores electrostatic interactions with other components having charged functional groups like ionomers, ion stabilized nanoparticles or proteins. ILs increase enzyme stability and activity [26] and this is perhaps an important factor for stability of enzyme modified electrodes [27,28].

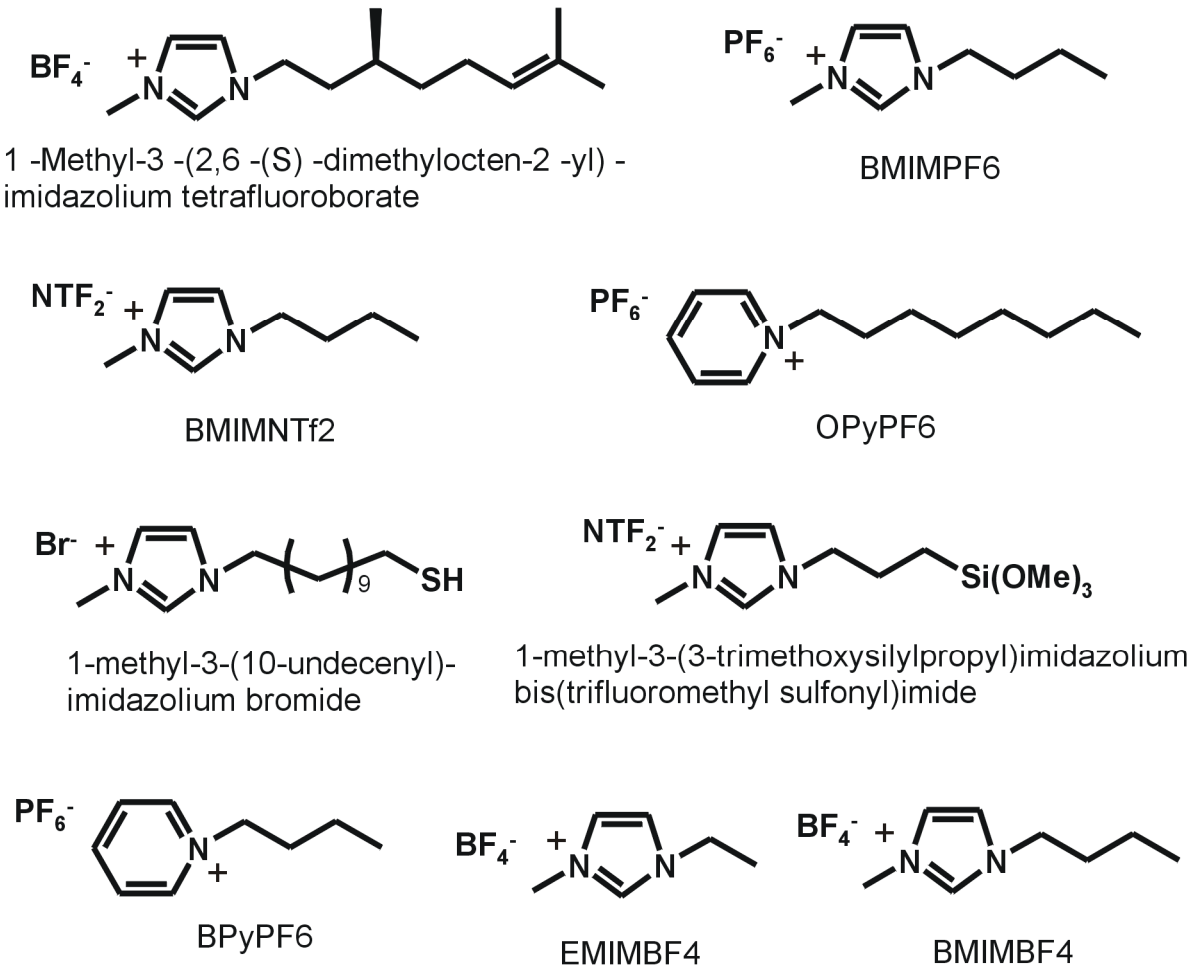

Fig. 3. The examples of ionic liquids used for electrode modification.

IL's ionic conductivity is usually ca. 10 mS cm^{-1} [29] and is certainly contributing to the properties of the prepared electrode material. Contrary to typical organic solvents ILs are characterized by non flammability and negligible vapor pressure. These properties make IL modified electrodes safe and easy to handle before their immersion into aqueous electrolyte. It allows for IL casting from the mixture with volatile solvent that helps for spreading over the all electrode surface [9,30]. Moreover, contrary to other liquid modified electrodes negligible IL's vapor pressure allows to study their morphology can be studied by SEM[27,31,32]. Viscosity of ILs typically used in electrochemical experiments is in the range of tens or hundreds of mPa s (at 25°C). It is by two or three orders of magnitude larger than that of typical polar organic solvents like acetonitrile and dimethylformamide or water [17]. However viscosity of large number of ILs is similar to that of Nujol or most viscous n-alkanes used as a binder for classic CPEs [12-14] and this contributes to popularity of IL based CPEs. Perhaps also in the case of film electrodes IL component acts as a binder as well.

The wide potential window is regarded as one of the most important advantages of ILs as electrolytes [11,17-21]. This seems to be not the case of IL modified electrodes, because they operate in contact with aqueous solution. It is already known that contamination of IL with water shrinks potential window to that exhibited in aqueous electrolyte solution [33]. This is also the case of most hydrophobic ILs composed of large 1-alkyl-3-methyl imidazolium cations and homologs of bis(trifluoromethanesulphonyl)imide anions. The solubility of water in these solvents is equal fraction of weight percent [11]. Therefore uptake of water is expected for IL deposit being in contact with aqueous electrolyte and the potential window of IL modified electrodes is typical for noble metal, carbon or CPEs immersed in aqueous solution. The solubility of hydrophobic ILs in water is much smaller than solubility of water in IL and in some cases is much below fraction of percent [11]. This property seems to be crucial from the point of view of stability of IL modified electrodes because of the possibility of microlitre-size liquid deposit dissolution in few milliliters of surrounding aqueous electrolyte. However, reported IL modified electrodes are stable at least in voltammetric time scale indicating slow dissolution in the case of more hydrophilic ILs. This is also the case of CPEs made of mixture of hydrophobic oil and more hydrophilic ILs like BMIMBF4, with solubility too high to form separate phase in water. Perhaps other phenomena like adsorption of IL on the electrode substrate or attractive interactions with other components of film electrodes have significant impact on IL modified electrodes stability and are difficult to quantify. The tendency of aggregation of some hydrophobic ILs [34] may also contribute to stability of their deposits. On the other hand the solubility of IL in water seems to be less important in the case of bulk modified electrodes CPE with IL as a binder, carbon ceramic electrode modified with ILs or CNT-IL gel electrodes because this bulk electrode material serves as reservoir of IL.

The presence of specific functionalities in ILs plays crucial role in their application for electrode modification. For example, the use of amino acid functionalized IL provides stable enzyme immobilization [35], whereas introduction of complexed metal ions like $[(C_4H_9)_2\text{-bim}]_3[La(NO_3)_6]$ [36] or $[(C_{10}H_{21})_2\text{-bim}]_2[CdCl_6]$ [37] allows to prepare electroactive IL modified electrode. Functionalization of IL, typically imidazolium cation, with reactive groups as thiolate [38-41], carboxylate [42], trialkoxy silicate [43] and others allows for preparation of IL appended modified electrodes.

1.2. Ionic liquid modified electrodes

1.2.1. Electrodes modified with ionic liquid droplets or film

In most cases electrodes modified with IL droplets or film are prepared by direct deposition of IL on the electrode surface [9,44,45] or from its diluted solution in volatile solvent [9]. These two procedures may provide different geometry of the deposit. Thin liquid film geometry can be obtained by surface coverage with Teflon membrane [9]. The preparation of IL modified electrode in situ by adsorption of IL from aqueous solution was also reported [46,47].

The appropriate selection of electrode substrate and IL is important to obtain stable liquid deposit in contact with aqueous solution in the absence of other film components. For some studies unmodified electrode substrates like basal plane pyrolytic graphite (BPPG) [9,28,48], glassy carbon [49,50], gold [45] or ITO [51] were applied. Also edge plane pyrolytic graphite [52] with well developed surface was used. In other studies the electrode substrate was pre-modified to achieve good wetting by IL. This was the case of gold pre-modified by self-assembled 2-aminoethanethiol [44] or paraffin impregnated graphite [53]. In all above mentioned cases micro liter amount of IL was deposited at working electrode and other electrodes remained in aqueous phase. The exceptional situation of embedded working, counter and reference electrodes covered by IL next immersed into aqueous solution was reported [54,55].

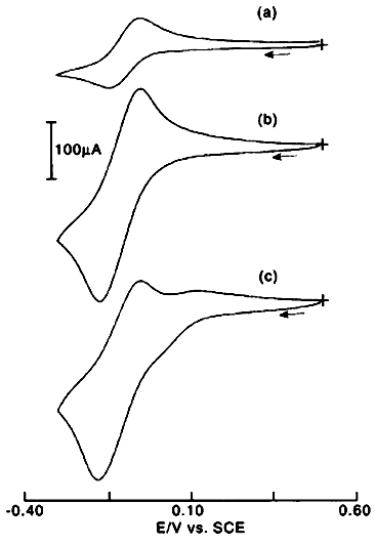

Fig. 4. Time dependence of the cyclic voltammetric response for the reduction of $K_3Fe(CN)_6$ in $NaBF_4$ at a basal plane pyrolytic graphite electrode modified with $MDIMBF_4$ ionic liquid after 30 s (a), 2 min (b) and 5 min (c) [9].

Thin film or micro droplets of 1-methyl-3-(2,6-(S)-dimethylocten-2-yl)-imidazolium tetrafluoroborate on bppg electrode is stable and selective partitioning of $Fe(CN)_6^{3-}$ anion into IL deposit phase was observed by cyclic voltammetry (Fig. 4) [9]. Despite to earlier reported use of IL in extraction process [56] this application of IL modified electrodes was not much later

developed, perhaps because exhaustive accumulation of redox active anions takes minutes or tens of minutes [9,43,51,54,55]. This is due to slow electrochemical probe transport in viscous IL film [55,57], hindered ion transfer and hydrophobic nature of deposit. Indeed such significant delay is not observed for molecular film of water miscible ILs on glassy carbon, but efficiency of such system is obviously not significant [47]. The interesting combination of extraction of Sr^{2+} and Cs^{+} cations into IL deposit containing macrocyclic ligands followed by their electroreduction at mercury electrode was reported [54]. The extraction of phenols into IL film covering electrode assembly is also noted [55].

Some attention was paid to electrochemical behavior of electrodes modified with insoluble redox probe deposit next covered by IL deposit [58,59] or modified with redox probe solution in IL [44,45,51-53,58]. The first approach was used to minimize the volume of ionic liquid, factor important at that time. The voltammetric behavior typical for simple redox couple was observed and for some systems and transition between thin layer to semi-infinite diffusion behavior was noted [58,59]. This is due to slow expansion of diffusive layer caused by high viscosity of IL.

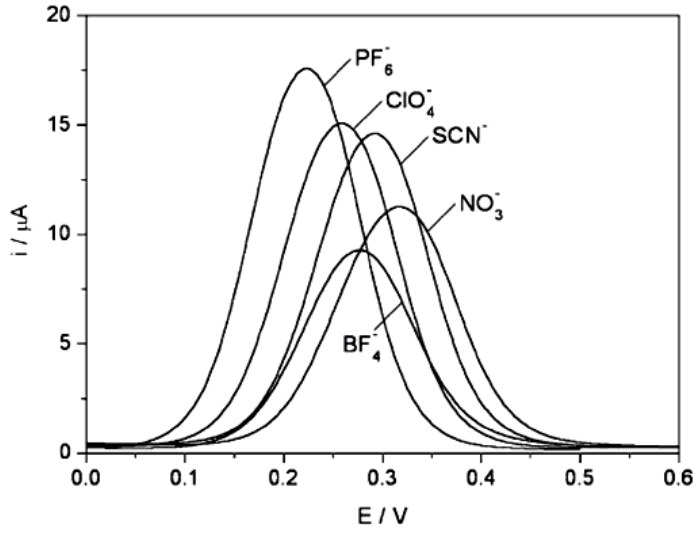

Fig. 5. The effect of selected anions on differential pulse voltammograms obtained with a Au electrode covered with tBuFc solution in C_{10}mimN(Tf)$_2$ immersed into the aqueous salt solution. Anions are marked on the figure [45].

Simple redox voltammetry was also observed for electrodes modified with liquid deposit of redox probe solution in IL [44,45,51-53]. The specific mechanism of electrode reaction was identified as ion transfer across ILlaqueous solution interface coupled to the electrochemical redox process. The latter creates imbalance of charge in IL phase which has to be overcame by ion insertion or ejection. It was proven that the oxidation of hydrophobic DMFc molecule dissolved in hydrophobic IL film is followed by ejection of IL cationic component, whereas

its re-reduction is accompanied by expulsion of the anionic one [44,53]. This indicates that the same redox reaction may drive cationic and anionic IL component across the IL|aqueous solution interface and the transition from one mechanism to another driven by concentration of aqueous electrolyte was noted [53]. The hydrophobicity of the deposited IL affects the mechanism of the electrode process [45]. The dependence of redox potential of tBuFc dissolved in 1-decyl-3-methyl imidazolium bis(trifluoromethylsulfonyl)imide [45], trihexyl(tetradecyl)phosphonium tris(pentafluoro ethyl)-trifluorophosphate [50] or 1-methyl-3-(3-trimethoxysilylpropyl) imidazolium bis(trifluoromethylsulfonyl)imide [51] on the anion of the aqueous electrolyte following Hofmeister series was identified as result of anion insertion into IL. For more hydrophilic ILs no such dependence was found and it suggests cation expulsion mechanism [45]. Interestingly, the redox process of extremely hydrophobic redox probe - Lutetium biphtalocyanine dissolved in hydrophobic IL results in expulsion of both hydrophobic IL components [52]. In this paper ion distribution between IL and aqueous electrolyte was taken into account. The complex interpretation of the observed medium effect on the ion transfer across IL|aqueous electrolyte interface coupled to electrochemical redox process was formulated [60].

The observation of redox voltammetric signal of metalloproteins like myoglobin [61] or cytochrome c [28] dissolved in IL film deposited on bppg electrode is noted. Blank experiments show that it is not observed for adsorbed protein and clearly IL promotes direct electron transfer to/from adsorbed enzyme and non mediated bioelectrocatalysis of O_2 reduction with myoglobin [61] (Fig. 6) or H_2O_2 reduction with cytochrome c [28].

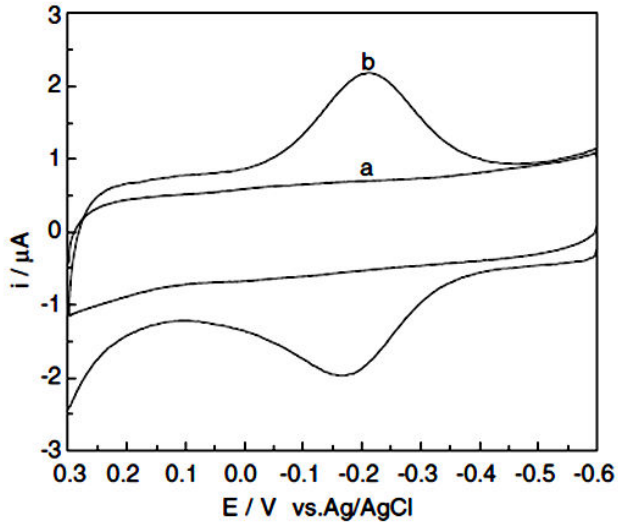

Fig. 6. CVs of BPG electrode in [HEMIm][BF_4] aqueous solution without (a) and with myoglobin (b) [61].

It was found that IL deposit provides suitable environment for further modification of the electrode surface. The IL droplets were used for cost effective deposition of Pt [62] and binary and ternary alloy [63] nanoparticles. The use of cyclodextrin functionalized IL for the same purpose is also mentioned [64]. In similar way IL thin film was applied for electrodeposition of composite polypyrrole-carbon nanotubes material [65]. These materials are reported to exhibit specific features obtained only in IL environment [62,63,66].

The presence of IL thin film increases catalytic activity of adsorbed inorganic catalyst – Prussian Blue [67] or enzyme [28,48]. Perhaps this property motivated later construction of large variety of IL containing hybrid electrode materials (see below).

1.2.2. Film electrodes with ionic liquid as one of the components

Although research on IL modified electrodes started from simple system – electrode substrate covered by droplets or liquid film, later attention switched to film electrodes with more complex composition. They are composed of organic or inorganic polymers, nanoparticles, nanotubes and other micro- or nanoobjects with IL as one of the component. These films range from relatively simple ones as polyvinylchloride plasticized with polyazacycloalkanes solution in BMIMPF6 [68] to most frequently prepared multi (typically three to five) component films consisting of polymer and/or conductive and/or isolating nanoparticles and IL.

The simple electrode consisting polymer membrane saturated with IL based ionophore solution exhibit ion selectivity and were used as ion selective electrode [68,69]. Others prepared on Ag|AgCl substrates served as reference electrodes [70,71] (Fig. 7). The gel composed of polymer (poly(vinylidene fluoride-*co*-hexafluoropropylene) and viscous IL (1-methyl-3-octylimidazolium bis-(trifluoromethyl-sulfonyl)imide) allows to obtain solid state and easy to miniaturize device without any other additives [71] (Fig. 8).

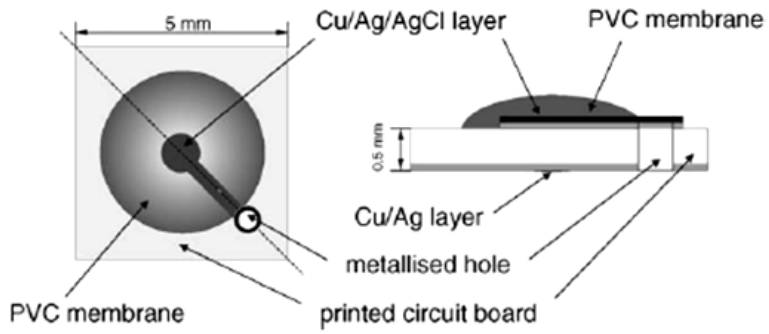

Fig. 7. Top view and schematic cross section (right) of the all-solid-state reference microelectrode based on PVC membrane containing IL and back-side contact Ag|AgCl transducer [70].

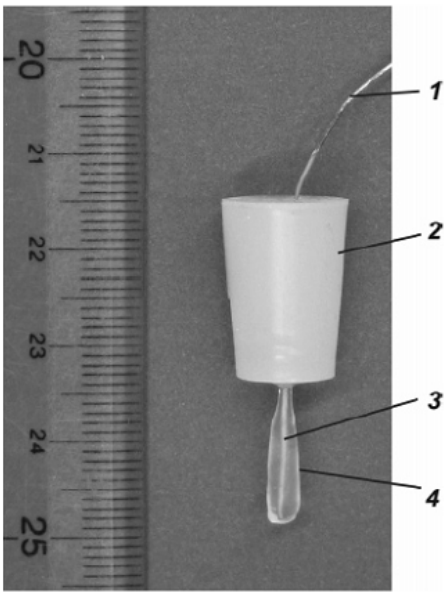

Fig. 8. Picture of gelled-[C_8mim^+][$C_1C_1N^-$]-coated Ag|AgCl electrode: 1, silver wire; 2, silicon rubber stopper; 3,Ag|AgCl; 4, [C_8mim^+][$C_1C_1N^-$] gel saturated with AgCl [71].

The molecules of different complexity were used as scaffolds to built up IL impregnated films. Fullerenes [72] and surfactants as cationic gemini surfactants [73-76] or phospholipids [77] are the simplest modifiers. Others are inorganic polymers like Nafion [78-81], silicate [27,82], mesocellular silicate foams [83], Teflon [9], Nafion - silicate composite [84] zeolites [85], hydroxyapatite [86] and clays [87-89]. However, most often polysaccharides like chitosan [90-94], gelatin [95], hyaluronate [96,97], gellan gum [98,99], konjac glucomannan [78] were applied. The multicomponent polymer films composed of Nafion and agarose [100] or prepared from fullerene-ferrocene solution in IL-chitosan and glucose oxidase employing layer-by-layer architecture [72] are other examples. The use of biomolecule - DNA as IL scaffolds [101] also having layer-by-layer architecture [102] has to be mentioned.

Other group of film electrodes is prepared from IL and conductive nanoobjects like carbon nanotubes or metal nanoparticles in the absence of any polymeric scaffold. The latter

is not necessary because of viscous IL consisting of charged species serves as a binder. The immobilized conducting elements include: multiwalled carbon nanotubes (MWCNTs) [35,92,103-107], amine functionalized MWCNTs [108], single walled carbon nanotubes (SWCNTs) [109-111], porous carbon nanofibers [112], graphenes [113], polymer functionalized graphene sheets [114], gold nanoparticles [115-117], PtCo alloy nanoparticles [64,118], CdTe quantum dots [119]. Perhaps strong interactions between nanoobjects and IL components results in stable film formation and low degree of aggregation what results in their enhanced electrocatalytic reactivity. The preparation of composite [120,121] and layer-by-layer assembled film [103] consisting of MWCNTs and Au nanoparticles was also reported. Direct decoration of MWCNT within IL film with PtAu alloy nanoparticles is also possible [107,122]. The film electrodes modified with Pt [123,124] and Au [40] nanoparticles stabilized by IL for electrocatalytic oxygen reduction have to be mentioned here.

Next are numerous variations of multicomponent films composed of IL, polymers, nanoparticles, nanotubes, proteins and others. These components contribute to mechanical and electrical properties of the film and many of them provide electrocatalytic activity. Combinations of polymer, conductive nanoparticles and IL [125,126], polymer and non-conductive nanoparticles [127,128], polymer, carbon nanotubes or nanofibers and IL [30,129-134] and polymer, IL and other particles as CuS microspheres [135] or CdS nanorods [136] are the examples. The preparation of film from surfactant, MWCNTs and IL has to be noted [76]. Multicomponent films of nanoparticles and CNTs with polymer and IL [122,137-140] were also prepared. In some cases sandwich configuration is employed consisting polymer matrix saturated with IL and AuNPs adsorbed on the top of the film with a help of functional groups [141]. Although in most cases IL is a free component of the film, it can be also used for functionalization of nanoparticles or nanotubes [142] to increase their dispersion or to decorate nanotubes with nanoparticles [143] before film is built. The preparation of conductive polymer – IL gel enriched with organic (polyaniline) or inorganic (Prussian Blue) coloring component for electrochromic devices has to be noted [144]. The ink prepared from IL and polyaniline tubes was applied for preparation of screen printed electrodes [145].

Similarly as in the case of free standing IL deposit the redox activity of the film was achieved by dissolution of redox active compound in IL component [30,72] or its drop deposition from volatile solvent together with IL [106]. Also for some of these electrodes the redox reaction driven ion transfer across IL|aqueous electrolyte interface has to be noted [30].

Film electrodes with IL as one of the components are useful for electrode reactions of other substrates which are difficult to oxidize or reduce. Quite often the magnitude of

voltammetric signal and/or overpotential decrease are good enough to apply these electrodes as electrochemical sensors. These reagents include inorganic anions as nitrite [146-148], nitrate [114], iodate [106] or gases like nitric oxide [149]. There is also large group of organic analytes as chloroamphenicol [150], 4-chloronitrobenzene [151], 4-nitrophenol [105] or biomolecules as L-tyrosine [152], cysteine [107], NADH [153] (Fig. 9), glucose [64], cholesterol [154] and DNA [145] which can be determined with these electrodes. They are also used for stripping voltammetry of trace metal ions employing their high solubility in IL [155 152]. Electrochemiluminescence of IL film containing quantum dots [119] has to be mentioned.

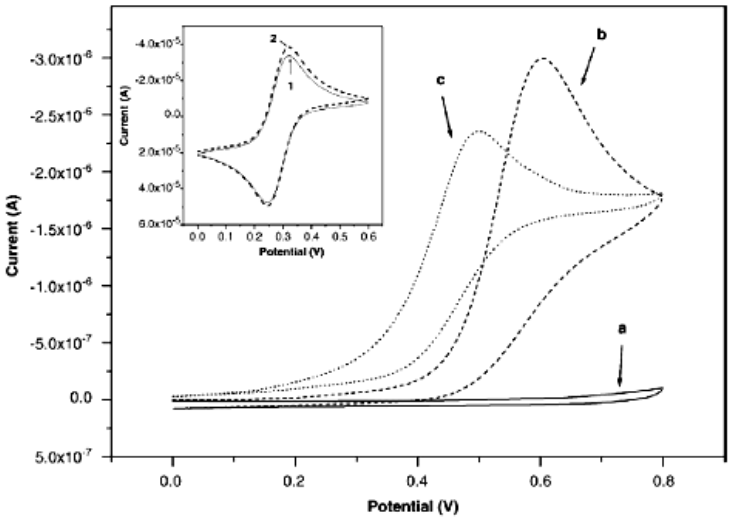

Fig. 9. CVs in the absence (a) or in the presence (b, c) of NADH at bare GC electrode (b) or C_{60}|$BMIPF_6$ composite modified GC electrode (a, c). Inset shows the CV of C_{60}|$BMIPF_6$ composite modified electrode in $K_3Fe(CN)_6$ solution, 1 and 2 are is the 1st the 50th cycle respectively [153].

IL containing film electrodes are important supports for enzyme immobilization. This is because IL provide suitable environment for stable immobilization of proteins [26]. As it was earlier mentioned some proteins dissolved in IL film exhibit reversible voltammetric behavior which cannot be seen for adsorbed biomolecule [28,61]. It was proven that IL additive enables to obtain direct electrochemical signal from immobilized protein [74,78,79,81,89,91,93] not just improve protein voltammetry. Also the increase of the magnitude and reversibility of voltammetric signal of metalloprotein with the increasing amount of IL in the film was reported [84] (Fig. 10). One can speculate that the presence of IL allows protein molecule to adopt conformation suitable to direct electron transfer as it was proven in few studies by UV-Vis and IR spectroscopy [81,112,156,157]. Bioelectrocatalytic function of IL-enzyme modified electrodes enable to apply them as electrochemical sensors. The immobilization of other biocomponents

as antibodies [82] or cells in film composed of IL stabilized biopolymer and SWCNTs composite [134] has to be also noted.

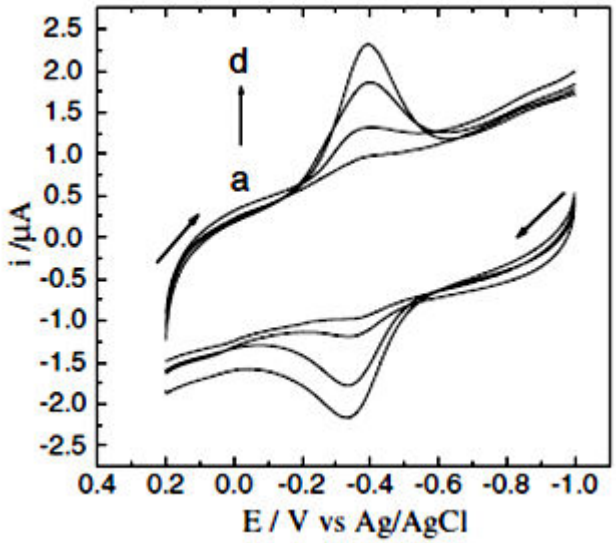

Fig. 10. CV of Hb\sol\IL\Nafion modified BPG electrode containing different amounts of IL: (a) 0, (b) 15, (c) 30, and (d) 45 μl 2% IL solution [84].

In particular IL containing film enables to observe direct electrochemistry of enzymes as horseradish peroxidase [27,74,75,79,91,93,99,100,136], hemoglobin [73,77,83,84,89,90,96,98,102,112,114,127,135,158-160], myoglobin [81,87,97,112,126,161], cytochrome c [92,103,112,115], catalase [108] and chloroperoxidase [78]. These and other electrodes are capable of mediatorless bioelectrocatalysis of H_2O_2 electroreduction with immobilized enzymes as horseradish peroxidase [27,75,79,91,94,95,99-101,136], hemoglobin [73,77,83,88,89,96,98,102,127,135,158-160], cytochrome c [92,103], myoglobin [81,87,97,126], catalase [108] or chloroperoxidase [78]. Other group of IL containing composite film electrodes modified with horseradish peroxidase [79], hemoglobin [77,84,88-90,127], cytochrome c [115] or chloroperoxidase [78] exhibits catalysis of oxygen reduction.

Direct electrochemistry of another important enzyme – glucose oxidase immobilized on film electrode containing IL [35,113,116,137,138,157,162] or its mixture with dimethylformamide [116,157,162] was also reported. These and other electrodes were applied for bioelectrocatalysis of glucose [35,72,113,116,118,122,137,138,157,162,163].

1.2.3. Carbon paste electrodes with ionic liquid as a binder and other bulk modified electrodes.

High viscosity of ILs makes them suitable binder for CPE [13,14]. Typically, hydrophobic ILs are used for IL based CPE (ILCPE) preparation and they compete with those made of Nujol or paraffin oil in terms of stability in aqueous solution. Contrary to classic CPEs their binder

is composed of charged species and exhibits ionic conductivity. These properties allows to employ solubility of ionic reagents in a binder and take advantage of electrostatic interactions between the electrode body and film on the top. It has to be mentioned that some research groups named ILCPE as CILE - Carbon Ionic Liquid Electrodes [164,165], what causes some confusion in extracting information from data bases.

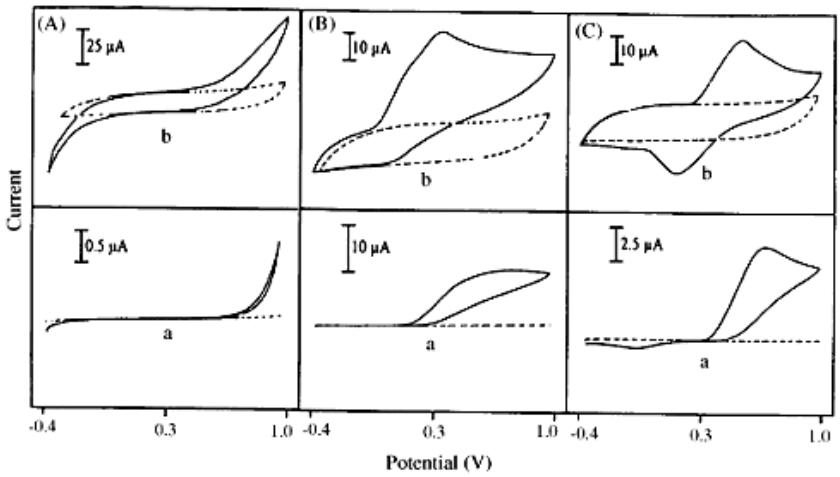

Fig. 11. CVs for H_2O_2 (A), ascorbic acid (B) and acetaminophen (C), at the mineral oil/graphite (a) and BMI-PF_6/graphite (b) paste electrodes [166].

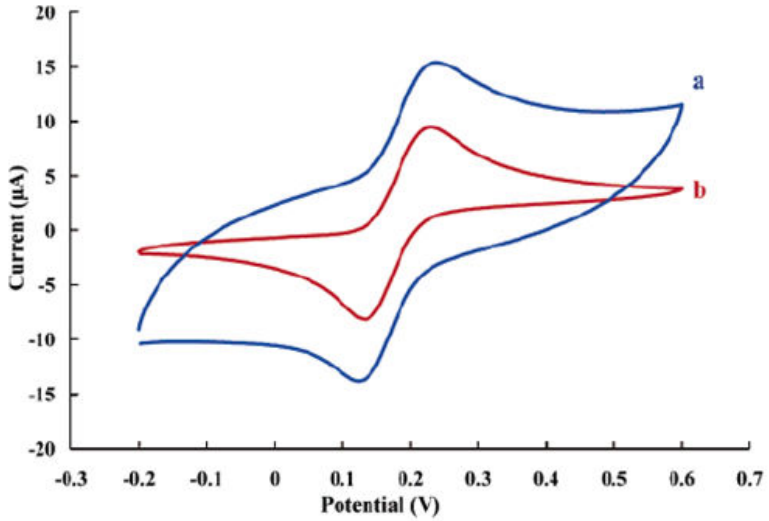

Fig. 12. CVs of catechol on CILE before (a) and after heating (b) [167].

Typically ILCPE is prepared in the same way as classic CPE by mixing or grinding of graphite particles with the IL [16] and placing the mixture in a cavity of the polymer or glass tube. After polishing the electrode is ready to use. The IL : graphite particles ratio has to be optimized from the point of view of not only mechanical stability, but also capacitive current, resistance and last not least specific electrode process [166,168] (Fig. 11). One can say that 30% of IL is a most popular composition. If IL with m.p. above room temperature as OPyPF6 are used, heating of the mixture is required to decrease capacitive current [167] (Fig. 12). The

preparation of CPE of different geometry like deposition of the film on screen printed electrode from suspension composed of carbon microparticles, IL and volatile solvent was also reported [169].

The composition of the binder is perhaps first choice factor affecting performance of ILCPE. Wide range of ILs and IL – organic solvent mixtures were used as binders. Generally two hydrophobic hexafluorophosphates: BMIMPF6 and N-butylpyridinium hexafluorophosphate (BPPF6) are the most often used for this purpose. Although the instability of these electrodes was not reported, they may suffer from solubility of the binder in water [170] and hydrolysis of PF_6^- anions [11]. The improvement of voltammetric signal (overpotential decrease, decrease of the difference between peak potentials and peak current increase) when mineral oil is replaced by IL was demonstrated [166,171,172]. The increase of the capacitive current may be considered as disadvantageous. However, replacement of oil with IL increases voltammetric signal to noise ratio because of the larger magnitude of the signal [167,171,173-175]. The problem of higher capacitive current can be also defeated by electrode rotation [166,171] or providing microdisc geometry [166,176].

Both increase of faradaic and capacitive current at ILCPE as compared with classic CPE is connected with larger electroactive area. This is because before electron transfer occurs some fraction of reactant is transferred across IL|aqueous electrolyte and electrode reaction occurs at carbon|IL interface. Perhaps this preconcentration effect overcomes slow diffusion of reactant in binder caused by IL's high viscosity and results in high faradaic current. The larger capacitive current is caused by electroactivity of fraction of carbon particles being in contact with IL and close to IL-aqueous solution interface. This is different than hydrophobic oil based CPEs, where electrochemical activity is limited to the surface of carbon particles surface sticking out to aqueous solution interface [13,14]. Only this surface contributes to capacitive current and its very low value is caused by adsorption of binder molecules on the graphite particles. The fast electron exchange and overpotential decrease at ILCPEs results from the absence of organic binder adsorption on electoactive surface. ILCPEs prepared with IL having melting point above room temperature [165,167,172,177-196] retain typical ILCPE's properties at room temperature. However heating of the cell above 70°C is recommended to not only increase the voltammetric signal [167,195,197] but increase signal to noise ratio what is important for electroanalytical applications.

In some cases the use of the mixture of oil and IL as binder was recommended to improve the signal obtained on classic CPE [36,198-207] or improve dispersion of Pt nanoparticles in electrode body [205]. The IL additives ranges from extremely hydrophobic tetradecyl-3-

methylimidazolium bis(trifluoromethylsulfonyl)imide [207], to moderately hydrophobic BMIMPF6 [198,204,205,208,209]. High melting point N-octylpyridium tetrafluoroborate was also selected as binder component [206]. Also more hydrophilic ILs as 1-ethyl-3-methylimidazolium tetrafluoroborate [199-203], 1-ethyl-3-methylimidazolium ethylsulphate [210], $BMIMBF_4$ [208,211,212], $[(C_4H_9)_2\text{-bim}]_3[La(NO_3)_6]$ [36] and $[(C_{10}H_{21})_2\text{-bim}]_2[CdCl_6]$ [37] were mixed with oil to prepare ILCPE. Perhaps the hydrophilicity of these ILs does not allow for preparation of mechanically stable CPE because of their solubility in water and only their mixture with hydrophobic viscous oil ensures mechanical stability. Making a binder from hydrophilic BMIMBF4 and solid organic substance - 5-(dimethylamino)naphthalene-1-sulfonyl 4-phenylsemicarbazide represents another strategy [213].

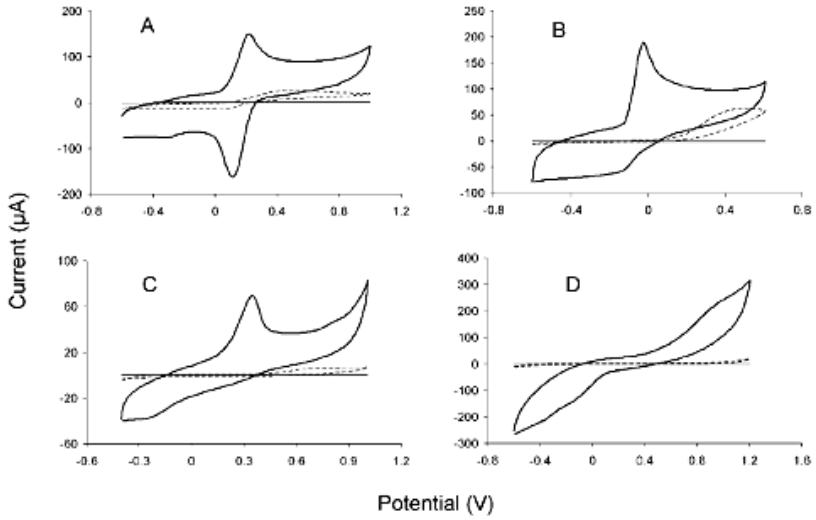

Fig. 13. CVs using MWCNT/OPFP (solid bold line), MWCNT/Mineral oil (dashed line) and Graphite/OPFP (solid regular line) for potassium ferricyanide (A), ascorbic acid (B), NADH (C) and hydrogen peroxide (D) [172].

Obviously the type of conductive component affect the performance of ILCPEs. MWCNTs [172,200,211-213] or SWCNTs [214] were added to improve performance of ILCPEs. Also stable ILCPE electrodes were made of only MWCNTs [172,195,204,215] or short SWCNTs [216]. Contrary to ILCPEs prepared from graphite particles these made of only MWCNTs require lower carbon loading, typically 10%, to optimize response [172]. Although their capacitive current is larger than that of ILCPE made of graphite microparticles, the magnitude of voltammetric signal is larger for such species as $Fe(CN)_6^{3-}$, ascorbic acid, hydrogen peroxide and NADH and overpotential decrease is also seen for the same systems [172] (Fig. 13). The increase of capacitive current is due to large active area of carbon nanotubes and their significant deaggregation as shown by scanning electron microscopy [172]. Glassy carbon microspheres [206] and ordered mesoporous carbon particles [210,217] were also applied as

conductive elements of ILCPEs. Ag and Au [209], Au [218] and Pt [205] nanoparticles additive were used to increase the efficiency of electrocatalytic process.

Many examples of increase of voltammetric current and overpotential decrease of number ionic and neutral substrates at simple ILCPE composed of IL based binder and carbon particles can be found in literature [165-169,173,175,176,179-181,185-188,195,197,206,214,219-232]. The electrochemical studies of DNA [182,187,210,216,223] and electrochemiluminescence [195,206,215,231,233,234] represent interesting application of ILCPEs. Employment of extraction properties at open circuit [220] and the use of ILCPE for potentiometry of metal ions compared with PVC membrane electrode [211-213] has to be noted.

The use of additional components dissolved in a binder of ILCPEs is important way of their further modification. As it was done with classic CPEs [15], dissolution [167,168,174,175,197,219,226,231] of redox active component in a binder provides electrodes electroactivity [16,169,215,234-237]. Another way to introduce redox activity was mixing oil with redox active hydrophilic ILs: $[(C_4H_9)_2\text{-bim}]_3[La(NO_3)_6]$ [36] (Fig. 14) or $[(C_{10}H_{21})_2\text{-bim}]_2[CdCl_6]$ [37]. These electrodes were used to study redox catalysis [16,36,37,169,236,237]. The study of ion transfer across IL-aqueous solution interface generated by redox probe dissolved in ILCPE binder has to be noted [235].

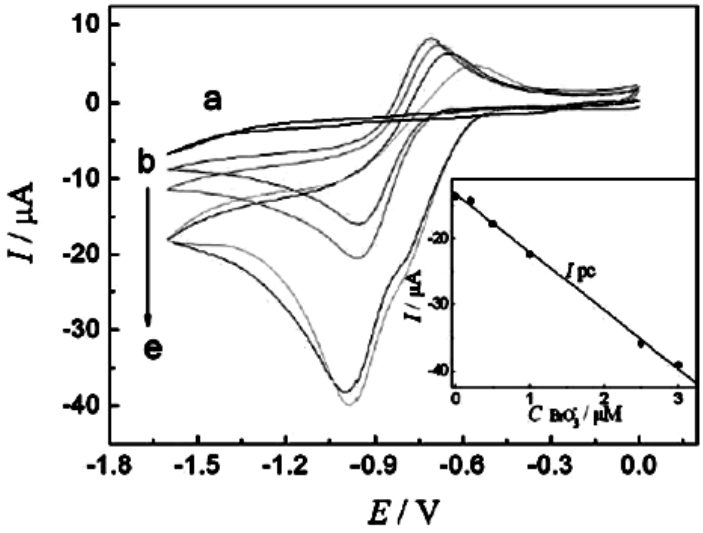

Fig. 14. CVs of (a) the bare CPE in solution containing 2 mM bromate; (b-e) La-CPE in solution containing 0, 0.5, 2.5 and 3 μM bromate respectively. Insert: the variation of peak current vs. bromate concentration [36].

As in the case of film electrodes with IL as one of the components enzymes are another important additive of a ILCPE binder due to stabilizing properties of IL. They are added by dissolution [168,172,198,205,207-209,238,239] or preadsorption on conductive component as mesoporous carbon [217]. In this way ILCPEs loaded with heme [198], glucose oxidase [168,172,217],

hemoglobin [238,239] and laccase [205,207-209] were prepared and applied for bioelectrocatalysis of wide range of substrates. The studies of DNA with ILCPEs also have to be mentioned [182,187,216,223].

ILCPE modification with non-conductive particles like sulfonate functionalized MCM-41 [240] and clay particles [233] premodified with tris(2,2'-bipyridyl)ruthenium(II) allows for observation of its electrochemiluminescence. ILCPE modified with hemoglobin immobilized on MCM41 particles promotes direct protein voltammetry and bioelectrocatalysis of trichloroacetic acid [241]. The addition of silica appended binuclear Ni^{2+} complex together with Au nanoparticles provides favorable conditions for electrocatalytic oxidation of fisetin [218]. The use of hydroxyapatite [190] enables preconcentration of Pb^{2+} and Cd^{2+} ions followed by stripping analysis. Also metal hydroxides were used for ILCPE modification [191,242]. With ILCPE modified with $Ni(OH)_2$ nanoparticles [242] electrooxidation of glucose in alkaline solution is observed whereas ILCPE modified with copper hydroxide nanoparticles allows for separation of electrochemical signals of glutathione and glutathione disulfide [191].

ILCPE were also used as easy to prepare support electrodes for wide range of deposits [88,147,156,164,177,178,184,189,192,196,200,201,203,214,227,243-258]. This important class of ILCPEs allows for use of minute amount of material for electrode modification without losing easy renewability of the surface. The methodology of their modification is almost the same as solid electrodes. The films deposited on the top of IL were composed of conductive nanoobjects like SWCNTs [255], beta cyclodextrins together with MWCNTs [256] or metal nanoparticles [184,192,248] including Au nanoparticles modified with antibodies [189] and MWCNTs, V_2O_5 nanobelts and chitosan composite film [196]. Electroactive polymer films like methylene blue [247], Prussian blue [259], or polyaniline [249] were obtained by electropolymerisation on the top of ILCPE.

Not surprisingly the surface of ILCPEs was used as support for adsorbed enzyme [156,177,178,214,246,250]. More complicated architectures were built on the surface of these electrodes for stable protein immobilization. They include enzyme covered by ionomer film [200], ionomer enriched with DNA [203] and CdS nanorods [252] and by electroactive polymer – polyaniline enriched with Fe_2O_3 nanoparticles [249]. Similar architecture was obtained with biopolymer [245,251,257,260,261], biopolymer film enriched with nanoparticles [227,253,262], biopolymer and MWCNTs [201,263], biopolymer with hydrophilic IL [156], biopolymer with Fe_2O_3 nanoparticles and IL different than used as a binder for ILCPE support [258] and Nafion together with electrodeposited Au nanoparticles [264]. Enzyme deposit covered by MWCNTs [201] represents another example. The stable layer-by-layer structure made of polyvinyl alcohol,

clay and enzyme was build on the top of ILCPE [254]. Most of enzyme modified ILCPEs exhibit direct protein voltammetry and bioelectrocatalytic properties employed for sensing. The alternative situation - modification of classic CPE with composite film prepared from Nafion, myoglobin and BMIMPF6 allowing for protein voltammetry and bioelectrocatalysis has to be noted [265].

Although this is not carbon paste electrode, the carbon ceramic electrode modified with ionic liquid [266] has to be mentioned here. It is composed of hydrophobic sol-gel processed silicate and carbon microparticles. The porosity of hybrid material allows to fill it with IL with no restriction on its viscosity, because in this case IL does not function as a binder. With carbon ceramic electrode modified with redox probe solution in IL ion transfer across IL|aqueous solution interface can be seen [266] similarly as for ILCPE [235].

1.2.4. Electrodes prepared of ionic liquid – carbon nanotubes gel

In 2003 it was found that imidazolium type ionic liquids tends to form physical gel when grounded with SWCNTs [267]. These materials are formed by physical cross-linking of the nanotube bundles, mediated by local molecular ordering of ILs. Similar, highly electroconductive material can be formed from polymerizable IL and SWCNTs [267,268]. ILCNT gel and similar material made of carbon microbeads and IL was first recognized by Dong as a suitable electrode material [31]. Further studies of ILCNT gel electrodes obtained from variety of hydrophobic or hydrophilic ILs show usefulness of this easy prepared electrode material which can be deposited in a form of thick film on solid conductive substrate. Their bioelectroanalytical application was recently reviewed [24].

Although most papers report ILCNT gel electrodes made of SWCNTs, but also MWCNTs [269-273] and mesoporous carbon [274] can form gel films suitable for electrode preparation.

As in the case of ILCPEs research on ILCNT gel electrodes is oriented towards examination of wide range of analytes [27,272-287]. Taking advantage of stabilizing IL properties enzyme modified ILCNT gel electrodes were also prepared and studied. Enzymes as microperoxidase (MP-11) [31], horseradish peroxidase [31,269,288], hemoglobin [269,289], myoglobin [288], cytochrome c [288] and laccase [290] were immobilized and their direct electrochemistry and bioelectrocatalytic O_2 and/or H_2O_2 reduction was studied (Fig. 15). ILCNT gel electrode is also suitable for glucose oxidase immobilization and bioelectrocatalytic glucose electrooxidation [276,291]. Other examples are immobilization of D-proline dehydrogenase for

amino acid oxidation [292] and organophosphorous hydrolase for determination of organophosphates [271]. It has to be emphasized that all enzyme modified ILCNT gel electrodes exhibit their direct electrochemistry.

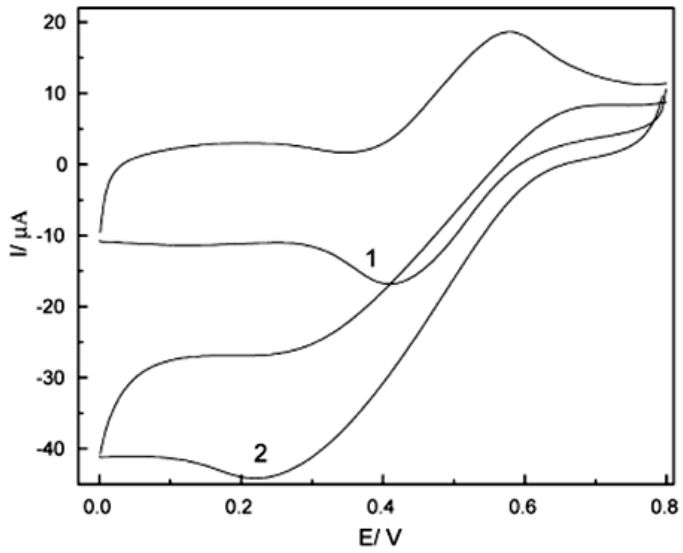

Fig. 15. CVs at laccase/CNTs-IL/graphite electrode in ABTS solution: (1) N_2 saturated solution and (2) O_2- saturated one [290].

An interesting ILCNT gel electrode was prepared with dual catalyst cobalt porphyrin for O_2 to H_2O_2 reduction and Prussian Blue nanoparticles for H_2O_2 reduction [293]. In this way non platinum four electron O_2 electroreduction catalytic electrode was obtained as proved by rotating ring disc electrode experiment [293]. MWCNTs forming gel can be electrochemically decorated with metallic nanoparticles. The example of ILCNT gel electrode modified with PtRuNi ternary alloy nanoparticles for ethanol oxidation was reported [270].

1.2.5. Electrodes modified with appended ionic liquids

The last class of ionic liquid modified electrodes surveyed in this review are electrodes modified with appended ionic liquids. They consist of imidazolium cation based substituent which is (i) self assembled on the electrode surface, (ii) covalently bonded to the electrode surface, (iii) covalently bonded to polymer deposited on the electrode surface or (iv) used for functionalization of conductive elements of the film. The counterion is electrostatically attracted to positively charged functionalities and can be exchanged after immobilization on the electrode surface.

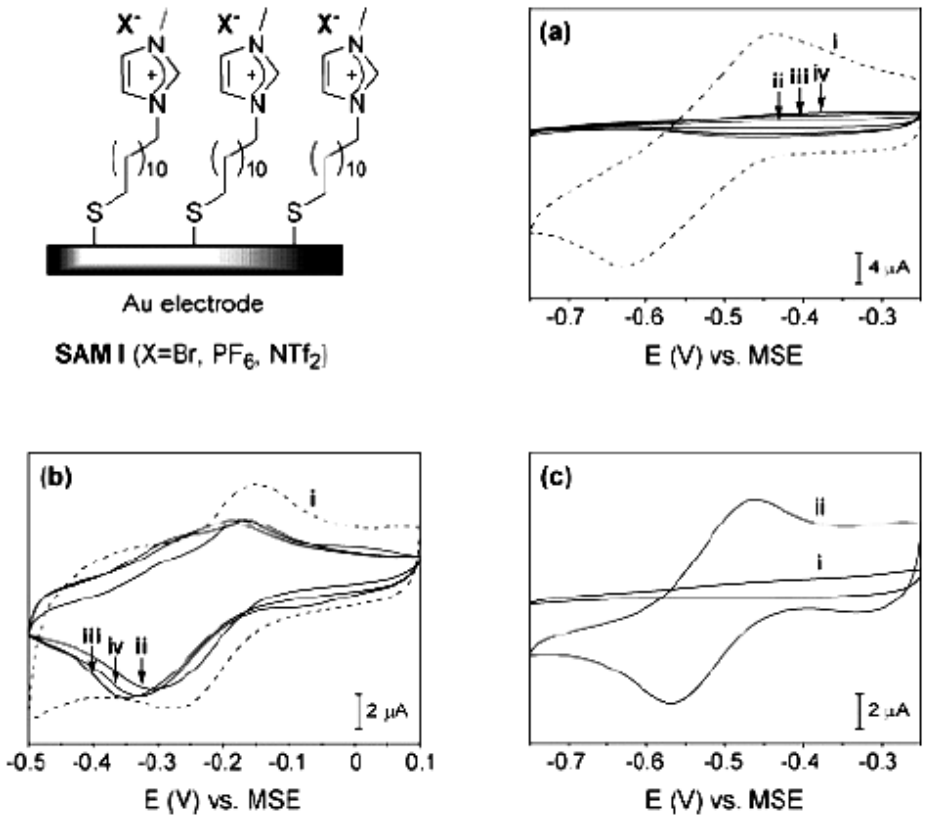

Fig. 16. CVs of (a) (i) bare gold and SAM I having (ii) X = Br, (iii) X = PF_6, and (iv) X = NTf_2 with $Ru(NH_3)Cl_3$; (b) (i) bare gold and SAM I having) X = Br, (iii) X = PF_6, and (iv) X = NTf_2 with $K_3Fe(CN)_6$; (c) SAM I (X = Br) with $Ru(NH_3)Cl_3$ (i) before and (ii) after pretreatment with $K_3Fe(CN)_6$ [39].

There are few reports on application of IL with thiol functionalities for gold electrode modification [38,39,41]. These modified surfaces are able to exchange anions [38,39]. This process allows for wettability control of the surface [38]. The monolayer is dense enough to control accessibility of the electrode surface by redox active ions and exhibits redox switching properties [39] (Fig. 16). Also boron doped diamond (BDD) surface can be modified by carboxylate functionalized IL [42]. Similarly the wettability of IL functionalized BDD can be controlled by anion exchanged and redox ion rectification in respect of charge is noted [42]. IL covalent bonding to the electrode surface was also achieved by solvent casting of IL functionalized SWCNTs [143] or graphene sheets [294]. The first electrode was further chemically modified with Au nanoparticles of narrow size distribution around 3.3 nm for electrocatalytic oxygen reduction [143]. The second electrode also modified with chitosan exhibits electrocatalytic behavior towards ascorbic acid, NADH and ethanol [294]. Further modification with alcohol dehydrogenase enables electrochemical sensing of ethanol [294].

Films of polymer appended ILs [43,51,295-302] are formed by chemical grafting and solution casting [295-298,302] surface initiated polymerization [299], polymerization of vinyl

appended imidazolium cation IL and solution casting [301] or by sol-gel process of the mixture of trimethoxysilane functionalized imidazolium cation and tetramethoxysilane [43,51,300]. The hybrid IL appended organic polymer – silicate film can be formed by sol-gel process of polymer solution in sol [298]. The preparation of electrodes of specific geometry as polymer brush [299] or the application of IL appended polymer as a linker for immobilization of carbon nanoparticles with anionic functionalities [300] or Prussian Blue nanoparticles [302] was also demonstrated. These electrodes combine advantages of ILs (high ionic conductivity, solubility) and polyelectrolytes (good adhesion, stability in aqueous solution). Electrode modification with these materials allows for electrochemical experiment in water in the absence of supporting electrolyte with prospective application for electropolymerisation of pyrrole [296] or in flow injection analysis [297]. IL grafted polymer modified electrode exhibits electrocatalytic properties towards biomolecules clearly due to the presence of imidazolium functional groups [295] (Fig. 17). The hybrid material composed of IL grafted polymer and silicate allows for stable immobilization of glucose oxidase for glucose sensing [298].

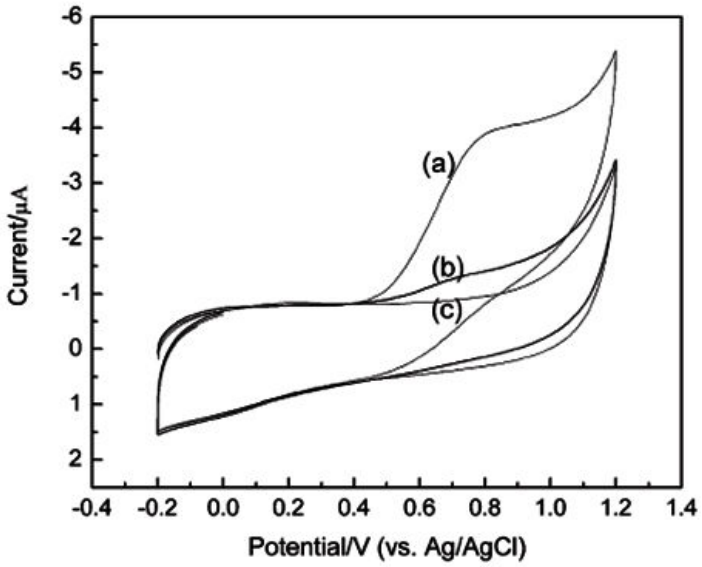

Fig. 17. CVs for NADH at PFIL-Nafion (a) and Nafion (b) modified GCE. Curve (c) was obtained for PFIL-Nafion modified GCE in clean buffer solution [295].

Immobilization of IL appended organic polymer represents another way of IL coupling to the electrode surface. The organic polymer microparticles require Nafion matrix for stable immobilization on the electrode surface and they were applied for glucose oxidase immobilization [303].

IL appended polymer wrapping of MWCNT was applied to obtained their deposit on the electrode surface with low degree of aggregation [304-306]. These modified nanotubes were

obtained by grafting of IL on MWCNTs earlier grafted with organic polymer [306] or by polymerization of vinyl appended IL monomer on MWCNT [304,305]. The electrodes obtained by solvent casting of IL polymer modified MWCNTs and some of them exhibits electrocatalytic behavior towards hydrogen peroxide [304] and oxygen [305]. After further modification with glucose oxidase [304,305] or tyrosinase [306] direct protein voltammetry and bioelectrocatalysis is observed. Similar strategy of IL appended polyelectrolyte wrapping was used for graphene sheets [307]. The electrodes modified with solvent casted IL appended graphene was used to observe direct glucose oxidase voltammetry and glucose sensing [307].

In this thesis the electrodes modified with covalently bonded ILs are described. Sulfur – gold bonding as well as co-condensation with TMOS have been utilized. The comparison of the electrochemical behavior of covalently bonded and non-bonded IL have been done.

2. Sol – Gel processing

The roots of sol-gel science can be found 17,000 years ago in the Lascaux in France. The pigments used for the cave walls decoration were in fact colloidal suspension of iron oxide, carbon and clays. Next, ceramics and pottery was developed in the ancient Mesopotamia, China and Egypt. Ancient Romans have been using concrete. A milestone in sol-gel chemistry was discovery of "water glass" by von Helmont in 1644. He has shown that acidification of alkaline solution of the silicate containing materials leads to the formation of silica precipitate. Synthesis of oxide materials from hydroxide gels had been successively developing during 19th century. In 1846 Ebelman has synthesized silicon alkoxides for the first time. He has also observed that new compounds have had a tendency to gel in the course of time. This experiment can be assumed as a starting point of the modern sol-gel science [308].

2.1. Basics of sol-gel processing

To understand what actually is the sol gel processing one has to introduce several basic definitions.

"A sol is a stable suspension of colloidal solid particles within a liquid." [309] For a sol to be stable dispersion forces must be greater than gravitational ones [310].

"A gel is an porous 3-dimensionally interconnected solid network that expands in a stable fashion throughout a liquid medium and is only limited by the size of the container." [310] One can divide gels for a colloidal and polymeric ones. They are composed respectively of colloidal and sub-colloidal chemical units [310].

"A sol-gel process is a colloidal route used to synthesize ceramics with an intermediate stage including a sol and/or gel state." [310] In other words sol-gel is a method which allows to obtain solid material from a starting precursor solution. One can divide sol-gel materials into two main groups: nonsilicates (based on transition metals, aluminates and borate systems) and silicates (based on hydrolysis and condensation of silicon alkoxides) [311]. Silicate materials have been exploited for modification of electrodes described in the experimental part of this work so they will be described in more details in this chapter.

Starting from silicon alkoxides one can obtained silica in sol-gel process. Several main steps of this process can be singled out:

1. **Hydrolysis** is the first step of sol-gel process. This reaction can be catalyzed either by acids (Fig. 18) or bases (Fig. 19).

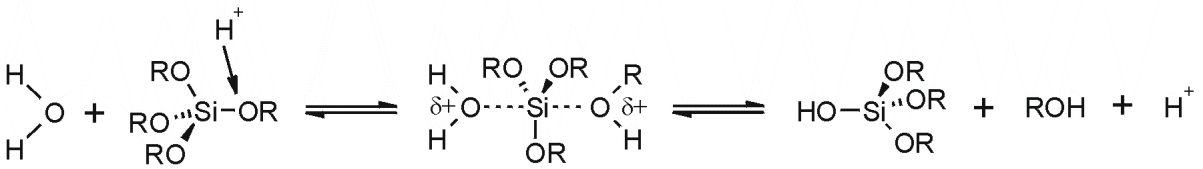

Fig. 18. Acid catalyzed hydrolysis reaction mechanism [308].

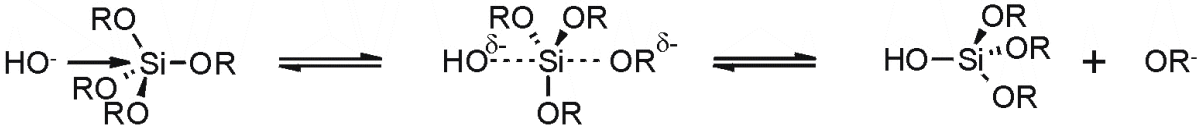

Fig. 19. Base catalyzed hydrolysis reaction mechanism [308].

2. **Condensation** reaction occurs simultaneously with the hydrolysis reaction. It can be catalyzed either by acids (Fig. 20) or basis (Fig. 21).

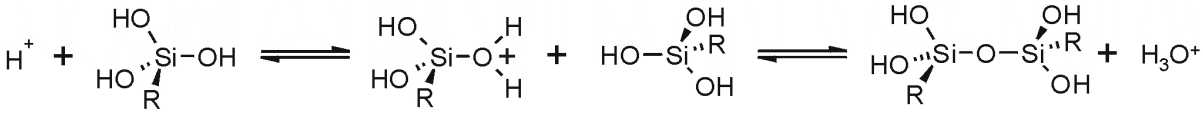

Fig. 20. Acid catalyzed condensation reaction mechanism [308].

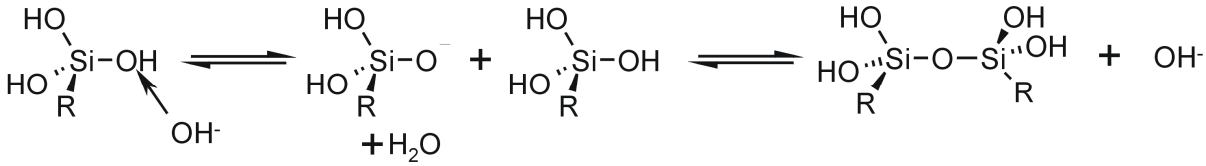

Fig. 21. Base catalyzed condensation reaction mechanism [308].

3. **Gelation** is the process in which colloidal silica particles arranges themselves into a 3-dimensional structure which stretch across reaction vessel. In gelation process solvent molecules as well as sol particles are trapped in the solid network. Many of the sol particles remains unbound and further ageing is needed to incorporate them into the network. Gelation starts in the gel-point which is defined as the "time at which the viscosity is observed to increase abruptly." [311](Fig. 22)

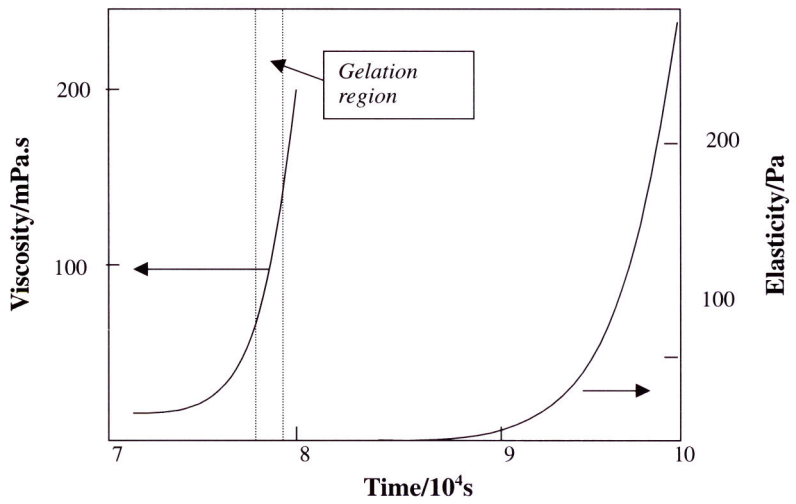

Fig. 22. Viscosity and elasticity changes in relation to gelation [308].

4. During **ageing** process the new covalent cross-linking bonds form inside the gel. From macroscopic point of view gel shrinks and becomes stiffer. This process has a vital influence on future material properties. One can control the process by adjusting the pH, temperature, pressure, ageing liquid medium and initial precursor composition [308].

5. **Drying** process can be divided into several stages. First, water evaporates and the gel shrinks to compensate the volume loss and this is called "constant rate period". After reaching the critical point network cannot shrink more and starts to crack because of the capillary forces. Next one observes the "first falling rate period" which is connected with the liquid's flow along the partially filled pores. After that there is a "second falling rate period" when evaporation starts to proceed inside the gel body and the vapors escapes by the diffusion [311].

6. **Densification** is realized by heat treatment of the gel material. During the sintering it is possible to obtain dense glasses and ceramic materials [308]. In spite of its advantages this process can only be used for materials which does not contain any organic nor biological molecules.

Very interesting idea binding sol-gel science with electrochemistry is electro-assisted generation of sol-gel films. The method was first introduced by Mandler and coworkers [312]. Conductive substrate was immersed into the pre-hydrolyzed sol solution as a working electrodes. The pH close to the electrode surface could be adjusted by electrochemical

generation of the OH^- ions. It is known that pH strongly affects the rate of the sol polycondensation reaction. Locally increased pH causes that polycondensation reaction goes fast close to the electrode surface and the film deposition is observed. This concept was further developed by other groups [313-316].

2.2. Surfactant templates in sol-gel process

Apart of many possibilities of controlling the sol-gel process by changing factors such as pH, temperature, pressure, humidity etc. one can change the material structure by adding surfactant to the sol solution. They are usually long chain organic amphiphile molecules which have an ability to decrease the surface tension [317]. Various types of surfactants are known. The first group there are anionic surfactants which consists of the long carbon chain with the anionic group on the end. The most popular are: carboxylic acid salts, sulfonic acid salts, sulphuric acid ester salts, phosphoric and polyphosphoric acid esters. In the second group one can find cationic surfactants. They usually are: long-chain amines and their salts, acylated diamines and polyamines and their salts, quaternary ammonium salts, polyoxyetylenated (POE) long-chain amines, quaternized POE long-chain amines and amine oxides. The third main group of the surfactants are non ionic ones. Representatives of them are: POE alkylphenols, POE straight-chain alcohols, POE polyoxypropylene glycol, POE mercaptans etc. Another possibility are the amphoteric or zwitterionic surfactants which have both anionic and cationic groups [318].

Interesting and potentially very useful property of the surfactant solutions is the formation of micelles – colloidal size clusters of surfactant molecules. Micelles start to form spontaneously when CMC is reached. The driving force of this phenomenon is minimization of the system's free energy. System tends to minimize the free energy by decreasing the distortion in solvent structure [318].

The first reports on surfactant template silicate materials synthesis were published in 1992 [319,320]. The new material group was named M41S. The pore size in the material was 1.5 nm to 10 nm. The pore structure was organized in hexagonal (MCM-41), cubic (MCM-48) and lamellar (MCM-50) way [310]. The main idea of the discovery was to use surfactant micelles as a template for silicate or other material network formation (Fig. 23). The materials were obtained from an acid solution of surfactant and sodium silicate heated to 100 °C for 114 h. [321] Of course particular conditions may vary for desirable material.

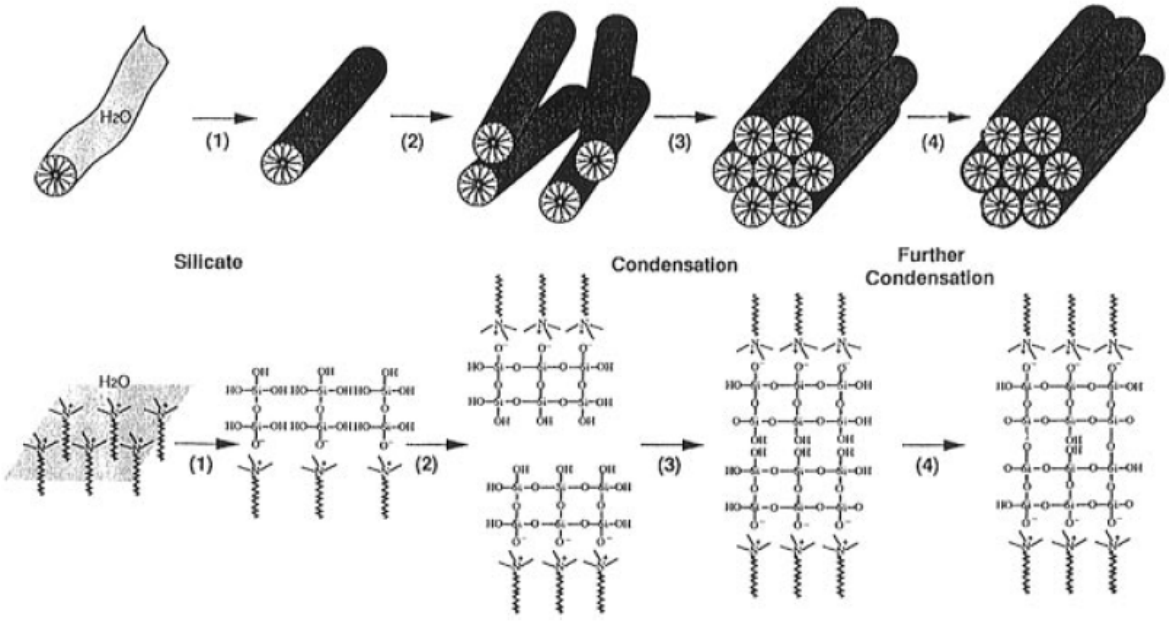

Fig. 23. Mechanism for the formation of MCM-41 [321].

2.3. Ormosils – hybrid materials synthesis

Structures and properties of the sol – gel materials can be strongly influenced by incorporation of the organic groups. Such materials belongs to the hybrid organic-inorganic materials. They are defined as "materials that includes two moieties blended on the molecular scale. Commonly one of these compounds is inorganic and other one organic in nature." [322]. Going further one can divide hybrid materials into two classes [322]. In Class I materials organic part is connected with inorganic part by week interactions (van der Waals, hydrogen bonds, electrostatic interactions). Class II materials shows strong chemical interactions between organic and inorganic part. (Fig. 24)

Hybrid materials can be obtained by adding organic compounds into the sol precursor solution. After gelation process organic are entrapped inside the gel material. Organic molecules must be durable enough to withstand the sol-gel process conditions such as water environment and particular pH. As it is well known sol-gel process needs conditions mild enough to immobilize a broad spectrum of biologically active compounds such as enzymes [323].

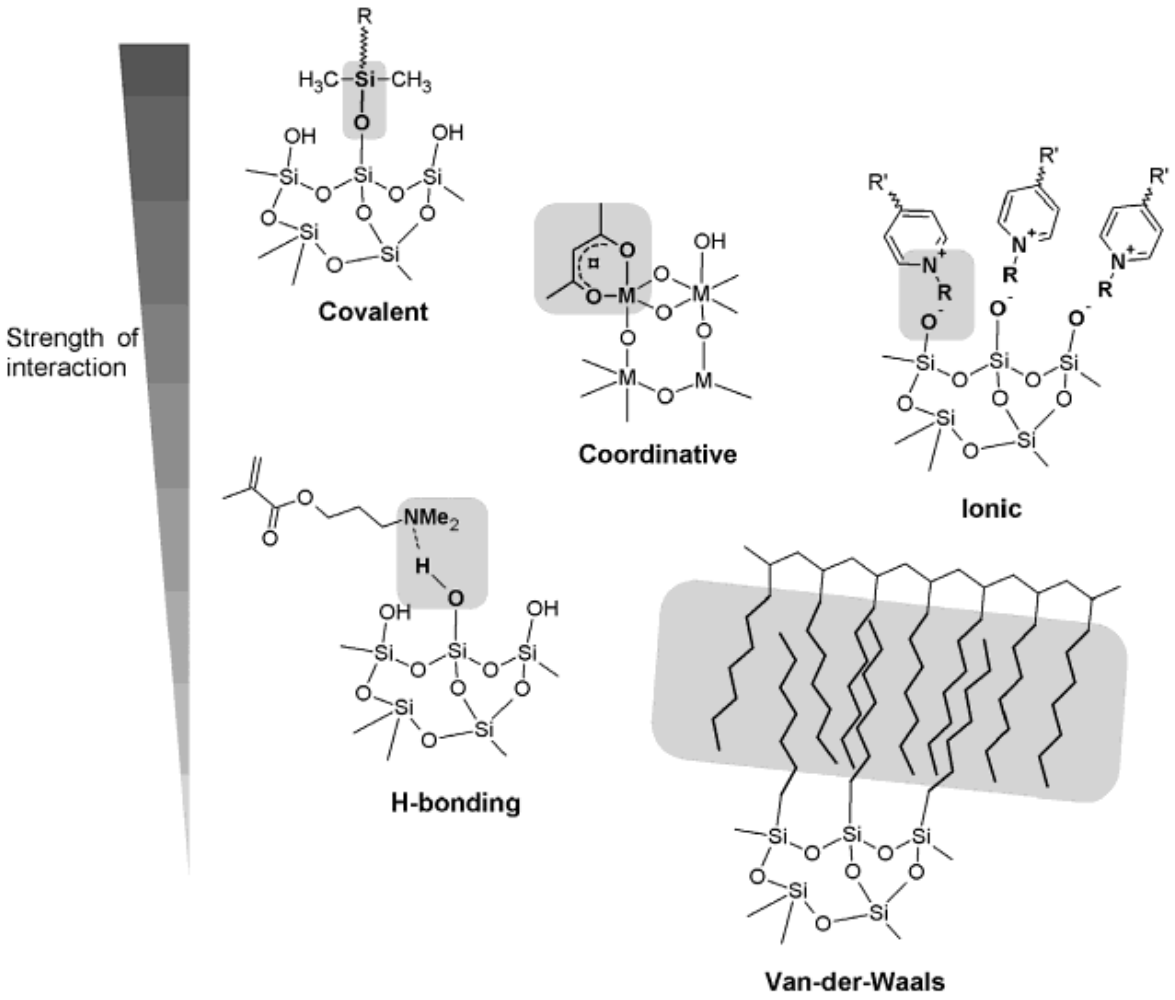

Fig. 24. Selected interactions typically exploited in hybrid materials and their relative strength [322].

Physical entrapment of organic compounds is very universal and simple. The main disadvantage of this method is leaching of the entrapped compound from sol-gel matrix. To avoid this problem organotrialkoxysilanes with particular functional groups (Fig. 25) are used.

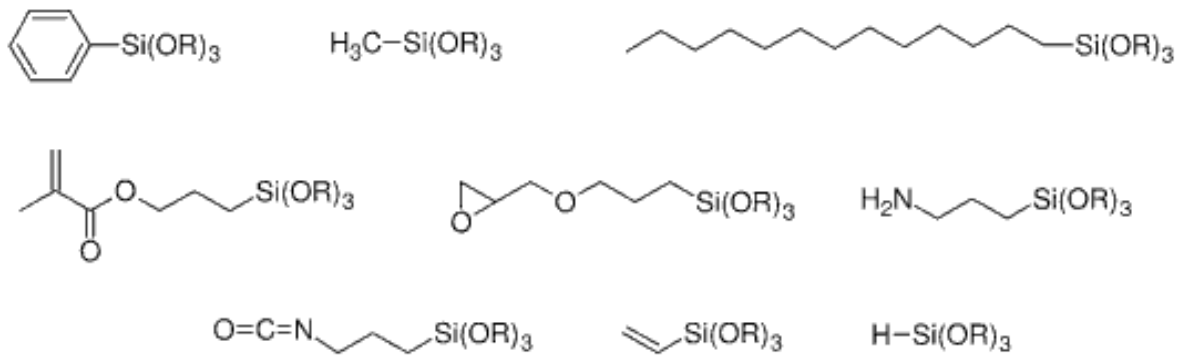

Fig. 25. The examples of trialkoxysilane precursors often used in sol-gel process [322].

The usual way of synthesizing silicate material with covalently bonded organic group is to prepare the sol from a mixture of organotrialkoxysilane and tetraalkoxysilane. It is very difficult to obtain gel material only from organotrietoxysilane because of the presence of bulky organic group. The steric hindrance problem can be bypassed by tetraethoxysilane addition. As a result of co-condensation silicate structure functionalized with organic groups is obtained. However such network has a lower interconnectivity in the bulk because of the presence of organic groups in the material [308]. Another way of introducing organic groups to the sol gel material is surface functionalization also known as a grafting. In this approach silanol groups of already formed gel reacts with organotriethoxysilane bearing the desired group. This strategy leads to the formation of well connected gel matrix with organically modified surface [324].

2.4. Mesostructured hybrid organic-inorganic materials

The interesting path in the new material synthesis is combining surfactant templated synthesis route with organic groups attachment. As a result of such fusion on can obtain organically modified mesoporous silicates materials. There are two main approaches to obtain such materials. (Fig. 26)

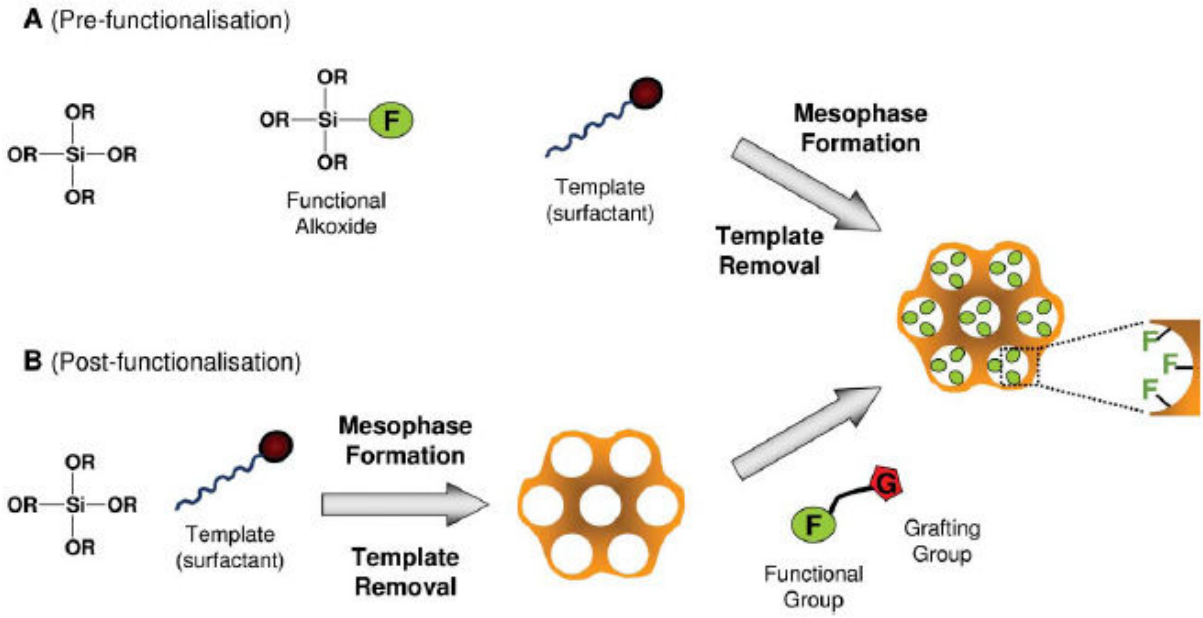

Fig. 26. Routes to mesostructured hybrid organic-inorganic materials synthesis [325].

The simplest way is so called one-pot synthesis [325]. In this approach tetraalkoxysilane is mixed together with organotrietoxysilane and surfactant. After co-condensation organically modified mesoporous material with surfactant template inside the pores forms. Surfactant is

removed in the next stage. Materials obtained in this process has organic groups both on the pores surface and in the bulk material. The addition of organotrialkoxysilane disturbs the organization in the sol solutions and very often leads to the final material without well defined organization [326]. However some organized mesoporous hybrid materials obtained via one - pot synthesis are reported [325,327].

Another approach to introduce organic groups to the mesoporous material is post-synthetic route also known as a grafting. In this case first mesoporous silicate material is synthesized and the surfactant is removed from the pores. In the next step organic groups are introduced in the reaction of precursor with the silicate surface [325]. In this approach the number of introduced organic groups is smaller in comparison to one-pot synthesized materials. They are located only at the surface of pores. The bulk of the silicate remains unmodified. This strategy can lead to well ordered organically modified mesoporous materials [328,329].

2.5. Sol-gel materials' shapes for various applications

Apart from various compositions and microstructures, sol-gel materials can be easily synthesizes in a great variety of shapes. The particular shapes of the sol-gel materials are often required for particular applications [311,330].

The first commercialized sol-gel materials were in the form of thin films and coatings [311]. Many examples of optical coatings are obtained in sol-gel process. Colored [331], antireflective [332], optoelectronic [333] and ones for optical memories [334] are the most important examples. Electronic films obtained in sol-gel procedure are used as photoanodes [335], high-temperature superconductors [336], conductors [337] and ferroelectrics [338]. Another type of sol-gel thin film are protective coatings. They can increase corrosion resistivity [339] of the surface but also make it planar [340], scratch resistive [341] and promote the adhesion [342]. The last type of films are porous coatings. These materials in combination with surface modification techniques are ideal candidates for sensors [343] and catalytic applications [344].

The sol-gel materials can be also obtained as monoliths. The main applications of such monoliths are different branches of optics. Optical fibers [345], lenses [346], graded refractive index glasses [347] and thermal insulators [348] can be obtained by sol-gel technology.

Another important group of sol-gel materials are powders. Different types of powders, grains and spheres of different shapes were synthesized. Such materials can be used as catalysts [349], chromatography immobilized phases [350], high temperature superconductors [336]

and abrasive materials [351]. Sol-gel fibers of different types are used mainly in reinforcement applications [352].

The last but very important to be mentioned sol-gel materials are unsupported films (membranes) [353]. The main application of such structures is filtration.

2.6. Electrochemistry of sol-gel materials

The important area where sol gel process is used are modified electrodes and electrochemical sensors either amperometric [354] or potentiometric [355]. Very fast developing branch of electrochemistry where sol-gel materials are widely applied is electrochemical biosensing. The first successful active enzyme encapsulation in sol gel material was described in 1990 [356]. This was the milestone, which has provided a new way of enzymes immobilization for sensors application. Papers describing sol-gel encapsulated enzyme based sensors have started to mushroom. Many different sensor projects have been presented [323] and the topic is still developing [357,358].

Electrodes can be modified in the bulk or only on the surface with thin sol-gel film. In the first case carbon particles are mixed together with sol solution and after gelation carbon ceramic electrode (CCE) [359] is obtained. Also another modifiers such as organometallic catalysts [360], inert metals [361], biological molecules [362] and others can be added to the sol to modify electrode properties. In the case of surface modified electrodes, charge mediators, chromophores, metal and organo-metallic catalysts, preconcentration agents, ionophores, and active proteins are immobilized in thin sol-gel film [363].

One can single out several groups of sol-gel processed systems utilized in electrochemistry. There are: interpenetrating organic inorganic systems, redox polymers, solid electrolytes, electrochromic materials, sol-gel encapsulated complexes and others. Electrochemistry can be also used for sol-gel process monitoring or even for sol-gel process control.

First group of sol-gel materials containing systems are interpenetrating organic-inorganic hybrids. Such material usually consists of sol-gel material and conductive polymer. They can be applied in lithium intercalation batteries, capacitors, electrochromic displays, electrochemical signal mediators, and ion-selective field effect transistor sensors [363]. Other important electrochemical topic connected to sol-gel process is redox polymers. The unique properties of sol-gel process make it relatively easy to bond redox moieties to the gel matrix [363].

Another discipline in which sol-gel materials are widely exploited is solid electrolytes. Several main types of solid electrolytes are known. There are: protonic conductors [364], sodium ion conductors [365] and lithium ion conductors [366]. Electrochromic materials can also be sol-gel processed. One can divide electrochromic materials into two main groups: transition metal oxides [367] and hybrid organic-inorganic electrochromic materials [368]. Electrochemistry can be also successfully applied to monitor sol-gel process, to observe structural transitions and to synthesize the sol-gel precursors [363]. It is possible to observe electrochemiluminescence from sol-gel encapsulated complexes [369].

3. Nanochemistry

"There's plenty of room at the bottom." In these words 1959 Richard Feynman has presented the idea that direct manipulation of atoms an molecules can be a strong alternative for classic synthetic chemistry. He has described the strategy of building sophisticated materials starting from the single molecules or atoms. In other words: "from the bottom up rather than top down." [370] He has also proposed the building of the miniaturized tools in atom by atom method and presented the idea of microscopes which allows to see objects much smaller than those possible to observe with scanning electron microscopes. However, some time was needed for people to use his idea in practice. It was only in 1982 when Binning and Rohrer invented the scanning tunneling microscopy [371]. They have been awarded with the Nobel Prize in 1986. However, this technique was limited to conductive samples. In 1986 the first paper about atomic force microscopy (AFM) was published [372]. This technique has made the observation of the insulating surface with atomic resolution possible. Soon the manipulation on the scale of single atoms has been demonstrated [373] and the synthesis of chemical molecules atom by atom was demonstrated to be possible [374]. In 1985 the fullerene molecule has been synthesized [375] by Kroto and coworkers which brought them a Nobel Prize in 1996. All of the experiments mentioned above and many others has convinced the scientific community that it is worthy to look closer at the world of nanoobjects.

3.1. Nanomaterials

According to the conventional definition nanomaterials are the materials "having a characteristic length scale less than about hundred nanometers. This length scale could be a particle diameter, grain size, layer thickness or width of a conducting line on an electronic chip." [376]

Nanoobjects can be presented as a transition between molecules and bulk materials. They often shows different physical properties than latter, because of large fraction of the surface atoms (Fig. 27). The well developed surface of nanomaterials is one of the factors which makes them interesting also from the electrochemical point of view. Their optical, magnetic, electronic and chemical properties are also very different than those of the bulk material [377]. The important group of nanomaterials are nanoparticles.

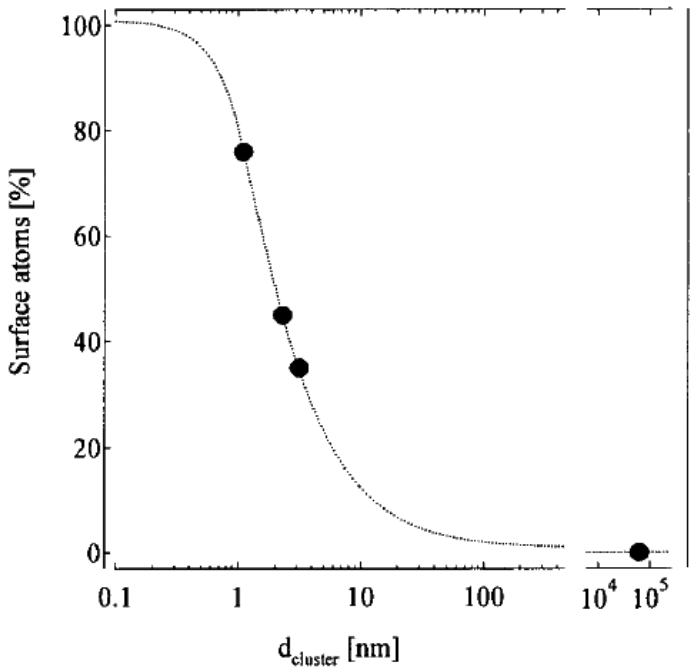

Fig. 27. The percentage of surface atoms changes vs. the cluster diameter [378].

3.2. Nanoparticles deposition

Nanoparticles have a massive influence on modern chemistry. However to fully utilize their potential in electrochemistry one needs to immobilize them on the electrodes. Crucial challenge of such immobilization is to provide electrical contact between the nanoparticle and the electrode. Various methods has been used such as "anchoring by electrostatic interactions, covalent linkage, and electrochemical deposition" [379].

The most obvious deposition method is adsorption from aqueous suspensions [380,381]. The attractive interactions between the nanoparticles and the surface result immobilization. One can tune these interactions by modifying the surface with different functional group and/or by varying the nanoparticles stabilizing agents. The good examples of such approach can be deposition of gold nanoparticles onto the thiolated glass surface [382] or binding the gold nanoparticles to the gold surface using dithiols [383]. To increase the load of nanoparticles on the surface sometimes additional linker molecules are used [381].

Another interesting approach to nanoparticles immobilization is application of sol-gel process. A thiol containing sol-gel matrix can be synthesized by hydrolysis and condensation of mercaptopropyltrimethoxysilane. The matrix can be immobilized on the gold surface by self assembling after electrode immersion into the sol solution. Such sol-gel modified electrode can by further modified with gold nanoparticles by immersion into their suspension. In this step they bind to –SH groups present in the sol-gel matrix [384]. Not only gold

nanoparticles can be immobilized via sol-gel processing. An interesting electrode was obtained by deposition of hydrophilic carbon nanoparticles in sol-gel matrix on the ITO surface [385]. Similar system was later applied for enzyme immobilization and it was found to promote the direct electron transfer between enzyme and electrode [386].

The next important strategy of nanoparticle deposition is incorporating them into the CPE [377]. The advantages of this method are a, facility of introducing additional components (e.g. enzymes) [387,388] to the paste, and b, easy electrode surface renewal. It can be done by simple removal of the top layer of the paste. Only a tiny amount of gold nanoparticles is needed to completely change CPE behavior [388]. This fact can be exploited to build much cheaper electroanalytical systems [389] than those containing bulk gold electrodes.

The easy and efficient way to obtain electrode covered with gold nanoparticles is electrochemical deposition. Similarly to the colloidal gold synthesis the basic solution is $HAuCl_4$ solution and potential is applied to the electrode instead of using chemical reducing agent. $AuCl_4^-$ anions are reduced and gold nanoctrystals are deposited on the electrode surface. By varying deposition conditions, such as applied potential, time etc., one can control size, shape and distribution of the deposited particles [377]. Above mentioned procedure allows to obtain dense deposits [390]. of nanoparticles on the surface which is not so trivial with non-electrochemical methods. Electrodes prepared accordingly to the procedure described above can be used as a base for more complexed systems such as biosensors [391], heavy metals sensors [392] etc.

3.2.1. Gold nanoparticles

Gold nanoparticles are among the most widely investigated nanostructures. They are usually synthesized via chemical or electrochemical reduction of the gold compounds such as $HAuCl_4$. The most commonly used reducing agent is sodium citrate but also others compounds such as $NaBH_4$ can be used [377]. The size and shape of the particles are strongly dependent on the preparation conditions.

Bare gold nanoparticles shows a tendency to aggregate because of their high surface energy. To obtain the stable suspension of AuNPs usually a stabilizing agent is necessary. The most commonly used ones for AuNPs are thiols or disulfides with variety of functional groups [393], but other compounds are also used. They attach to the nanoparticle's surface and prevents the aggregation and precipitation. The additional role of the stabilizing agent can be

nanoparticles' surface functionalization (Fig. 28). Functionalized nanoparticles are suitable building blocks for more complex systems.

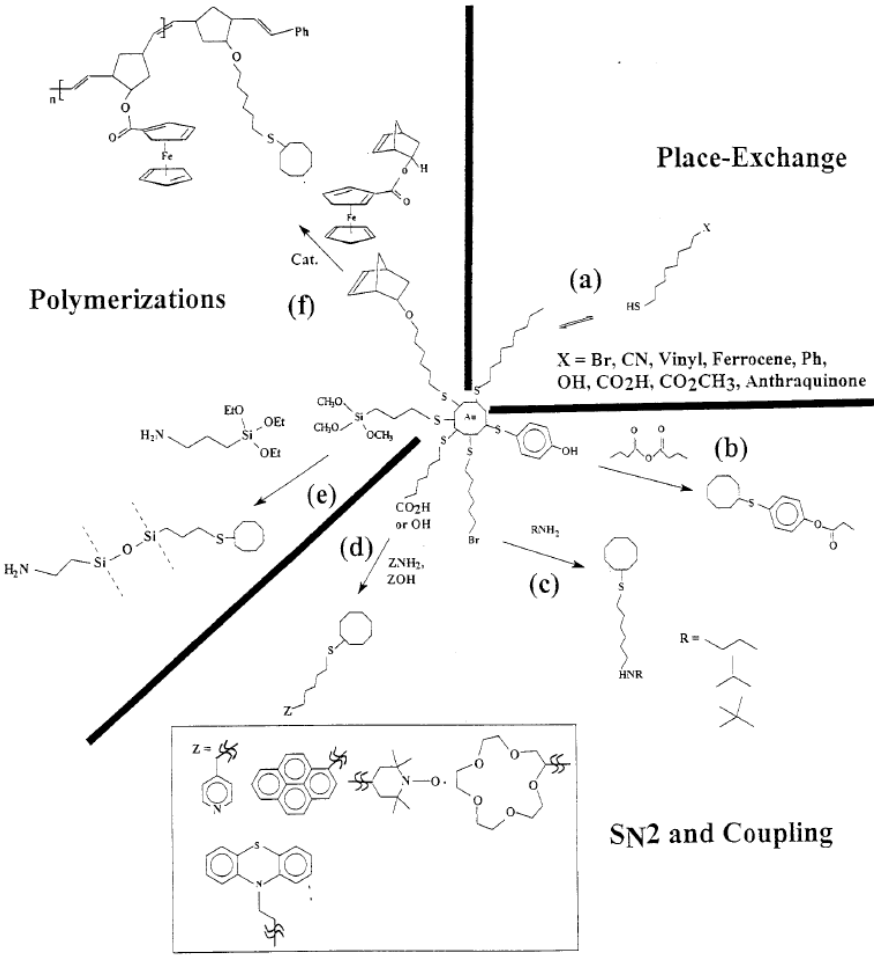

Fig. 28. Reactivity of monolayer protected clusters [393].

For a great number of applications, especially electrochemical ones, there is a need to immobilize AuNPs on the solid surface (electrode). There is a number of methods, which allows one to immobilize gold nanoparticles on the electrode. As it was said above, the most important are: adsorption from water suspensions, immobilization in a carbon paste and electrochemical deposition.

The big problem with adsorption from the water solutions is small number of immobilized [380]. It can be increased if linker molecules are used [377]. This approach helps in increasing the number of nanoparticles on the surface but on the other hand can suppress their catalytic activity because of the surface blocking effect. Another approach is to immobilize gold nanoparticles in carbon paste electrode [388]. It is easy to mix nanoparticles with the paste. The surface of the electrode prepared this way can be easily renewed by removing the top layer of the paste. Next process which allows to obtain gold nanoparticles modified electrode

is electrochemical deposition. One can generate them on the surface of the electrode immersed to the $HAuCl_4$ solution by applying a particular potential. This electrochemical process can be controlled relatively easy which results with good reproducibility [377]. Glassy carbon [394], basal plane pyrolytic graphite [394] and bulk gold electrodes [395] can be modified this way.

Electrodes modified with gold nanoparticles are suitable candidates for electroanalytical applications [377]. There were used for cadmium, copper and nickel detection [392]. Catalytic oxygen reduction on nanoparticulate gold electrode was also studied [396]. Arsenic detection is the next example of electroanalytical application of AuNPs [389]. NPs immobilized on the electrode surface provides well developed surface. Interactions between analytes and crosslinking molecules are the crucial factor which allows to build selective or even specific sensors [397]. Due to their catalytic properties gold nanoparticles can selectively decrease the overpotential of some reactions which allows to analyze substances in the presence of commonly appearing interfering agents [398]. NPs can be used as a building block in construction of chemiresistors [399]. Such devices can be used as sensors. Their selectivity depends on the nature of organic matrix which binds nanoparticles together. Incorporating analyte molecule between the nanoparticles changes the distance between them, which causes the increase of the chemiresistor resistivity. This phenomenon has been successfully exploited for the detection of toluene and tetrachloroethylene vapors [400] or toluene, dichloromethane and ethanol dissolved in electrolyte solutions [401]. Some electrochemical sensors has been prepared by crosslinking gold nanoparticles with compounds able to form complexes with π-donor substances [402]. This type of sensors was found to be very effective in preconcentration of the analyte on the electrode surface, however voltammetric detection makes them useful only for redox active analytes. To bypass above mentioned disadvantage, ion sensitive field effect transistors (ISFET) [403] were applied.

However one of the most spectacular fields where gold nanoparticles are utilized is bioelectrochemistry. Electrochemical biosensors, bioelectronic devices, biofuel cells, electrochemical immunosensors and DNA-sensors are only the most obvious examples of the AuNPs impact on bioelectrochemistry [404]. Gold nanoparticles starts to play more and more important role in biosensors construction [405]. The big challenge in biosensing is to provide good electrical connection between enzyme active center and the electrode. Several methods such as use of diffusional mediator [406], binding redox-relay group to the protein [407] or immobilization of enzyme in the redox-active polymer [408] have been tried. AuNPs provides additional option of enzyme wiring to the electrode. One can build a sensor by simple Au

nanoparticles and enzyme co-deposition [409], but more effective way is enzyme reconstitution [383]. In this method gold nanoparticles are functionalized with enzyme cofactors (e.g. flavin adenine dinucleotide). After that apo-enzyme (e.g. apo-glucose oxidase) is reconstituted with the cofactor functionalized nanoparticle which results in nanoparticle enzyme hybrid. Such system can be immobilized at the electrode surface with different dithiols as a linkers (Fig. 29). This approach allows to eliminate random enzyme arrangement factor which usually causes poor electric contact [404].

Unique plasmon absorbance properties of nanoparticles has been used for DNA [410] and antibody-antigen [411] analysis. However this type of analysis can be also done with electrochemical signal transduction. Moreover application of metal nanoparticles as tags for stripping voltammetry allows to lower the detection limit by 3 to 4 orders of magnitude in comparison to commonly applied methods [404]. The main idea is that single recognition event results in release of many ions which can be directly detected in electrochemical way – one nanoparticles consists of many atoms. The amplifying effect can be additionally increased by electroless deposition of metals (e.g. silver) on the nanoparticles which causes that even more ions can be released and detected.

The similar strategy has been applied for the immunosensors design. The only difference is that antibody-antigen interaction is exploited rather than DNA complementary strands hybridization [412]. (Fig. 30)

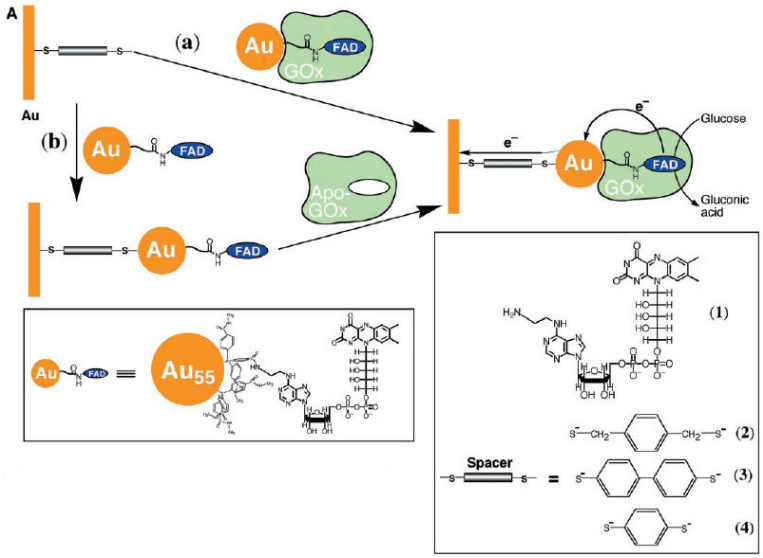

Fig. 29. Assembly of Au-NP–reconstituted GOx electrode by (a) the adsorption of Au-NP–reconstituted GOx to a dithiol monolayer associated with a Au electrode and (b) the adsorption of Au-NPs functionalized with FAD on the dithiol-modified Au electrode followed by the reconstitution of apo-GOx on the functional NPs [383].

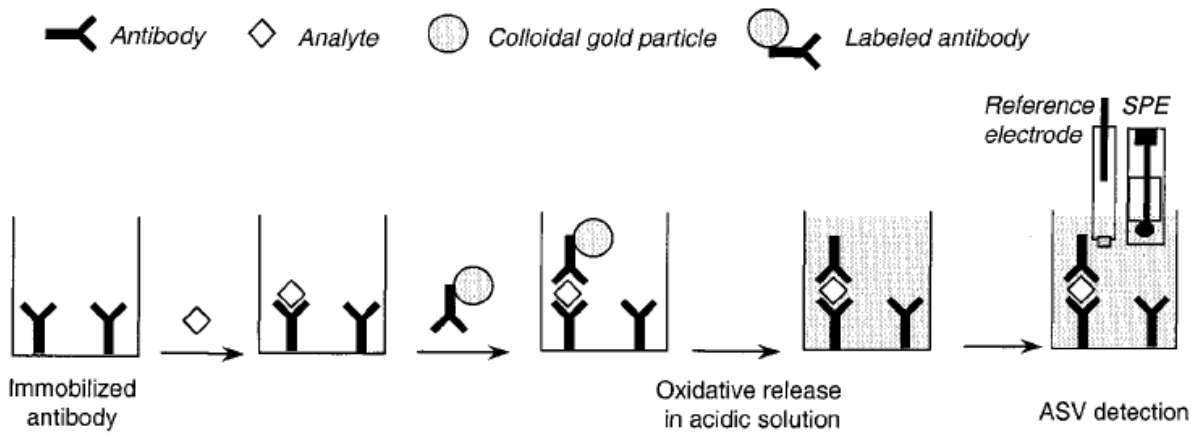

Fig. 30. Schematic representation of the noncompetitive heterogeneous electrochemical immunoassay based on a colloidal gold label [412].

3.2.2. Tosyl functionalized carbon nanoparticles

There are many reports on the electrodes modified with carbon nanostructures as carbon nanotubes [413], fullerenes [414], graphene [415] or carbon nanofibers [416]. However only a few papers reports modification with carbon nanoparticles. The idea of use tosyl functionalized carbon nanoparticles as a nanotechnological building blocks analogically to the metal nanoparticles has been developed in Marken's group [417]. First they were used to stabilize the liquid|liquid interface [418]. The most important strategies of CNPs immobilization are: immobilization in LbL film with different binders, entrapment in sol gel silicate matrix and others, usually more complexed, systems.

ITO electrode modified with carbon nanoparticles and poly(diallyldimethylammonium chloride) (PDDAC) by layer-by-layer method have been found to bind negatively charged redox probes such as indigo carmine. No binding was observed for the positively charged ferrocenyltrimethylammonium. This was caused by the excess of positive charged binding sites in the film. The film was also demonstrated to strongly affect electron rate transfer for hydroquinone oxidation. It was also used to detect micromolar concentration of dopamine in the presence of milimolar concentration of ascorbate [417]. Properties of the film was further investigated and application of it for detection of triclosan was proposed [419]. Similar film was build with carbon nanoparticles and chitosan as a binder. Physisorption of indigo carmine and hemisorption of 2-methyleneanthraquinone was observed. It was demonstrated that the number of binding sites can be controlled by varying the amount of chitosan in the film [420]. Chemisorptive properties of the film was also demonstrated for 2-bromo-methyl-anthraquinone in acetonitrile [421]. Only recently, the method of conversion of the original negatively charged sulfonate modified carbon nanoparticles into the positively charged ones was developed [422]. First the original sulfonate group was converted to sulfonylchloride. In the

second step sulfonamide was formed in the reaction with an amine (Fig. 31). In the same paper layer-by-layer film preparation from positively and negatively charged carbon nanoparticles without additional binder was demonstrated.

Carbon nanoparticles entrapment in sol-gel silicate matrix leads to the porous material with the high specific capacitance and good stability [423]. Such material can be potentially applied in energy storage devices. An hydrophilic silicate sol-gel matrix with encapsulated carbon nanoparticles was also deposited on ITO electrode by drop deposition [385]. Highly porous electrode with high double layer capacitance have been obtained. The electrode was further investigated in the presence of hydrogen peroxide or tert-butylferrocene. These experiments have shown well developed electrochemically active surface of the electrode. The sol-gel hybrid film has been demonstrated as a suitable binder for carbon nanoparticles immobilization [300]. The layers of carbon nanoparticles were deposited subsequently with the layers of imidazolium modified silicate.

More complex systems containing carbon nanoparticles has been also constructed. Glassy carbon electrode modified with the hemoglobin-carbon nanoparticles-polyvinyl alcohol film has shown good electrocatalytic properties towards hydrogen peroxide, oxygen and nitrite reduction [424]. The hybrid film has been demonstrated as a good matrix for proteins immobilization for biosensing applications. Electrode made of laccase adsorbed on carbon nanoparticles immobilized in sol-gel silicate matrix has been successfully applied as an biocathode in a zinc oxygen battery [386]. Biocompatibility of carbon nanoparticles has also been exploited in bacteria immobilization. Electrode made of carbon particles, *proteus vulgaris* and Teflon emulsion has been applied as an anode in microbial fuel cell [425]. A glucose biosensor based on glucose oxidase encapsulated in carbon nanoparticles-nafion film has recently been described [426]. Chitosan-carbon nanoparticles film has been recently used for electrochemical mercury nanodroplets formation. Such nanodroplets modified electrode was demonstrated as an efficient tool for Cu^{2+} and Pb^{2+} detection [427].

Recently the glassy carbon electrode was modified with carbon nanoparticles by simple drop coating procedure. Modified electrode was than successfully applied in detection of drugs such as acetaminophen and tramadol [428]. After addition of Nafion electrode was found to be suitable for naltrexone detection [429]. A suspension of tosyl functionalized carbon nanoparticles can be also applied for extraction and subsequent electrochemical detection of phenolic pollutants such as 2-hydroxy-4-methoxybenzophenone or 5-chloro-2-(2,4-dichlorophenoxy)phenol [430]. The extraction step have been followed by the drop coat deposition and electrochemical detection in this case.

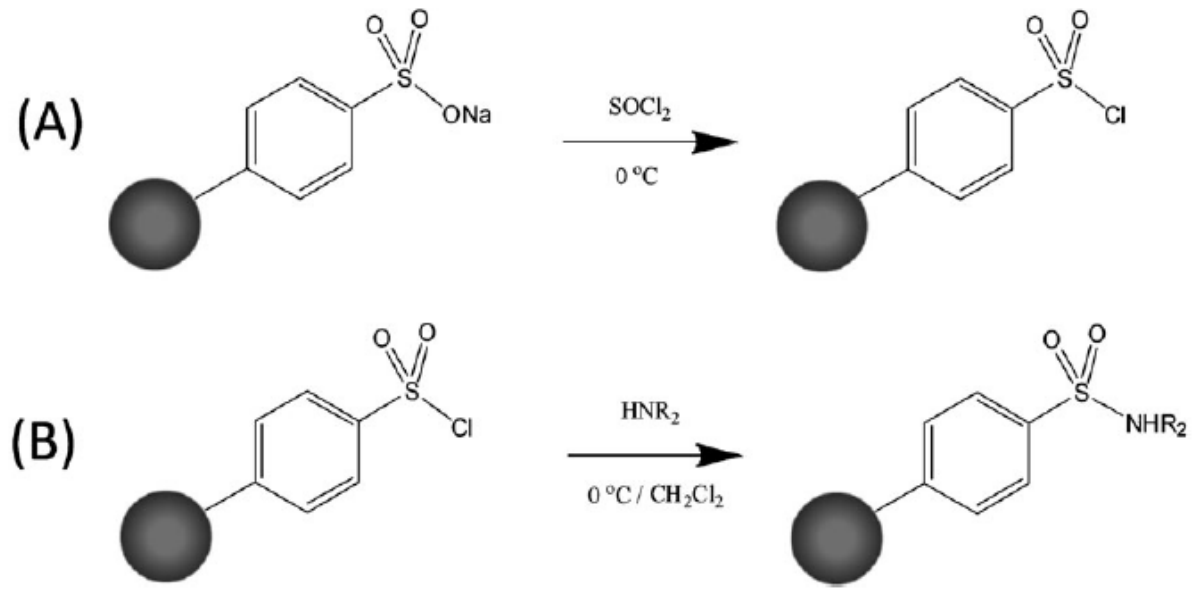

Fig. 31. Negatively and positively charged functionalized carbon nanoparticles [422].

3.3. Layer-by-layer deposition

Layer-by-layer deposition method is rooted in the experiments described by Iler in 1966. [431] He has shown that positively charged colloidal particles have a tendency to bind negatively charged colloidal particles. Multilayered structure can be obtained by subsequent immersion of the substrate into the suspensions of particles of the opposite charge [370]. (Fig. 32)

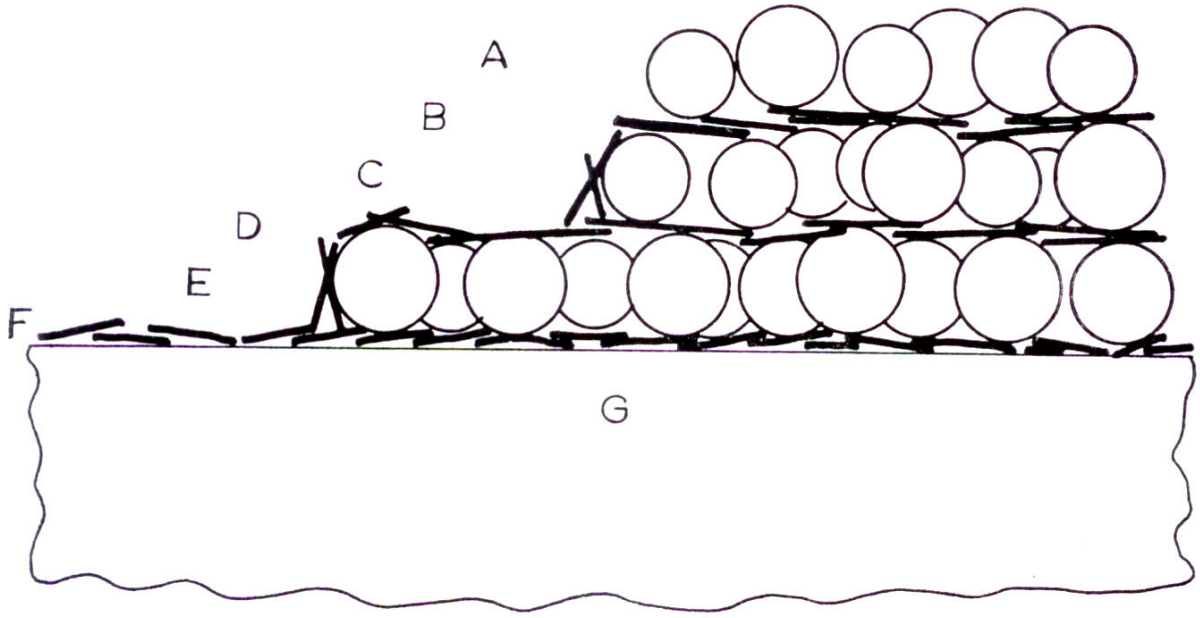

Fig. 32. "Schematic cross section of a multilayer film: A, C, and E represents layers of 100 μm silica; B, D, and F, layers of colloidal boehemite fibrils; G, the glass substrate." [431]

This interesting idea was further developed by Decher and coworkers [432-435]. They have shown that LbL approach is a suitable method for polyelectrolyte multilayered structures

formation. In order to deposit a thin polyelectrolyte film one need to immerse charged substrate into the solution of polyelectrolyte of the opposite charge. Electrostatic interactions between the surface and the polyelectrolyte leads to thin layer formation. This process can be repeated many times until the film of desired thickness will be obtained (Fig. 33).

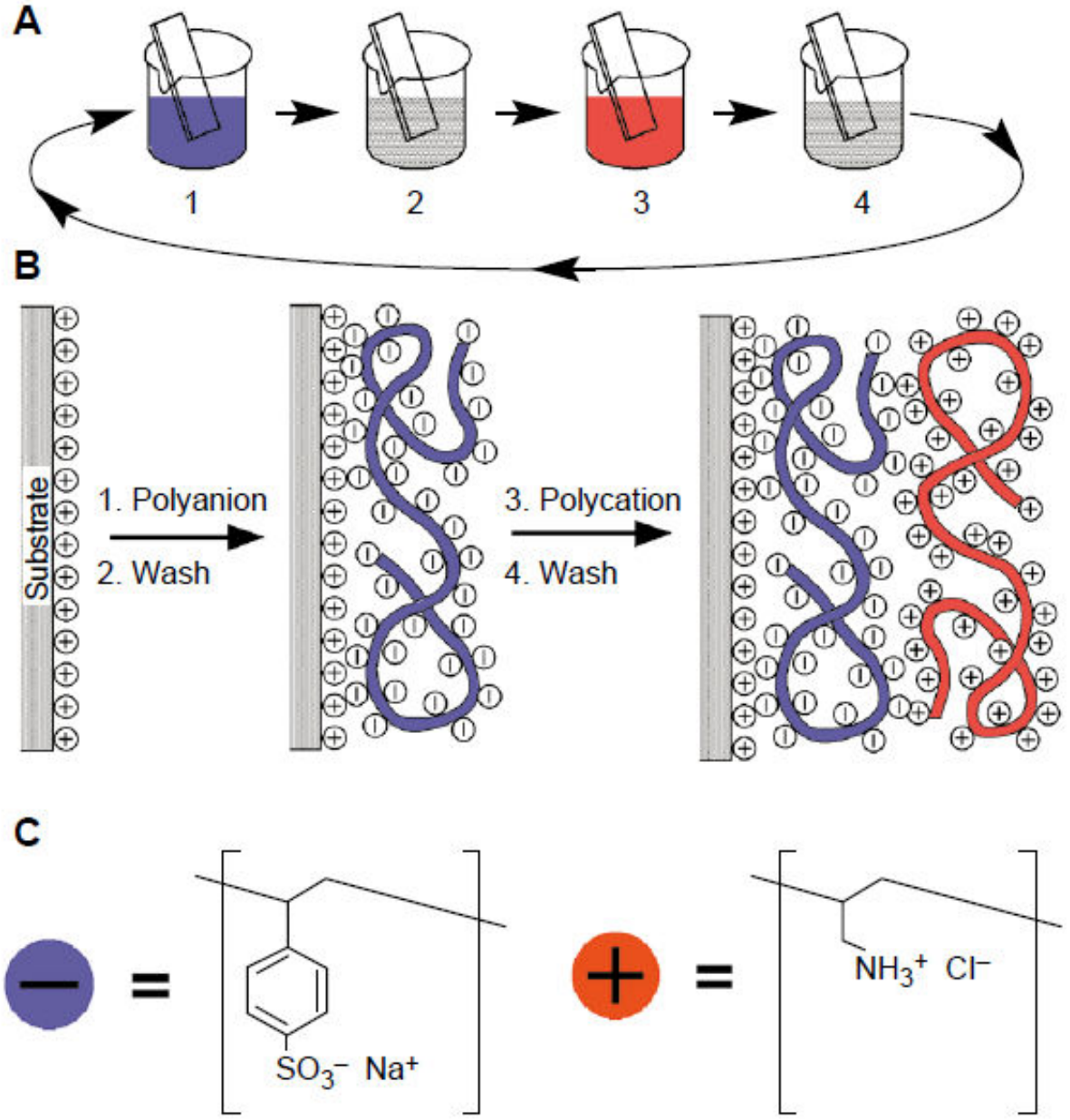

Fig. 33. Original scheme of the LbL deposition method [432].

Soon it was shown that similar strategy can be successfully applied not only for polyelectrolytes but also for a great variety of different systems such as polymeric nanocrystals, nanoparticles, dendrimers, proteins, enzymes, DNA, cell membranes and viruses [436].

LbL thin films recently find application in electrode modification [436]. There are many papers on electrochromic compounds incorporated in the LbL structures. The good example is preparation of phthalocyanine/chitosan composite film [437]. The film formation was monitored wit UV-VIS spectroscopy. Electrodes obtained with particular metalphtalocyanines were shown to be suitable tools for dopamine detection in the presence of ascorbic acid [437]. Another interesting use of LbL method is nanoparticles deposition. AuNPs were deposited alternately with 1,4-benzenedimethanethiol self assembled monolayers. Such system shows electrocatalytic properties towards oxygen reduction [438]. Not only free nanoparticles are used for LbL electrodes modification. An interesting class of compounds called dendrimers is used for nanoparticles immobilization. AuNPs embedded in sixth-generation polyamidoamine has been deposited layer by layer with myoglobin. Above mentioned electrode was discovered to efficiently catalyze hydrogen peroxide reduction reaction [439]. Generally LbL approach seems to be ideal technique for biomolecules immobilization. Biologically active compounds are usually sensitive to harsh processing conditions. LbL deposition can be performed in relatively mild conditions, which makes the technique suitable for enzymes and other biomolecules immobilization. The good example of LbL enzyme immobilization is the work by Wang and coworkers [440]. In the above mentioned paper gold electrode modified with polycationic redox polymer and negatively charged enzyme: glucose oxidase (GOx) has been described. In the same paper, one can find description of the influence of carbon nanotubes on the sensor response. Nanotubes were also deposited in LbL method. Another interesting paper on the similar topic is one where the GOx were deposited LbL with ferrocene-derivatized poly(allylamine) redox polymer [441]. LbL enzyme modified electrode was also shown to be a suitable base for one-compartment biofuell cell construction [442].

Usually in LbL systems at least one of the components is non particulate material such as polymer. However there are some examples in literature where particles of the opposite charges have been immobilized on the surface in the absence of any additional binder [443-448] Moreover, only recently such a procedure involving conducting and insulating nanoparticles was applied for film electrode preparation [449].

In this thesis the application of LbL method to carbon-silicate and carbon-gold composite electrodes preparation is described. The successful enzyme immobilization on these supports is also reported.

4. Goal

The goal of this thesis was to prepare and investigate electrochemical properties of the electrodes modified with imidazolium functionalized materials obtained from ILs. Two main strategies of IL covalent bonding have been applied.

The electrodes modified with IL covalently bonded to the sol-gel processed silicate material were prepared and investigated. This system have been chosen, because of the relatively easy film formation on the electrode surface and the possibility to tune its properties by changing the processing conditions. Silicate materials with confined IL were investigated as the thin films and as submicrometer particles immobilized at the electrode surface. Another part of the thesis is devoted to gold electrodes modified with thiol moiety bearing IL. IL was immobilized on planar gold electrodes and used as an AuNPs stabilizing agent. Finally the electrodes prepared by LbL method from IL modified silicate particles and functionalized CNPs as well as IL stabilized AuNPs and functionalized CNPs were investigated.

The general aim of this thesis was to develop further the area of covalently bonded IL modified electrodes.

Experimental Part

Several physicochemical techniques have been used to investigate electrodes and materials prepared during this research. Thin films have been studied with infrared spectroscopy (IR) and optical profilometry. Silicate and hybrid nanoparticles have been investigated with gas porosimetry. These materials and modified electrodes have been observed with SEM and TEM. The main, most broadly used techniques in the research were electroanalytical methods such as CV, CA and DPV. The main principles of these above mentioned techniques will be briefly summarized below.

5. Techniques

5.1. Infrared spectroscopy

Spectroscopy is based on the interactions between the matter and the electromagnetic radiation. Its root is a quantum chemistry, and its fundamental statement that the energy can only be emitted or absorbed in the specific portions called quanta of energy.

Electromagnetic radiation can be described in two ways: either as an electromagnetic wave propagating in space and time or as a stream of photons. The former is characterized by two related parameters: wavelength λ and frequency ν:

$$\lambda = \frac{c}{\nu} \tag{1}$$

where c – speed of light in vacuum ($c = 3 \cdot 10^8$ m s^{-1}).

Photons have no rest mass. However, when in motion they have a particular energy which can be calculated from Planck equation:

$$E = h\nu \tag{2}$$

where E – energy, ν – frequency and h – Planck constant ($h = 6.626 \cdot 10^{-34}$ J s). This equation combines together the wave-like and particle-like nature of electromagnetic radiation.

IR spectroscopy is the technique in which the interactions of infrared region ($0.8 \leq \lambda \leq 1000$ μm) radiation with molecules are investigated. When the molecule absorbs a quantum of radiation from this range it changes its vibrational level. When the molecule is changing its vibrational level to the lower one, it emits a quantum of IR radiation. A particular vibration is related to the particular wavelength. Analyzing the IR spectrum which is plot of the absorbance or emittance as a function of wavelength, one can get an idea what vibrations are present in the molecule. The IR spectrum is sometimes called a fingerprint of the molecule, because its shape is characteristic for a given compound and is very useful in its

identification. Therefore IR spectroscopy is the most widely exploited in organic chemistry. Together with nuclear magnetic resonance NMR it is the most important technique which allows one to determine the molecular structure of the compound. However, IR spectroscopy can be also a powerful tool in the inorganic compounds analysis.

The reflectance IR technique allows to study composition of surface functional groups and thin films [450]. The IR radiation is directed on the sample under the certain angle of incidence which is dependant on the sample thickness. The measured reflected radiation bears information about surface or thin film composition. In this work IR spectroscopy was used for silicate gel film formation monitoring.

5.2. Optical profilometry

Optical profilometry is a non contact method which allows to get information about the surface topography and roughness. Its principles are based on the interferential properties of light waves. The light is divided into two beams. One is reflected by the inner mirror and another one is directed to the specimen surface. The beam reflected from the investigated surface interferes with the internally reflected beam producing the interference pattern (Fig. 34). It is than recorded with a CCD camera and after processing is used to build the 3D surface profile [451].

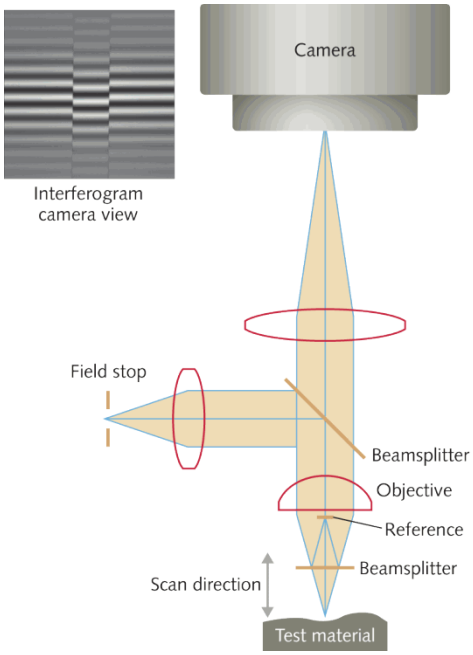

Fig. 34. Optical profilometer scheme [451].

The optical profilometer have been utilized in the research described in this thesis to measure the IL modified silicate film thickness and to get information about film surface morphology.

5.3. Gas porosimetry

Pores volume and their size distribution in the material have a substantial influence on the materials properties and potential applications. The rough idea on the material porosity one can get from images obtained by microscopic techniques such as: optical microscopy, scanning electron microscopy, transmission electron microscopy, atomic force microscopy etc. However, microscopic techniques have several limitations. First of all, it is impossible to visualize pores smaller than the resolution of the method. Another problem is to get any information about the pores which are hidden below the material surface. Porosimetry is an efficient tool to bypass above-mentioned limitation.

Mercury and gas porosimetry are two main types of this technique. In this work nitrogen adsorption porosimetry was used. To perform the porosimetric experiment the sample has to be degassed to remove the adsorbed gas from the sample surface. Usually it's done under the vacuum in the increased temperature. Then the nitrogen is introduced to the chamber and the adsorption isotherm is recorded. The adsorption process can be described with different models. The popular and well working model is Brunauer, Emmett, Teller (BET) isotherm [452]. (3)

$$v = \frac{v_m c P}{(P_0 - P)\{1 + (c-1)\frac{P}{P_0}\}} \tag{3}$$

where v – adsorbed gas volume, v_m – maximal volume of adsorbed gas with complete surface coverage, P – equilibrium pressure, P_0 – saturation pressure.

$$c = \exp(\frac{-(\Delta H_{a,1} - \Delta H_k)}{kT}) \tag{4}$$

where $\Delta H_{a,1}$ – heat of adsorption in the first layer, ΔH_k – heat of condensation, k – Boltzman factor, T – absolute temperature.

BET isotherm is the root of porous materials structural analysis. Analyzing the amount of adsorbed nitrogen as the function of relative pressure one can determine the specific surface, volume and pore's diameters for various porous materials [452]. Adsorption on the porous materials is quite complicated process. In the first stage the smallest pores are filled with gas and the condensation takes place. Next gas starts to adsorb on the surface of bigger pores. When the surface becomes completely covered multilayers start to form. The last stage is when the bigger pores are filled completely and the gas condenses inside (Fig. 35).

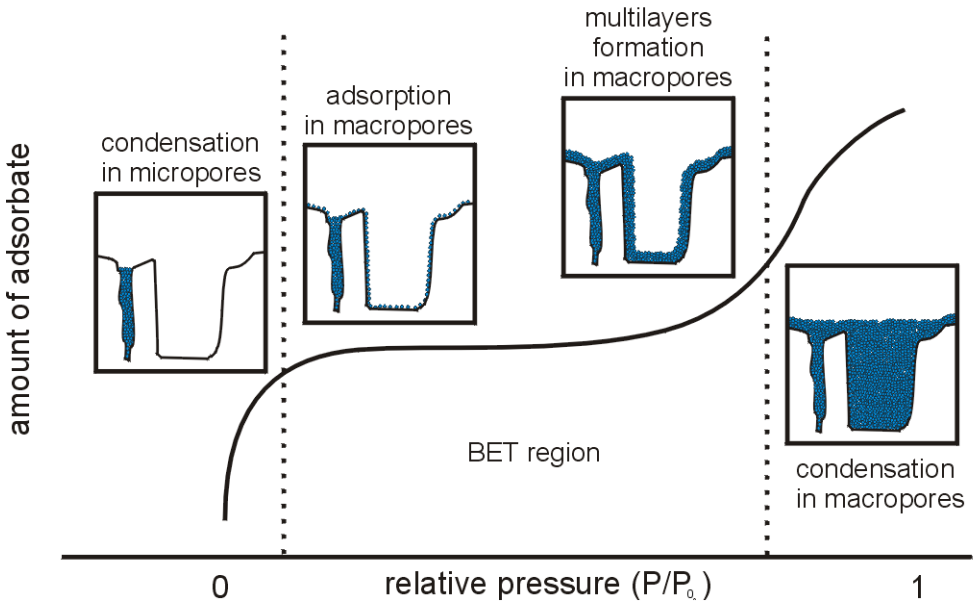

Fig. 35. Adsorption on porous material.(Adapted from [452]).

This step-by-step mechanism is related to the capillary condensation phenomenon. The vapor pressure above the concave surface is lower than above the flat one. This phenomenon is described by Kelvin equation (5).

$$\ln\frac{P}{P_0} = -\frac{2\sigma V}{rRT}\cos\Theta \qquad (5)$$

where V – molar volume of the liquid, σ – surface tension, r – capillary radius, Θ – contact angle [452].

The gas porosimetry was used in the research described in this thesis to determine the pore size distribution and the specific surface area of the IL modified silicate submicroparticles. The specific surface area was determined using BET model and the pore size distribution was determined using Dubinin-Astakhov equation [453].

5.4. Scanning electron microscopy

Scanning electron microscopy became a popular microscopic technique in the modern science. Nowadays its is hard to find a material science paper without SEM image.

SEM allows to obtain much higher magnification than optical techniques. The main difference between SEM and optical methods is the way how one gets a picture. In this method electron beam is equivalent of visible light in optical microscopy. Electrons are generated on thermionic, Schottky or field emission cathode. Next, they are accelerated in the electric field. The acceleration voltage can vary from $0.1 \cdot 10^3$ V to $50 \cdot 10^3$ V [454]. Accelerated

electrons beam is focused by the system of electromagnetic lenses. A system of coils allows operator to scan the beam across the sample (Fig. 36).

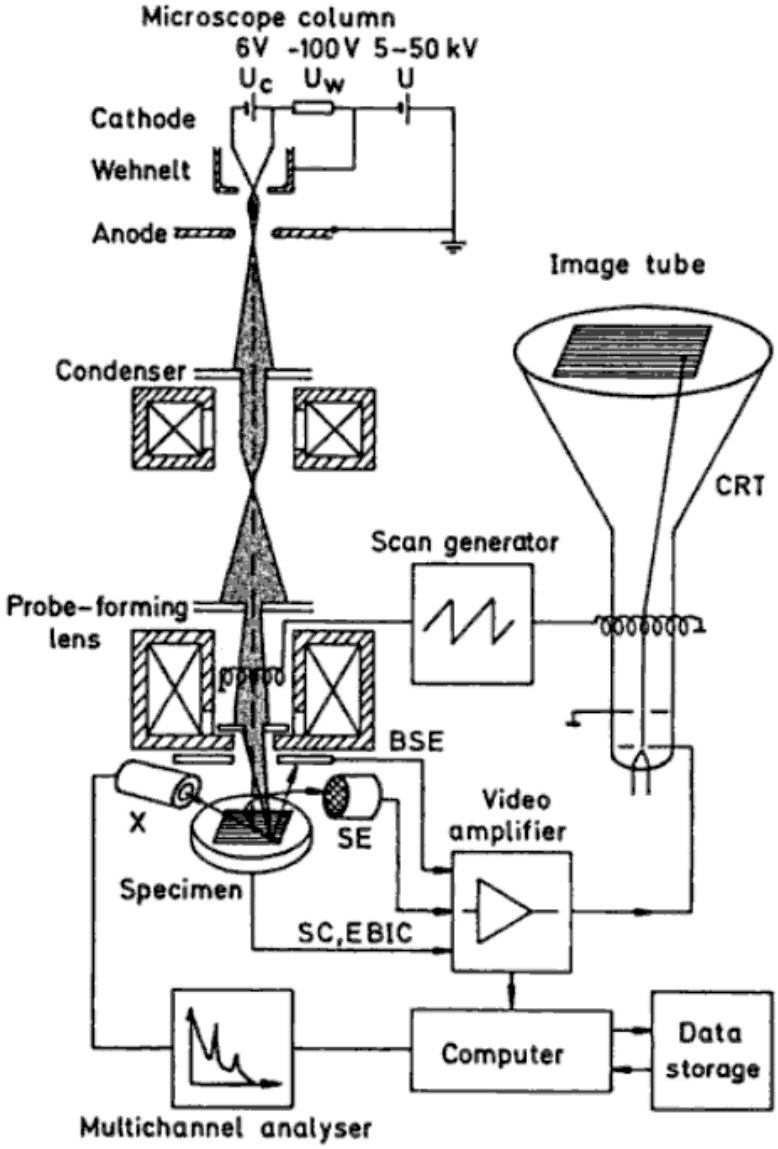

Fig. 36. "Principle of scanning electron microscope (BSE = backscattered electrons, SE = secondary electrons, SC = specimen current, EBIC = electron-beam-induced current, X = X rays, CRT – cathode-ray tube)" [454]

When electron hit the sample several phenomena ca occur. Electron can be backscattered without the energy loss, can be absorbed by the sample what causes the emission of low energy (< 50 eV) secondary electron and X rays. Electron can be also absorbed by the sample with emission of light. The latter phenomenon is called cathodoluminescence. The beam of electrons can also cause the electric current flow in the sample. Although all of the above-mentioned effects can be potentially used to create the picture of the sample, usually the secondary electrons detector is used.

Secondary electrons are selectively attracted to the grid which posses the slightly (50 V) more positive potential than the sample. Behind the grid there is a disc made of scintillator covered with the thin layer of aluminum. Electron pass through the grid and hit the disc causing the light emission. The light is transported by optical fiber to the photomultiplier where the light is transferred into the voltage. Electrons that comes from the small spot on the sample surface produce the particular voltage. It is then visualized at the screen as the spot of specific brightness. The final picture is built with single pixels one by one.

There are no lenses responsible for magnification in SEM. The magnification effect is produced due to the differences between the scanned surface and the surface of the screen. The date collected for the relatively small scanned area, are later presented as a pixels of relatively high surface area. The smaller surface is scanned the greater the magnification is.

The SEM have been widely used during the research described in this thesis to investigate the new materials and electrodes morphology.

5.5. Transmission electron microscopy

Transmission electron microscopy is the microscopic technique where electrons transmitted through the sample are used to create the sample image. Electrons are generated and focused on the sample in the similar way like in SEM. After hitting the sample some of them are transmitted through it and can be detected on the fluorescent screen below the sample (Fig. 37).

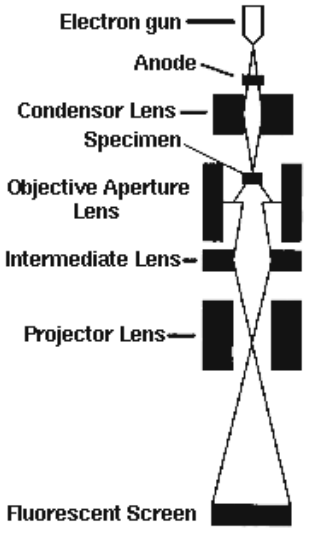

Fig. 37. TEM apparatus scheme [455].

The biggest advantage of TEM is very high resolution. It was demonstrated that it is possible to obtain resolution less than 50 pm with the most sophisticated devices [456]. The main drawback is a complicated sample preparation. The sample have to be no thicker than ca. 200

nm. If the original sample is not thin enough it is necessary to cut it. Unfortunately, during this procedure the original sample structure can be destroyed.

Despite above-mentioned drawbacks TEM is a powerful device for new materials characterization. It is particularly suitable for thin films, powders and nanoobjects characterization. In these cases sample preparation is substantially simplified and the results can give one a lot of information about the sample.

In this work TEM was used to characterize the electrogenerated thin film. In particular this was done to observe its organized mesoporous structure.

5.6. Contact angle measurement

Angle of contact is "the angle between the surface of a liquid and the surface of a partially submerged object or of the container at the line of contact. Also known as contact angle." [457] (Fig. 38).

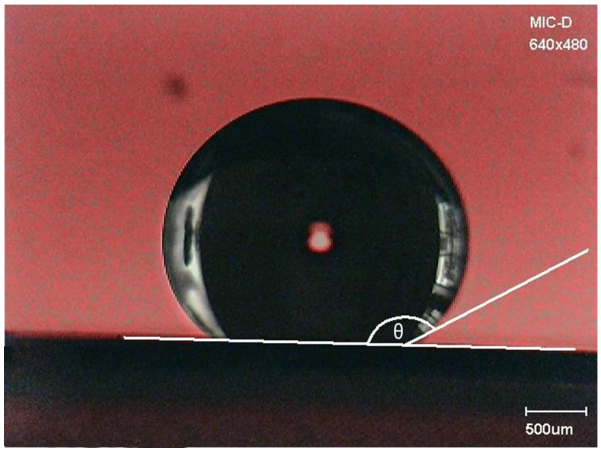

Fig. 38. Contact angle (θ).

Measuring the contact angle of water droplet on the solid surface in air can give us important information about the surface properties. If the water droplet is put on the hydrophilic surface the contact angle is close to 0° because water is strongly attracted to the hydrophilic surfaces. Generally for hydrophilic surfaces the contact angle is smaller than 90°. If the surface is hydrophobic the contact angle is higher than 90° up to 150° for super hydrophobic surfaces.

In experiments described in this thesis the contact angle was measured with the simple homemade device. The source of light, table and microscope have been fixed to the optical bench. In order to perform the experiment the sample is placed on the table. Then a droplet of water is casted on the surface. The droplet is lighted from the back and the photo with optical microscopy is taken. Then the contact angle is measured with simple geometric method.

5.7. Cyclic voltammetry

Cyclic voltammetry is one of the most popular electroanalytical techniques. Although it is sometimes difficult to interpret, the result of the measurement (cyclic voltammogram) usually provides a lot of information about redox process thermodynamics, kinetics and mechanism. The method is also suitable for investigating the new electrode materials.

CV is an example of potential sweep technique. The potential of working electrode is varied linearly with time. After reaching the particular potential E_λ the direction of potential changes is reversed. (Fig. 39a) During the potential sweeping the current is recorded (Fig. 39b). Lets consider the case where the reduced form of the redox active species (Red) is present at the solution. When the potential increases Red starts to be oxidized. The electron is transferred from Red to the electrode and the oxidized form of redox active species (Ox) forms. The higher the potential is, the faster the process goes and the higher is the oxidation current. The current starts to decrease when all Red from the electrode close proximity are already oxidized.

From the first Fick's law (6) one knows that the mass flux is proportional to the gradient of concentration.

$$J = -D\frac{dc}{dx} \tag{6}$$

J – flux, D – diffusion coefficient, c – concentration, x – distance.

When the Red depleted layer is growing, the concentration gradient decreases. This means that the transport of electroactive species to the electrode surface becomes slower. The slower the transport, the lower the current and the anodic peak forms.

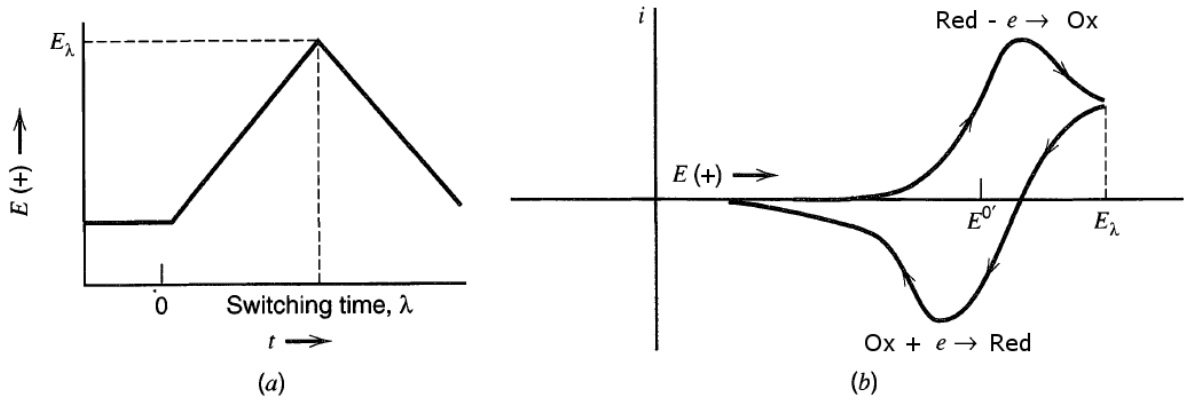

Fig. 39. (a) Cyclic potential sweep. (b) Resulting cyclic voltammogram. (Figure modified to match up IUPAC recommendations) [458].

Then the potential changes are turned back. When it reaches the particular value the reduction process is taking place. Ox produced in the first step gets an electron from the electrode and becomes Red again. The lower the potential, the faster the process until the transport limited conditions are reached again. Then cathodic peak forms.

In this work CV was widely used for studying ions accumulation process, electrocatalysis and bioelectrocatalysis.

5.8. Chronoamperometry

Chronoamperometry is one of the potential step methods. In this work single potential step chronoamperometry have been used. First the potential E_1 where no faradaic process occurs is applied to the working electrode (Fig. 40a) so no faradaic current is recorded. Next the potential is rapidly changed to the value E_2 where faradaic process occurs. The current is recorded (Fig. 40c). During the faradaic process the concentration of substrate in the proximity of the electrode is decreasing. The diffusion layer is growing thicker and thicker with time. It means that the concentration profile's slope is decreasing (Fig. 40c). From the Fick's law (6) we know that the smaller concentration gradient the lower flux is. When the flux decreases the faradaic current also decreases.

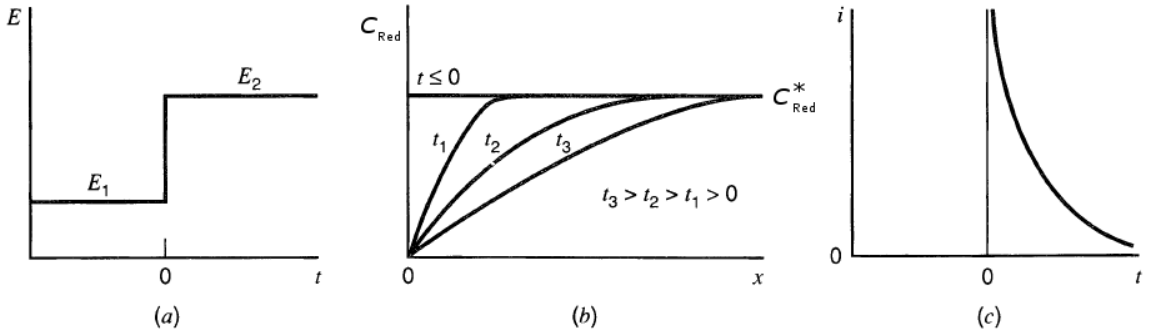

Fig. 40. (a) Waveform for CA experiment. (b) Concentration profiles for various times into the CA experiment. (c) Current vs. time in CA experiment [458]*. (Figure modified to match up IUPAC recommendations)*

The current drop in CA experiment is described by Cottrell equation: [458]

$$i(t) = \frac{nFAD^{1/2}C^*}{\pi^{1/2}t^{1/2}} \qquad (7)$$

where: n – number of electrons transferred, F – Faraday's constant, A – electrode area, D – diffusion coefficient, C^* - redox probe concentration in bulk, t – time.

In this work CA method have been used to monitor the changes in bioelectrocathalytic activity of the enzyme modified electrode.

5.9. Differential pulse voltammetry

Differential pulse voltammetry belongs to the family of the pulse voltammetry methods. The advantage of this method is the possibility of capacitive current elimination. Also DPV allows one to determine the redox potential of the redox probe much more precisely than CV and for this reason it was used in this work.

In DPV the potential pulses are applied to the working electrode. The amplitude and the lifetime of the pulses are constant, but the base potential changes from pulse to pulse. (Fig. 41a) In DVP two current samples are taken for each data point. First the current just before the pulse is measured $i(\tau')$. Next current sample $i(\tau)$ is taken late in the pulse (Fig. 41b).

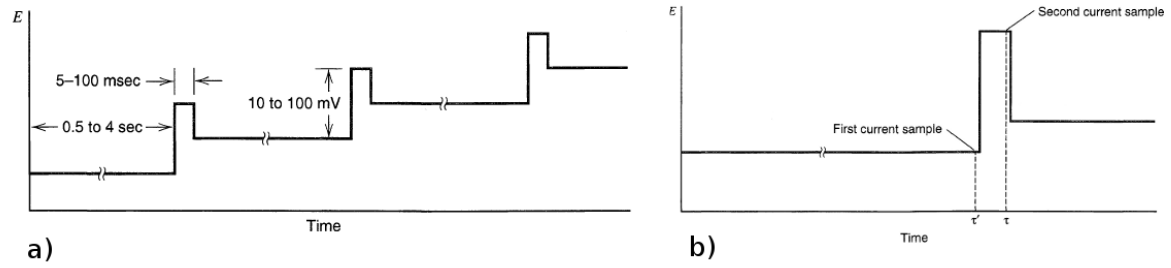

Fig. 41. (a) Potential program scheme in DPV.(b) Currents sampling scheme in DPV [458].

The difference between $i(\tau)$ and $i(\tau')$ is calculated for every data point (8).

$$\delta i = i(\tau) - i(\tau') \tag{8}$$

where: δi – current difference

Next, the current differences are plotted as a function of base potential what results in differential pulse voltammogram (Fig. 42).

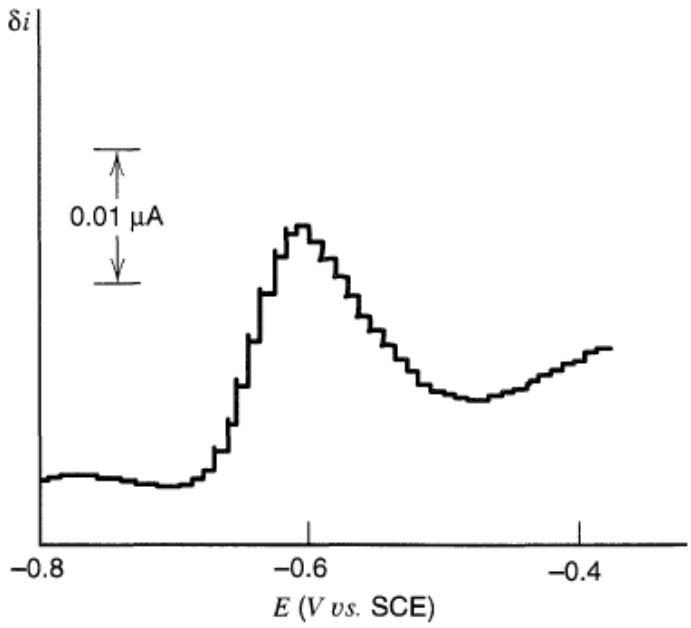

Fig. 42. Typical example of differential pulse voltammogram [458]. (Figure modified to match up IUPAC recommendations)

The height of the peak in DPV is given by the equation: [458]

$$(\delta i)_{\max} = \frac{nFAD^{1/2}C^{*}}{\pi^{1/2}(\tau-\tau')^{1/2}} \cdot \left(\frac{1-\sigma}{1+\sigma}\right) \tag{9}$$

where: $\sigma = \exp\left(\frac{nF}{RT}\frac{\Delta E}{2}\right)$

where: ΔE – pulse height

6. Experimental conditions and procedures

6.1. Chemical reagents and materials

- Ferrocenedimethanol (99%), $NaClO_4$, NaSCN, methanol, ethanol, hexane, $(NH_4)_2ABTS$, CH_3CN, CTAB, FA, hexadecane, NADH, TEOS, TMOS, PAH, $TBAPF_6$ – Aldrich
- tBuFc (99%), K_3IrCl_6 – ABCR
- KNO_3, KCl, KOH, KBr, NaF, $K_4Fe(CN)_6$, $K_3Fe(CN)_6$, H_2SO_4, HNO_3, HCl, H_3PO_4, Na_2HPO_4, NaCl, $NaNO_3$, $KClO_4$ – POCh
- KPF_6 – Merck
- SDS, DMFc, - Fluka
- Citric acid, H_2O_2, NaOH, NH_3 – Chempur
- $Ru(NH_3)_6Cl_3$ – Strem Chemicals, Inc.
- BOx – Amano Enzymes
- Laccase (Cerrena unicolor) – separated and purified by prof. dr hab. Jerzy Rogalski
- P(TMOS)MIMNTF2 – synthesized by dr Cecile Rizzi
- MIUSHCl – sythetized with a help of dr Maciej Paszewski

All chemicals were used as received. Water was purified by an ELIX system (Millipore).

- Tin-doped indium oxide nanoparticles as water suspension – ITO_{part} (d = 21 nm) – NanoTek
- CNPs with phenylsulfonic acid surface functionalities (ca. 7.8 nm mean diameter) (Emperor 2000) - Cabot Corporation (Dukinfield, UK).
- Graphite powder UPC-1-M (ca. 1 μm mean diameter) – Graphite Pold
- 1-(11-mercaptoundecyl)-3-methyl-imidazolium chloride modified gold nanoparticles ((+)AuNPs -) and sodium 11-mercapto-1-undecane sulfonate modified gold nanoparticles ((-)AuNPs) – synthesized by dr Maciej Paszewski

Reference electrodes: platinum wire d = (1 mm), $Ag|AgCl|KCl_{sat.}$ n-Lab.

Counter electrode: platinum wire (d = 0.5 mm)

Working electrodes: gold disc (d = 1.6 mm) in Kel-F, n-Lab; ITO coated glass (d = 5.0 mm, resistivity 30 Ohm per square), Image Optics Ltd.

Electrochemical experiments have been performed in the standard three electrode cell except for electroassisted film generation experiments where a dedicated cell have been used (Fig. 43).

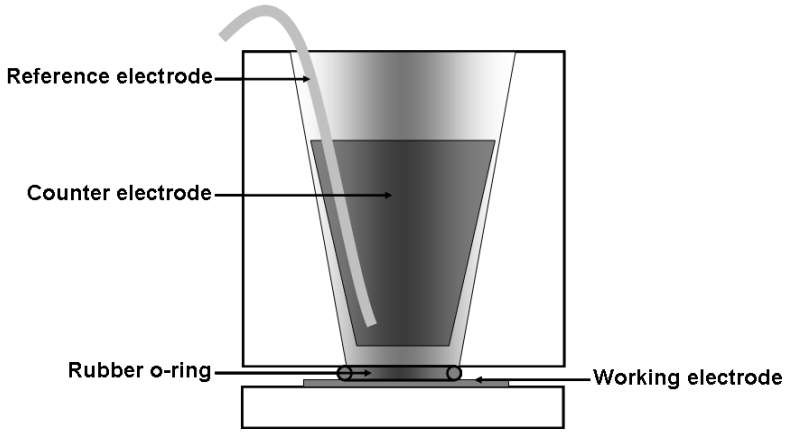

Fig. 43. Scheme of the cell used for electroassisted film generation.

6.2. Instrumentation

- FTIR and FTIRRAS spectra were measured with FTIR 8400 Shimadzu spectrometer. FTIR spectrum of the liquid gel precursor was recorded as thin liquid film between KRS-5 plates. The reflectance spectrum of ionic liquid modified silicate film was obtained using the variable angle reflectance accessory model 500 from SpectraTech Inc at 80° incidence angle by dr Barbara Pałys.
- SEM images were obtained with a JEOL JSM6310 or with a Leo 1530 field emission gun scanning electron microscope system by dr Adam Presz
- TEM images were obtained with a Philips CM20 microscope operating at 200 keV
- Profilometry was performed with WYKO NT100 optical profiler by dr Martin Jönsson-Niedziółka
- Dip-coating was done with a KSV dip-coating unit (KSVInstruments Ltd.).
- Surface area and porosity of the particles were measured with an ASAP2020 V3.01 H analyzer (Micromeritics) by dr Janusz Malinowski.
- CV, CA and DPV experiments were done with an Autolab (Eco Chemie) electrochemical system in a conventional three-electrode cell with dedicated software.
- Furnace for ITO electrode cleaning Elite tube furnace, model TSH 12/65/550
- Optical microscopy pictures were obtained with Nikon Eclipse LV150 optical microscope.

Results and discussion

7. Ionic liquid appended sol-gel film electrodes

This chapter concerns mainly the sol-gel processed films modified electrodes. The film obtained with IL sol-gel precursor (Fig. 44) will be further called silicate confined IL film (SCILF). The electrodes covered with the films of various composition and thickness have been prepared and investigated. Various redox probes have been used to test the electrodes properties. The enzyme - laccase has been also immobilized on some of the electrodes and the oxygen reduction reaction has been investigated. Some electrodes have been premodified with the ITO nanoparticles by dipcoating.

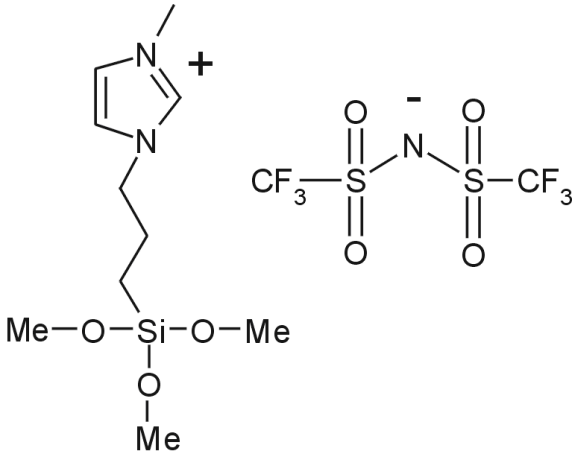

Fig. 44. 1-methyl-3-(3-trimethoxysilylpropyl)imidazolium bis(trifluoromethyl sulfonyl)imide (P(TMOS)MIMNTF2) formula.

7.1. Ionic liquid appended sol-gel film electrodes - preparation

The ITO electrodes were cleaned with ethanol, deionized water and hot redistilled water subsequently. In some experiments ITO was additionally heat treated (30 min in 500°C) to remove the remaining contaminations. The electrode surface was defined by masking off an area of 0.2 cm^2 with a scotch tape. The electric contact was assured by using a piece of copper tape.

The sol stock A solution was prepared by mixing 0.3209g of P(TMOS)MIMNTF2, 196 µl of TMOS and 370 µl of FA. The stock B solution was prepared by mixing 0.3209g of P(TMOS)MIMNTF2, 98 µl of TMOS and 370 µl of FA. The stock C solution was prepared by mixing 0.4806g of P(TMOS)MIMNTF2, 49 µl of TMOS and 370 µl of FA. These mixtures were sonicated for 10 min. Then the stock sol was diluted with methanol at 1:10, 1:100 or 1:1000 volume ratio.

For electrode modification, 5 µl of diluted stock sol was deposited onto the electrode surface. The modified electrodes were left for drying for at least 12 h at room temperature to let the silicate film form (Fig. 45).

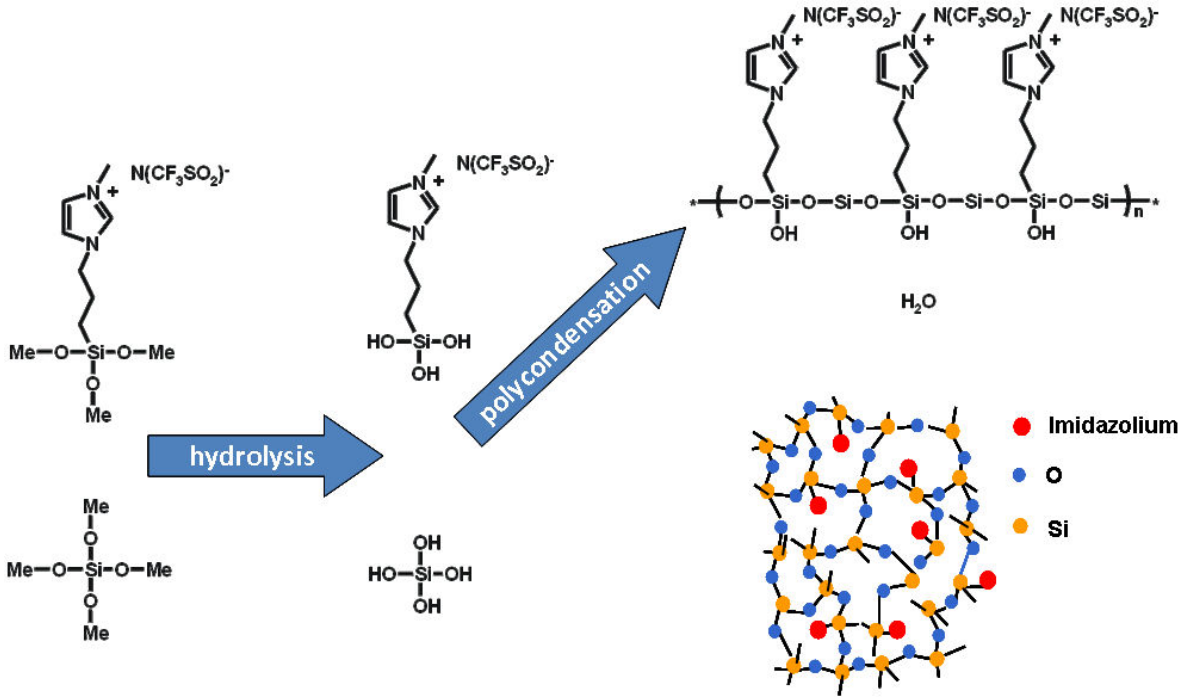

Fig. 45. Ionic liquid appended sol-gel film formation scheme.

The sol-gel modified electrodes have been compared with the electrodes modified with the thin film of liquid P(TMOS)MIMNTF2 (Fig. 44). 0.0428 g P(TMOS)MIMNTF2 in 1 ml of acetonitrile was prepared. For the electrode modification, 5 µl of solution was deposited onto the electrode surface and left for solvent evaporation.

7.2. IR characterization of silicate film

IR spectroscopy has been used to confirm the silicate network formation. The IR transmittance spectra of P(TMOS)MIMNTF2 and TMOS have been compared with the reflectance spectra of the sol-gel film. Such approach has been earlier demonstrated as a suitable method of sol-gel films investigation [459-461].

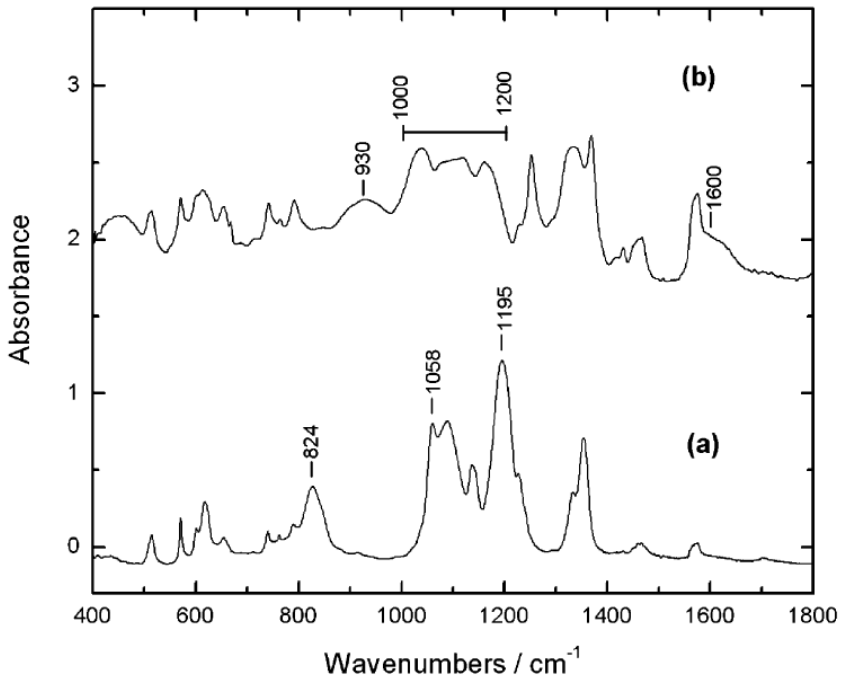

Fig. 46. FTIR spectra of liquid precursors (a) and sol–gel processed film (b).

The bands at 824 cm^{-1} and 1058 cm^{-1} have been assigned to the Si-O-C modes of P(TMOS)MIMNTF2 and TMOS and band at 1195 cm^{-1} originates from $SiOCH_3$. These bands present in the spectrum of liquid precursors (Fig. 46a) have been replaced by Si-O-Si band at 1000-1200 cm^{-1} in the spectrum of sol-gel film. (Fig. 46b). Such behavior clearly indicates the silicate network formation [459-461]. In the film spectrum there is also relatively intense band at 960 cm^{-1}. It has been assigned to the unreacted Si-OH groups. The broad bands observed at 1600 and 3300–3700 cm^{-1} (not shown) originate probably from mixed contributions of Si–OH and water trapped during the sol–gel process [462]. The imidazole mode at 1575 cm^{-1} and S–O stretching modes at 1353 and 1333 cm^{-1} become very intense after the gel formation process indicating strong interaction between the ionic liquid and the gel matrix. Since imidazolium groups are strongly electronegative, they may serve as proton acceptor from Si–OH groups.

7.3. Optical microscopy characterization of the sol-gel film.

The sol-gel film obtained by the deposition of ten times diluted stock sol A on the ITO electrode have been investigated with optical microscope (Fig. 47).

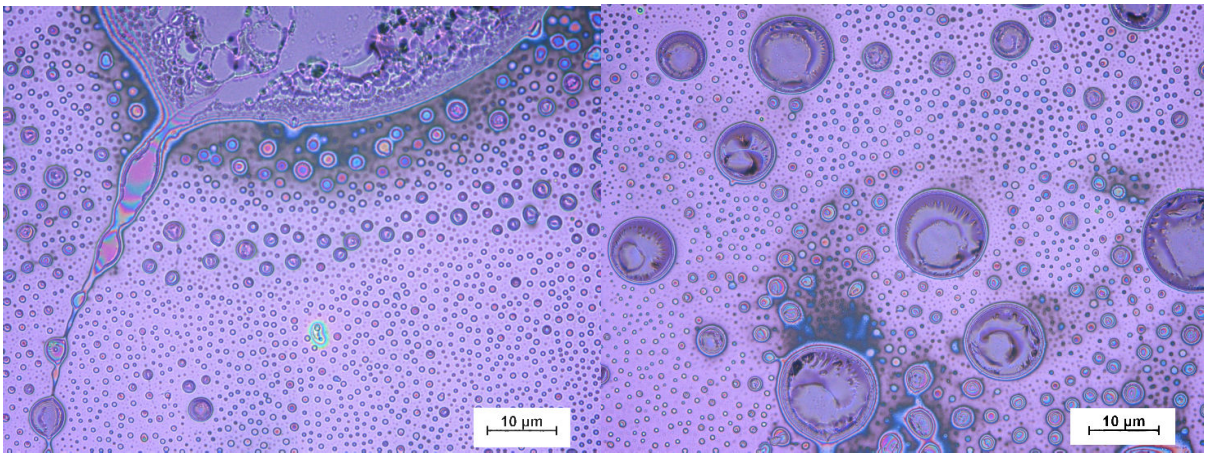

Fig. 47. Pictures of the sol-gel processed film obtained with optical microscope.

Film covers the substrate almost completely, however, it is not homogenous. There are many bubble-like structures on the film surface. Probably the film structure results from the method of film deposition (sol drop deposition).

7.4. SEM of the sol-gel film.

The sol-gel film obtained by the deposition of ten times diluted stock sol A on the ITO electrode have been also investigated with SEM (Fig. 48). The SEM analysis confirmed the structure observed with the optical microscope at smaller scale. There are several cracks and bubbles visible in the film structure.

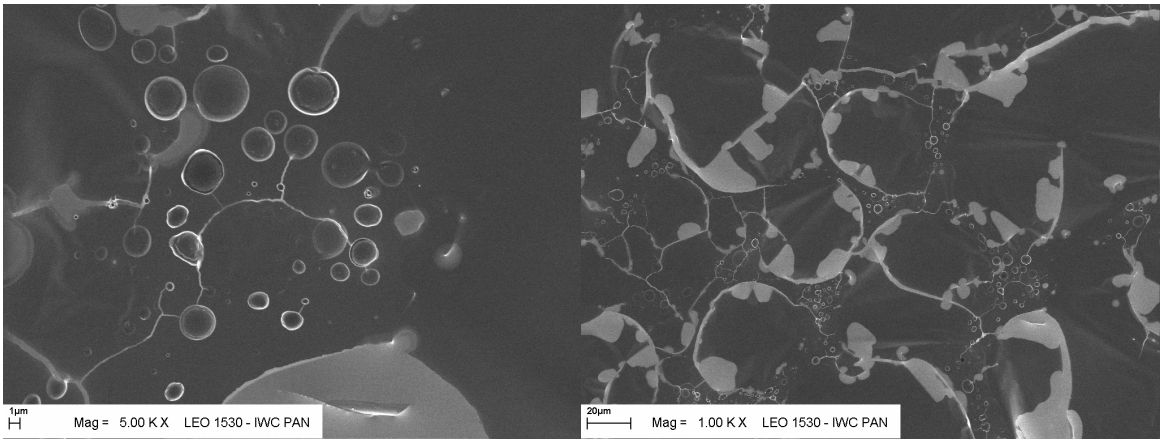

Fig. 48. Pictures of the sol-gel processed film obtained with SEM.

7.5. Optical profilometry of the sol-gel film.

In order to get information about sol-gel film thickness and morphology the optical profilometry experiment has been done. For the thickness measurement the film was scratched with the needle. The cross like shape is well visible at the surface map (Fig. 49a).

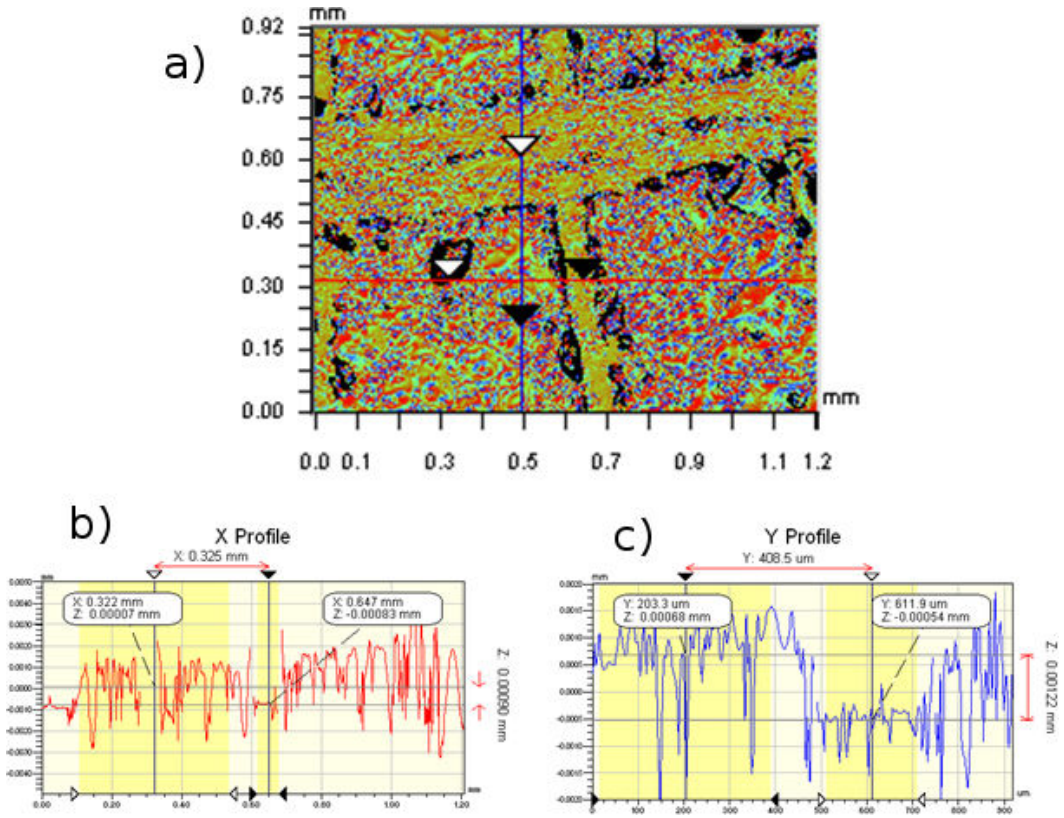

Fig. 49. a) The surface map of the sol-gel film modified electrode. b) Profile along the red line. c) Profile along the blue line.

Two profiles were recorded: one along the red line (Fig. 49b) and another one along the blue line (Fig. 49c). For every profile two average height values have been calculated. One from the film covered part of thr substrate and another one from the surface at the bottom of the scratch. As a result of the above-mentioned values subtraction the film thickness has been obtained. Two values has been calculated: 0.9 μm and 1.22 μm. The significant difference between those two values is the result of the heterogeneous nature of the film confirmed in previous experiments.

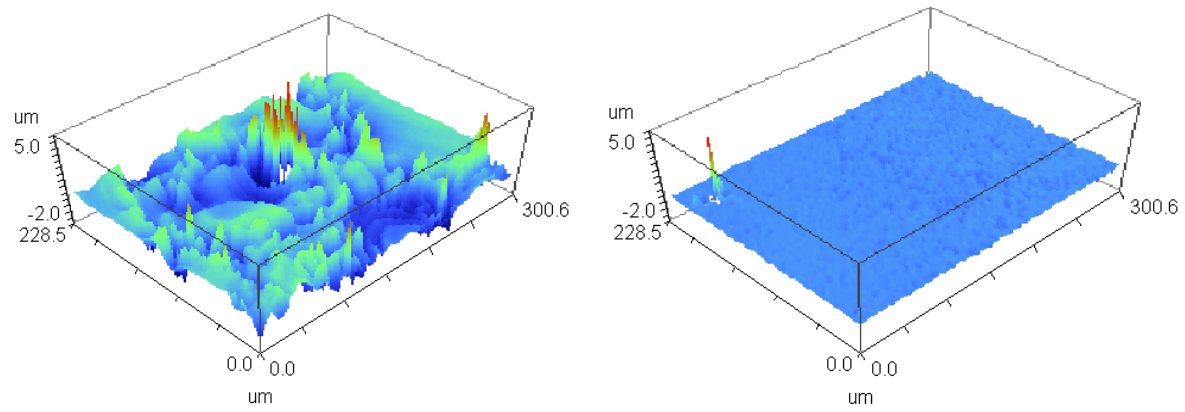

Fig. 50. Surface topography plots obtained with optical profilometry for sol-gel film modified electrode (a) and bare ITO (b).

From the surface topography measurements (Fig. 50) the surface roughness has been calculated (10).[463]

$$R_a = \frac{1}{n}\sum_{i=1}^{n}|Z_i - \overline{Z}| \qquad (10)$$

where: R_a – roughness parameter, n – number of data points, Z_i – height for the i^{th} point, $\overline{Z}$ - average height. The calculated R_a parameters were 762 nm and 70 nm for the sol-gel film and the clean ITO respectively. This result shows that the sol-gel processed film has a very well developed surface. This observation stays in the agreement with SEM and optical microscopy data. In spite of the non conductive character high film roughness can be very useful for electrochemical application. The electrochemical investigation of the film will be described in details in the next chapter.

7.6. Electrochemistry of the sol-gel processed ionic liquid film electrodes.

7.6.1. Voltammetry of the different redox probes

7.6.1.1. Voltammetry in $K_3Fe(CN)_6$ solution.

The electrochemical properties of the sol-gel film modified electrodes have been studied in the presence of various electroactive ions to investigate the interactions between the imidazolium moieties and redox probes of various charges. The first results have been obtained for the electrode immersed into the 0.1 mM $K_3Fe(CN)_6$ solution in aqueous 0.1 M $NaClO_4$ solution have been chosen as supporting electrolyte. The peak shaped voltammogram was observed (Fig. 51a). The faradaic current recorded during the experiments was connected with the following reaction:

$$Fe(CN)_6^{3-} + e^- \leftrightarrow Fe(CN)_6^{4-} \quad (11)$$

Both cathodic and anodic peak current increase have been observed during the experiment. This is because of the ion accumulation process, which starts directly after the modified electrode immersion into the redox probe solution. This is because some fraction of NTf_2^- anions during the accumulation process are replaced with $Fe(CN)_6^{3-}$ anions. The supporting electrolyte anions can also take part in the process [39]. The peak current vs. time dependences almost reach plateau after ca. 0.5 h of the experiment (Fig. 51b).

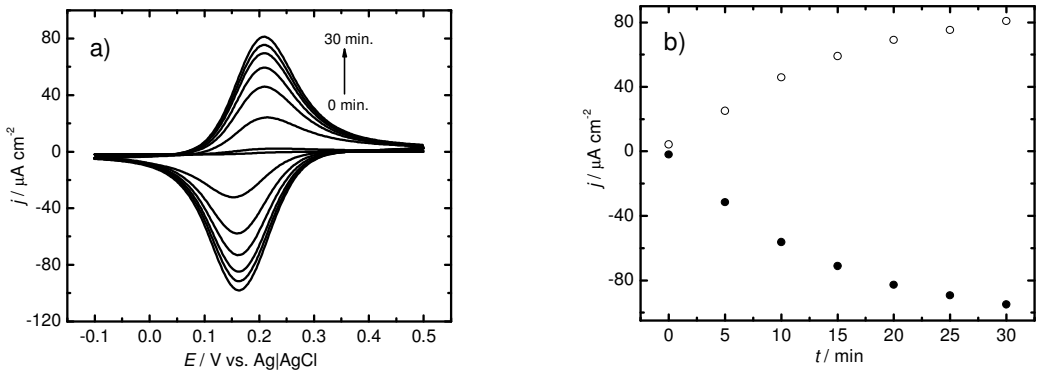

Fig. 51. a) CVs of SCILF modified electrode immersed to 0.1 mM $K_3Fe(CN)_6$, 0.1 M $NaClO_4$. Arrow shows the time changes. b) Anodic (○) and cathodic (●) peak current vs. time plot. v = 10 mV s^{-1}.

To investigate how an accumulation process depends on the amount of imidazolium moieties three types of electrodes has been prepared. The sol-gel films have been obtained from sol of different dilution 1:1000, 1:100 and 1:10 on ITO electrodes according to the previously described procedure.

The electrodes have been immersed into the 0.1 mM solution of $K_3Fe(CN)_6$ and CV experiments have been performed. 0.1 M $NaClO_4$ solution has been used as supporting electrolyte. The cyclic voltammograms have been recorded until the stable voltammogram have been obtained (Fig. 53). After the accumulation process the electrode was flushed with deionized water and immersed into the supporting electrolyte solution.

There is clearly visible relationship between the film thickness and the accumulation properties. The stable voltammogram (after accumulation) obtained for the electrode modified with the thinnest film (1:1000) is hardly distinguishable from the one obtained for the clean ITO (Fig. 52). The medium thickness (1:100) film covered electrode exhibits significantly higher current response in comparison to the clean ITO. The highest current was obtained for

the electrode modified with the thickest film (1:10). The peak currents are about one order of magnitude higher than ones obtained with the clean ITO. Unfortunately the film obtained from sol diluted less than 1:10 was cracking and falling off the electrode in contact with water solution or even just during the drying process. That was the reason why we decided to use the electrode prepared from 1:10 diluted stock solution in further investigations.

The redox potential obtained on film covered electrodes shift towards cathodic potentials indicates the stabilizing properties of the film. $Fe(CN)_6^{3-}$ ion have been stabilized by the film probably because of the stronger electrostatic interactions with imidazolium moieties.

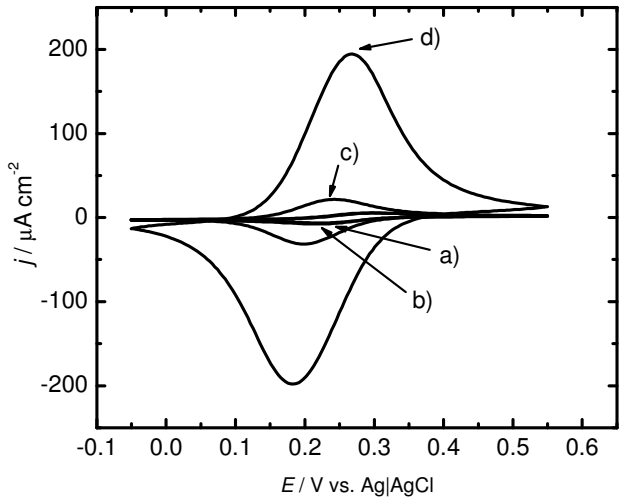

Fig. 52. CVs obtained after accumulation in 0.1 mM $K_3Fe(CN)_6$, 0.1 M NaClO4 for the bare ITO (a), ITO modified with SCILF (1:1000) (b), ITO modified with SCILF (1:100) (c) and ITO modified with SCILF (1:10) (d).

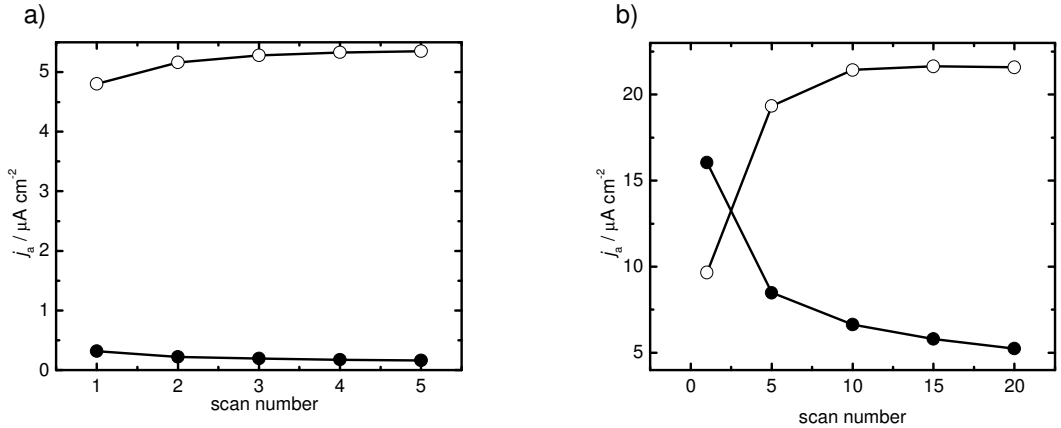

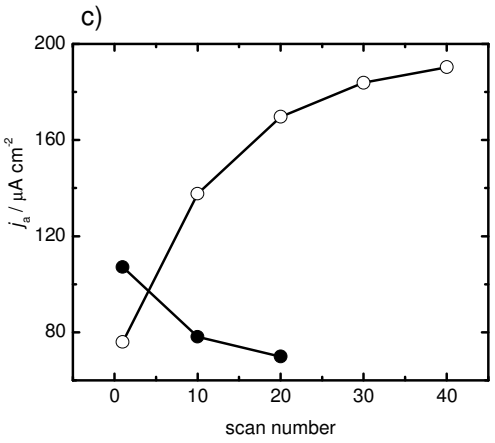

Fig. 53. Anodic peak currents vs. scan number for accumulation (○) and washing out (●) of the $K_3Fe(CN)_6$ from electrode modified with the SCILF obtained from 1:1000 (a), 1:100 b) and 1:10 c) diluted stock sol.

The peak current increases with time because of the anion accumulation (Fig. 53). One can notice that its kinetics is strongly dependent on the film thickness. The thicker the film is the more time is needed to reach the plateau but the plateau peak current is also significantly higher. This is because redox active ions needs more time to diffuse into the thicker film structure, but the ion exchanging capacity of such film is also higher.After the electrode was immersed into the supporting electrolyte solution the current decreases. The electroactive $Fe(CN)_6^{3-}$ or $Fe(CN)_6^{4-}$ anions have been exchanged with ClO_4^- anions from the supporting electrolyte. The kinetics of washing out process is also dependent on the film thickness. Similarly as for accumulation the thicker the film the slower the washing out process.

7.6.1.2. Accumulation of the redox probes of various charges.

To learn more about the accumulation process voltammetry in solution of redox probes of various charges $IrCl_6^{2-}$, $Fe(CN)_6^{3-}$, $Fe(CN)_6^{4-}$ was performed and compared. The sol-gel film modified electrodes have been immersed into the redox probes solutions and the cyclic voltammogram was recorded in every 5 min. One can see that the less negative the redox probe charge the more efficient accumulation process. This dependence is especially clearly visible for cathodic peak currents (Fig. 54).

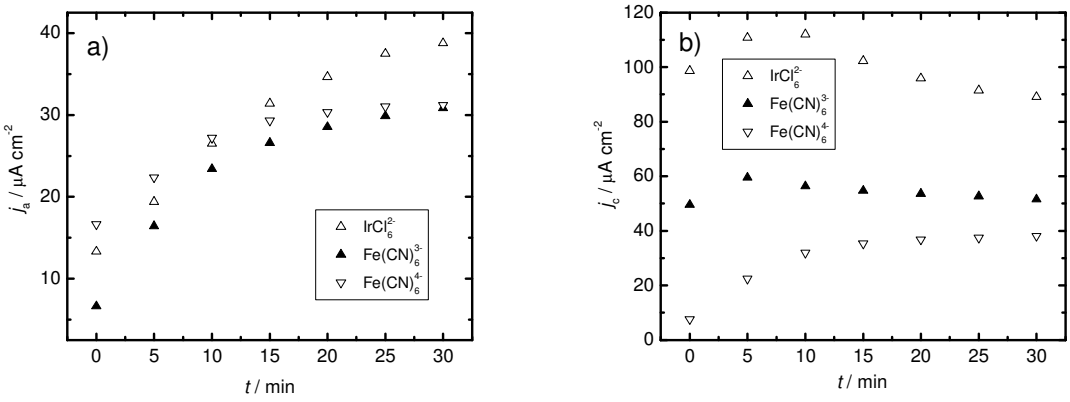

Fig. 54. a) Anodic peak current densities for the SCILF (1:10)modified electrode vs. time for various electroactive anions. b) Cathodic peak current densities for the electrode modified with sol-gel film (1:10) vs. time for various electroactive anions marked on the figure.

The phenomenon mentioned-above can be explained on the basis of electrostatics. The hybrid sol-gel film contains a particular amount of positively charged imidazolium groups. In the initial state all the groups are neutralized by NTf_2^- anions. After electrode immersion into the redox probe solution the certain amount of NTf_2^- anions is exchanged for the electroactive anions. The most efficient accumulation was observed in the case of $IrCl_6^{2-}$ anions. Next was the $Fe(CN)_6^{3-}$ and $Fe(CN)_6^{4-}$.The lower the redox active ion's charge is the more ions is needed to compensate the film charge. Another factor may be that because of the electrostatic interactions the ions of the lower charge can be packed denser than the highly charged ones.

7.6.1.3. The influence of the supporting electrolyte on the accumulation process.

As it was mentioned above not only redox active anions are taking part in the anion exchange. The charge can be compensated by any negatively charged species. The concentration of the supporting electrolyte is at least two orders of magnitude higher than concentration of the redox probe, so the significant influence of the type of supporting electrolyte anions on the accumulation of the redox probe was expected. Therefore voltammetric experiments were performed also in nitrate and chloride salt solutions.

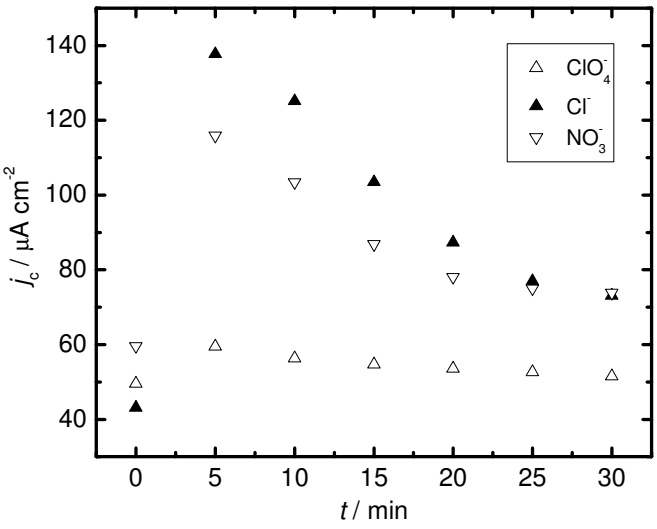

Fig. 55. Cathodic peak current densities for the SCILF (1:10) modified electrodes vs. immersion time for 1 mM $Fe(CN)_6^{3-}$ in various 0.1 M supporting electrolytes (marked on the plot).

Analyzing the plot (Fig. 55) one can see that the $Fe(CN)_6^{3-}$ accumulation process is the most efficient when there are Cl^- anions present in the supporting electrolyte. The anions from supporting electrolyte compete to neutralize positively charged imidazolium groups with $Fe(CN)_6^{3-}$ anions. The higher the supporting electrolyte's affinity to the imidazolium groups the less efficient the $Fe(CN)_6^{3-}$ accumulation. One can conclude that among selected anions this effect is the strongest for Cl^- anions. For weekly hydrated NO_3^- and ClO_4^- these interactions are weaker.

7.6.1.4. Neutral redox probe interactions with the SCILF

It was already demonstrated that the SCILF accumulates negatively charged ions. To learn more about SCILF electrochemical properties the experiment with the neutral redox probe has been performed. 1,1'-ferrocenedimethanol (FDM) have been chosen as a redox probe. The FDM redox reaction can be described with the equation:

$$FDM \leftrightarrow FDM^+ + e^- \qquad (12)$$

The SCILF modified electrode have been immersed into the 1 mM FDM in 0.1 M $NaClO_4$. The cyclic voltammograms have been recorded in every 5 min.

The peak current density obtained in this condition for the SCILF modified electrode was ca. 4 times smaller than one obtained for the clean ITO electrode (Fig. 56). Such behavior was earlier observed for sol-gel processed films on electrodes [459]. It is caused by blocking the electrode surface by silicate film. Furthermore the sigmoidal shape of the voltammograms indicates the spherical diffusion, resulting from the micrometer size defects present in the film. Such electrode covered with imperfect silicate film acts as an array of microelectrodes [464].

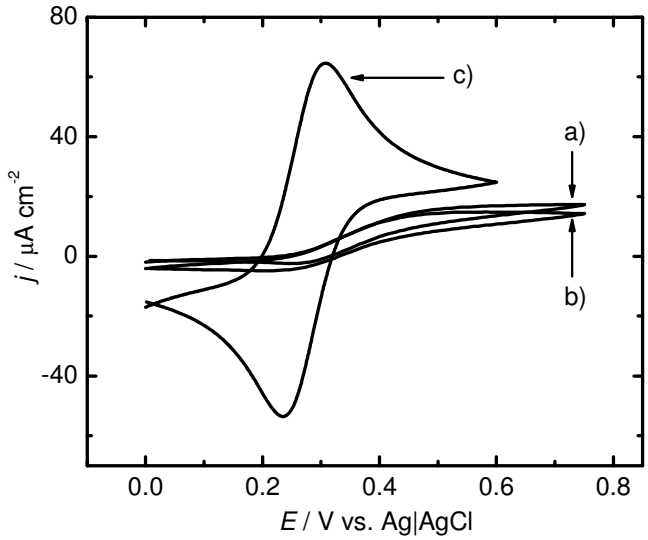

Fig. 56. Cyclic woltammograms obtained for SCILF (1:10) modified electrode immerse into the 1 mM FDM, 0.1 M $NaClO_4$ immediately a) and 30 min b) after immersion. Curve c) was obtained for the bare ITO electrode in the same conditions. v = 10 mV s^{-1}.

No significant change in current vs. time indicates the lack of the FDM accumulation. The redox potential of the FDM/FDM^+ redox couple was shifted on SCILF modified electrode ca. 100 mV towards anodic potentials in comparison to the clean ITO electrode. This indicates that positively charged imidazolium groups hinder the formation of the cation from the neutral molecule (12).

7.6.1.5. Positively charged redox probe interactions with SCILF

The hybrid sol-gel film with imidazolium groups has been also investigated in the presence of the positively charged redox probe $Ru(NH_3)_6^{3+}$.

First the bare ITO electrode has been immersed into the 0.1 mM $Ru(NH_3)_6Cl_3$ in 0.1 M $NaClO_4$ solution and the oxygen has been removed from the system by bubbling argon through the solution for 30 min. A pair of well defined peaks have been observed on CV. This was assigned to the following reaction:

$$Ru(NH_3)_6^{3+} + e^- \leftrightarrow Ru(NH_3)_6^{2+} \quad (13)$$

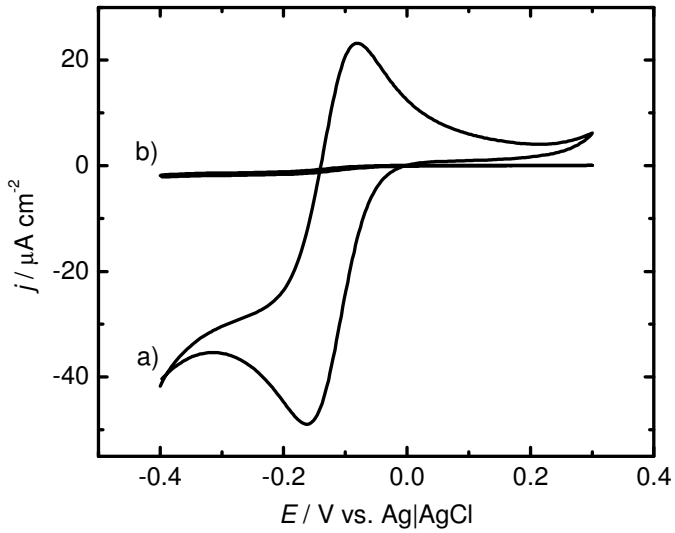

Fig. 57. Cyclic woltammogram recorded in 0.1 mM $Ru(NH_3)_6Cl_3$, 0.1 M $NaClO_4$ for bare ITO a) and SCILF (1:10) modified electrode. v = 10 mV s^{-1}.

With SCILF electrode in the same conditions current peaks were not observed. It means that the electrode reaction was blocked. It was demonstrated in the previous experiments that the sol gel film has a porous structure which is permeable for negatively charged redox probes (Fig. 51). Here both, oxidized and reduced, forms of the redox probe bears the positive charge. The positively charged imidazolium groups may block access of $Ru(NH_3)_6^{3+}$ or $Ru(NH_3)_6^{2+}$ to the ITO surface. The vestigial faradaic current is caused by the imperfect character of the film. The sigmoidal shape of the voltammogram indicates the hemispherical diffusion regime. This indicates that some pores in the film allows the positively charged redox probe to reach the electrode surface.

7.6.1.6. Influence of covalent bonding on IL's accumulation properties.

In the previous chapters it was demonstrated that the covalently bonded ionic liquid has the anion accumulation properties. There is also the electrode surface blocking effect

demonstrated for the neutral and the positively charged redox probe. To understand how strong is the influence of the covalent bonding of the ionic liquid on the ion accumulation properties the next set of experiments with unconfined ionic liquid modified electrode have been performed. 5 μl of 0.0428 g of P(TMOS)MIMNTF2 in 1 ml of acetonitrile was deposited onto the electrode surface and left for volatile solvent evaporation.

Let's consider the negatively charged redox probes first. One can observe little anion accumulation process on the thin P(TMOS)MIMNTF2 liquid film covered electrodes (Fig. 58, Fig. 59, Fig. 60). However the peak currents ware ca. 100 times lower than for the electrodes covered with SCILF in the same conditions. This is because of the strongly damped transport caused by the high viscosity of the ionic liquid. The obtained currents were much lower than ones obtained on the bare ITO. One can also see that the cyclic voltammograms obtained for the electrodes covered with non-bonded ionic liquids are not very well shaped. It can be also connected with the slow transport (Fig. 58ac, Fig. 59ac, Fig. 60ac).

In contrast to the P(TMOS)MIMNTF2 liquid film covered electrodes the SCILF modified electrodes have shown the well developed cyclic voltammetry curves. There is no transport hindrance observed for these systems. The imidazolium groups are easily accessible for the redox probes and it is easy to exchange the electrons between the redox probe and the electrode.

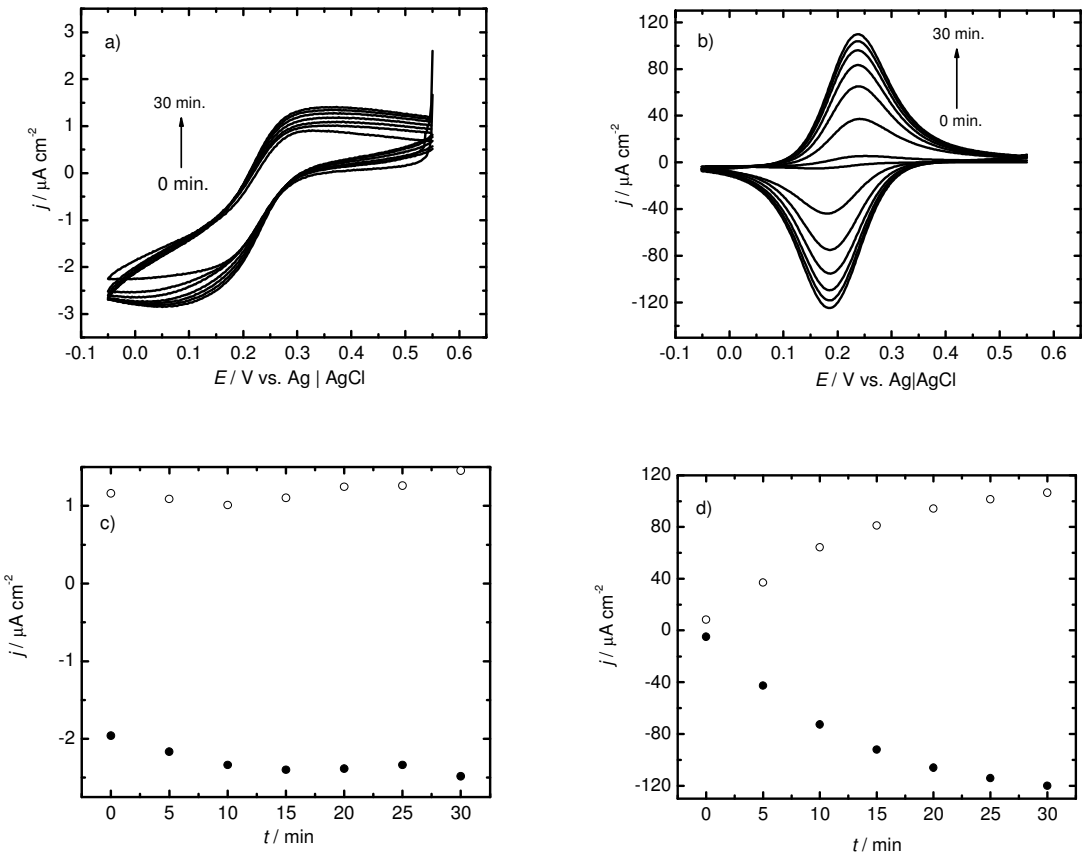

Fig. 58. a) cyclic woltammnograms obtained for ITO electrode modified with the thin film of P(TMOS)MIMNTF2 immersed in the 0.1 mM $K_3Fe(CN)_6$, 0.1 M $NaClO_4$. Arrow shows the flow of time. b) cyclic woltammnograms obtained for ITO electrode modified with SCILF immersed in the 0.1 mM $K_3Fe(CN)_6$, 0.1 M $NaClO_4$. Arrow shows the flow of time. c) and d) anodic (○) and cathodic (●) peak current density vs. of time for the system described in a) and b) respectively.

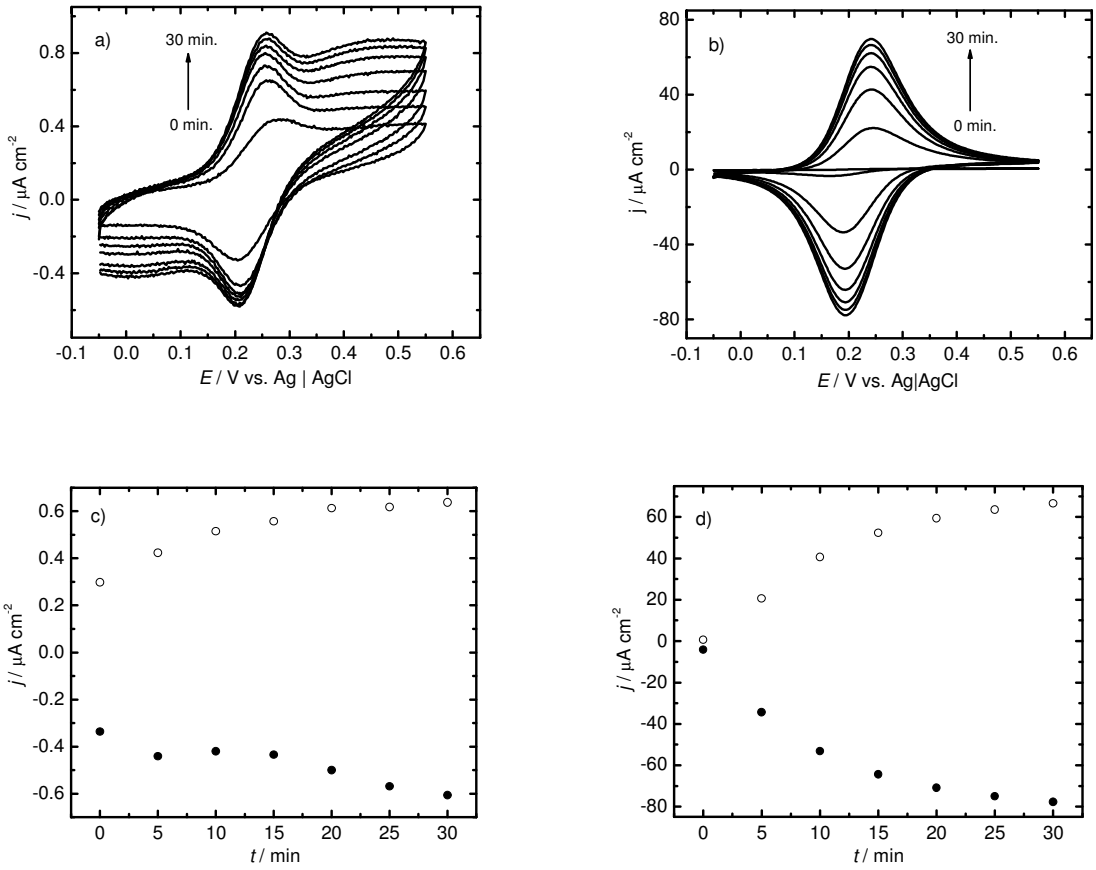

Fig. 59. a) cyclic woltammnograms obtained for ITO electrode modified with the thin film of P(TMOS)MIMNTF2 immersed in the 0.1 mM $K_4Fe(CN)_6$, 0.1 M $NaClO_4$. Arrow shows the flow of time. b) cyclic woltammnograms obtained for ITO electrode modified with SCILF immersed in the 0.1 mM $K_4Fe(CN)_6$, 0.1 M $NaClO_4$. Arrow shows the flow of time. c) and d) anodic (○) and cathodic (●) peak current density vs. of time for the system described in a) and b) respectively.

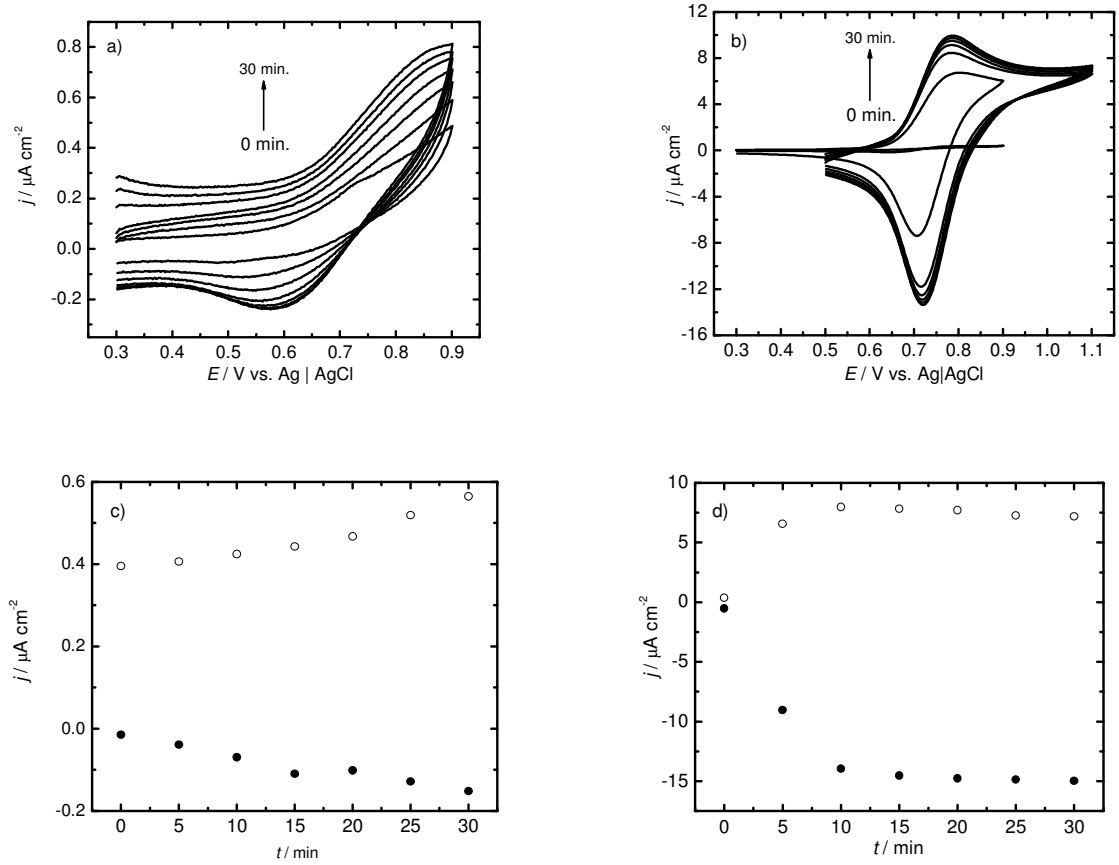

Fig. 60. a) cyclic woltammnograms obtained for ITO electrode modified with the thin film of P(TMOS)MIMNTF2 immersed in the 0.1 mM K_3IrCl_6, 0.1 M $NaClO_4$. Arrow shows the flow of time. b) cyclic woltammnograms obtained for ITO electrode modified with SCILF immersed in the 0.1 mM K_3IrCl_6, 0.1 M $NaClO_4$. Arrow shows the flow of time. c) and d) anodic (○) and cathodic (●) peak current density vs. of time for the system described in a) and b) respectively.

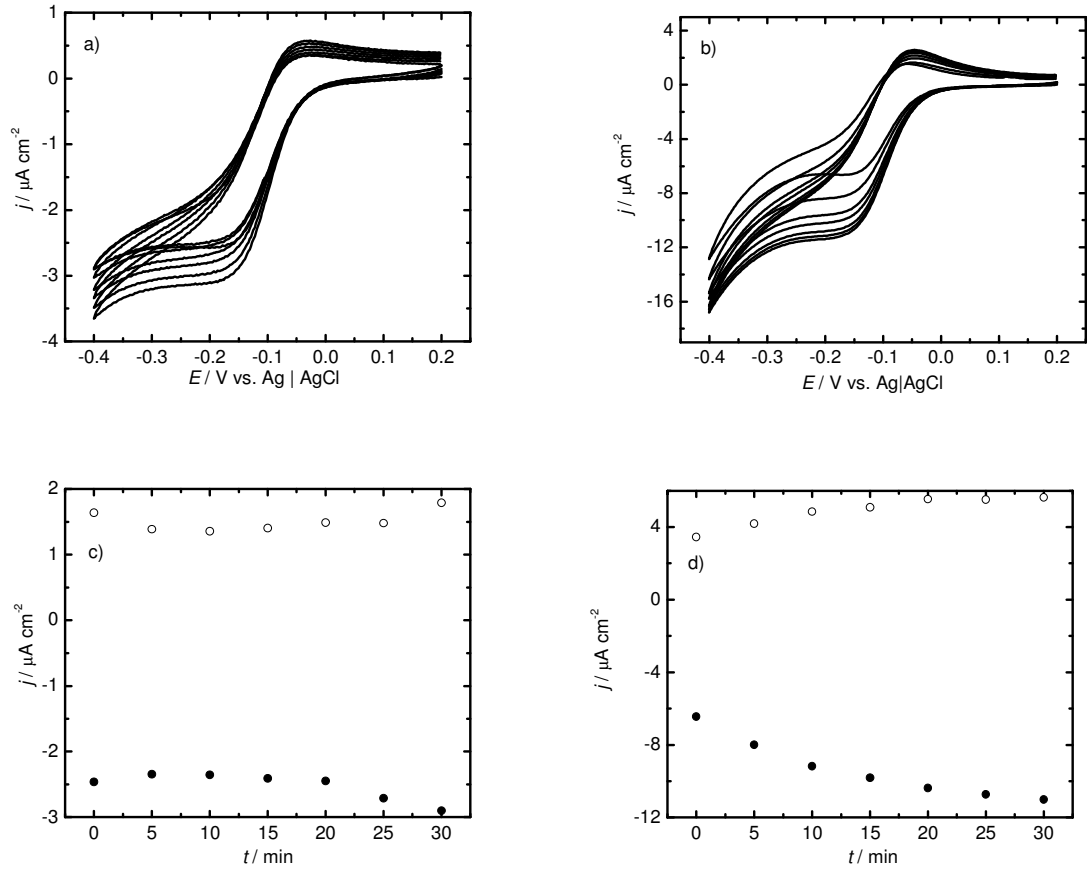

Fig. 61. a) cyclic woltammnograms obtained for ITO electrode modified with the thin film of P(TMOS)MIMNTF2 immersed in the 0.1 mM $Ru(NH_3)_6Cl_3$, 0.1 M $NaClO_4$. Arrow shows the flow of time. b) cyclic woltammnograms obtained for ITO electrode modified with SCILF immersed in the 0.1 mM $Ru(NH_3)_6Cl_3$, 0.1 M $NaClO_4$. Arrow shows the flow of time. c) and d) anodic (○) and cathodic (●) peak current density vs. of time for the system described in a) and b) respectively.

In the case of the positively charged redox probe there is a low current observed on the P(TMOS)MIMNTF2 film modified electrodes (Fig. 61ac). Similarly as in the previous cases the mass transport is hindered by the high viscosity of the ionic liquid.

When the SCILF modified electrode was used instead surprisingly the larger current in time have been observed. The effect if probably caused by the presence of pinholes in the film structure. The film can change it's structure during the experiment exposing higher and higher electrode area. However, the peak current is still significantly lower than one obtained for the bare ITO electrode.

Concluding, the covalent bonding of the IL have a fundamental influence on the accumulation properties of the electrodes. The advantages of covalent bonding of the ionic liquid to the porous silicate film is that the imidazolium groups present in the porous film

structure are easily accessible for the species dissolved in the electrolyte. In combination with high specific surface of the hybrid material it makes the SCILF modified electrodes ideal candidates for anion accumulation. SCILF permeability allows the redox active ions and the electrolyte to penetrate the film.

7.6.1.7. Redox switching on the SCILF modified electrode.

Self assembled monolayer of imidazolium ion terminated thiol compounds on gold was earlier demonstrated to form the ion exchange promoted redox switch towards $Ru(NH_3)_6^{2+/3+}$ [39]. In this chapter the similar behavior of the hybrid sol-gel film modified electrode will be described.

Three solutions has been prepared for the experiment: 0.1 mM $Ru(NH_3)_6Cl_3$, 10 mM $K_3Fe(CN)_6$ and 10 mM NaSCN. First the 0.1 mM $Ru(NH_3)_6Cl_3$ solution has been deoxygenated. The 0.1 M $NaClO_4$ has been used as supporting electrolyte. The hybrid sol-gel film modified electrode has been immersed into the redox probe solution and the cyclic voltammetry experiment has been performed. For the reason described in chapter 14.1.7.5. nearly no faradaic current have been observed (Fig. 62).

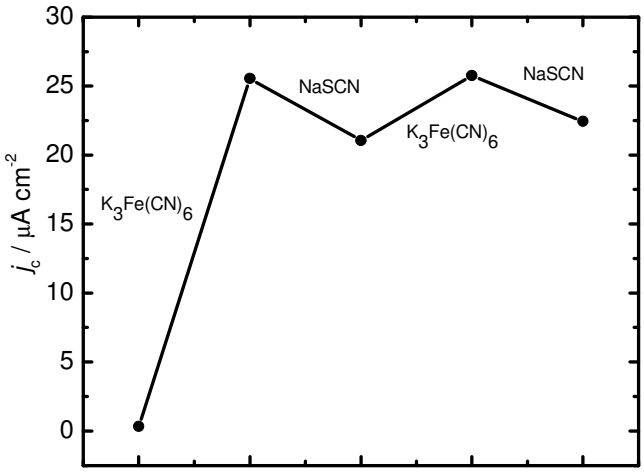

Fig. 62. Cathodic peak current values for hybrid sol-gel modified electrode immersed in the 0.1 mM $Ru(NH_3)_6Cl_3$, 0.1 M $NaClO_4$. Starting from second experiment the electrode was pretreated in either 10 mM $K_3Fe(CN)_6$ or 10 mM NaSCN as indicated on the plot.

Next the electrode was rinsed with deionized water and immersed into the 10 mM $K_3Fe(CN)_6$ for 10 min. Again the electrode was rinsed with deionized water, immersed into

the 0.1 mM $Ru(NH_3)_6Cl_3$ and the cyclic voltammogram has been recorded. Now the peak current density is much higher.

In the next step, the electrode was rinsed with deionized water and immersed into the 10 mM NaSCN solution for 10 min. After that the electrode was rinsed with deionized water, immersed into the 0.1 mM $Ru(NH_3)_6Cl_3$ solution and the cyclic voltammogram has been recorded. This time the current density decreases (ca. 20 μA cm^{-2}), however it is still much higher than for the electrode without any pretreatment. Above-described sequence has been repeated and similar result is seen (Fig. 62).

To explain this phenomenon the anion exchange process has to be taken into consideration. In the initial hybrid sol-gel film the positive charge is compensated by $NTf2^-$ anions. As it was described in chapter 14.1.7.5. such film is quite impenetrable and prevents $Ru(NH_3)_6^{3+}$ from electron exchange. When the electrode was immersed into the $K_3Fe(CN)_6$ solution some fraction of the $NTf2^-$ anions is exchanged with $Fe(CN)_6^{3-}$ anions. The latter are known to promote the electron transfer between the positively charged redox probe and the electrode, however the mechanism is still unexplained [39]. The electron transfer is now possible and the faradaic currents connected with reaction (13) can be observed.

Although $Fe(CN)_6^{3-}$ anions are relatively strongly associated with imidazolium groups [39] their exchange for SCN^- or OCN^- anions is possible [39]. Here some of the $Fe(CN)_6^{3-}$ anions have been exchanged for SCN^- anions. The peak current connected with reaction (13) was lower, because the SCN^- anions do not promote the electron transfer between the positively charged redox probe and the electrode. This current is not as low as for the initial film with $NTf2^-$ counterions because still some $Fe(CN)_6^{3-}$ anions are present in the film and reaction (13) can occur. This is perhaps caused by slow ion exchange and 10 min. allows only for some fraction of $Fe(CN)_6^{3-}$ anions to be exchanged as it was demonstrated in initial accumulation experiments (Fig. 51).

When the electrode has been immersed into the $K_3Fe(CN)_6$ solution again, the faradaic current increase was observed. The amount of $Fe(CN)_6^{3-}$ anions inside the film has increased and the reaction (13) can run efficiently again.

7.6.1.8. The influence of ITO nanoparticles on SCILF modified electrodes accumulation properties.

Electrochemically active surface development is an important issue in electrochemistry, because it allows for the current increase without increase of the apparent geometric area.

In order to develop the ITO electrode surface the methanol suspension of ITO nanoparticles (d = 21 nm) has been prepared. Water was evaporated from this suspension and the 300 mg of ITO nanoparticles was suspended in 10 ml of methanol.

The ITO electrodes were modified with the ITO nanoparticles by dip coating method [465]. The freshly cleaned slide was immersed into the ITO nanoparticles suspension and than withdraw from it. The immersion and withdrawal speed was 85 mm min^{-1}. During the withdrawal step the methanol is evaporating and ITO nanoparticles are left on the surface. Then the electrode was left to dry in the ambient condition for ca. 20 s. The deposition process could be repeated several times depends on how thick deposit was needed. After the premodification with ITO nanoparticles the electrodes was covered with hybrid sol-gel film according to the previously described procedure (14.1.1.).

Four different types of electrodes have been prepared by: zero (ITO|SCILF), one (ITO|1L ITO_{part}|SCILF), three (ITO|3L ITO_{part}|SCILF) and six (ITO|6L ITO_{part}|SCILF) times immersing into the ITO nanoparticles suspension. Then imidazolium appended hybrid sol-gel film was deposited on the electrodes.

The 2,2'-azino-bis(3-ethylbenzothiazoline-6-sulphonic acid) (ABTS) (Fig. 64) have been chosen as a redox probe. The $ABTS^{2-}$ is commonly used as a mediator for the laccase enzyme [466]. From the previously described experiments (14.7.1.) it is known that the hybrid sol-gel film acts as a sponge for anions. Therefore possibility of $ABTS^{2-}$ immobilization in the SCILF have been tested. The electrodes have been immersed into the 0.1 mM ABTS solution in 0.1 M phosphate buffer (pH = 4.8) and the CV experiments have been performed (Fig. 63).

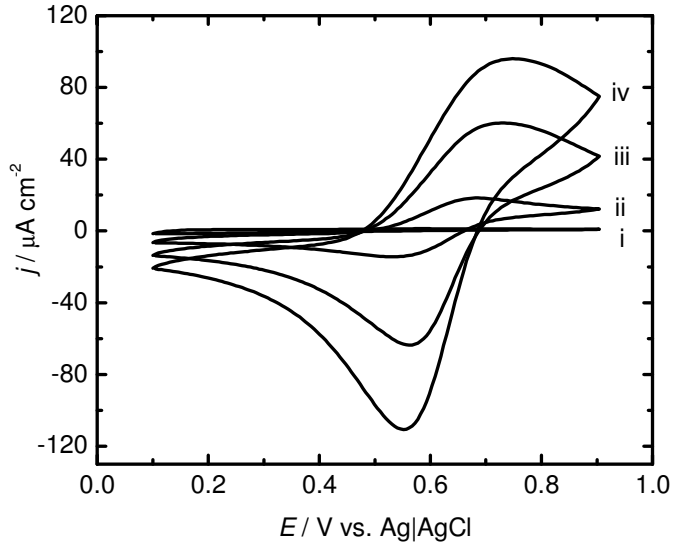

Fig. 63. CVs obtained with the ITO\3L ITO$_{part}$\SCILF electrode immersed to the 0.1 mM ABTS solution in 0.1 M phosphate buffer (pH = 4.8). 1st (i), 30th (ii), 60th (iii) and 90th scan. v = 10 mV s^{-1}.

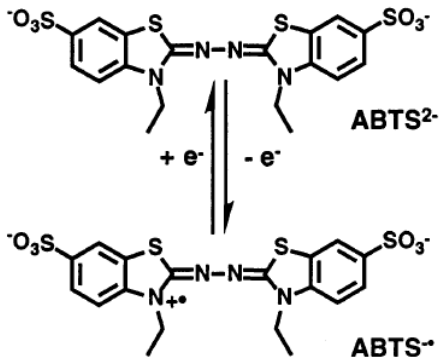

Fig. 64. The redox reaction of ABTS [466].

After the accumulation process electrodes have been rinsed with deionized water and immersed into 0.1 M phosphate buffer (pH = 4.8) in order to trace the leaking process. Then cyclic voltammetry experiments have been performed.

Indeed the $ABTS^{2-}$ accumulation process have been observed (Fig. 65). One can also see that the electrode pre-modification with ITO nanoparticles results with the current increase. This phenomenon is connected to the electrode surface development [465]. One can say that if the electrode surface is well developed, the bigger amount of the accumulated ions is able to exchange the electron with the electrode.

The highest current density was obtained for the electrode modified with one layer of ITO nanoparticles. This is not surprising, because for the ITO|ITO_{part} system it was earlier observed that initial deposition steps provide the largest increase of electrochemically active

surface. When the electrode is already covered with the nanoparticulate deposit further deposition does not increase this effect much [467].

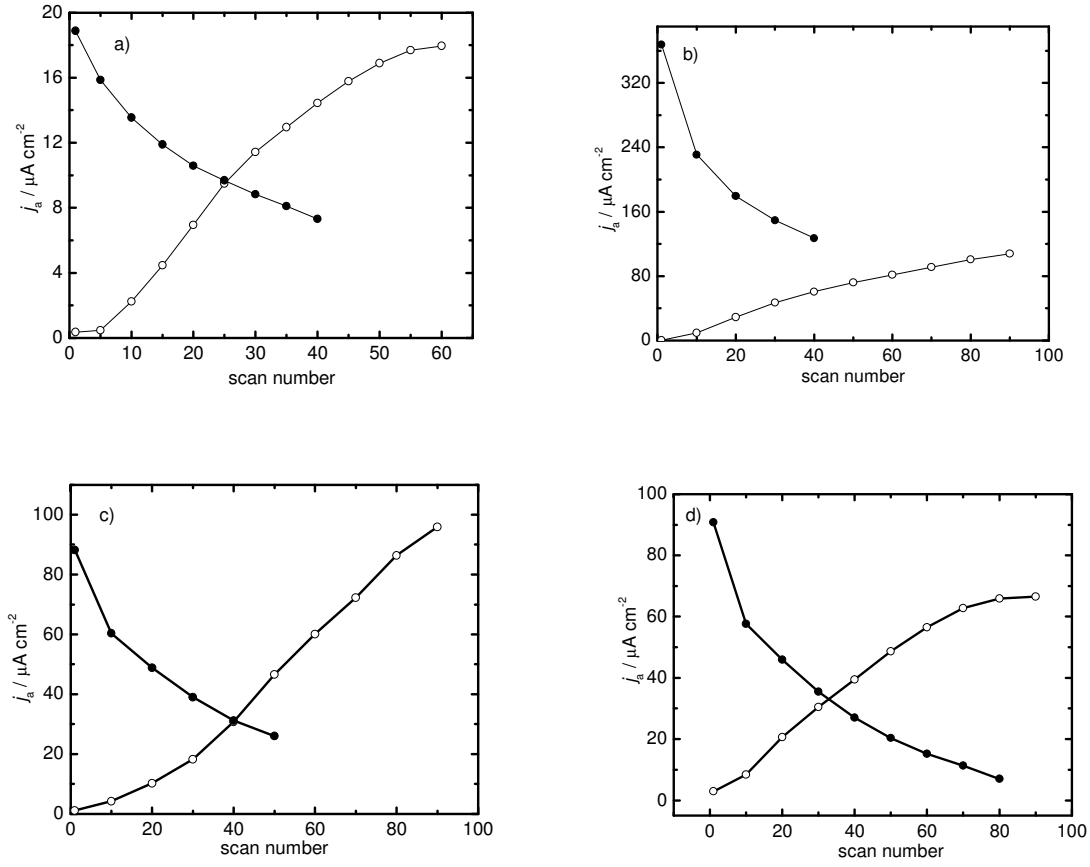

Fig. 65. Anodic peak current density vs. scan number plots for ITO|SCILF a), ITO|1L ITO$_{part}$|SCILF b), ITO|3L ITO$_{part}$|SCILF c), ITO|6L ITO$_{part}$|SCILF d) electrodes immersed into 0.1 mM ABTS, 0.1 M phosphate buffer (pH = 4.8) (○) and into 0.1 M phosphate buffer (pH = 4.8) (●) after previous accumulation. v = 10 mV s^{-1}.

It was noticed that even 90 scans wasn't enough for the current density to reach the plateau. This is because of the slow kinetics of the accumulation process. To learn more about the new electrodes' sorption properties the additional experiment have been performed.

The ITO|SCILF, ITO|1L ITO$_{part}$|SCILF, ITO|3L ITO$_{part}$|SCILF, ITO|6L ITO$_{part}$|SCILF electrodes have been immersed in the 0.1 mM ABTS solution in 0.1 M phosphate buffer overnight. After the accumulation the cyclic voltammograms have been recorded (Fig. 66). One can see that the highest current was obtained for the electrode pre-modified with three layers of ITO nanoparticles. One can conclude that the surface development was the best in this case. The electrons can be efficiently transferred between the adsorbed ABTS molecules and the electrode. ITO|3L ITO$_{part}$|SCILF electrode have been chosen for further experiments with adsorbed enzyme .

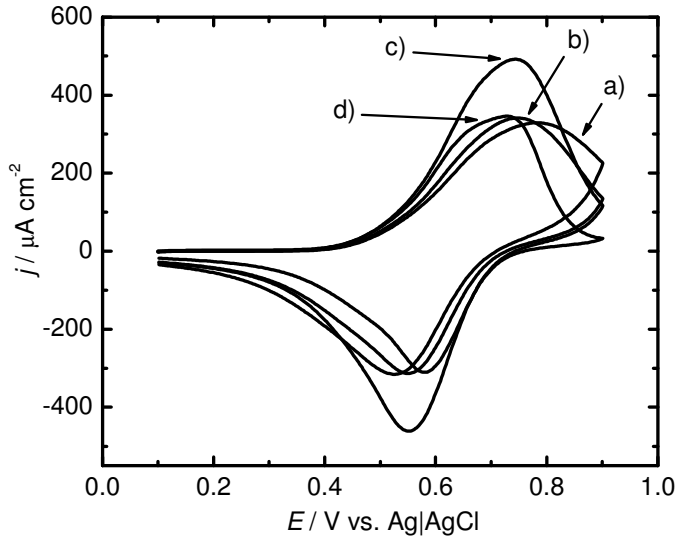

Fig. 66. CVs obtained for ITO|SCILF a), ITO|1L ITO$_{part}$|SCILF b), ITO|3L ITO$_{part}$|SCILF c), ITO|6L ITO$_{part}$|SCILF d) immersed into the 0.1 mM ABTS, 0.1 M phosphate buffer (pH = 4.8) after overnight accumulation.

7.6.2. Hybrid sol-gel film as support for enzyme immobilization.

Biofuel cells are the devices which allows for direct conversion of chemical energy into the electrical one by the utilization of the catalytic properties of the biological systems. One of the most popular and broadly studied type of the enzymatic biofuel cells is the glucose-oxygen biofuel cell [468]. There glucose is oxidized in the anodic part of the biofuel cell by the enzyme. In the cathodic part the oxygen is reduced by an enzyme to water. Above mentioned reactions causes the electron flow in the outer circuit. In order to construct the one compartment biofuel cell one has to immobilize the cathodic and anodic enzymes on the electrode surfaces as well as anodic and cathodic mediators (if needed) [469,470]. In this chapter the attempt to construct biofuel cell's cathode based on SCILF will be described.

First the electrodes have been prepared according to the procedure described in previous chapter and modified with $ABTS^{2-}$. For modification with enzyme laccase-TMOS sol was prepared. First the **stock 1** solution have been prepared by mixing together 500 µl of TMOS, 125 µl of water and 27.5 µl of HCl. It was then sonicated for 20 min. Next the **stock 2** solution was obtained by mixing 250 µl of **stock 1**, 25 µl of 0.1 M phosphate buffer (pH = 5.8) and 225 µl of water. It was sonicated for 2-3 min. Next the **stock 3** was prepared by mixing 25 µl of **stock 2**, 125 µl of laccase standard solution, 25 µl of 0.1 M phosphate buffer (pH = 5.8) and 75 µl of water. It was sonicated for 2-3 min. The final **stock 4** solution was obtained by mixing 25 µl of the **stock 3** solution, 125 µl of laccase standard solution, 25 µl of

0.1M phosphate buffer solution (pH = 5.8) and 75 µl of water. After 2-3 min sonication it was ready for casting onto the electrode surface. Next the two portions (10 µl each) of **stock 4** solution was deposited by drop coating one by one onto the electrode surface. After 1.5 h of drying two portions (10 µl each) of 1.56 mM PAH solution was deposited onto the electrode surface to create a diffusion barrier and to retain immobilized mediator anions within the electrode.[471] The electrodes was left to dry for 20 h in ambient conditions.

The electrochemical experiment was performed in 0.1 M phosphate buffer (pH = 4.8). The electrodes were immersed into the phosphate buffer solution previously saturated with the oxygen and the cyclic voltammograms were recorded (Fig. 67).

One can observe the sigmoidal shape of the voltammograms indicating electrocatalysis. The onset potential of biocatalytic oxygen reduction was about 670 mV vs. Ag|AgCl. The highest catalytic current have been observed for the clean ITO electrode modified with laccase embedded in sol-gel matrix covered with PAH. However it is very unstable and decreases rapidly with subsequent scans. The highest stable current have been obtained for the ITO|3L ITO_{part}|SCILF electrode.

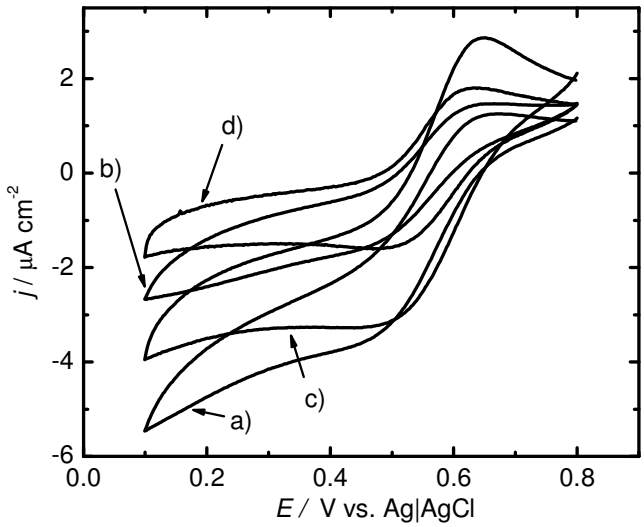

Fig. 67. Cyclic voltammograms obtained for ITO\SCILF a), ITO\1L ITO_{part}\SCILF b), ITO\3L ITO_{part}\SCILF c), ITO\6L ITO_{part}\SCILF d) modified with ABTS and sol-gel immobilized laccase covered with the layer of PAH immersed into 0.1 M phosphate buffer (pH = 4.8) saturated with oxygen.

The appearance of the highest current density for ITO|3L ITO_{part}|SCILF modified electrode can be explained by two oppositely acting effects. First of all, the more nanoparticles is deposited on the electrode surface, the better the surface is developed and the higher current

can be obtained. On the other hand, the thicker the nanoparticulate deposit is the more difficult is for the oxygen to diffuse to the inner parts of the deposit and the electrode support. Therefore the ITO|3L ITO_{part}|SCILF electrode have been chosen for the comparison with clean ITO|SCILF modified electrode.

The electrodes have been further modified with the sol-gel embedded laccase and PAH according to the standard procedure. Then they were immersed into the oxygenated 0.1 M phosphate buffer (pH = 4.8) and the oxygen was pumped over the solution during all experiment. The working electrode potential have been set for 450 mV vs.Ag|AgCl and the current density was recorded as a function of time (Fig. 68).

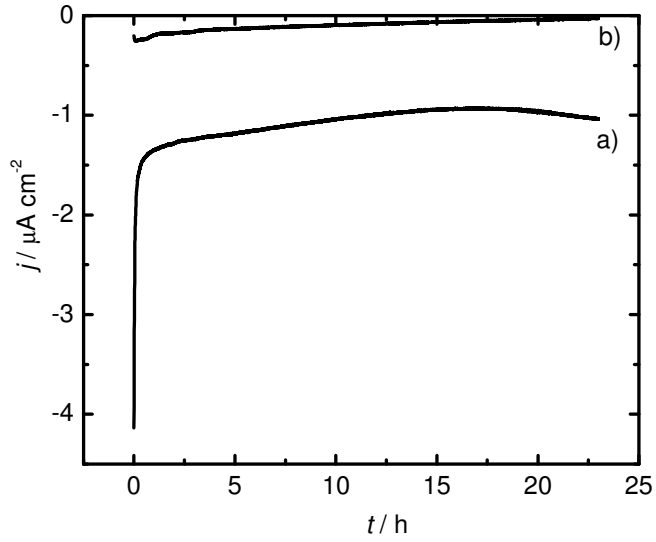

Fig. 68. Chronoamperometric curves obtained for the ITO|3L ITO_{part}|SCILF a) and ITO|SCILF b) electrodes with accumulated ABTS modified with sol-gel embedded laccase and PAH. The experiment was performed in the oxygenated 0.1 M phosphate buffer (pH = 4.8). Applied potential was set on 450 mV vs. Ag|AgCl.

Despite the fact that that biocatalytic current density obtained for the electrode built on the ITO|$3L_{part}$ substrate was rapidly decreasing with time in the first period of the experiment it was still significantly higher than the one obtained for the electrode built on the clean ITO. The current was stable for more than 20 hours. It is also clearly visible that biocatalytic current density obtained for the electrode built on the clean ITO is very low (<0.5 µA cm^{-2}) and constantly decreases in time (Fig. 68b).

The above-mentioned experiments have shown that SCILF can be used as a substrate for the negatively charged enzyme mediator immobilization. The premodification of the electrode with particular amount of the ITO nanoparticles can facilitate the electron transfer

and make the bioelectrocatalysis process more efficient. Comparing these results with the actual state of art [472] one can conclude that this electrodes are not promising.

7.6.3. Electrochemistry of redox liquid deposit.

Ion transfer across liquid|liquid interfaces is very important process in biological systems. Three phase junction approach to study these processes have been introduced by Marken [4]. This system can be potentially applied in electroanalysis, electrocatalysis, electroorganic synthesis and electrochemically driven extraction and separation processes. For its development the design of new materials is an important issue [473].

tBuFc have been chosen as the redox probe for the experiments. This redox liquid has been deposited on the SCILF covered electrode's surface or clean ITO surface. To investigate the influence of covalent bonding on the ion transfer properties of the ionic liquid t-butylferrocene dissolved in the P(TMOS)MIMNTF2 liquid deposit have been also investigated.

For electrode modification 1µl of t-butylferrocene was dissolved in 1ml of hexane. The mixture was stirred well and the 5 µl of the resulting solution was deposited either on the clean ITO or the SCILF modified ITO electrode. In the second system the tBuFc (1µl) solution in P(TMOS)MIMNTF2 (0.2 ml) have been prepared. Small droplet (ca. 5 µl) of the resulting solution have been deposited on the clean ITO electrode surface.

The electrodes have been immersed into the 0.1 M solutions of KPF_6, $NaClO_4$, NaSCN, KNO_3, KBr, KCl and NaF. The different electrolytes have been tested to check the $E_{\mathrm{tBuFc/tBuFc^+}}$ dependence on standard transfer potential of anions from water to nitrobenzene. This information was needed to conclude the charge compensation mechanism. The CV and DPV experiments have been performed.

The electrode reaction can be described by the simple equation: [465]

$$\mathrm{tBuFc} \leftrightarrow \mathrm{tBuFc^+} + \mathrm{e^-} \qquad (14)$$

When reaction (14) occurs the positively charged t-butylferrocenium ion is created. However the droplet electroneutrality have to be retained. Either the newly created cation can be expelled from the oil droplet (Fig. 70b.)

$$\mathrm{tBuFc(org)} \leftrightarrow \mathrm{tBuFc^+(aq)} + \mathrm{e^-(electrode)} \qquad (15)$$

or the anion present in the water phase can be transferred into the oil droplet (Fig. 72b.).

$$\mathrm{tBuFc(org) + X^-(aq) \leftrightarrow tBuFc^+(org) + e^-(electrode) + X^-(org)} \quad (16)$$

The anion dependence of the redox potential ($E_{red/ox}$) can be described by the following Nernstian type equation: [6]

$$E_{red/ox} = E^0_{tBuFc^+_{tBuFc}/tBuFc_{tBuFc}} + \Delta^{tBuFc}_{aq}\varphi^0_{X^-} - \frac{RT}{F}\ln c_{X^-_{aq}} + \frac{RT}{F}\ln\frac{c^*_{tBuFc_{tBuFc}}}{2} \quad (17)$$

where $E^0_{tBuFc^+_{tBuFc}/tBuFc_{tBuFc}}$ is the standard redox potential for the $tBuFc^+$/tBuFc couple in the tBuFc droplet, $\Delta^{tBuFc}_{aq}\varphi^0_{X^-}$ is the standard transfer potential of anion X^- from water into the tBuFc phase, and $c_{X^-_{aq}}$ and $c^*_{tBuFc_{tBuFc}}$ are the initial concentrations of X^- and tBuFc in aqueous solution and tBuFc, respectively. If the electrooxidation of tBuFc is followed by anion insertion to the tBuFc phase one should expect a linear plot of $E_{tBuFc^+_{tBuFc}/tBuFc_{tBuFc}}$ vs. $\Delta^{tBuFc}_{aq}\varphi^0_{X^-}$ with unit slope. The latter parameter is unavailable and can be replaced [45] by the standard transfer potential of X^- from water to nitrobenzene ($\Delta^{NB}_{aq}\varphi^0_{X^-}$) as a measure of the anion hydrophobicity. If the droplet electroneutrality is maintained by cation expulsion the $E_{tBuFc^+_{tBuFc}/tBuFc_{tBuFc}}$ should be independent from $\Delta^{tBuFc}_{aq}\varphi^0_{X^-}$.

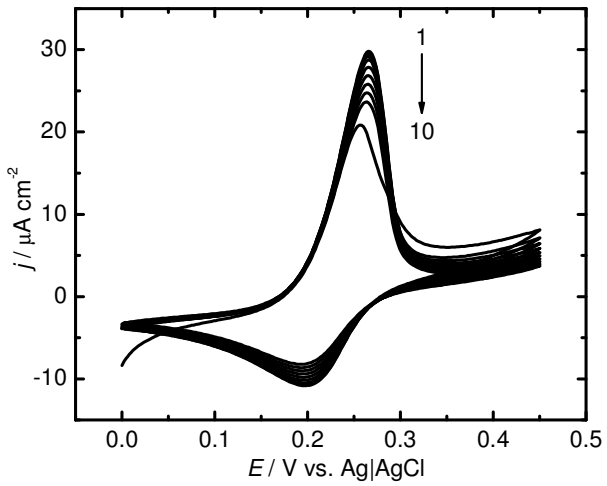

Fig. 69. CVs obtained for ITO electrode modified with t-BuFc immersed into the 0.1 M $NaClO_4$. Arrow show the dictection of current changes in subsequent scans. v = 10 mV s^{-1}

In the CV experiment (Fig. 69) relatively symmetric CV have been obtained. The ratio of anodic to cathodic charges calculated by integration of CV was Q_a/Q_c = 1.3. The peak current densities were slowly decreasing in subsequent scans. The above mentioned observation indicates the fact that some t-BuFc cation expulsion have been also present.

It was found that ITO electrode modified with t-butylferrocene shows anion sensitive voltammetry (Fig. 70a). There is a linear dependence of $E_{tBuFc^+_{tBuFc}/tBuFc_{tBuFc}}$ vs. $\Delta^{tBuFc}_{aq}\varphi^0_{X^-}$ observed with the slope 1.2 ± 0.1. This can be explained by assuming a significant contribution of anion (X^-) insertion from the aqueous phase to the tBuFc deposit.

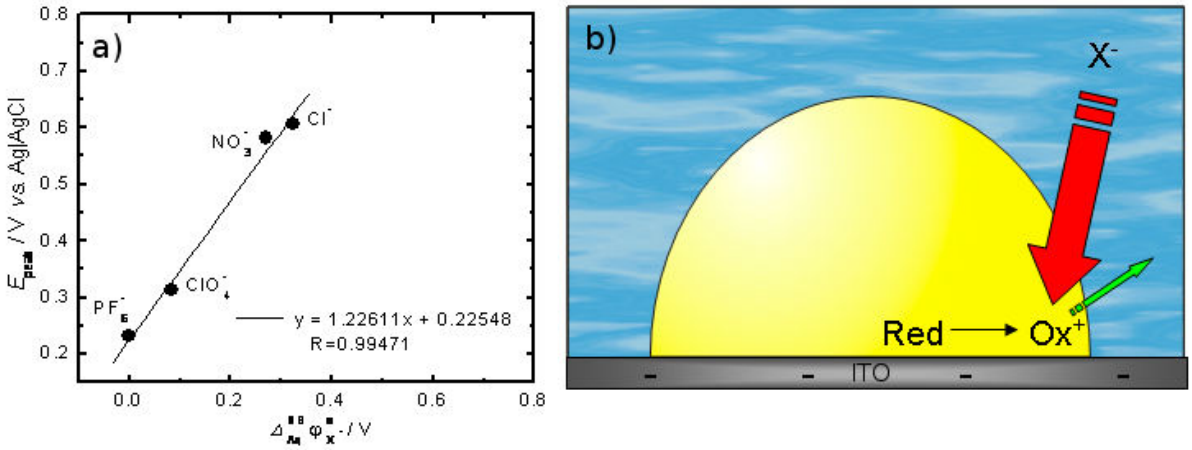

Fig. 70. a) E_{peak} vs. $\Delta^{NB}_{Aq}\varphi^0_{X^-}$ plot obtained with ITO electrode modified with t-butylferrocene immersed into 0.1 M aqueous salt solutions. The anions are marked on the plot. The solid line was obtained by a linear fit of the data marked by dots. b) Scheme the tBufc oxidation followed by anion insertion into the oil phase.

When the tBuFc droplet was deposited on the SCILF covered ITO or ITO|3L ITO_{part} different charge neutralization mechanisms proportion have been observed. The ratio of anodic to cathodic charge much higher than unity (Q_a/Q_c = 3.9) calculated by integration of the CVs and a significant decrease of the peak current during continuous scanning (ca. 80% after first five scans) was observed (Fig. 71).

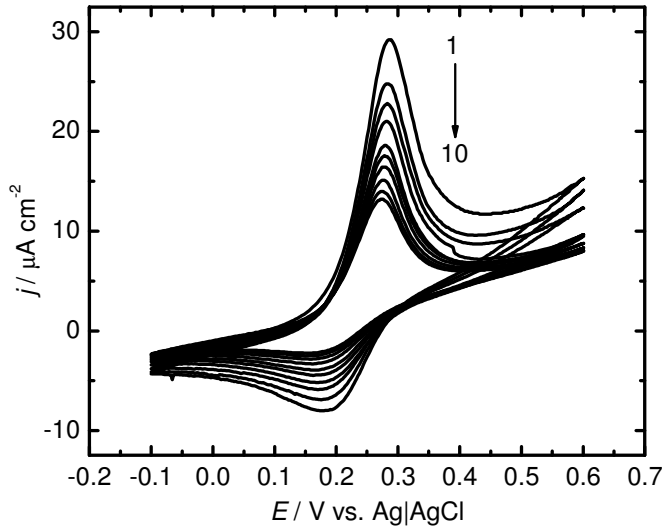

Fig. 71. CVs obtained for ITO|SCILF electrode modified with t-BuFc immersed into the 0.1 M$NaClO_4$. Arrow show current changes in subsequent scans. v = 10 mV s^{-1}

This indicates significant number of $tBuFc^+$ ejection as the result of the t-butylferrocene oxidation (15). Moreover nearly no anion influence on the $tBuFc^+$/tBuFc couple's redox potential was observed (Fig. 72a). This fact also confirms the cation ejection mechanism. There was no significant difference between the behavior of electrodes obtained with the ITO|SCILF and the ITO|3L ITO_{part}|SCILF as substrates.

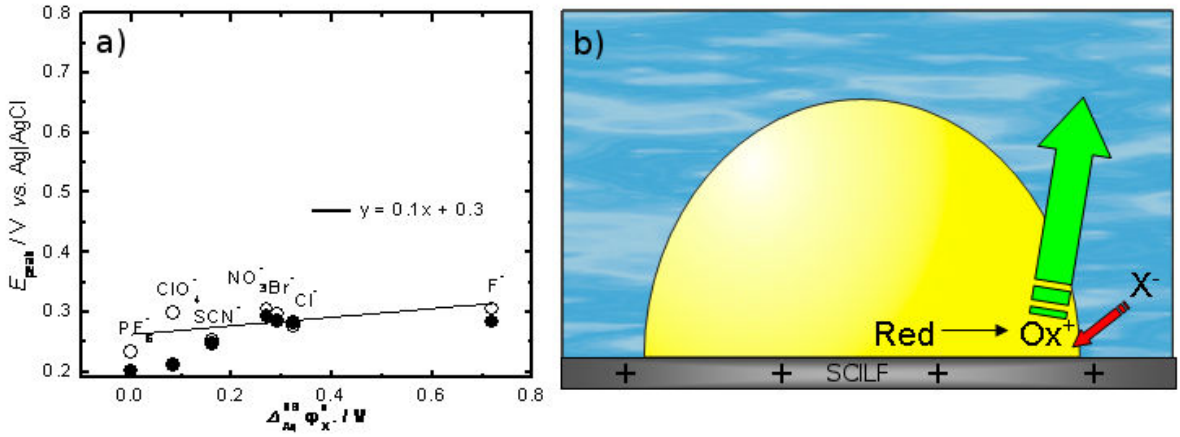

Fig. 72. a) E_{peak} vs. $\Delta^{NB}_{Aq}\varphi^0_{X^-}$ plot obtained with ITO (○) and ITO|3L ITO_{part} (●) electrode modified with SCILF and t-butylferrocene immersed into 0.1 M aqueous salt solutions. The anions are marked on the plot. The solid line was obtained by a linear fit of the data marked by dots. b) Scheme the t-butylferrocene oxidation followed by cation expulsion from the oil phase.

In the case of ITO electrode modified with t-butylferrocene dissolved in P(TMOS)MIMNTF2 the redox potential can be described by the equation similar to equation (17):

$$E_{red/ox} = E^0_{tBuFc^+_{P(TMOS)MIMNTF2}/tBuFc_{P(TMOS)MIMNTF2}} + \Delta^{P(TMOS)MIMNTF2}_{aq}\varphi^0_{X^-} - \frac{RT}{F}\ln c_{X^-_{aq}} + \frac{RT}{F}\ln\frac{c^*_{tBuFc_{P(TMOS)MIMNTF2}}}{2} \qquad (18)$$

where $E^0_{tBuFc^+_{P(TMOS)MIMNTF2}/tBuFc_{P(TMOS)MIMNTF2}}$ is the standard redox potential for the $tBuFc^+$/tBuFc couple in the P(TMOS)MIMNTF2 droplet, $\Delta^{P(TMOS)MIMNTF2}_{aq}\varphi^0_{X^-}$ is the standard transfer potential of anion X^- from water into the P(TMOS)MIMNTF2 phase, and $c_{X^-_{aq}}$ and $c^*_{tBuFc_{P(TMOS)MIMNTF2}}$ are the initial concentrations of X^- and tBuFc in aqueous solution and P(TMOS)MIMNTF2 phase, respectively.

Although some scattering of the data is observed (Fig. 74) a linear dependence with slope equal to 0.46 ± 0.19 can be found. This is quite below unity and can be explained by some $tBuFc^+$ or 1-methyl-3-(3-trimethoxysilylpropyl)imidazolium cations expelled into the aqueous solution. A similar dependence was already found for different electrodes modified with the hydrophobic RTIL – 1-decyl-3-methylimidazolium bis(trifluoromethylsulfonyl)-imide [30,45,235]. It indicates a significant contribution of anion insertion into the ionic liquid precursor deposit (16). This conclusion is strengthened by the value of Q_a/Q_c not much larger than unity (1.07) (Fig. 73) and by an modest decrease peak current during subsequent potential scanning (10%) after the first five voltammetric scans (not shown).

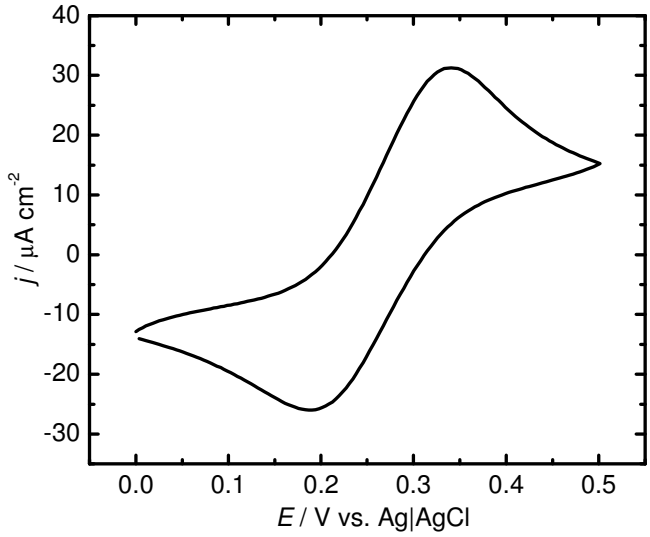

Fig. 73. CV obtained for ITO electrode modified with 2×10^{-9} mol tBuFc solution in P(TMOS)MIMNTF2 immersed in 0.1 M $NaClO_4$. v = 10 mV s^{-1}.

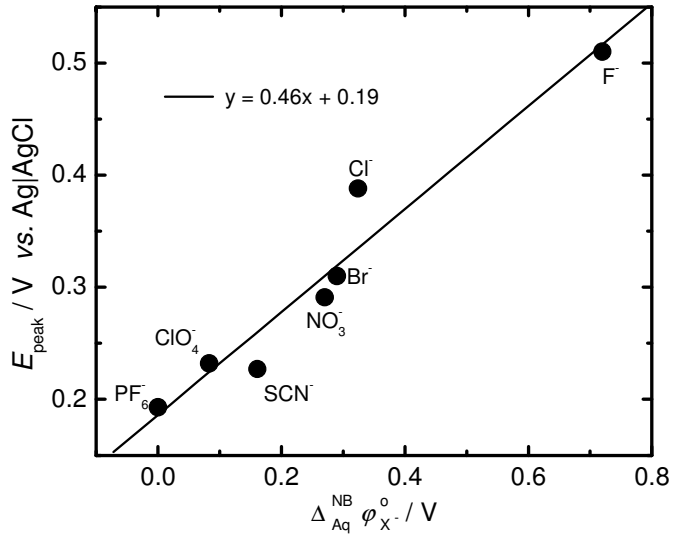

Fig. 74. $E_{Red/Ox}$ vs. $\Delta^{NB}_{aq}\varphi^{0}_{X^-}$ plot obtained with ITO electrode modified with 2×10^{-9} mol tBuFc solution in P(TMOS)MIMNTF2 immersed into 0.1 M aqueous salt solutions. The anions are marked on the plot. The solid lines were obtained by a linear fit of the data marked by dots.

These experiments shows the influence of P(TMOS)MIMNTF2 on the ion transfer driven by tBuFc redox reaction. It was demonstrated that the electroneutrality of the tBuFc droplet on the ITO electrode is maintained mainly by anion transfer from water phase to the oil one. When tBuFc was dissolved in P(TMOS)MIMNTF2 droplet deposited on the ITO electrode its electroneutrality was maintained by both anion insertion and cation expulsion. If the tBuFc droplet was deposited on SCILF modified electrode its electroneutrality was

maintained mainly by cation expulsion to the water phase. As one can see the ion transfer process driven by the redox reaction is different for unconfined or covalently bonded P(TMOS)MIMNTF2.

7.6.4. Decametylferrocene oxidation on the SCILF covered ITO electrode

As a continuation of the previous experiments the redox probe more hydrophobic than tBuFc, DMFc, have been chosen to test at the SCILF modified electrodes. Contrary to tBuFc this redox probe is solid at room temperature.

Three different DMFc modified electrodes have been prepared. 1 mg of the DMFc have been deposited from hexane onto the clean ITO, ITO|SCILF and ITO|3L ITO_{part}|SCILF modified electrodes. After the solvent evaporation the crystals of the DMFc could be easily observed with the optical microscope (Fig. 75).

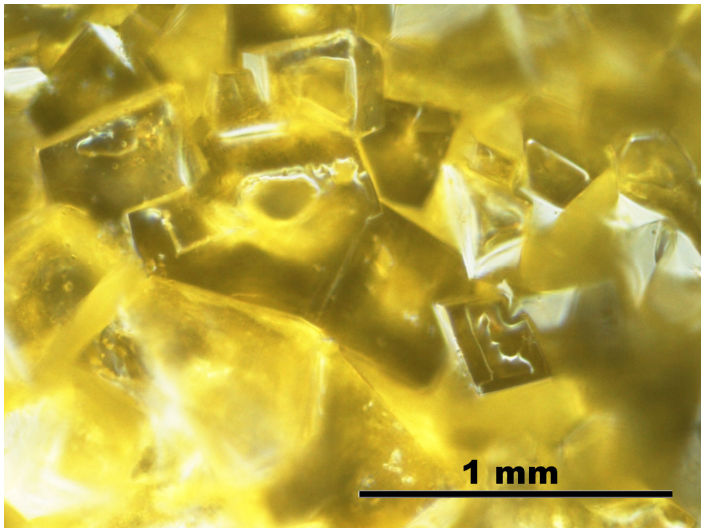

Fig. 75. Optical microscopy picture of the DMFc deposit on the ITO surface.

Then DMFc modified electrodes were immersed into the 0.1 M $NaClO_4$ solutions and the CV experiment have been performed. On the CV curve the well defined redox peak have been observed (Fig. 76). The peaks have been assigned to the DMFc oxidation and reduction:

$$DMFc \leftrightarrow DMFc^{+} + e^{-} \qquad (18)$$

The Q_a/Q_c ratio is ca. 1.5 and ca. 0.75 for bare ITO and SCILF modified electrode respectively. However, the latter value is very uncertain because of the very low currents and difficulties in baseline corrections. On can see that the current densities obtained on the SCILF supports are ca. 20 times smaller than ones obtained on bare ITO support. This can be explained by the surface blocking properties of the SCILF.

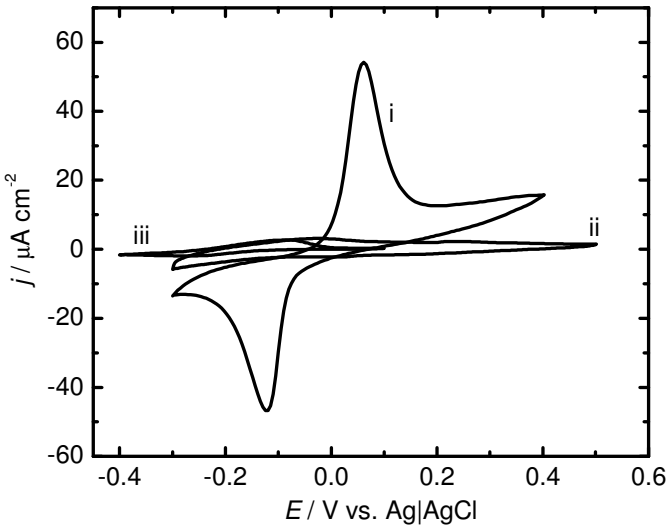

Fig. 76. CVs obtained for the DMFc modified ITO (i), ITO|SCILF (ii) and ITO|3L ITO_{part}|SCILF (iii) electrodes immersed to 0.1 M $NaClO_4$.

Clearly the anion independent voltammetry have been observed for the DMFc deposited on bare ITO (Fig. 77). After the oxidation process the $DMFc^+$ cation is expelled from the DMFc crystal into the water solution. It is hardly probable that anion will be transferred into the DMFc crystal structure from solution to compensate the charge. This observation is in contradiction with the results of the previous experiments where anion influence on DMFc CVs was observed [474]. Probably the DMFc deposition method is an important factor which influences on its electrochemical behavior.

The data obtained for the film covered electrodes are strongly scattered and the reproducibility was poor. This can be explained by the differences among the individual copies of the electrodes and by the blocking effect of the film. It is known that the sol-gel process is extremely sensitive to the processing conditions such as: temperature, humidity etc. [328] In these experiments it was impossible to control the mentioned-above factors with sufficient accuracy.

In spite of the great data scattering it is clearly see that SCILF causes the decrease of the $DMFc/DMFc^+$ couple redox potential. The presence of the film on the electrode surface stabilizes the oxidized form of the redox probe. It is understandable if one takes into consideration fact that both $DMFc^+$ and SCILF surface have the positive charges. The electrostatic repulsion between them makes it difficult to rereduce the $DMFc^+$ cation. There is no significant effect of ITO particles on the $DMFc/DMFc^+$ couple redox potential observed.

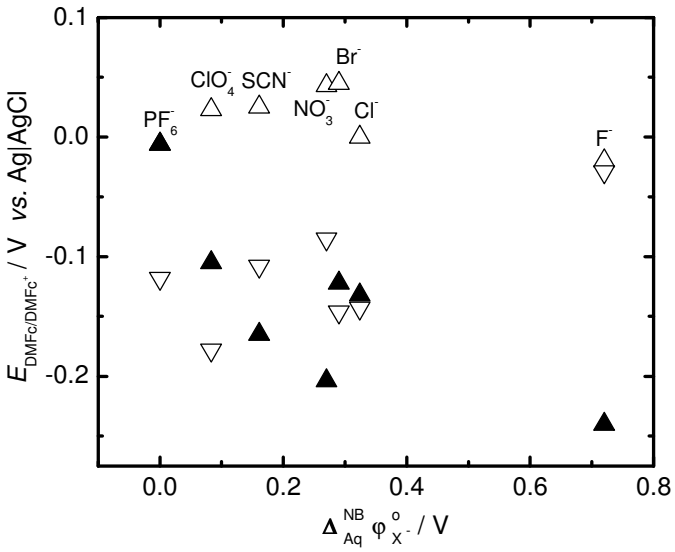

Fig. 77. $E_{DMFc/DMFc^+}$ vs. $\Delta^{NB}_{aq}\varphi^{0}_{X^-}$ plot obtained with ITO electrode (open triangle), ITO|SCILF electrode (inversed open triangle) and ITO|3L ITO_{part}|SCILF electrode (full triangle) modified with 1 mg of DMFc deposited from hexane, immersed into 0.1 M aqueous salt solutions. The anions are marked on the plot.

8. Electroassisted generation of hybrid sol-gel films

8.1. Co-deposition

The TEOS and P(TMOS)MIMNTF2 have been used first to obtain mesoporous, organized, silicate thin film modified with imidazolium groups. TEOS was used instead of TMOS because previously reported organized films have been obtained from this precursor [313].

8.1.1. Sol-gel film preparation procedure

The starting sols have been obtained by mixing together the sol components as shown in the Table 1. To name the film obtained from the particular sol the deposition time was added to the name of sol. The different sol composition have been tested to find the optimal one for the organized film modified with imidazolium groups deposition. After mixing the pH of the sol have been adjusted by addition of HCl and the sol have been vigorously stirred for 2 h in order to hydrolyze precursors.

Table 1. Compositions of various sols used for the films electrodeposition.

sol code	sol composition
S1	20 ml EtOH 20 ml (0.1 M $NaNO_3$, 100 mM TEOS, 150 mM CTAB) in H_2O
S2	8 ml CH_3CN 16 ml EtOH 16 ml (0.125 M $KClO_4$, 125 mM TEOS, 187.5 mM CTAB) in H_2O
S3	8 ml CH3CN 16 ml EtOH } 2 mmol $TBAPF_6$ 16 ml (125 mM TEOS, 187.5 mM CTAB) in H_2O
S4	20 ml CH_3CN + 2 mmol $TBAPF_6$ 20 ml (0.125 mM TEOS, 187.5 mM CTAB) in EtOH
S5	8 ml CH_3CN 16 ml EtOH 16 mM (0.125 M $NaNO_3$, 0.125 mM TEOS, 187.5 mM CTAB)
S6	8 ml CH_3CN + 430 µl TEOS (95%) + 0.0525 g P(TMOS)MIMNTF2 (**5% IL**) 16 ml ETOH 16 ml (0.125 M $NaNO_3$ + 1.0934 g CTAB) in H_2O

S7	8 ml CH_3CN + 0.0525 g P(TMOS)MIMNTF2 (**5% IL**) 16 ml ETOH 16 ml (0.125 M $NaNO_3$ + 1.0934 g CTAB+ 430 µl TEOS (95%)) in H_2O
S8	8 ml CH_3CN + 0.0210 g P(TMOS)MIMNTF2 (**2% IL**) 16 ml ETOH 16 ml (0.125 M $NaNO_3$ + 1.0934 g CTAB+ 443 µl TEOS (98%)) in H_2O
S9	8 ml CH_3CN + 0.0105 g P(TMOS)MIMNTF2 (**1% IL**) 16 ml ETOH 16 ml (0.125 M $NaNO_3$ + 1.0934 g CTAB+ 448 µl TEOS (99%)) in H_2O
S10	8 ml CH_3CN + 0.105 g P(TMOS)MIMNTF2 (**10% IL**) 16 ml ETOH 16 ml (0.125 M $NaNO_3$ + 1.0934 g CTAB+ 407 µl TEOS (90%)) in H_2O
S11	8 ml CH_3CN + 0.0420 g P(TMOS)MIMNTF2 (**4% IL**) 16 ml ETOH 16 ml (0.125 M $NaNO_3$ + 1.0934 g CTAB+ 434 µl TEOS (96%)) in H_2O
S12	8 ml CH_3CN + 0.0736 g P(TMOS)MIMNTF2 (**7% IL**) 16 ml ETOH 16 ml (0.125 M $NaNO_3$ + 1.0934 g CTAB+ 421 µl TEOS (93%)) in H_2O
S13	8 ml CH_3CN + 0.2625 g P(TMOS)MIMNTF2 (**5% IL**) 16 ml ETOH 16 ml (0.125 M $NaNO_3$ + 1.0934 g CTAB+ 2150 µl TEOS (95%)) in H_2O
S14	8 ml CH_3CN + 0.3152 g P(TMOS)MIMNTF2 (**30% IL**) 16 ml ETOH 16 ml (0.125 M $NaNO_3$ + 1.0934 g CTAB+ 317 µl TEOS (70%)) in H_2O
S15	8 ml CH_3CN + 1.8914 g P(TMOS)MIMNTF2 (**30% IL**) 16 ml ETOH 16 ml (0.125 M $NaNO_3$ + 0.3461 SDS+ 1900 µl TEOS (70%)) in H_2O

Then the ITO electrode have been immersed into sol. The platinum wire and the stainless steel sheet have been used as a quasi reference electrode and a counter electrode respectively. The deposition potential of 1.3 V vs. Pt wire have been applied to the working electrode for various periods of time (10 - 180s). The formation of white film was visible at the ITO surface with the naked eye. After the deposition process the electrodes have been

kept at 130 °C overnight. This was in order to finalize the gelation process and to remove the remaining solvent from the film. After the heat treatment the films was ready to use, however in some cases it was necessary to remove the surfactant template from the pores. It was achieved by the immersion of the film into the 0.1 M HCl solution in ethanol and vigorous stirring for 15 min.

8.1.2. TEM analysis

In order to analyze the film structure the TEM experiment have been performed. The surfactant have been removed from the S5_20s film. Then the film was scratched of the ITO surface with the needle. The film slivers were transferred onto the TEM grid.

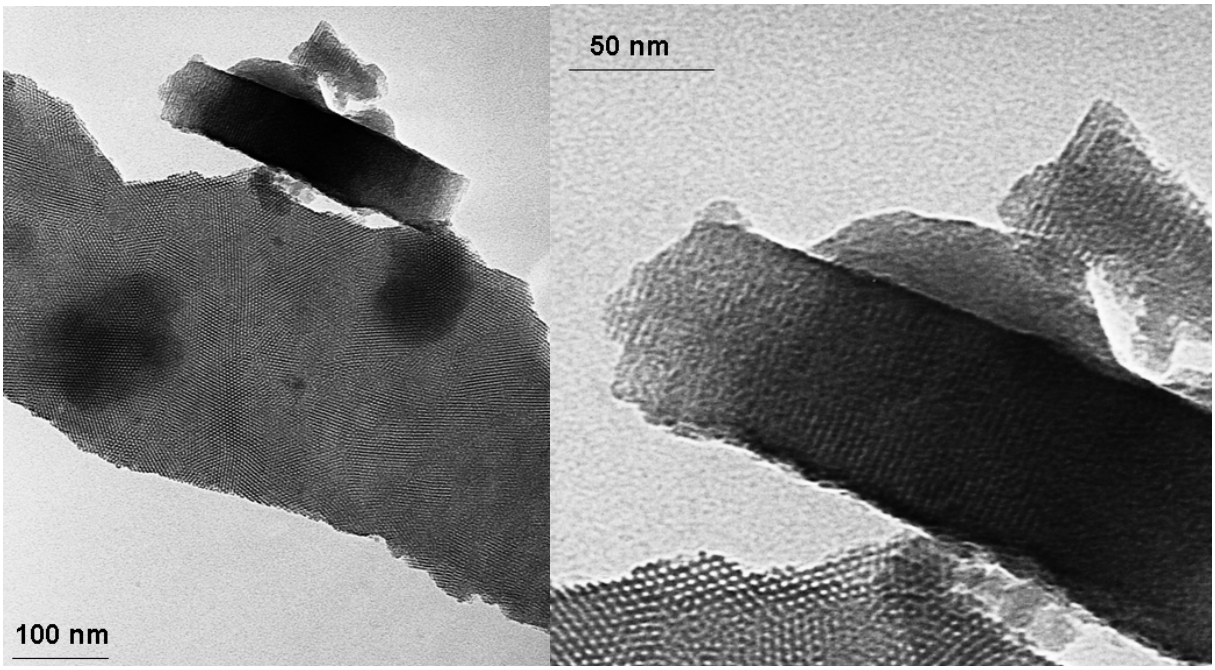

Fig. 78. TEM images of the S5_20s film.

On the TEM micrographs (Fig. 78) the porous structure of the film is clearly visible. On can see the film domains with hexagonally ordered pores. Moreover, the pores have been perpendicular to the electrode surface. The pore size was estimated at several nanometers which is in agreement with the CTAB molecule size. The film thickness have been estimated at 72 nm which is the reasonable value for this type of materials [313].

8.1.3. Electrochemical properties

First the S1 sol was prepared and the films of different thickness were deposited by applying potential for 10, 15 and 20 s. It is known from the literature that film thickness is proportional

to the deposition time [315]. Here the film obtained by 15 s anodization was found to be optimal for further experiments. It was thick enough that one can be sure that whole electrode surface was covered with it, but still as thin as possible.

In order to investigate if the film covers whole electrode surface, electrochemical experiments have been performed. The data obtained during the experiments have been also used to demonstrate the porous structure of the film.

First, the electrode covered with S1_15s was immersed into the 5 mM $Ru(NH_3)_6Cl_3$. 0.1 M $NaNO_3$ was used as a supporting electrolyte. The CV experiment have been performed. The same experiment have been performed for the S1_15s film modified electrode after surfactant removal. The curve for the bare ITO was also recorded to be used as a reference.

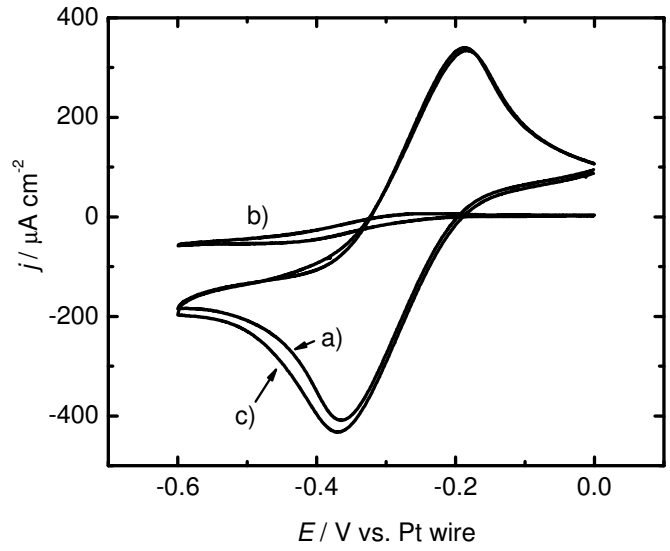

Fig. 79. Cyclic voltammograms obtained in 5 mM $Ru(NH_3)_6Cl_3$, 0.1 M $NaNO_3$ on the bare ITO electrode (a), S1_15s film modified electrode before (b) and after (c) surfactant removal. v= 20 mV s^{-1}.

One can clearly see that the S1_15s film covered electrode's surface was nearly completely blocked towards the $Ru(NH_3)_6^{3+}$ cations. (Fig. 79b) The currents are significantly lower than on the bare ITO electrode in the same conditions. (Fig. 79a.) This indicates that the film covers the whole electrode surface and is tight enough to prevent electroactive $Ru(NH_3)_6^{3+}$ cations from electron exchange. Perhaps the pores present in the film structure are blocked with the surfactant template. The redox potential red from the vestigial current is shifted towards cathodic potential, what is caused by the interactions between CTAB and $Ru(NH_3)_6^{3+}$. After the surfactant removal from the pores another CV curve have been

recorded. In this case the current response was nearly the same as for clean ITO electrode. This indicates that the pores in the film are open on both sides and the film have nearly no influence on electroactive species transport to the electrode surface. This allows to think of such films as a suitable supports for further electrode modification.

The similar experiment have been performed with the more hydrophobic redox probe – FDM. The same set of electrodes have been tested in 0.5 mM FDM, 0.1 M $NaNO_3$.

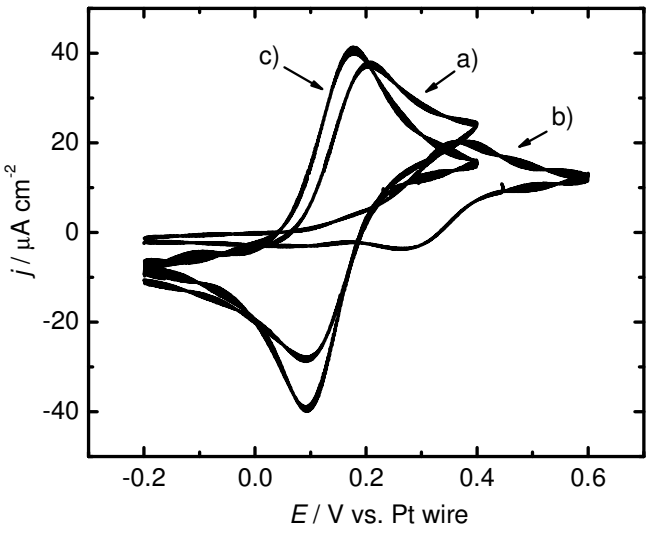

Fig. 80. CVs obtained in 0.5 mM FDM, 0.1 M $NaNO_3$ on the clean ITO electrode (a), S1_15s film modified electrode before (b) and after (c) surfactant removal. v= 20 mV s^{-1}.

The shape of the voltammograms results from the (12) redox reaction. It was found that the S1_15s film covered electrode is not completely blocked for the FDM (Fig. 80b). However the FDM redox potential have been significantly shifted towards anodic potentials. Such behavior have been observed before [313] and it is connected with the accumulation of the neutral redox probe in the CTAB liquid-crystal-like phase [475]. The positively charged CTA^+ cations stabilize the reduced form of FDM. After the surfactant removal the redox potential is almost not shifted (Fig. 80c.) comparing to the bare ITO electrode (Fig. 80a.). It means that the surfactant was removed from the pores and the pores volume can be penetrated by aqueous electrolyte.

For later experiments it was necessary to find solvent composition for dissolution of IL precursor and TMOS. The suitable solvent mixture contains CH_3CN, EtOH and water in ratio 1:2:2. $NaNO_3$ was found as suitable electrolyte for all sols.

To investigate how this solvents mixture influences the film properties the electrodes covered with S5_15s (Fig. 81) and S5_20s (Fig. 82) films have been prepared. Both films covered electrodes have been tested in the $Ru(NH_3)_6Cl_3$ and FDM solutions.

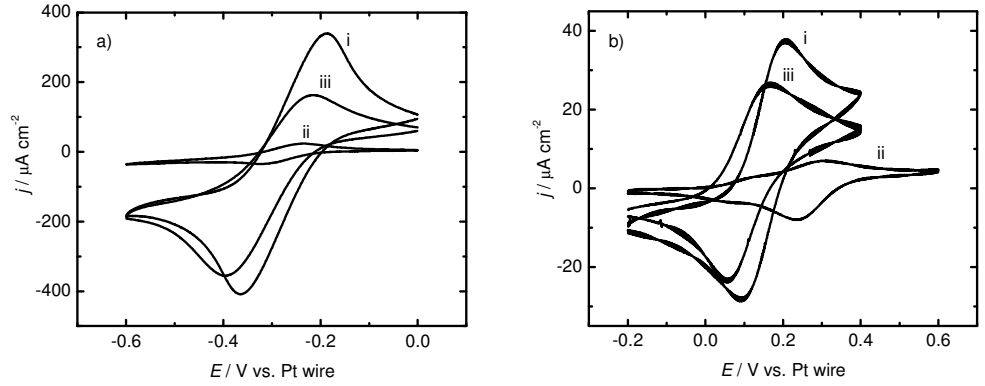

Fig. 81. a) Cyclic voltammograms obtained in 5 mM $Ru(NH_3)_6Cl_3$, 0.1 M $NaNO_3$ on the clean ITO electrode (i), S5_15s film modified electrode before (ii) and after (iii) surfactant removal. v= 20 mV s^{-1}. b) Cyclic voltammograms obtained in 0.5 mM FDM, 0.1 M $NaNO_3$ on the clean ITO electrode (i), S5_15s film modified electrode before (ii) and after (iii) surfactant removal. v= 20 mV s^{-1}.

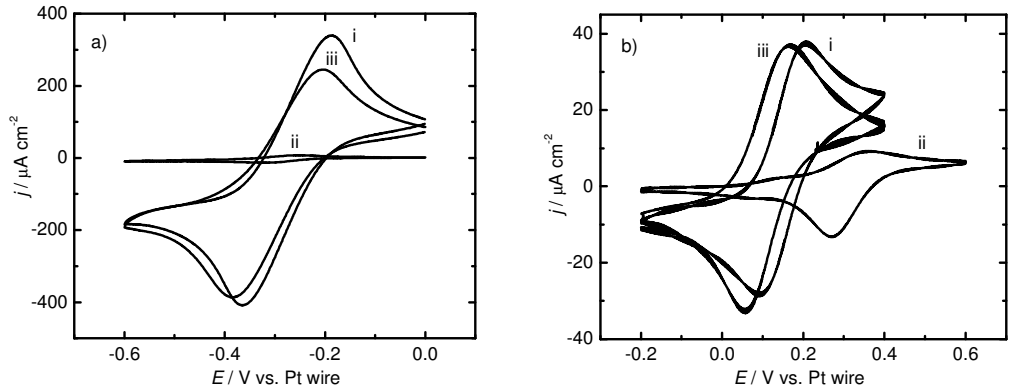

Fig. 82. a) Cyclic voltammograms obtained in 5 mM $Ru(NH_3)_6Cl_3$, 0.1 M $NaNO_3$ on the clean ITO electrode (i), S5_20s film modified electrode before (ii) and after (iii) surfactant removal. b) Cyclic voltammograms obtained in 0.5 mM FDM, 0.1 M $NaNO_3$ on the clean ITO electrode (i), S5_20s film modified electrode before (ii) and after (iii) surfactant removal. v= 20 mV s^{-1}.

The similar behavior as for the S1_15s film covered electrode have been observed in this case. However the S5_15s film blocking effect (Fig. 81) towards $Ru(NH_3)_6^{3+}$ is slightly smaller than for the S1_15s. After surfactant removal the current increases significantly, but it is still lower than that obtained for the clean ITO. The similar behavior was observed for the FDM. The above-mentioned differences may be connected with the incomplete electrode coverage and the less ordered structure of the film obtained from the mixture of solvents.

Probably some parts of the film are not porous or the wormlike and/or closed pores are present. This hinders the mass transport to the electrode and results in the lower peak currents.

To produce the full coverage of the electrode the deposition time have been elongated to 20 s then the white deposit is visible on the whole electrode surface. The obtained film covered electrodes have been tested in $Ru(NH_3)_6^{3+}$ and FDM solutions. This time the blocking effect of the film for $Ru(NH_3)_6^{3+}$ was clearly visible (Fig. 82b). After surfactant removal (Fig. 82c) the current was only slightly lower than the one obtained for the clean ITO in the same conditions (Fig. 82a). The similar behavior have been observed for the S5_20s film covered electrode immersed into the FDM solution. The strong blocking effect of the film gives evidence of the complete electrode surface coverage. The small differences in currents obtained on the clean ITO electrode and the S5_20s film covered electrodes after surfactant removal indicates the well ordered structure of the film. For the reasons described above the 20 s deposition time was used as a standard for further experiments with these films.

8.1.4. Electroassisted deposition of the hybrid film

The goal of the experiments described in this chapter was to introduce the imidazolium moieties to the electrogenerated film by cocondensation of the TEOS and P(TMOS)MIMNTF2 ionic liquid precursor.

First the 5% P(TMOS)MIMNTF2 sol have been prepared. It was found impossible to prepare the homogeneous sol by using the (S6) composition because of the lack of solubility of the TEOS in the acetonitrile. The sol preparation procedure has been changed. The P(TMOS)MIMNTF2 was dissolved in acetonitrile and TEOS was dissolved in water and both solutions have been mixed afterwards (S7).

The film obtained from S7 have been deposited on the ITO surface by applying the anodic potential for 20 s. Two types of films have been prepared. One (S7_20s) was deposited using the standard procedure with 2 h ageing step. Second one (S7_ON_20s) was aged overnight ageing (> 12 h). These films have been tested by voltammetry in $Ru(NH_3)_6Cl_3$ and K_4FeCN_6 solutions.

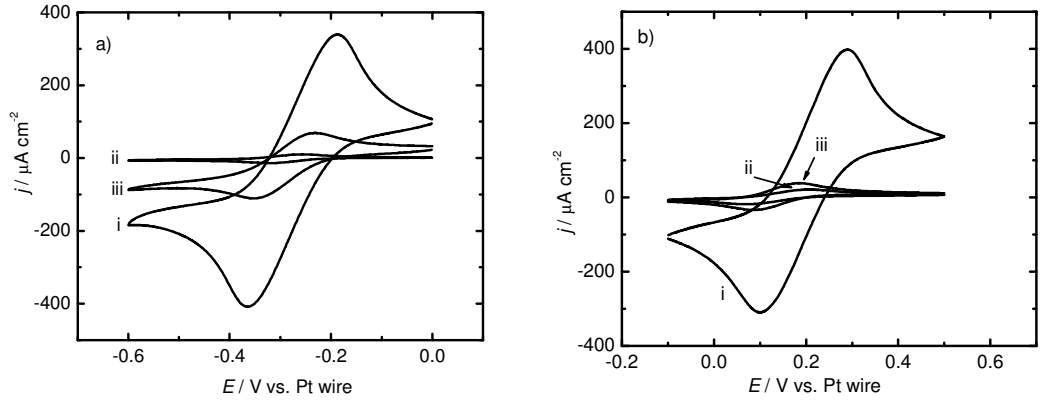

Fig. 83. a) Cyclic voltammograms obtained in 5 mM $Ru(NH_3)_6Cl_3$, 0.1 M $NaNO_3$ on the clean ITO electrode (i), S7_20s film modified electrode before (ii) and after (iii) surfactant removal. b) Cyclic voltammograms obtained in 5 mM K_4FeCN_6, 0.1 M $NaNO_3$ on the clean ITO electrode (i), S7_20s film modified electrode before (ii) and after (iii) surfactant removal. v= 20 mV s^{-1}.

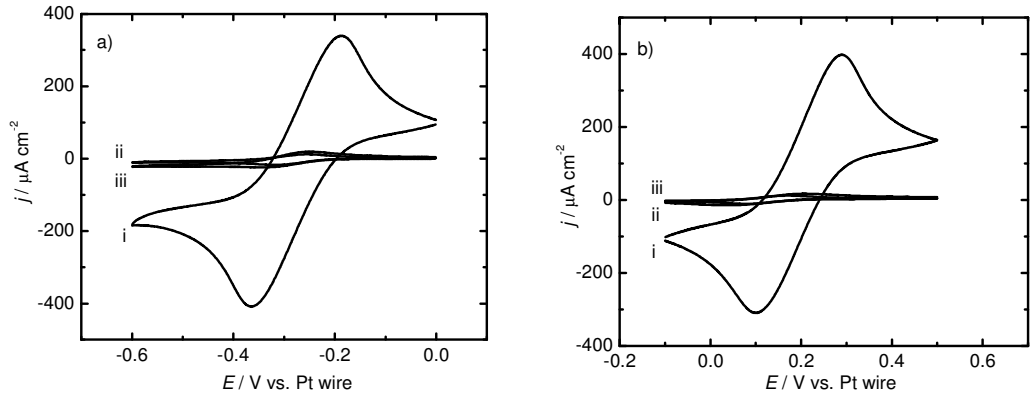

Fig. 84. a) Cyclic voltammograms obtained in 5 mM $Ru(NH_3)_6Cl_3$, 0.1 M $NaNO_3$ on the clean ITO electrode (i), S7_ON_20s film modified electrode before (ii) and after (iii) surfactant removal. b) Cyclic voltammograms obtained in 5 mM K_4FeCN_6, 0.1 M $NaNO_3$ on the clean ITO electrode (i), S7_ON_20s film modified electrode before (ii) and after (iii) surfactant removal. v= 20 mV s^{-1}.

The strong blocking effect of the S7_20s film was observed for both $Ru(NH_3)_6^{3+}$ and $Fe(CN)_6^{4-}$ redox probes (Fig. 83) even after surfactant removal. This can be caused by the different film structure film structure. Unlike for the films prepared from TEOS only, the pores in the S7_20s film seems to be strongly disorganized and their majority have no connections with electrode surface.

To be sure that the precursor molecules present in the initial sol have been well hydrolyzed the overnight aging step have been performed. However the peak currents obtained on such electrodes are even smaller (Fig. 84) than on standard ones (Fig. 83). It have

been concluded that these films are even less organized than ones obtained from sol aged for 2 h only.

One can conclude that even the small (5%) addition of P(TMOS)MIMNTF2 affects strongly the film structure. To get more information on this effect films from the sols with various P(TMOS)MIMNTF2 to TEOS molar ratios have been prepared. The electrodes behavior have been investigated in K_4FeCN_6, $Ru(NH_3)_6Cl_3$ and FDM solutions.

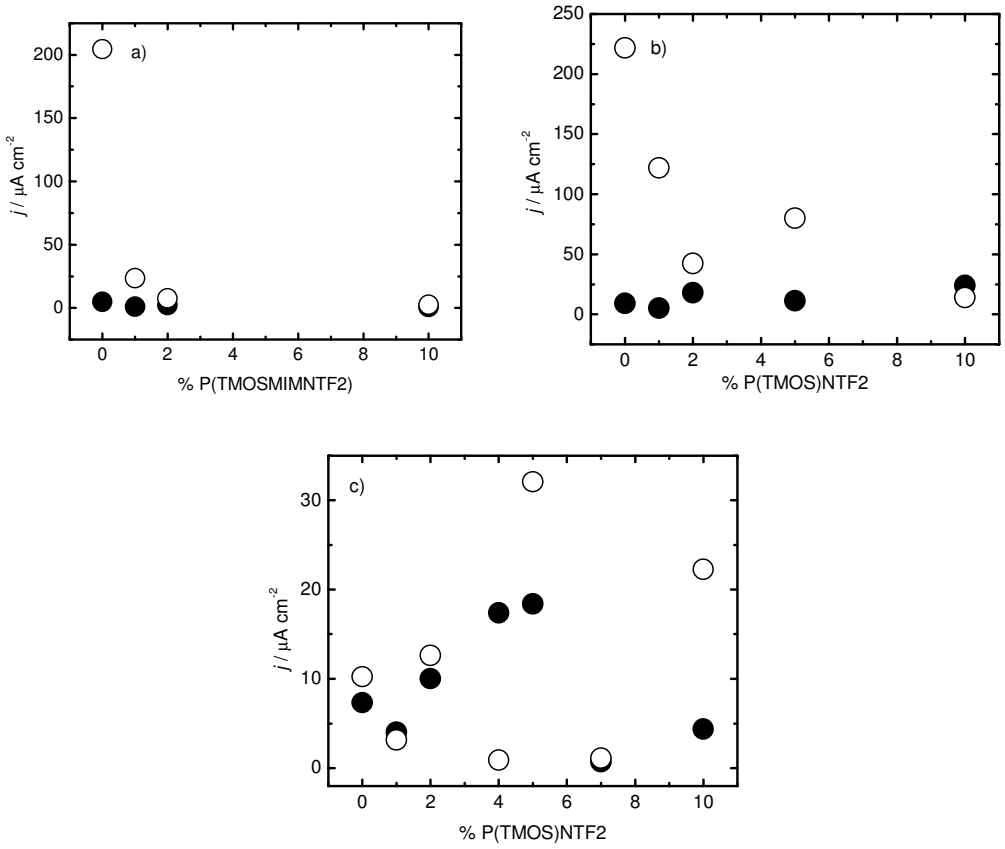

Fig. 85. Dependences of the peak currents on the P(TMOS)MIMNTF2 content for electrogenerated film modified electrodes before (●) and after (○) surfactant removal immersed into the 0.5 mM FDM (a), 5mM $Ru(NH_3)_6Cl_3$ (b) and 5 mM K_4FeCN_6 (c). 0.1 M $NaNO_3$ was used as a supporting electrolyte. v = 20 mV s^{-1}.

Let's consider the experiment with the FDM as a redox probe first (Fig. 85a.). On can see that when 1% of P(TMOS)MIMNTF2 was added into the initial sol, the resulting currents were lower than for the electrodes covered with films obtained from TEOS only. It can be concluded that the presence of the P(TMOS)MIMNTF2 molecules prevents forming the organized film structure. The higher the P(TMOS)MIMNTF2 content, the stronger the blocking effect of the film and the lower the film organization. Very similar behavior have

been observed for the electrodes immersed into the $Ru(NH_3)_6Cl_3$ solution (Fig. 85b.). Again the more P(TMOS)MIMNTF2 was added to the sol the less permeable the resulting film was.

Quite complex behaviour have been observed for the $Fe(CN)_6^{4-}$ redox probe (Fig. 85c.). In the case of 1% P(TMOS)MIMNTF2 addition the typical current drop connected to the distortion of the film structure was observed. However, when more P(TMOS)MIMNTF2 was present in the sol the current increase was observed. It is not surprising taking into the consideration the results described in chapter 14.7.1. In general the more imidazolium groups have been introduced into the material the stronger the anion accumulation is. It seems that both above-mentioned parallel effects explains the presence of the maximum on the plot starts to be justified.

It is important to emphasize that the peak currents obtained for the P(TMOS)MIMNTF2 containing films modified electrodes are at least an order of magnitude lower than ones recorded for the clean ITO electrodes in the same conditions. This is the reason why the collected date were so scattered.

In order to increase anion accumulation two different approaches have been attempted. First the precursors concentration was increased to 250 mM (10 times more than usual) (S13) with the ratio of P(TMOS)MIMNTF2 to TEOS equal 5%. The second approach was to increase the P(TMOS)MIMNTF2 to TEOS ratio up to 30% leaving the precursors concentration on 25 mM level (S14). In both cases the currents observed for the film covered electrodes were still much lower than for the clean ITO electrode even though there was an anion accumulation effect observed on the S14_20s film covered electrode immersed into the K_4FeCN_6 solution (Fig. 86).

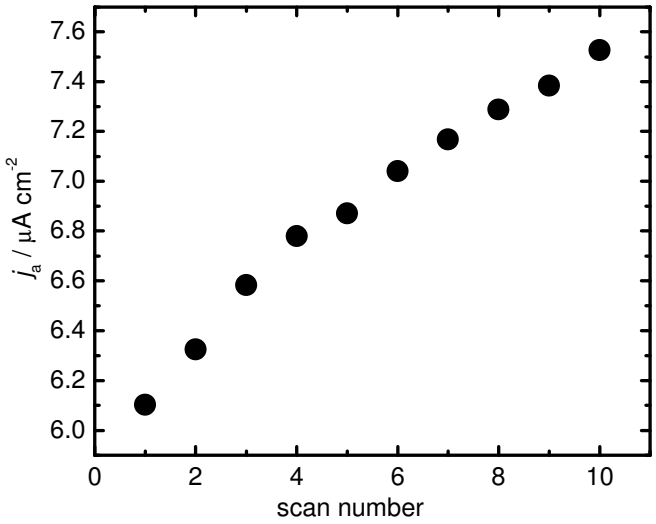

Fig. 86. Anodic peak current vs. scan number for the S14_20s film covered electrode immersed into the 5 mM K_4FeCN_6, 0.1 M $NaNO_3$. v = 20 mV s^{-1}.

In the next experiments sodium dodecyl sulfate (SDS) have been used as a template instead of CTAB (S15). It was necessary to optimize the deposition time for the new sol and the stable films are obtained within 50s. The 15_50s film covered electrodes were next investigated in K_4FeCN_6 and FDM solutions.

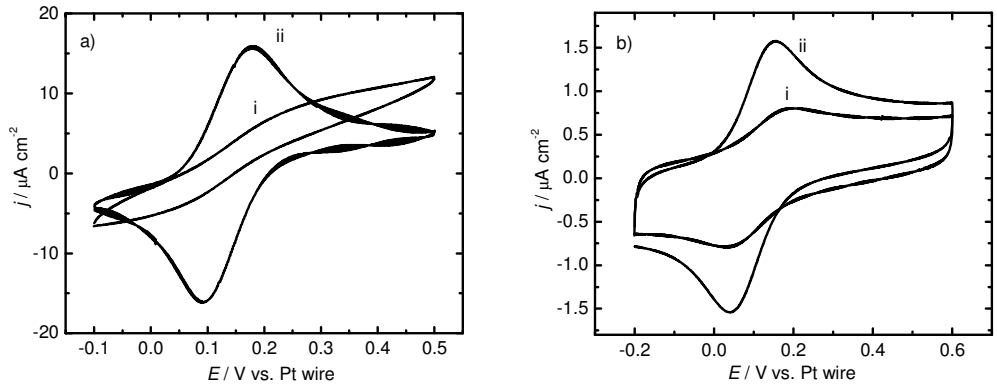

Fig. 87. Fig. 40. a) CVs obtained in 5 mM K_4FeCN_6, 0.1 M $NaNO_3$ on the S15_50s film modified electrode before (i) and after (ii) surfactant removal. b) CVs obtained in 0.5 mM FDM, 0.1 M $NaNO_3$ on the S15_50s film modified electrode before (i) and after (ii) surfactant removal. v= 20 mV s^{-1}.

Clearly, the obtained film strongly blocks the electrode surface towards $Fe(CN)_6^{4-}$ and FDM redox probes (Fig. 87). After the surfactant removal procedure the CV curves was found to be well defined (Fig. 87a curve i, b curve i) However peak currents are significantly lower than ones obtained on the clean ITO. Perhaps it is difficult to form the pores with the good

contact with electrode surface. This can be explained by the repulsion forces between the negatively charged surfactant molecules and the negatively polarized electrode surface necessary for sol gel film deposition.

Concluding, electroassisted deposition is not the best method to obtain hybrid imidazolium group bearing silicate films with good accumulation properties. The biggest problem is that increase of the amount of ionic liquid precursor which increases the material accumulation properties also decreases organization of the film. So even though a great amount of anions is perhaps accumulated in the film they cannot be electrochemically detected, because of blocked access to the electrode surface. On the other hand when the film is highly permeable, the amount of imidazolium groups is not sufficient to get the significant accumulation effect.

8.2. Grafting

In order to deal with the problems described in the previous chapter, the new approach to synthesizing the imidazolium bearing hybrid films have been applied.

First the pure silicate films with well developed hexagonal structure have been prepared. Next the surfactant have been removed from the pores with the 0.1 M HCl_{aq} ethanol mixture (1:1) (5 min vigorous stirring). The grafting mixture have been prepared by dissolving the 0.0525g of P(TMOS)MIMNTF2 in 100 ml of acetonitrile. The acetonitrile have been chosen because of the good solubility of P(TMOS)MIMNTF2 in this solvent. To graft imidazolium group onto the silicate film the ITO slide with the film on it was immersed into the grafting solution. The mixture was refluxed for 2 h. After the grafting procedure the electrodes have been rinsed with acetonitrile and left to dry.

These electrodes have been immersed into the 1 mM $K_3Fe(CN)_6$, 0.1 M KCl solution and the CVs have been recorded (Fig. 88a). It can be seen that the film covered electrode was strongly blocked against $Fe(CN)_6^{3-}$ ions even after surfactant removal. This behavior can be explained by the electrostatic repulsion between the negatively charged redox probe and the negatively charged SiO_2 film pores' walls.

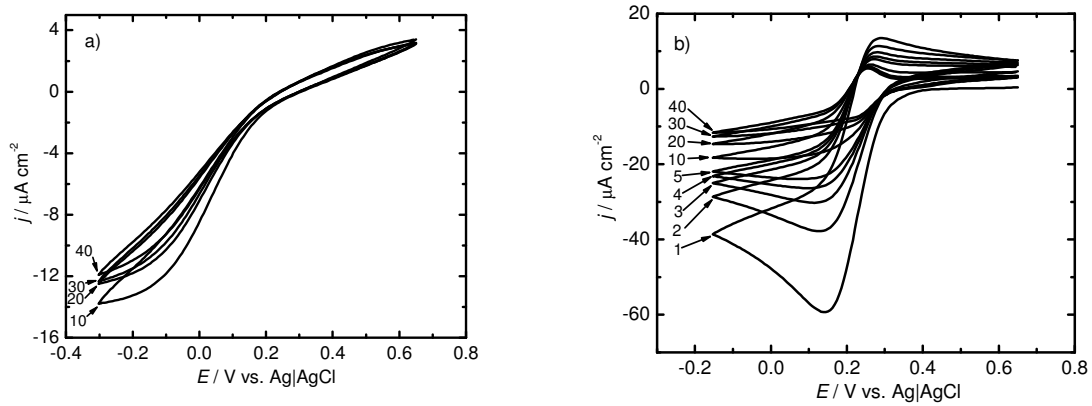

Fig. 88. CVs obtained with ordered silicate film covered ITO electrodes before (a) and after (b) grafting procedure immersed into the 1 mM $K_3Fe(CN)_6$, 0.1 M KCl. The numbers on the pictures indicates subsequent scans. v = 10 mV s^{-1}.

After the grafting procedure the current clearly increased (Fig. 88b). The shape of the CV has also changed. Well defined peaks connected with the $Fe(CN)_6^{3-/4-}$ redox couple reactions have appeared. The presence of the imidazolium groups facilitates the negatively charged redox probe transport through the film to the electrode surface. However, there is a current decrease observed during the experiment. This is probably connected with the film degradation. The peak currents are higher than for the pure silicate film covered electrode, but still significantly lower then for the bare ITO electrode.

The reason for low currents obtained for describe electrodes may be that there was some water present in the silicate film. Its presence may cause the P(TMOS)MIMNTF2 deposition not only on the pore walls, but also gel formation in the volume of pores. The above mentioned process could lead to the pores blocking and to limitation of the current.

9. Imidazolium modified silicate particles

Electrodes modified with particles and nanoparticles have many advantages over the standard electrodes like: enhancement of mass transport, catalytic properties, high effective surface and possibility to control the electrode microenvironment [377]. It was demonstrated that mass transport for the particulate can be rather described by hemispherical not linear diffusion model [476]. More importantly, the nanoparticles can decrease overpotential of some reactions [398]. This allows to separate the electrochemical response from various analytes (e.g. dopamine and ascorbic acid) which interferes with each other if macroelectrode is being used [398]. The high effective surface area is connected to the high surface atoms fraction in nanoparticles. The combining of other materials with nanoparticles allows for the latter immobilization and control the electrode microenvironment. Many of such composite materials have been shown to posses the unique properties which are not observed for the pure components [288].

In this chapter the synthesis of P(TMOS)MIMNTF2 modified silicate particles will be described. These particles have been characterized by SEM and gas porosimetry. Non-conductive character of the material causes that the electrochemical investigation of the particles was possible only after their immobilization in the carbon paste electrode, carbon ceramic electrode or directly on the ITO electrode surface by solvent evaporation.

9.1. Synthesis and characterization of particles

9.1.1. Synthesis

The P(TMOS)MIMNTF2 modified silicate particles have been synthesized via modified Stober method [326]. 0.5 g CTAB, 3 ml NH_3 (25%) and 9 ml methanol with 10 ml H_2O was mixed together. A mixture of 0.105 g of P(TMOS)MIMNTF2, and 0.58 g of TMOS and 1 ml methanol was added to the solution and have been stirred vigorously. The ammonia catalyst causes the formation of pseudospherical particles [477] and the surfactant acts a template for porous material formation [326]. After 2 h a white precipitate was filtered off, rinsed with ethanol and left to dry in ambient conditions. After 24 h of drying the white powder was refluxed in a mixture of ethanol and 1 M HCl (ratio 1:1) for another 24 h to remove the surfactant. The final product was filtered, rinsed with ethanol and left to dry (Fig. 89). Non modified particles for blank experiments were prepared in the similar way from only TMOS as a precursor.

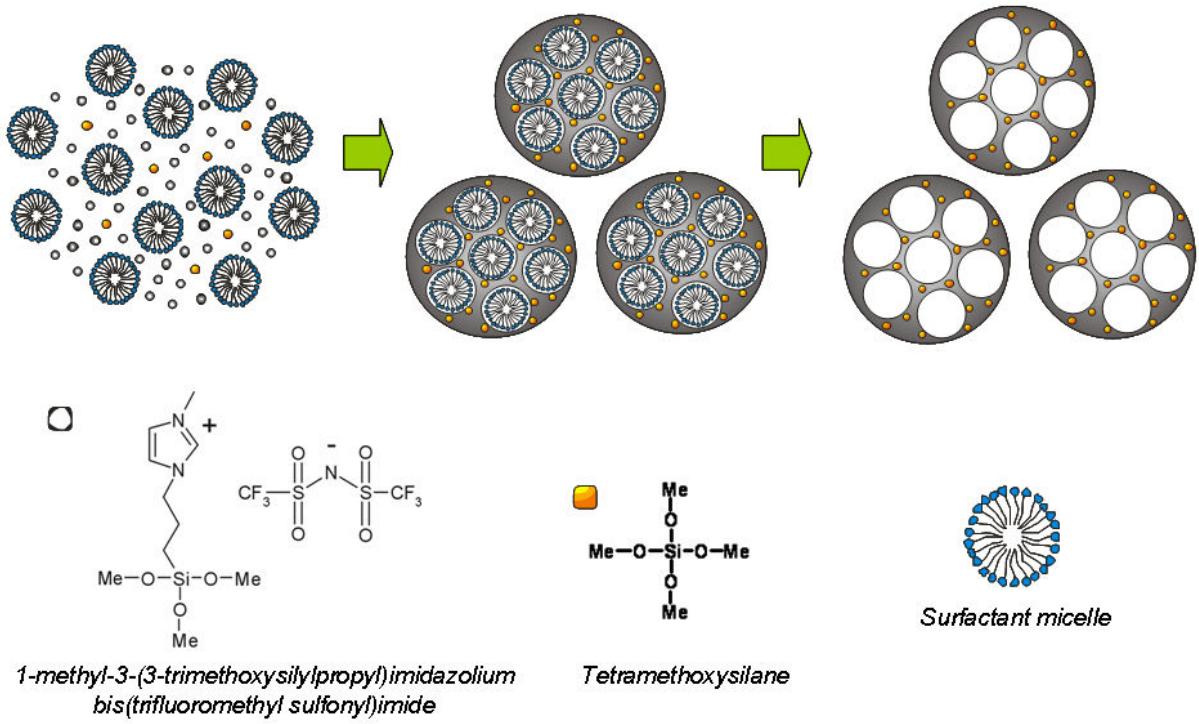

Fig. 89. Ionic liquid modified silicate particles' synthesis scheme

9.1.2. SEM analysis

Ionic liquid particles have been observed with SEM. Because of the non-conductive character of particles a carbon sputtering was necessary to obtain the image.

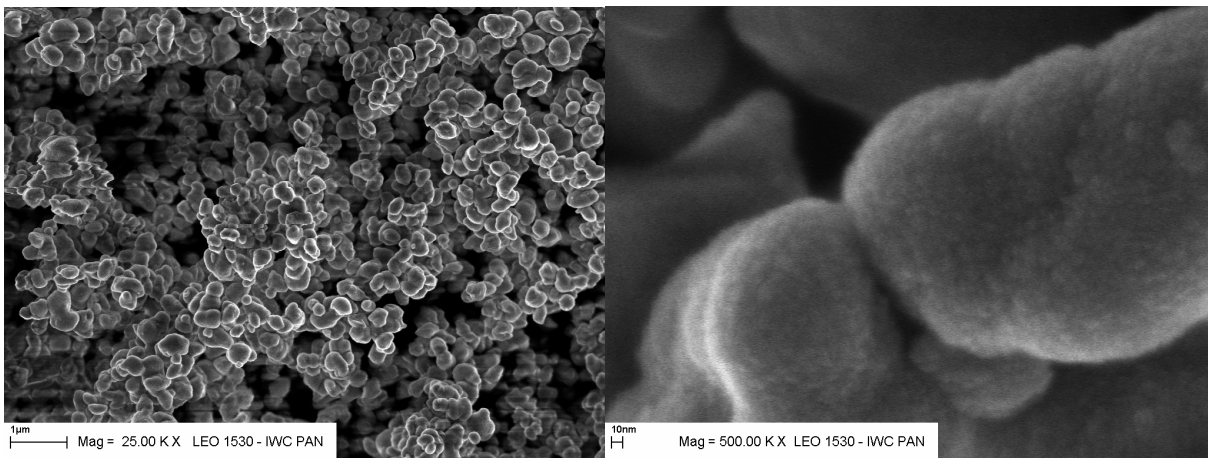

Fig. 90. SEM images of P(TMOS)MIMNTF2 modified silicate particles.

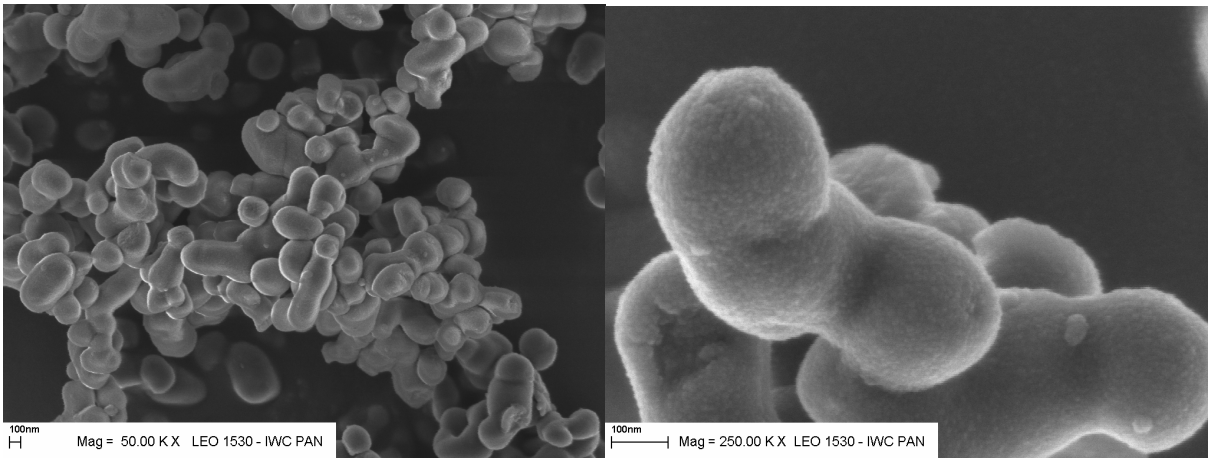

Fig. 91. SEM images of the silicate particles.

On the SEM micrographs the particulate character of the obtained material can be observed. The shape of particles is irregular and their average size was estimated to ca. 200 nm. On some parts of the electrode the bigger agglomerates of several particles have been found (Fig. 90). The presence of P(TMOS)MIMNTF2 influences the obtained particles morphology. The shape of the hybrid particles is more angular and their surface have looked less smooth then of the pure silicate particles (Fig. 91).

9.1.3. Gas porosimetry

To learn more about the porosity of the new material the gas porosimetry experiment have been performed. The nitrogen adsorption measurements at 77 K confirm that the obtained hybrid nanoparticles are porous. Their specific surface area determined with the BET method is 860 ± 30 m^2 g^{-1}. It is somewhat smaller than that of silicate particles (995 ± 47 m^2 g^{-1}) obtained by the same method. These average pore width is equal ca. 2 nm (Fig. 92). Therefore according to the IUPAC notation [478] this material can be classified between micro- and mesoporous material.

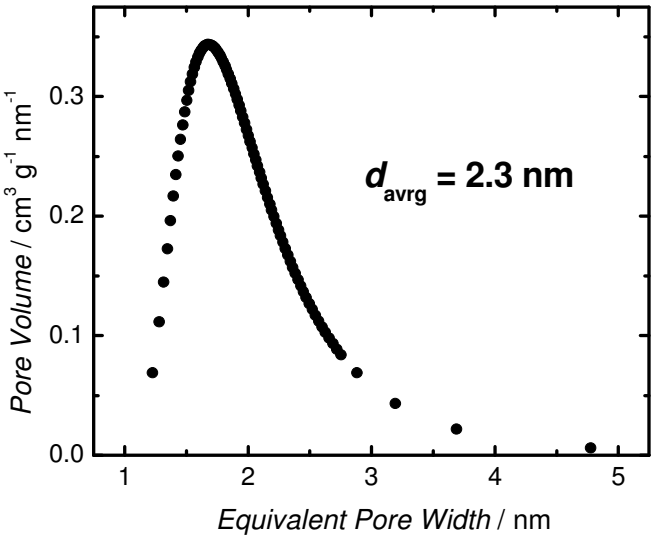

Fig. 92. Porosity diagram of IL modified particles

9.2. Electrodes modified with imidazolium modified silicate particles.

9.2.1. Carbon paste electrodes.

A typical approach to investigate non-conductive materials with electrochemical methods is to incorporate such materials in the carbon paste electrode [14]. The carbon paste electrodes described in this chapter were prepared by mixing suitable amounts of graphite powder (1μm), ionic liquid modified or pure silicate particles and a binder (Table 2).

Table 2. Compositions of various pastes used for CPE preparation.

Code	Paste composition	Particles content
P1	70 μl hexadecane 0.025 g graphite powder 0.025 g P(TMOS)MIMNTF2 modified silicate particles	50%
P2	70 μl hexadecane 0.05 g graphite powder 0.005 g P(TMOS)MIMNTF2 modified silicate particles	9%
P3	70 μl hexadecane 0.05 g graphite powder 0.0125 g P(TMOS)MIMNTF2 modified silicate particles	20%
P4	70 μl hexadecane 0.05 g graphite powder	30%

	0.0214 g P(TMOS)MIMNTF2 modified silicate particles	
P5	70 µl hexadecane 0.05 g graphite powder 0.0214 g pure silicate particles	30%
P6	70 µl hexadecane 0.05 g graphite powder	0%
P7	70 µl hexadecane 0.05 g graphite powder 0.0125 g pure silicate particles	20%
P8	70 µl P(TMOS)MIMNTF2 0.05 g graphite powder	0%

The paste components have been mixed and placed in the 2 mm deep cavity of the 1.55 mm inner diameter glass tubing filled tightly with a cooper wire. The electrode front was polished with a smooth paper and its geometric surface area is 0.02 cm^2 (Fig. 93).

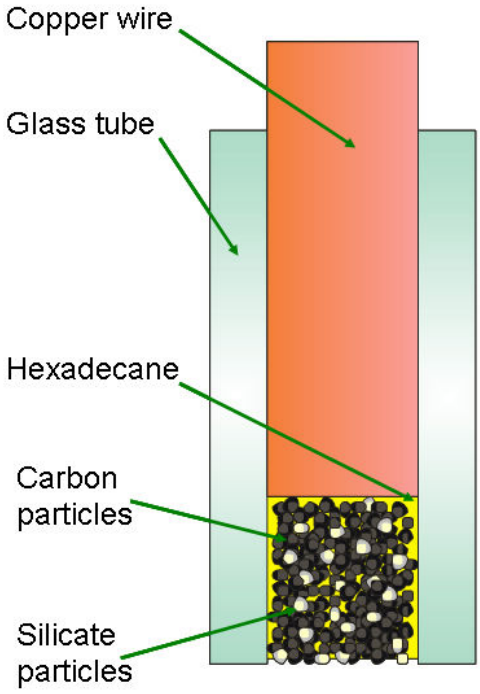

Fig. 93. Carbon paste electrode construction's scheme.

9.2.1.1. Contact angle measurements

Surface hydrophobicity may have high impact on electrochemical behavior of the electrode. To get information about CPEs surface hydrophobic properties, contact angle measurements have been performed. For this experiment CPEs were prepared in an usual way in the glass tubing with 5 mm inner diameter. The water droplet (2 µl) have been placed on the CPE surface and the contact angle have been measured with the home made device (Fig. 94). There were ten measurements performed for each type of the electrode: CPE (P6), pure silicate particles modified CPE (P7) and P(TMOS)MIMNTF2 modified silicate particles modified CPE (P3).

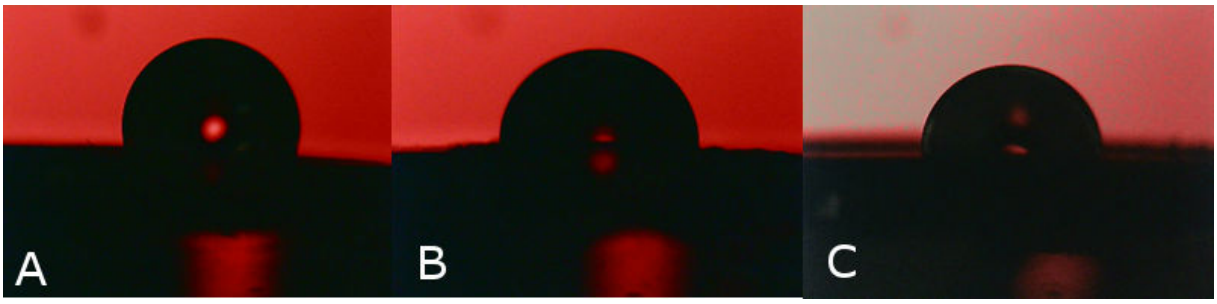

Fig. 94. Water droplet on the surface of CPE (A), pure silicate particles modified CPE (B) and P(TMOS)MIMNTF2 modified silicate particles modified CPE (C).

It was found that the largest contact angle measured is for the CPE electrode (θ = 84.4 ± 3.5). It means that the CPE surface was relatively hydrophobic. The addition of pure silicate particles makes the electrode surface more hydrophilic (θ = 81.2 ± 5.3). If the P(TMOS)MIMNTF2 modified silicate particles was added to the paste the surface of the electrode was even more hydrophilic (θ = 74.6 ± 2.9). This indicates that the modified particles are more hydrophilic than unmodified ones. As it will be described in the next chapter these properties have a strong impact on electrochemical behavior of the electrodes.

9.2.1.2. Electrochemical measurements

The series of electrochemical experiments have been performed in order to characterize a new IL modified silicate material. First the CPE (P6), pure silicate particles modified CPE (P7) and P(TMOS)MIMNTF2 modified silicate particles modified CPE (P3) were immersed into the 1 mM $K_3Fe(CN)_6$, 0.1 M KCl solution and the CV experiment have been performed. The potential was swept constantly and the 100^{th} scans have been compared (Fig. 95).

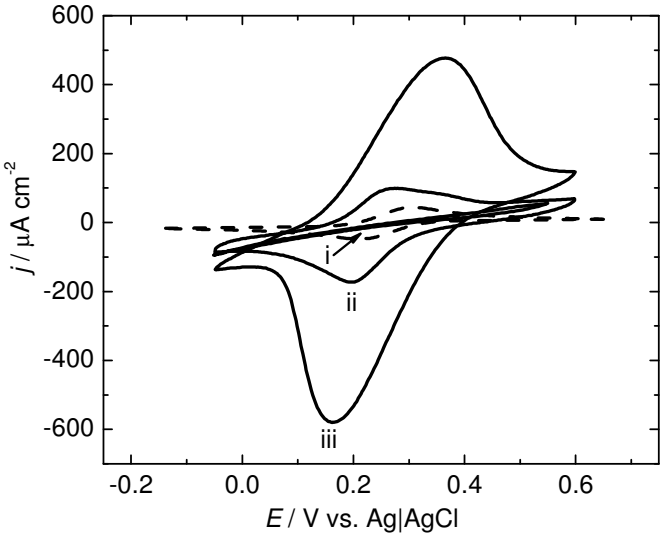

Fig. 95. 100th CV scans obtained for CPE (P6) (i), pure silicate particles modified CPE (P7) (ii) and P(TMOS)MIMNTF2 modified silicate particles modified CPE (P3) (iii) immersed into the 1 mM $K_3Fe(CN)_6$, 0.1 M KCl solution. Dashed line was obtained for the bare ITO electrode in the same conditions.

It can be clearly seen that in the presence of the pure silicate particles in the paste the peaks from $Fe(CN)_6^{4-}/Fe(CN)_6^{3-}$ redox couple are well visible (Fig. 95 curve ii) in comparison to the non-modified CPE (Fig. 95 curve i). This is probably caused by the electrochemically active surface development. The porous silicate particles incorporated in the paste can be penetrated with the electrolyte what makes the electrode surface accessibility for the redox probe much higher. There is no CV signal corresponding to $Fe(CN)_6^{4-}/Fe(CN)_6^{3-}$ redox couple on the unmodified CPE electrode (P6). Probably the carbon particles are covered by insulating and hydrophobic binder blocking access of hydrophilic redox active anions to carbon particles.

One can see that the peak currents are even higher for the CPE modified with P(TMOS)MIMNTF2 modified silicate particles then for the pure silicate particles modified CPE. In the first case besides of the surface development effect also anion accumulation process takes place. This is because of the presence of positively charged imidazolium groups in the particles structure. One can see that currents densities were higher than one obtained on ITO electrode for both (P7) and (P3) CPEs. This is caused by above-mentioned factors: surface development and ion accumulation process.

The next step was to check how the amount of IL modified particles influences on the electrochemical response from $Fe(CN)_6^{4-}/Fe(CN)_6^{3-}$ redox couple. Three electrodes with

different amount of modified particles have been immersed into the 1 mM $K_3Fe(CN)_6$, 0.1 M KCl solution and the CVs have been recorded (Fig. 96). It was impossible to perform such experiment for the electrode with 50% IL modified particles (P1). The water penetrates the electrode up to the cooper wire, what is caused by the high content of hydrophilic material in the paste.

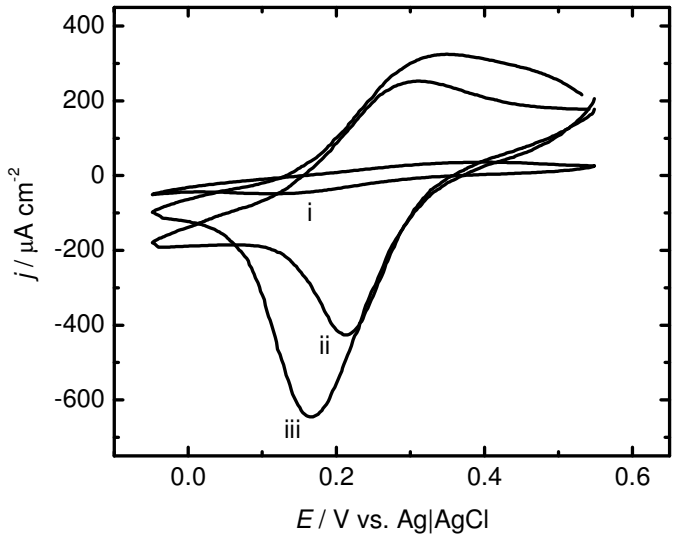

Fig. 96. 60th CV scans obtained for CPE modified with 9% (i), 20% (ii) and 30% (iii) P(TMOS)MIMNTF2 modified silicate particles immersed in the 1 mM $K_3Fe(CN)_6$, 0.1 M KCl solution.

It was found that the higher the content of IL modified particles in the paste the higher the faradic current is. In other words, the higher the content of imidazolium groups the more effective is the anion accumulation. This observation is in the agreement with earlier experiments obtained earlier for the film modified electrodes (Fig. 52).

CPE with 20% silicate (P7) or IL modified (P3) silicate particles have been chosen for further experiments. This amount is high enough to allow one to observe their influence on the electrode behavior and small enough to prevent water penetrating of the electrode material. Various redox probes such as $IrCl_6^{3-}$, $Fe(CN)_6^{3-}$, $Fe(CN)_6^{4-}$ and $Ru(NH_3)_6^{3+}$ have been tested on both electrodes. Electrodes have been immersed into the 0.1 mM solutions of the redox probes in the 0.1 M $NaClO_4$. Cyclic voltammograms have been recorded in every 5 min. The results obtained for CPE modified with the pure and IL modified silicate particles modified electrodes have been compared.

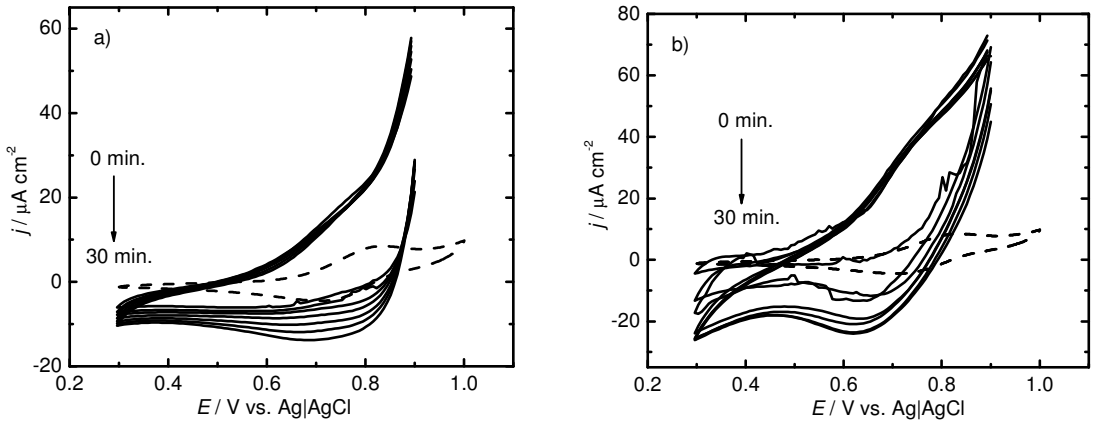

Fig. 97. CVs obtained for the pure (a) or IL modified (b) silicate particles modified CPEs immersed into the 0.1 mM K_3IrCl_6, 0.1 M $NaClO_4$. CVs were recorded in every 5 min. v = 10 mV s^{-1}. Dashed curves were obtained for bare ITO electrodes in the same conditions.

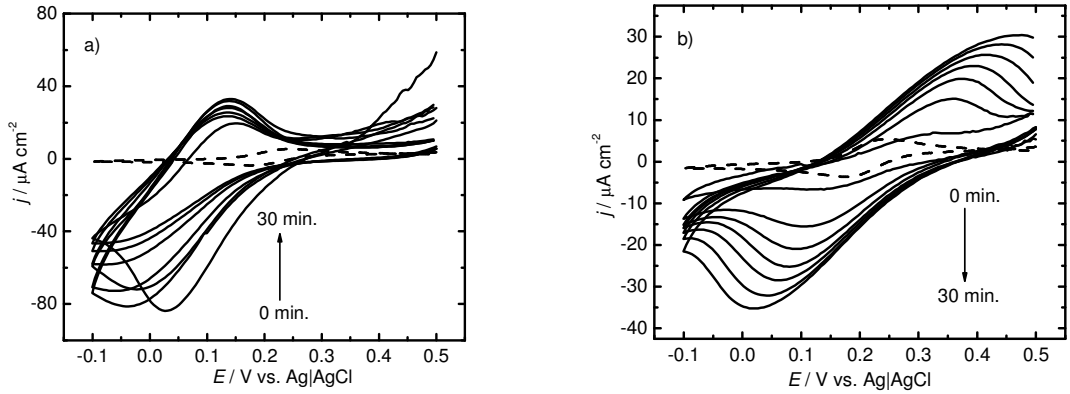

Fig. 98. CVs obtained for the pure (a) or IL modified (b) silicate particles modified CPEs immersed into the 0.1 mM $K_3Fe(CN)_6$, 0.1 M $NaClO_4$. CVs were recorded in every 5 min. v = 10 mV s^{-1}. Dashed curves were obtained for bare ITO electrodes in the same conditions.

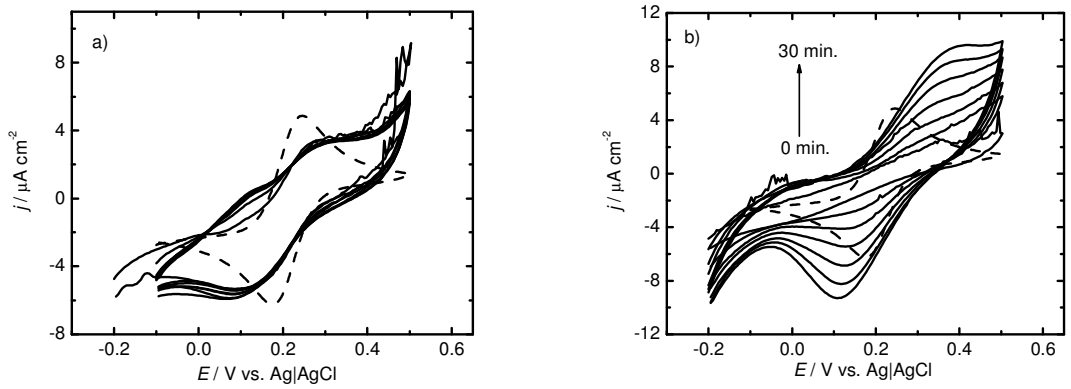

Fig. 99. CVs obtained for the pure (a) or IL modified (b) silicate particles modified CPEs immersed into the 0.1 mM $K_4Fe(CN)_6$, 0.1 M $NaClO_4$. CVs were recorded in every 5 min. v = 10 mV s^{-1}. Dashed curves were obtained for bare ITO electrodes in the same conditions.

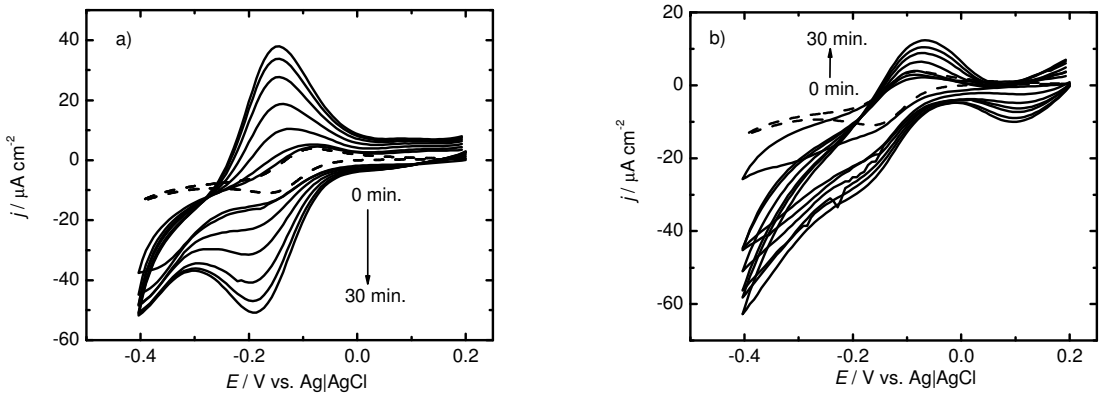

Fig. 100. CVs obtained for the pure (a) or IL modified (b) silicate particles modified CPEs immersed into the 0.1 mM $Ru(NH_3)_6Cl_3$, 0.1 M $NaClO_4$. CVs were recorded in every 5 min. v = 10 mV s^{-1}. Dashed curves were obtained for bare ITO electrodes in the same conditions.

The peak current is ca. 50% higher on the electrode with IL modified particles in comparison to one modified with silicate particles in the presence of $IrCl_6^{3-}$ electroactive anion (Fig. 97). The effect is connected with electroactive anions accumulation. There is an additional cathodic process observed on the voltammograms and its nature is not clear.

The effect of the presence of imidazolium groups have been clearly observed in the case of $Fe(CN)_6^{3-}$ / $Fe(CN)_6^{4-}$ redox couple (Fig. 98, Fig. 99). Anion accumulation process was only observed for the hybrid particles modified electrodes. There was no such effect for the electrodes modified with pure silicate particles. This phenomenon clearly indicates that the presence of positively charged imidazolium groups causes the anion accumulation.

An interesting behavior have been observed for the electrodes immersed in the $Ru(NH_3)_6Cl_3$ solution. If the electrode was modified with hybrid particles no accumulation effect have been observed (Fig. 100b) It was because of electrostatic repulsion of the redox probe by imidazolium groups present in the electrode material. Surprisingly the accumulation effect have been observed on the electrode modified with pure silicate particles (Fig. 100a). This can be explained by the presence of the negative charge on the SiO_2 surface. In order to understand it better an additional experiment have been performed. The electrodes modified with pure silicate particles have been immersed into the 0.1 mM $Ru(NH_3)_6Cl_3$ solutions in 0.1 M citrate buffers of various pHs. Every electrode have been kept in the solution for 30 min. and CV have been recorded.

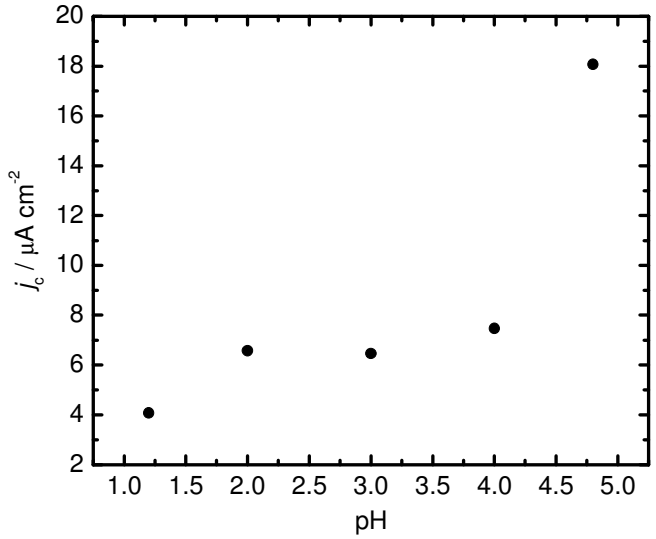

Fig. 101. Cathodic current densities vs. solution pH plot for the CPE electrode modified with pure silicate particles (P7) immersed into the 0.1 mM $Ru(NH_3)_6Cl_3$ solutions in 0.1 M citrate buffers of various pHs. $v = 10$ mV s^{-1}.

It was found that cathodic peak current connected with the (2) reaction is nearly constant for the low pH (< SiO_2 isoelectric point). At low pH groups present on the oxide surface are protonated and the surface charge is positive and it repels $Ru(NH_3)_6^{3+}$ cations. When the solution pH reach 5 (higher then SiO_2 isoelectric point) a significant increase of the current density have been observed (Fig. 101). This is because many OH groups present on the oxide surface are deprotonated and the charge of the surface is negative. It can be compensated, among others, by $Ru(NH_3)_6^{3+}$ cations.

During the investigation of the CPE modified with pure silicate particles other interesting observation have been done. After immersion of this electrode into the 1 mM

$K_3Fe(CN)_6$, 0.1 M KCl a CV experiment have been performed. The first scan had a typical shape for the $Fe(CN)_6^{3-}/Fe(CN)_6^{4-}$ redox couple. However in the next scans the new pair of peaks have appeared (Fig. 102a). The mid-peak potential is ca. 150 mV vs. Ag|AgCl with peak separation ca. 50 mV what has suggested the surface nature of the process. It was concluded that observed pair of the peaks is due to the Prussian blue growth in the silicate particles' pores (19) [67].

$$K_2Fe^{II}[Fe^{II}(CN)_6] \leftrightarrow KFe^{III}[Fe^{II}(CN)_6] + e^- + K^+ \quad (19)$$

To verify this hypothesis the experiment have been repeated with wider potential range. Now the characteristic Prussian Blue growing voltammetric pattern could be clearly observed (Fig. 102b). It is known from the literature [479] that the $Fe(CN)_6^{3-}$ anion may react as follows:

$$Fe^{III}(CN)_6^{3-} + 6H^+ \leftrightarrow Fe^{3+} + 6HCN \uparrow \quad (20)$$

The acidic environment necessary for Fe^{3+} cations formation results probably from HCl used for the surfactant removal. If the particles were carefully rinsed with ethanol no Prussian blue growing pattern have been observed.

When the Fe^{3+} cations and the $Fe(CN)_6^{3-}$ anions have been already present in the reaction mixture the Prussian blue could be formed in the usual way:

$$Fe^{3+} + Fe^{III}(CN)_6^{3-} \rightarrow Fe^{III}[Fe^{III}(CN)_6] \quad (21)$$

Additionally the cathodic peak current was found to be linearly dependent on the square root of the scan rate (Fig. 102a). Such behavior indicates the diffusion limited process. Despite of the fact that the Prussian Blue was adsorbed at the electrode surface a diffusion process was the limiting step. The most probably the diffusion of the K^+ cations is necessary to maintain the electroneutrality of the different forms of the deposit [480].

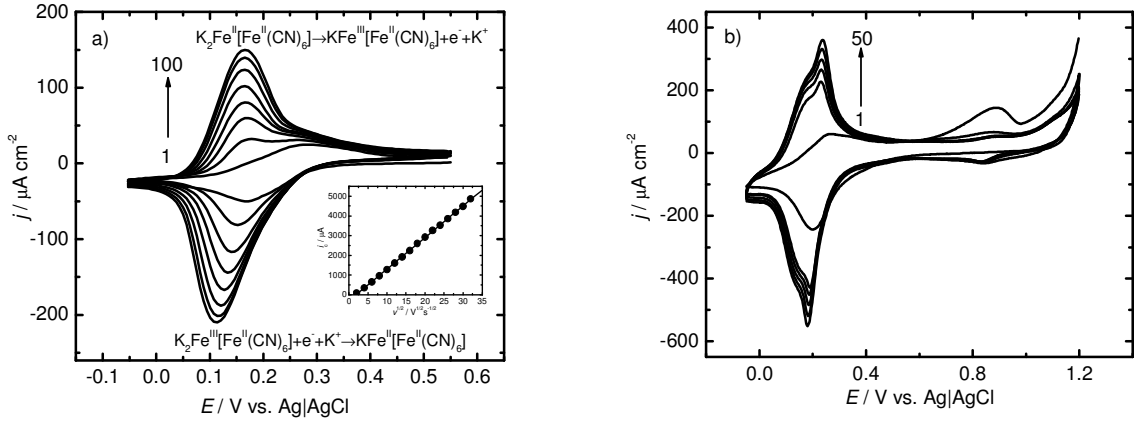

Fig. 102. CVs obtained for the pure silicate particles modified CPE (P7) immersed into the 1 mM $K_3Fe(CN)_6$, 0.1 M KCl. A potential was scanned between -0.5 V and 0.55 V vs. Ag|AgCl. Inset shows the dependence of the cathodic peak current on the square root of the scan rate. (a) or 0 V and 1.2 V vs. Ag|AgCl (b). Arrow shows the direction of current changes from scan to scan. Every fifth scan have been plotted. v = 10 mVs^{-1}.

9.2.2. Suspension drop deposition.

Despite of the fact that the incorporation of ionic liquid modified silicate particles in CPEs have given us a lot of information about the new material this method is not most convenient. There are several problems with preparation of the silicate modified CPEs. The reproducibility of the electrochemical results is not satisfactory. The biggest problem was the penetration of the electrode material by the electrolyte especially in the case of higher load of hydrophilic particles. This made impossible to obtain the electrode with high silicate particles content. To bypass all these problems an alternative approach based on the suspension drop deposition was proposed.

For particles deposition ITO electrodes were rinsed with ethanol, then with deionized water and finally with hot redistilled water. Next they were heated in 500 °C for 30 min to remove organic impurities. The active surface was defined by masking off an area of 0.2 cm^2 with a scotch tape. Electric contact was assured by using a piece of copper tape. For electrode modification 5 mg of particles was suspended in 1 ml of methanol. After 30 min sonication 5 µl of the suspension was cast onto the freshly prepared ITO surface. After solvent evaporation the electrode was ready for experiments.

9.2.2.1. Electrochemical measurements

The electrodes obtained by the suspension drop deposition have been investigated with electrochemical methods. The hybrid particles modified electrode have been immersed into

the 1 μM $K_3Fe(CN)_6$, 0.1 M $NaClO_4$. The series of CV curves have been recorded (Fig. 103a). It was clearly visible that accumulation process takes place. The voltammogram characteristic for the $Fe(CN)_6^{3-}/Fe(CN)_6^{4-}$ redox couple obtained just after immersion was nearly the same as for the clean ITO in the same conditions. However peak current are increasing in subsequent scans to reach ca. five times higher value in the 60th scan indicating the accumulation (Fig. 103).

In order to check stability of redox anion accumulation the electrode saturated with $Fe(CN)_6^{3-}$ anions was immersed into the clean supporting electrolyte. The current decrease from scan to scan was observed in this case (Fig. 103bii). The observed behavior clearly shows that large fraction of the accumulated $Fe(CN)_6^{3-}$ anions are gradually exchanged with the nonelectroactive ClO_4^- anions.

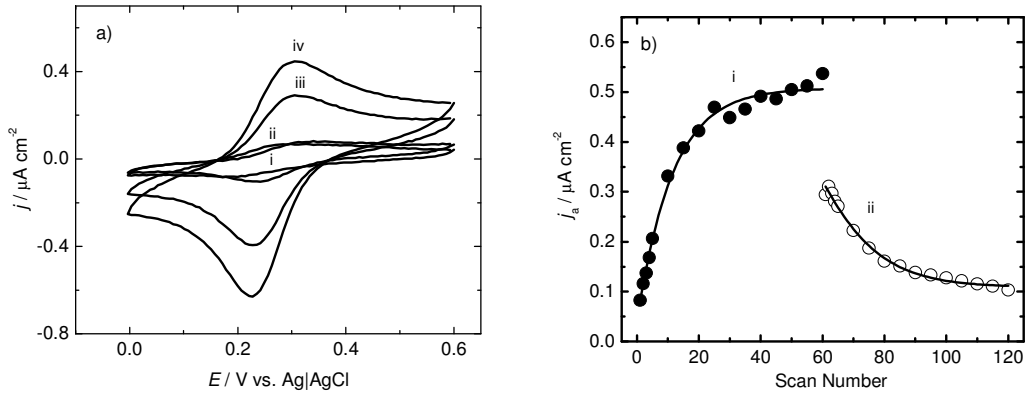

Fig. 103. a) Cyclic voltammograms obtained for the clean ITO electrode (i) or hybrid particles modified electrode (1st (ii), 10th (iii) and 60th (iv) scan) immersed in the 1 μM $K_3Fe(CN)_6$, 0.1 M $NaClO_4$. b) Anodic current density vs. scan number for the hybrid particles modified electrode immersed into the 1 μM $K_3Fe(CN)_6$, 0.1 M $NaClO_4$ (i) and 0.1 M $NaClO_4$ (ii) subsequently. v = 10 mVs^{-1}

9.2.3. Immersion followed by solvent evaporation deposition

The attempts with suspension drop deposition the attempt was also made to increase the number of deposited particles by immersion and withdrawal to hybrid particles suspension as it was earlier done for ITO nanoparticles [465].

To check the idea, ITO substrates were cleaned subsequently with ethanol and deionized water. Then they were heated for 30 min. in a tube furnace (Barnstead International) at 500 °C in air to remove any remaining contamination. They were immersed for 2 s in 5 mg ml^{-1} suspension of hybrid particles in MeOH. Each immersion step was

followed by electrode immersion into clean water to remove weakly immobilized particles and drying step. This procedure was repeated a number of times (Fig. 104).

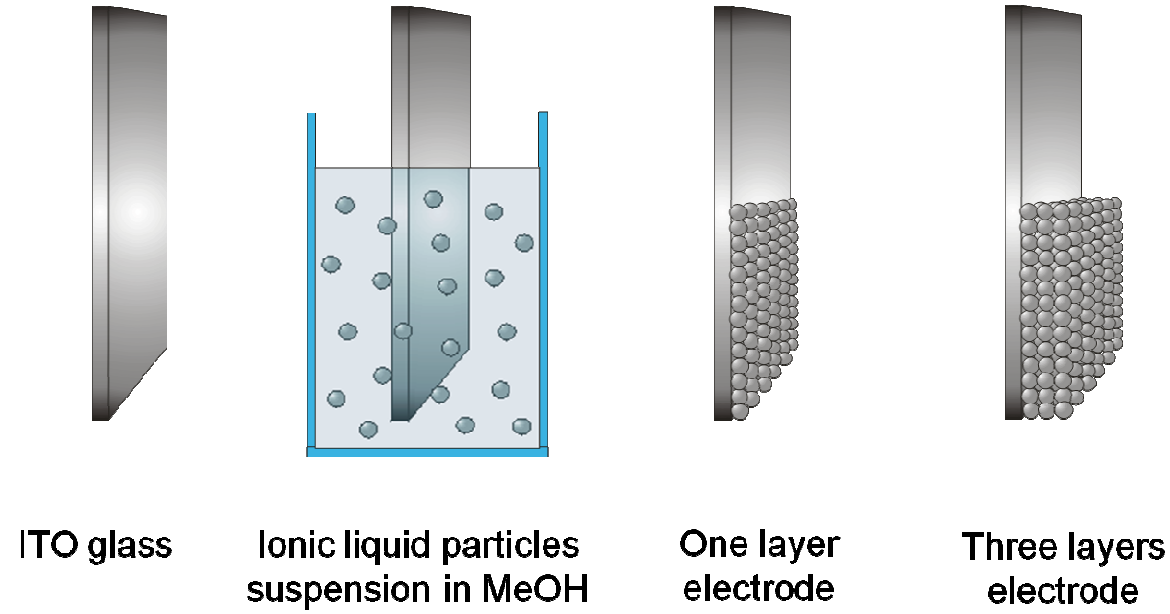

Fig. 104. Scheme of electrode modification by immersion into the hybrid particles suspension and solvent evaporation.

9.2.3.1. SEM analysis

Ready electrodes have been investigated with SEM (Fig. 105).

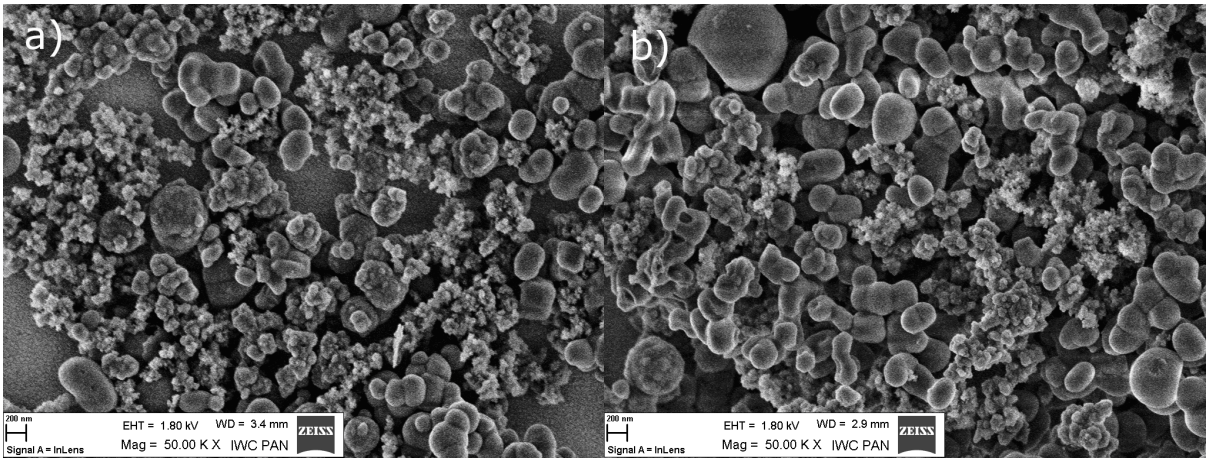

Fig. 105. SEM images of ITO electrodes modified by 1 (A) and 3 (B) immersion into the hybrid particles suspension steps.

From the SEM micrographs it can be clearly seen that the ITO surface has been covered with hybrid particles during the deposition process. The deposit was not ordered because of the broad particles size distribution. One can see there are some uncovered ITO areas on the one step modified electrode (Fig. 105a). The coverage of the three steps modified electrode was found to be larger (Fig. 105b).

9.2.3.2. Electrochemical measurements

The electrodes have been investigated in the electrochemical way. They have been immersed in the 1 μM $K_3Fe(CN)_6$, 0.1 M $NaClO_4$ and the CVs have been recorded. The accumulation process have been observed for the electrodes modified by one and three step procedures (Fig. 106).

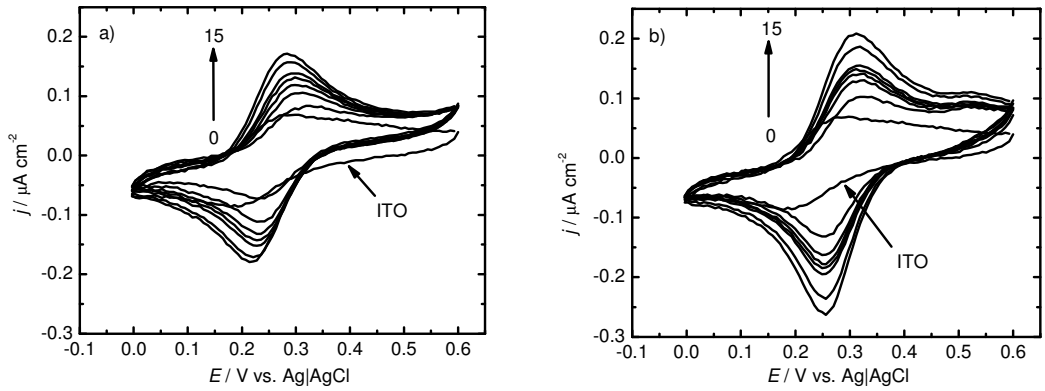

Fig. 106. Fig. 61. CVs for the 1 (a) and 3 step (b) hybrid particles modified electrodes immersed in the 1 μM $K_3Fe(CN)_6$, 0.1 M $NaClO_4$. Arrow indicates current changes from scan to scan. v = 10 mVs^{-1}.

For the three step modified electrode the peak currents are slightly higher than for the one step modified one. It's because of the bigger amount of the particulate deposit on the electrode surface. However only the particles next to the electrode influence electrochemical response. This is in agreement with the SEM experiment.

The most important is the fact that it was possible to immobilize the hybrid particles on the electrode surface without any additional binder. It was also possible to modify ITO electrode with pure silicate particles with the same procedure but, obviously, there is no anion accumulation observed in that case (Fig. 107).

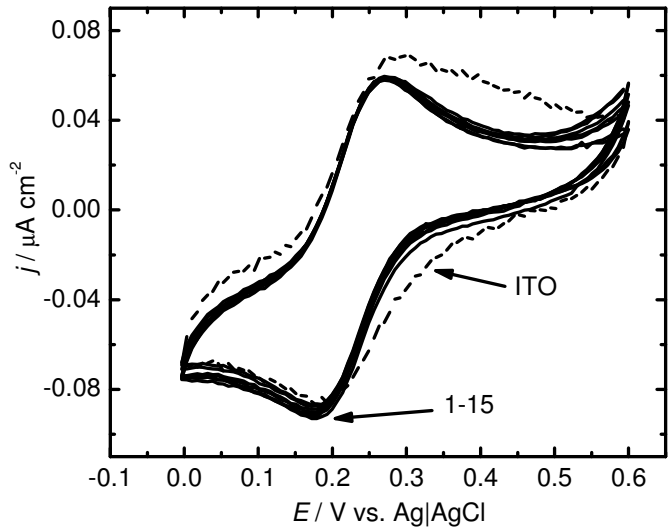

Fig. 107. CVs for the 1 step pure silicate particles modified ITO electrode immersed in the 1 μM $K_3Fe(CN)_6$, 0.1 M $NaClO_4$. v = 10 mVs^{-1}.

The electrocatalytic properties of imidazolium groups towards the NADH oxidation reaction have been earlier observed [295,481]. The electrocatalytic properties of new electrodes towards NADH oxidation have been investigated. This is a biologically important compound which is known to undergo the oxidation reaction [481]:

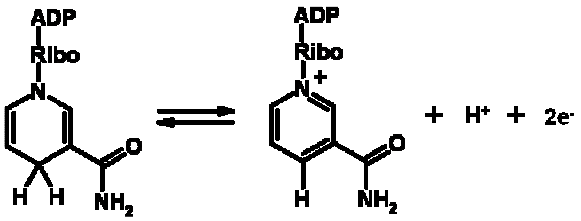

(22)

Electrodes modified by one and three steps immersion into the hybrid particles suspensions have been immersed into the 0.1 mM NADH, 0.1 M phosphate buffer solution (pH = 7.4) and the CV experiment have been performed. It was observed that NADH oxidation onset potential on hybrid particles modified electrodes (Fig. 108 curve iii and iv) is shifted ca. 100 mV towards cathodic potentials in comparison to the clean ITO electrode (Fig. 108ii). The observed catalytic effect is probably connected with the presence of imidazolium groups in the electrode surface vicinity [481]. Unfortunately the NADH oxidation potential is ca. 800 mV higher than one obtained on the graphene-IL composite material [481].

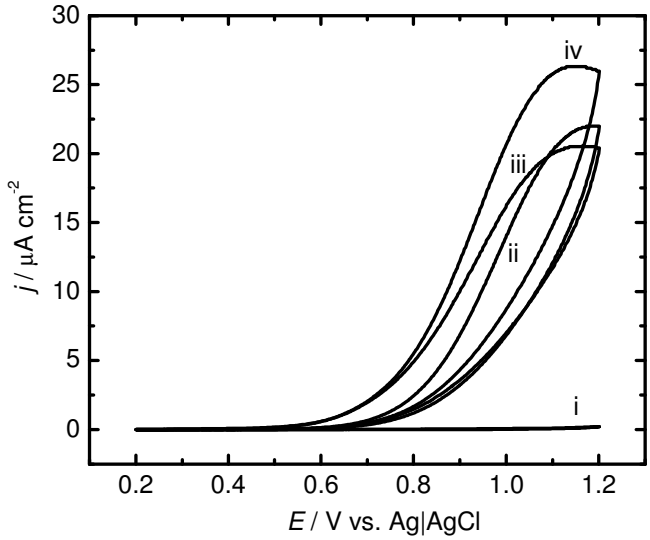

Fig. 108. CVs obtained for the clean ITO (ii), one step hybrid particles modified electrode (iv) and three steps hybrid particles modified electrodes (iii) immersed to the 0.1 mM NADH, 0.1 M phosphate buffer solution (pH = 7.4). Curve (i) was obtained for the one step hybrid particles modified electrode immersed in the buffer solution without NADH. v = 10 mV s^{-1}.

9.2.4. Layer by layer deposition

The peak current connected with redox reaction of anions accumulated on hybrid particles modified electrode is low in comparison to the SCILF modified one. Therefore, the deposition of higher amount of particles was highly desirable. To do it an additional component of the film acting as a binder for hybrid silicate particles – sulfonated carbon nanoparticles was used. They have negatively charged sulfonate groups which were supposed to bind electrostaticaly imidazolium groups attached to the hybrid particles surface. The second advantage of this carbon material is its high conductivity what allows to develop the electrochemically active surface.

To test the interactions between the positively charged hybrid particles and negatively charged sulfonated carbon particles the preliminary experiment have been performed. 0.5 mg ml^{-1} suspension of sulfonated carbon nanoparticles have been prepared (Fig. 109a). Such suspension is usually stable longer than a month. In the next step ca. 5 mg of hybrid particles were added to the suspension. As a result rapid precipitation have been observed (Fig. 109b).

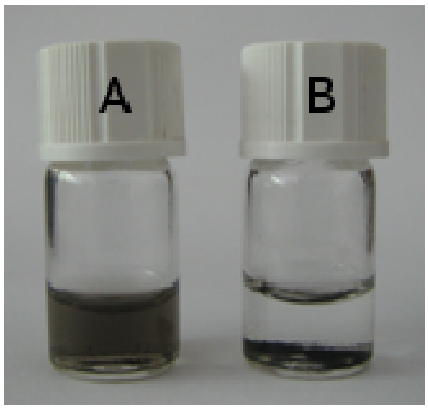

Fig. 109. 0.5 mg ml^{-1} suspension of sulfonated carbon nanoparticles before (a) and after addition of hybrid particles (b).

This phenomenon can be explained by the electrostatic interactions between negatively charged carbon particles and positively charged hybrid ones [482]. Here these interactions were exploited to build the hybrid-carbon particles electrode structure by layer by layer method.

ITO substrates were cleaned subsequently with ethanol and deionized water. Then they were heated for 30 min. in a tube furnace (Barnstead International) at 500 °C in the air to remove any remaining contamination. They were immersed for 2 s in suspensions of cationic and anionic particles subsequently. The cationic particles suspension was prepared by mixing 5 mg of particles with 1 ml of methanol and the mixture was sonicated for 30 min. Carbon nanoparticles with phenylsulfonic acid surface functionalities (ca. 7.8 nm mean diameter, with a typical bulk density of 320 g dm^{-3}, Emperor 2000) were obtained from Cabot Corporation (Dukinfield, United Kingdom). Their suspension was obtained by mixing 5 mg of particles with 1 ml of water and the mixture was sonicated for 30 min. Each immersion step was followed by electrode immersion into clean water to remove weakly immobilized particles. This procedure was repeated a varying number of times depends on how thick deposit was desired. In this way the carbon ceramic nanoparticulate film electrode (CCNFE) have been obtained (Fig. 110). For the sake of clarity the amount of material deposited by single immersion in silicate submiroparticles suspension and single immersion in sulfonated carbon nanoparticles suspension is called bilayer.

The electrodes with different number of bilayers have been prepared. It was clearly visible with the naked eye that more immersion and withdrawal steps results in larger amount of material deposited an the electrode (Fig. 111). In other words the more bilayers were deposited the more carbon was present at the electrode surface – the thicker the deposit was.

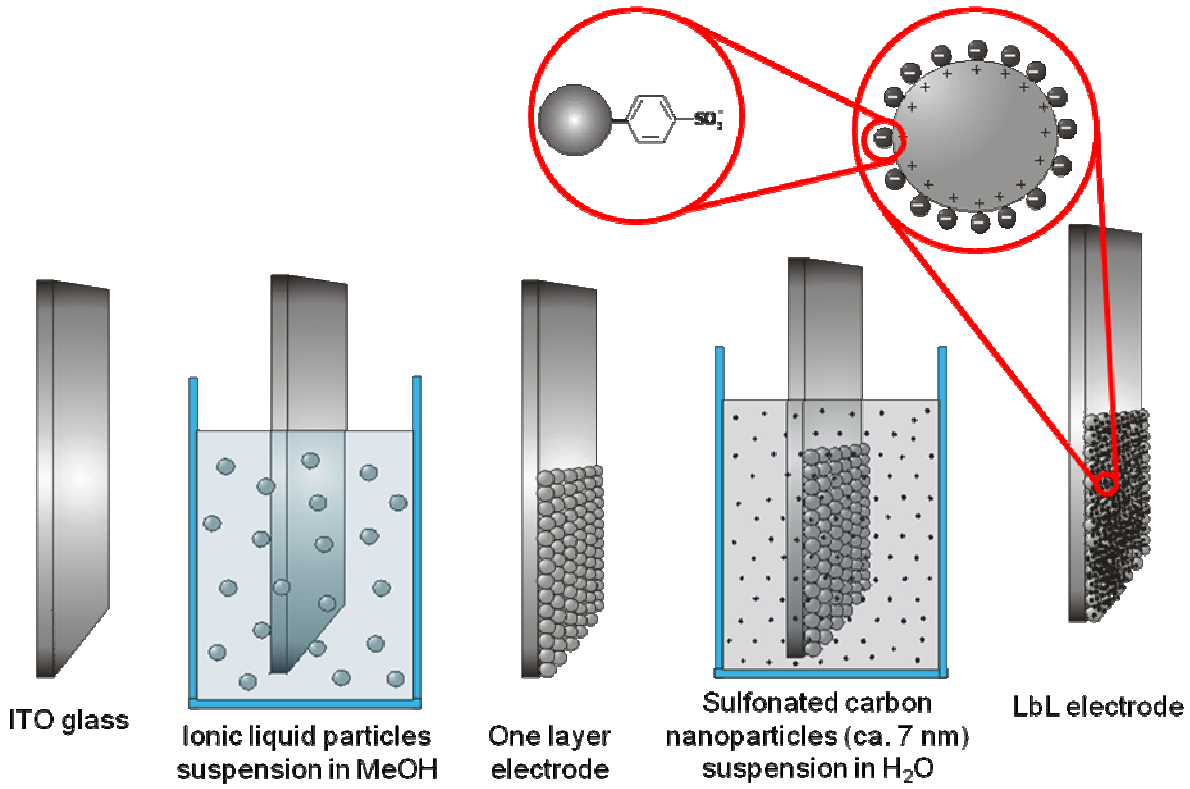

Fig. 110. Scheme of CCNFE preparation by LbL method.

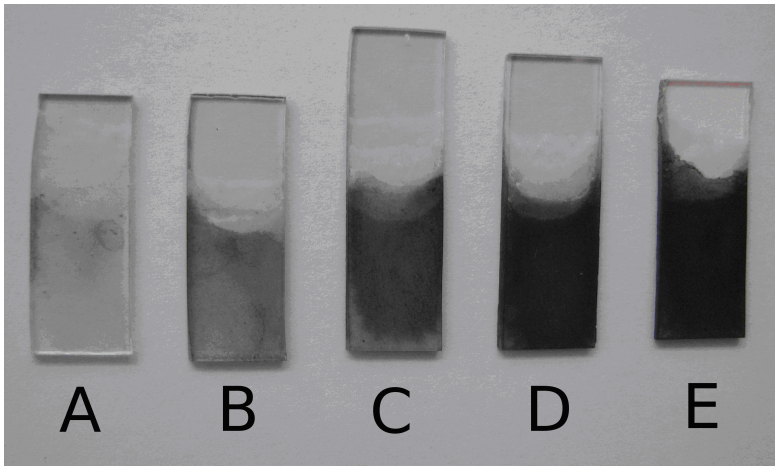

Fig. 111. Picture of CCNFE prepared by 1 (A), 3 (B), 6 (C), 9 (D) and 12 (E) immersion and withdrawal steps.

9.2.4.1. SEM analysis

The growth of the deposit obtained by subsequent immersion and withdrawal steps have been confirmed with SEM analysis (Fig. 112).

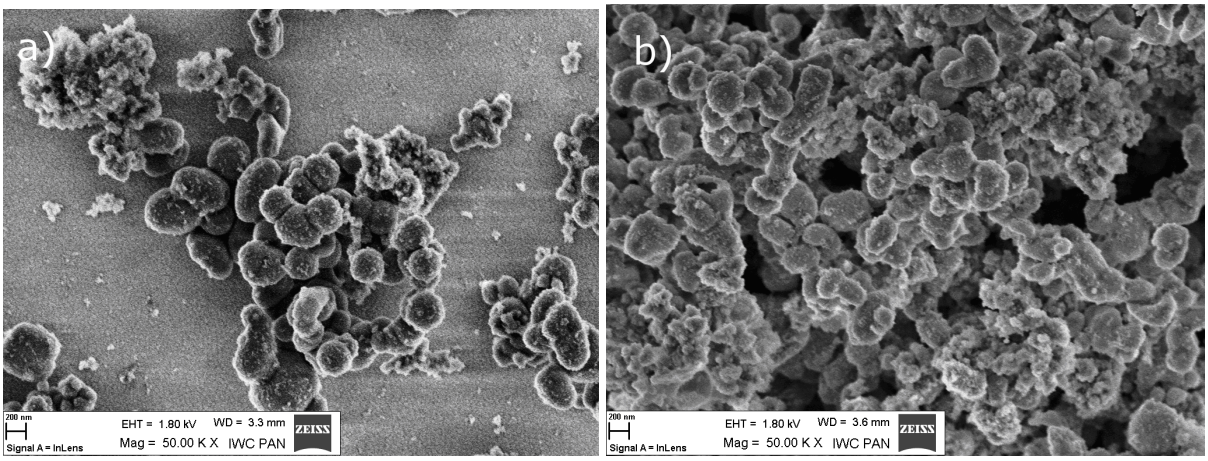

Fig. 112. SEM images of CCNFE prepared by 1 (a) and 12 immersion and withdrawal steps (b).

One can still see the surface of ITO electrode when CCNFE is prepared by one immersion and withdrawal step only. After 12 immersion and withdrawal steps the deposit is much thicker and all ITO is covered. The deposit looks similar to the hybrid particles. However, the particles surface looked much more textured than in the absence of carbon nanoparticles. This perhaps results from their decoration with carbon nanoparticles.

9.2.4.2. Electrochemical measurements

Anion accumulation properties of CCNFE have been investigated. The one and three bilayers CCNFE have been immersed into the 1 μM $K_4Fe(CN)_6$, 0.1 M $NaClO_4$ and the CV experiment have been performed.

It was found that the current response of the 1 bilayer CCNFE is significantly higher than the one obtained for the clean ITO electrode (Fig. 113a). However there is no current changes observed with time. This may be because of the fast kinetics of the accumulation process. In other words all the anions possible to exchange have been exchanged immediately after electrode immersion. The current obtained for the 3 bilayers CCNFE was several times higher than the one for the one bilayer CCNFE. The capacitance current in both cases was much higher than one for the clean ITO electrode. The double layer capacitances ware estimated to be 0.3 μF cm^{-2} for bare ITO electrode and 1.2 μF cm^{-2} and 4.5 μF cm^{-2} for CCNFE electrodes prepared by 1 and 3 immersion and withdrawal steps respectively. This is connected with the electrode surface development.

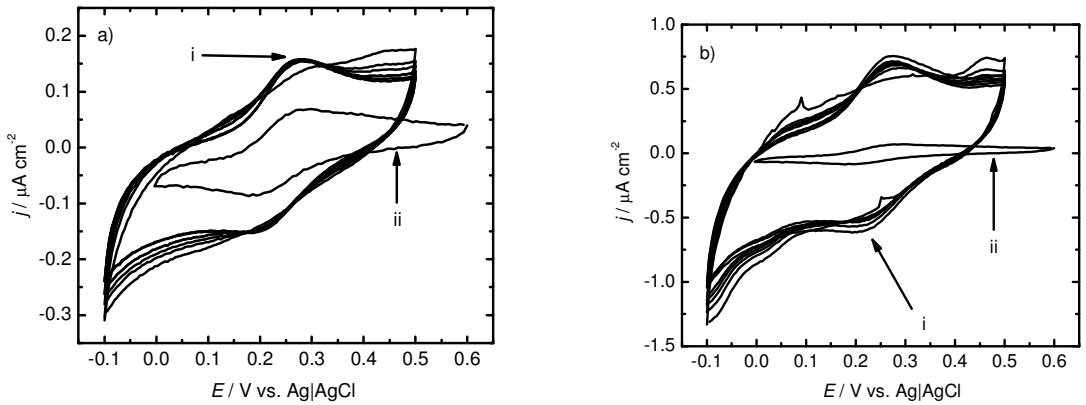

Fig. 113. a) CVs obtained for the 1 bilayer CCNFE immersed in 1 μM $K_4Fe(CN)_6$, 0.1 M $NaClO_4$ scans 1-20 (i) and CV obtained for the clean ITO electrode in the same conditions (ii). b) CVs obtained for the 3 bilayer CCNFE immersed in 1 μM $K_4Fe(CN)_6$, 0.1 M $NaClO_4$ scans 1-20 (i) and CV obtained for the clean ITO electrode in the same conditions (ii). v = 10 mV s^{-1}.

The new electrode was further characterised. The CCNFE electrodes have been immersed in the 0.05 M H_2O_2, 0.1 M H_2SO_4. It is known that H_2O_2 undergoes the reduction reaction according to the equation:

$$H_2O_2 + 2H^+ + 2e^- \rightarrow 2H_2O \qquad (23)$$

This reaction is slow, what makes it ideal candidate for investigating the surface development because the redox probe have enough time to penetrate the whole deposit. It was found that the current obtained for the 1 bilayer CCNFE is hardly distinguishable from the one obtained for the clean ITO in the same conditions. However it is much larger for the 6 bilayers modified electrode (Fig. 114). Further deposition of nanoparticulate material (12 and 24 bilayers) results in 10–20% decrease of the current as compared to 6 steps electrode and may be ascribed to depletion of the substrate within the more dense porous film. It shows that despite the fact that individual bilayer is very thin it is possible to build a three dimensional nanoparticulate film by repeating the deposition steps.

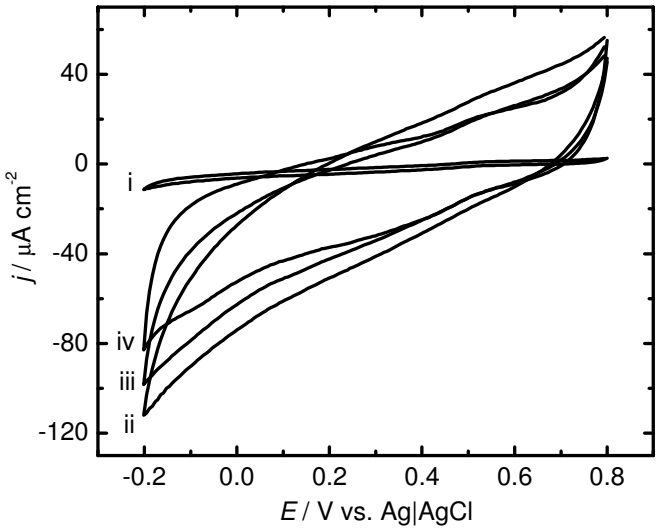

Fig. 114. CVs obtained for the CCNFEs prepared by (i), 6 (ii), 12 (iii) and 24 (iv) immersion and withdrawal steps immersed to 0.05 M H_2O_2, 0.1 M H_2SO_4. v = 10 mV s^{-1}.

Also the electrocatalytic properties of CCNFEs towards NADH electrooxidation reaction (23) have been investigated. The one bilayer CCNFE have been immersed into the 0.1 mM NADH, 0.05 M phosphate buffer solution (pH = 7.4) and the CV have been recorded (Fig. 115).

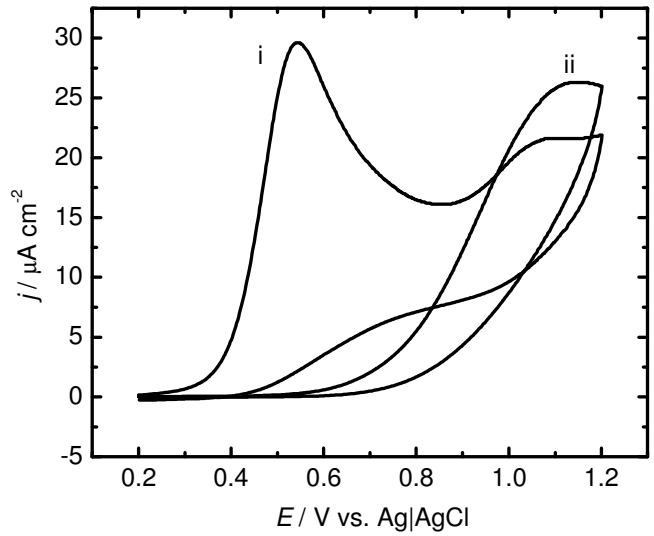

Fig. 115. CVs obtained for the 1 bilayer CCMFE (i) and 1 layer hybrid particles modified ITO electrode (ii) immersed to the 0.1 mM NADH, 0.05 M phosphate buffer solution (pH = 7.4). v = 10 mV s^{-1}.

The decrease of NADH oxidation reaction overpotential of ca. 400 mV is observed for the CCMFE in comparison to the only hybrid particles modified electrode. The catalytic effect is

clearly caused by the presence of carbon particles in the electrode structure. The second peak at potential ca. 1.1 V comes from NADH oxidation reaction on the uncovered ITO.

Several experiments were performed to check the new CCMFE electrode's usefulness as a support for enzyme immobilization. The one, twelve, twenty four, and thirty six bilayer CCMFEs have been prepared. Actually thirty six bilayers seems to be the limit and thicker film is fragile and have shown the tendency to peel of the electrode. These electrodes have been further modified with enzyme by adsorption. CCMFE electrodes have been immersed in the 0.7 mg cm^{-3} laccase solution in 0.1 mol dm^{-3} McIlvaine's buffer (pH 4.8) solution for 2 h in ca. 5 °C. The ready electrodes have been further immersed in oxygen saturated 0.1 mol dm^{-3} McIlvaine buffer (pH 4.8) and the CV have been recorded (Fig. 116).

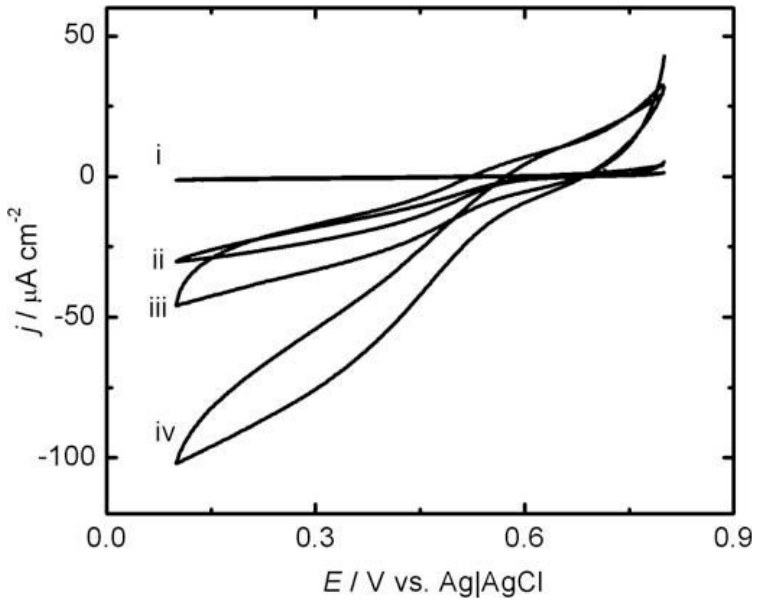

Fig. 116. CVs obtained in oxygen saturated 0.1 mol dm^{-3} McIlvaine buffer (pH 4.8) at ITO electrode coated by one (i), twelve (iii), twenty four (iii) and thirty six (iv) immersion and withdrawal steps to cationic silicate particles and carbon nanoparticles suspension alternatively followed by laccase adsorption. v = 1 mV s^{-1}.

The sigmoidal curves characteristic for the electrocatalytic oxygen reduction have been observed. Such mediatorless process is provided by laccase adsorbed on carbon nanoparticulate film. This signal is absent where the electrode was not modified by laccase or in argon saturated solution. Moreover, the magnitude of the plateau current is proportional to the number of immersion and withdrawal steps up to 36 steps. Above this value deposited film starts to be mechanically unstable and shows a tendency to peal of the electrode. After successful attempt of laccase immobilization on the CCMFE the possibility of another enzyme – bilirubin oxidase (BOx) immobilization have been checked. First the voltammetry of film CCMFEs (made of positively charged silicate submicroparticles and negatively

charged CNPs) was run in 1 mmol dm^{-3} $(NH_4)_2ABTS$ aqueous solution. The appearance of voltammetric peaks and increase of peak currents during subsequent scans was observed indicating accumulation of $ABTS^{2-}$ dianions. After transfer into phosphate buffer (pH = 4.8) 10-20% decrease of the peak current is observed, but finally the surface connected voltammetric signal remains stable (Fig. 117). The amount of immobilised mediator is larger for larger amount of deposited material.

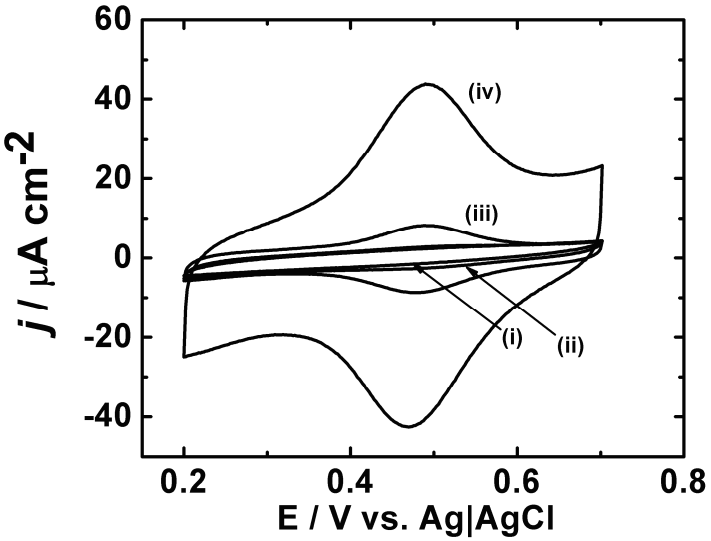

Fig. 117. CVs obtained in 0.1 mol dm^{-3} phosphate buffer (pH = 4.8) at an CCMFE prepared by one (i) six (ii), twelve (iii) or twenty four (iv) immersion and withdrawal steps further modified with $ABTS^{2-}$. v = 10 mV s^{-1}

The redox potential of $ABTS^{2-/\bullet-}$ redox couple remains almost unchanged for CCMFE as compared to bulk solution value. This indicates irreversible adsorption of mediator due to interactions between the extended π electron system of $ABTS^{2-}$ and the carbon surface as earlier seen for microporous carbon [483,484] or multiwalled carbon nanotubes [357,485,486].

After the mediator immobilization the enzyme adsorption have been performed. Enzyme adsorption was performed by immersion of CCMFE in 1 mg cm^{-3} BOx solution in pH = 4.8 phosphate buffer for 2 hours in ca. 5°C. After adsorption of BOx on CCMFE, which had earlier been modified with mediator, experiments were performed in oxygen saturated pH = 4.8 phosphate buffer solution.

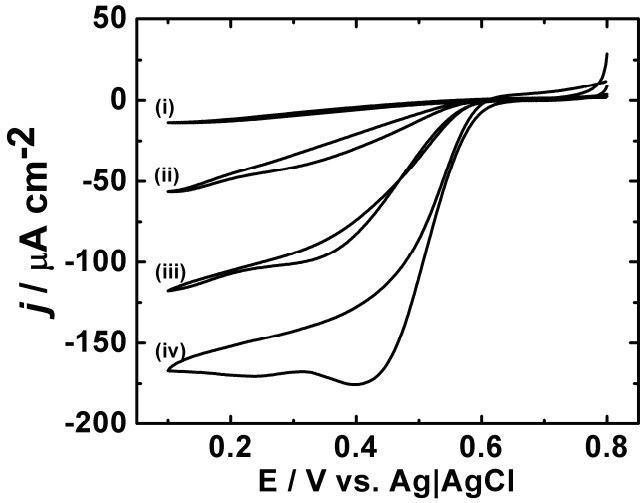

Fig. 118. CVs obtained in oxygen saturated 0.1 mol dm^{-3} phosphate buffer (pH = 4.8) at a CCMFE prepared by one (i) six (ii), twelve (iii) or twenty four (iv) immersion and withdrawal steps further modified with ABTS^{2-} and BOx. v = 1 mV s^{-1}

The sigmoidal shape of voltammetric signal (Fig. 118) indicates that CCMFE exhibits efficient oxygen reduction bioelectrocatalysis (Fig. 119). The magnitude of the signal is proportional to the amount of the adsorbed material. The ORR onset potential was comparable and the obtained catalytic current was ca. 30% higher than it was earlier reported for the similar system[487,488].

The voltammetric curves obtained at scan rates from 0.001 to 0.1 V s^{-1} exhibit a gradual transition from sigmoidal to peak shaped (Fig. 120) indicating slow kinetics of catalytic reaction. At slower scan rate a large fraction of reduced form of mediator is consumed in the catalytic reaction, whereas at faster scan rate it is reoxidised electrochemically. This pattern was earlier observed for ABTS^{2-} - laccase system within the same range of scan rates [471,486,489]. The pattern seems not to be connected with electrode architecture, but rather to be the result of the slowest reduction step where four Cu ions at the active site of the enzyme are fully oxidized [490,491].

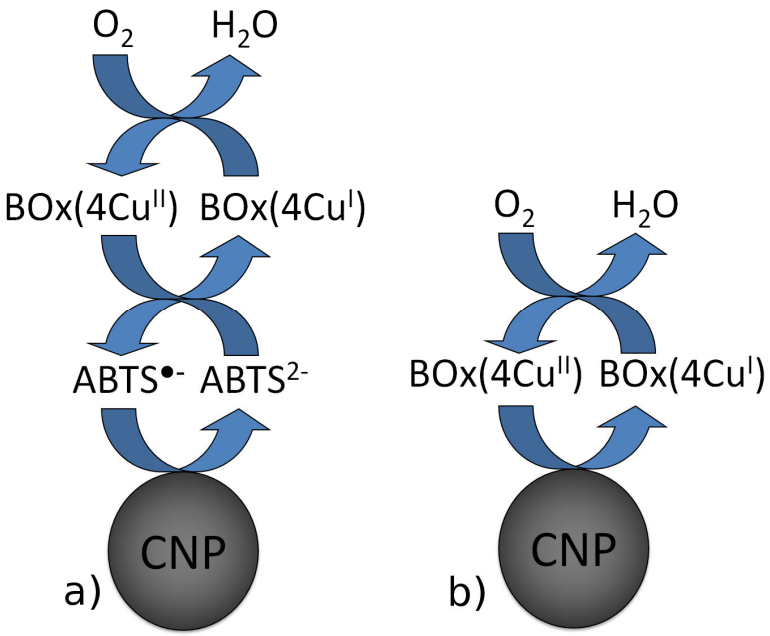

Fig. 119. Scheme of mediated (a) and nonmediated (b) oxygen reduction by bilirubin oxidase.

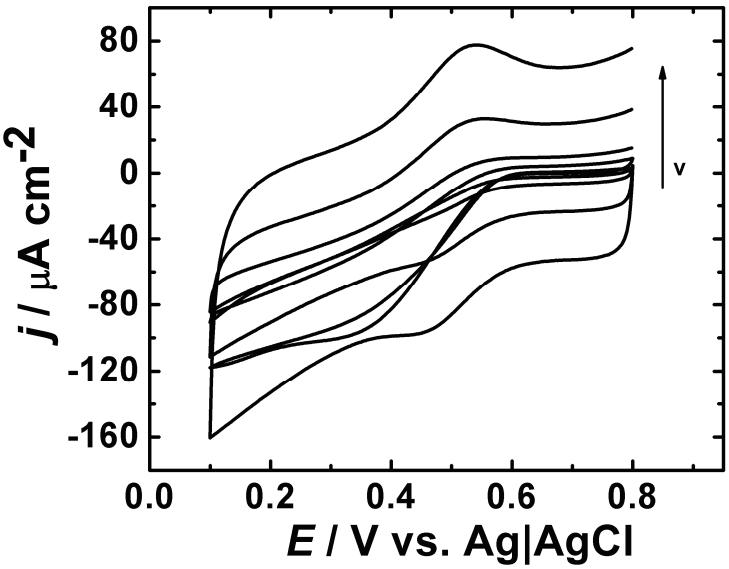

Fig. 120. CVs obtained in oxygen saturated 0.1 mol dm^{-3} phosphate buffer (pH 4.8) at an CCMFE prepared by twenty four immersion and withdrawal steps further modified with $ABTS^{2-}$ and BOx. Scan rates: 0.001, 0.01, 0.02, 0.05 and 0.1 V s^{-1}. Arrow shows increasing scan rate.

10. Thiol functionalized ionic liquid modified electrodes

It is known that thiols have an ability to form covalent bonds with gold [492]. These bonds are commonly for gold surface modification with thiol self assembled monolayers. Various thiols have been also used for AuNPs stabilization [492]. In this chapter the synthesis of thiol moiety bearing IL have been described. This thiol functionalized IL have been further used for modification of gold disc electrodes and gold nanoparticles. This immobilization method have been used as an alternative for sol-gel processing.

10.1. Thiol functionalized ionic liquid synthesis

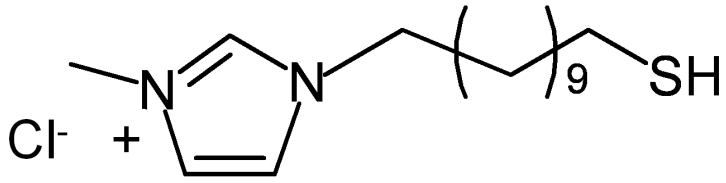

Fig. 121. 1-(11-mercaptoundecyl)-3-methyl-imidazolium chloride formula.

1-(11-mercaptoundecyl)-3-methyl-imidazolium chloride (MIUSHCl) (Fig. 121) have been synthesized according to the following procedure. To a solution of 1-methylimidazole (4.92 g, 60 mmol) in 50 ml of methanol 11-bromo-1-undecene (6.99 g, 30 mmol) was added. The mixture was stirred for 72 h at room temperature, filtered and concentrated under vacuum. Methylene chloride (30 ml) was added and solid residues were filtered off again. While vigorous stirring, 400 ml of n-hexane was gradually added to precipitate 1-methyl-3-(10-undecenyl)-imidazolium bromide as a white crystals. The product was filtered off under vacuum and dried (8.97 g, 28.5 mmol, yield 95%). Three grams (9.5 mmol) of the product was placed in a 100 ml round bottom flask. Methanol (40 ml), thioacetic acid (10 ml) and 1,10-azobis(cyclohexanecarbonitrile) (400 mg, 1.64 mmol) were added and the mixture was irradiated with UV light (high pressure mercury lamp) overnight under argon atmosphere with stirring. The mixture was concentrated under vacuum and 1-(11-acetylsulanyl-undecyl)-3-methyl-imidazolium bromide was purified by column chromatography (hexane then hexane/EtOAc then CHCl3/methanol, yellow oil (2.83 g, 7.23 mmol, 76%). This oil was dissolved in 40 ml of degassed methanol, 10 ml of 1.25 M HCl in methanol were added and the mixture was reflux under argon atmosphere for 8 h. 1-(11-mercaptoundecyl)-3-methylimidazolium chloride was purified by column chromatography. **^{1}H NMR** (Bruker 300) ($CDCl_3$): 10.74 (s, 1H, C(2)H), 7.26 (s, 1H, C(5)H), 7.21 (s, 1H, C(4)H), 4.31 (t, 2H, J = 7.4 Hz, N(3)–CH_2), 4.12 (s, 3H, N–CH_3), 2.51 (m, 2H, CH_2–S), 1.95–1.85 (m, 2H), 1.65–1.55

(m, 2H), 1.4–1.2 (m, 14H). **HRMS** (Marinner) M+ (LSIMS in methanol): calculated for $C_{15}H_{29}N_2S$: 269.2046, found 269.20556.

10.2. Gold electrodes modified with thiol functionalized ionic liquid's self assembled monolayer.

In this chapter polycrystalline gold electrodes modified with the self assembled monolayers of thiol functionalized ionic liquid are described. The electrode surface area was 0.02 cm^2. Before modification gold electrodes were polished on the cloth subsequently with 1, 0.3, 0.5 μM alumina powders. The last step was polishing on the cloth without addition of any powder. After that the electrodes have been rinsed with deionized water, then sonicated for ca. 5 min and rinsed with deionized water again. After cleaning procedure the electrode have been dried in the stream of argon.

The 1 mM MIUSHCl solution in methanol have been prepared for electrodes modification. The electrodes have been immersed in the solution for ca. 10 h. Then they have been rinsed with methanol and dried in the stream of argon.

The very first experiment on the new MIUSHCl modified electrodes was performed to check their electrochemical properties towards negatively ($Fe(CN)_6^{4-}$) and positively ($Ru(NH_3)_6^{3+}$) charged redox probes. First the electrode have been immersed in the 1 mM $K_4Fe(CN)_6$, 0.1 M KBr solution. The CV have been recorded (Fig. 122).

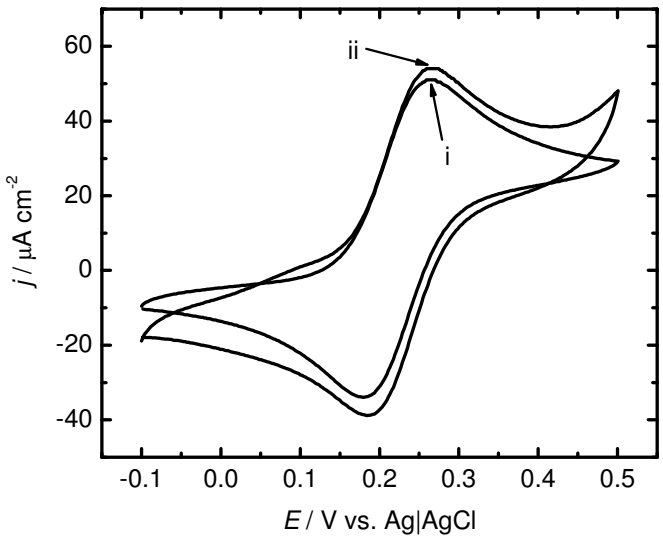

Fig. 122. CVs obtained for the MIUSHCl modified electrode(ii) and bare gold electrode (i) immersed in the 1 mM $K_4Fe(CN)_6$, 0.1 M KBr solution. v = 10 mV s^{-1}.

Almost no difference between voltammograms obtained with MIUSHCl modified electrode and the clean ITO electrode was found. The current obtained for the modified electrode was slightly higher then the one obtained for the clean ITO perhaps because of the some accumulation effect. This effect is small because of small number of functional groups. What was found interesting in this system was the lack of the electrode surface blocking effect in spite of the presence of relatively long chain thiol monolayer at the surface. Probably the thiol layer is not very well organized, what allows $Fe(CN)_6^{4-}$ to exchange electron with the electrode.

Completely different behaviour was noted for $Ru(NH_3)_6^{3+}$ redox probe. One can see that the electrode modification with the MIUSHCl monolayer nearly completely suppressed the electrochemical response from the $Ru(NH_3)_6^{3+}$ (Fig. 123). This behavior can be explained by the electrostatic repulsion interactions between the positively charged redox probe and the positively charged imidazolium groups at the electrode surface. Moreover the obtained result gives us information that the obtained monolayer is tight enough to prevent the redox probe from reacting directly at the gold surface [493].

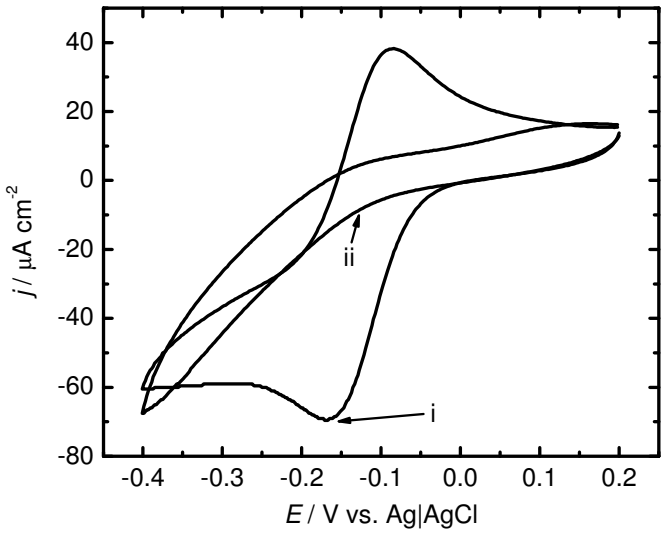

Fig. 123. CVs obtained for the MIUSHCl modified electrode(ii) and clean ITO electrode (i) immersed in the 1 mM $Ru(NH_3)_6Cl_3$, 0.1 M KBr solution. v = 10 mV s^{-1}.

Finally the redox-switch experiment have been performed (Fig. 124). The MIUSHCl modified electrode was immersed to 1 mM $Ru(NH_3)_6Cl_3$, 0.1 M KBr solution and the CV have been recorded. After that the electrode was conditioned in 10 mM $K_3Fe(CN)_6$ solution to exchange the Cl^- anions for the $Fe(CN)_6^{4-}$ anions. It was rinsed with deionized water and

immersed again in 1 mM $Ru(NH_3)_6Cl_3$, 0.1 M KBr solution. The CV curve have been recorded (Fig. 124ii). It is clearly visible that electrode has been activated towards $Ru(NH_3)_6^{3+}$ reduction reaction. The $Fe(CN)_6^{4-}$ anions present in the ionic liquid monolayer have made the electron transfer possible. Such behavior have been earlier described in the literature for the similar system [39]. Next there was an attempt made to exchange the $Fe(CN)_6^{4-}$ anions with another ones which don't promote the electron transfer between $Ru(NH_3)_6^{3+}$ and the electrode. The electrode have been immersed for 10 min in the 0.2 M KSCN. After that it was removed from the solution and tested once again in 1 mM $Ru(NH_3)_6Cl_3$, 0.1 M KBr (Fig. 124iii). One can see that the electron transfer between electrode and $Ru(NH_3)_6^{3+}$ is still possible. It looks that $Fe(CN)_6^{4-}$ anions are not exchanged for the SCN^- ions as have been earlier observed [39].

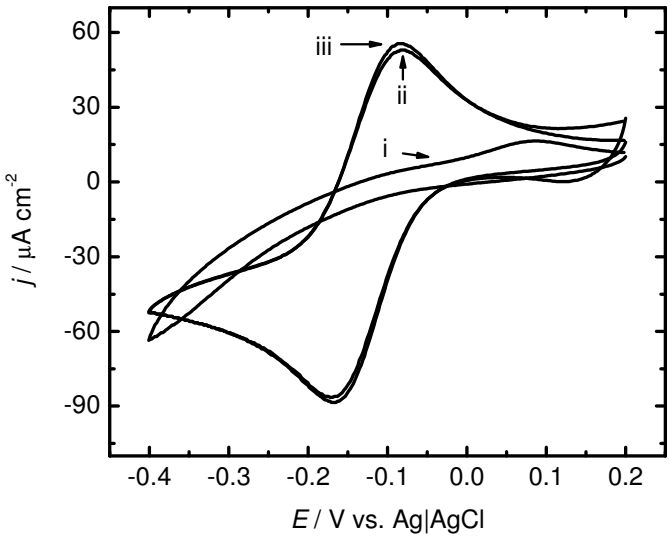

Fig. 124. CV of MIUSHCl modified electrode without pretreatment(i), pretreated 10 min in10 mM $K_3Fe(CN)_6$ solution (ii) and in 0.2 M KSCN solution (iii) immersed in 1 mM $Ru(NH_3)_6Cl_3$, 0.1 M KBr. v = 10 mV s^{-1}

10.3. Electrodes modified with thiol functionalized ionic liquid stabilized gold nanoparticles and carbon nanoparticles.

In this chapter the electrodes modified with gold nanoparticles stabilized with MIUSHCl (AuNPs) and carbon nanoparticles (CNPs) are described.

To modify the electrodes with AuNPs and CNPs the similar procedure as for hybrid particles and CNPs have been utilized. ITO slides have been cleaned as described before. It was immersed alternately into the AuNPs suspension in methanol (5 mg cm^{-3}) CNPs

suspension in water (5 mg cm^{-3}) for 2 s. Every step was followed by drying and immersion in clean solvent for 2 s to remove weakly bonded particles. Always the immobilization sequence Was finished with AuNPs deposition (Fig. 125).

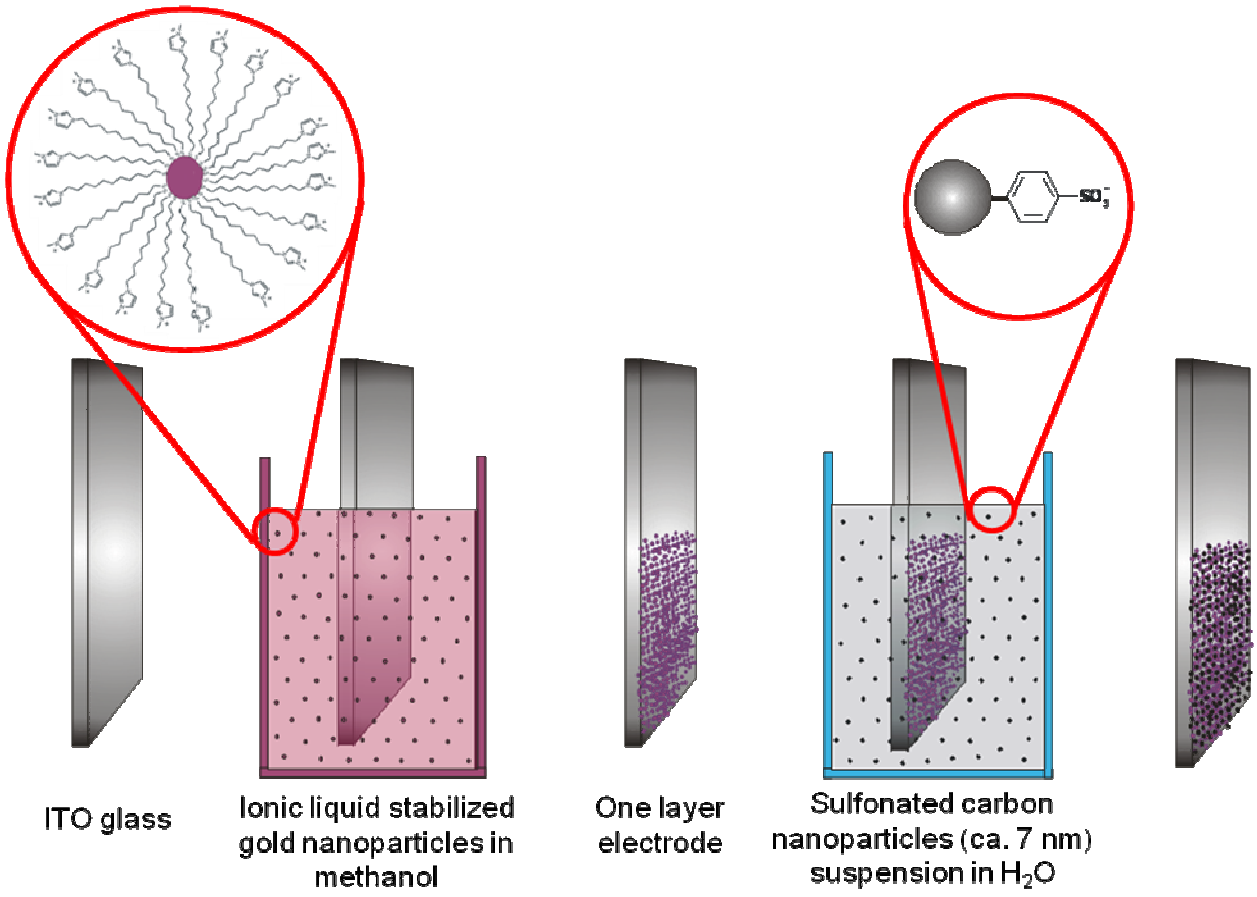

Fig. 125. Scheme of AuNPs-CNPs electrode preparation by LbL method.

10.3.1. SEM analysis

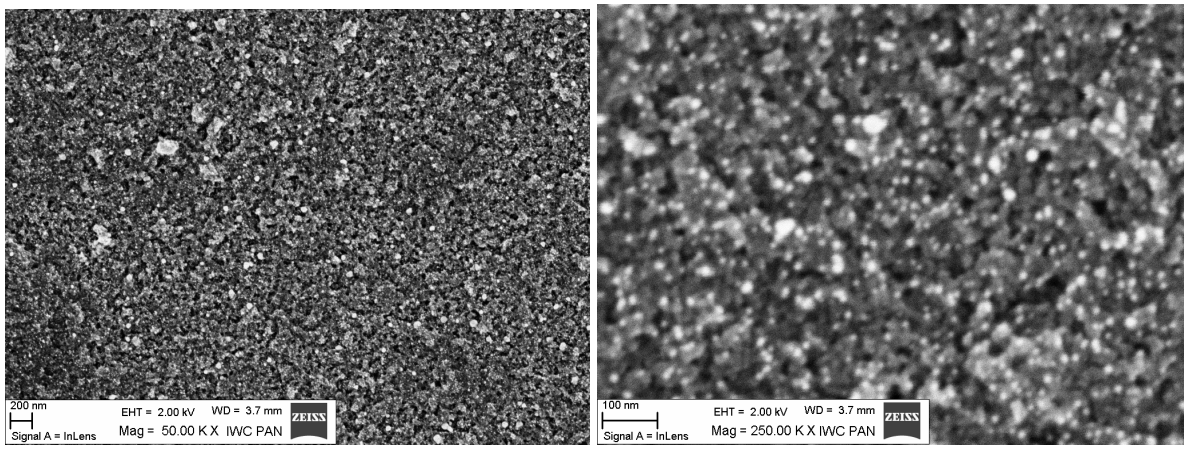

Fig. 126. The SEM image obtained for the 3 bilayers AuNPs-CNPs electrode.

SEM image of gold and carbon nanoparticles modified electrode (Fig. 126) shows that three immersion and withdrawal steps produce the complete coverage of the substrate by three dimensional film. One can also see that gold particles and their small aggregates (smaller than ca. 50 nm in diameter) are dispersed in carbon nanoparticulate material. The gold aggregations can be responsible for the golden shine of the electrodes observed by naked eye. Clearly electrostatic forces between particles made of different material plays an important role in carbon-gold nanoparticulate film formation.

10.3.2. Electrochemical characterization of electrodes modified with thiol functionalized ionic liquid stabilized gold nanoparticles and carbon nanoparticles.

As gold on carbon is known to be the oxygen reduction reaction (ORR) catalyst [494] it was a natural choice to test the newly obtained material ORR electrocatalytic properties. Therefore one, three, six and nine bilayers AuNPs-CNPs electrodes have been immersed in the oxygen saturated 0.5 mol dm^{-3} H_2SO_4 and the CVs have been recorded.

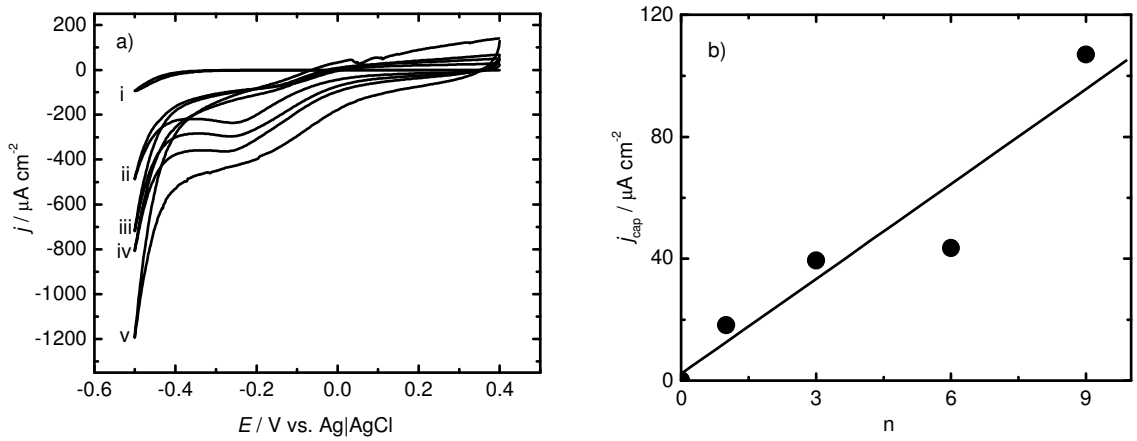

Fig. 127. a) CVs obtained in oxygen saturated 0.5 mol dm^{-3} H_2SO_4 at a bare ITO electrode (i) or an electrode coated by one (ii), three (iii), six (iv) and nine (v) immersion and withdrawal steps to cationic AuNPs and anionic CNPs alternatively. v = 50 mV s^{-1}. b) Relationship between capacitive current density (j_{cap}) at potential 0.2 V obtained in the same voltammetric conditions and the number of immersion and withdrawal steps.

The voltammetric experiments reveal that the capacitive current is proportional to the number of immersion and withdrawal steps (Fig. 127b). This indicates an increase of the electrochemically active surface and good contact with the ITO electrode substrate.

The onset of oxygen electroreduction is shifted from c.a. -0.4 V to 0.1 V in comparison to ITO electrode (Fig. 127a) what clearly indicates new material electrocatalytic properties towards ORR. Most importantly, the catalytic current is proportional to the number

of immersion and withdrawal steps indicating the increase of the Au nanoparticulate material accessible for oxygen dissolved in aqueous electrolyte.

The catalytic properties towards ORR in alkaline environment have been also investigated. The one, three, six and nine bilayers AuNPs-CNPs electrodes have been immersed in the oxygen saturated 0.1 mol dm^{-3} KOH. And the CVs have been recorded (Fig. 128).

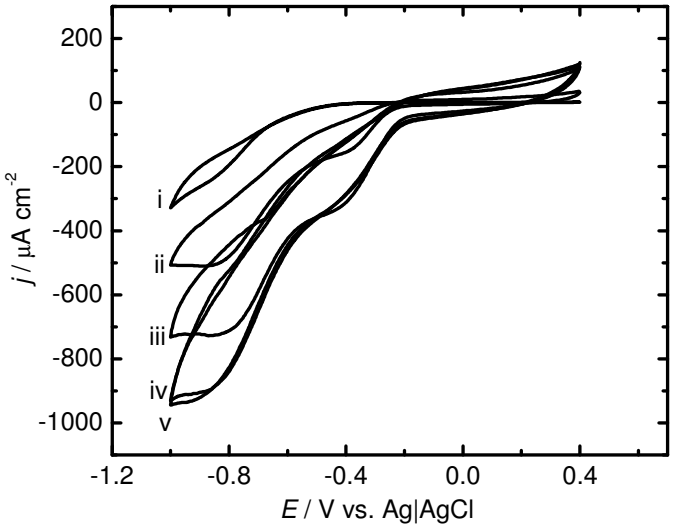

Fig. 128. CVs obtained in oxygen saturated 0.1 mol dm^{-3} KOH at a bare ITO electrode (i) or an electrode coated by one (ii), three (iii), six (iv) and nine (v) immersion and withdrawal steps to cationic AuNPs and anionic CNPs alternatively. v = 50 mV s^{-1}

In this case the onset of oxygen electroreduction is shifted from c.a. -0.4 V to -0.2 V in comparison to the ITO electrode. The catalytic current is proportional to the number of immersion and withdrawal steps indicating the increase of the Au nanoparticulate material accessible for oxygen dissolved in aqueous electrolyte similarly as in the acidic solution. The ORR reaction onsets potential are comparable with ones observed on the AuNPs modified electrodes described in the literature[495,496].

The bilirubin oxidase have been also immobilized on the AuNPs-CNPs electrodes. Enzyme adsorption was performed by immersion of the nanoparticulate film electrode into 1 mg cm^{-3} BOx solution in 0.1 mol dm^{-3} phosphate buffer (pH 4.8) solution for 2 h in ca. 5 °C. It was found that the onset potential of oxygen reduction can be shifted further to ca. 0.55 V after BOx adsorption (Fig. 129). Clearly, the studied material promotes mediatorless bioelectrocatalysis. The effect of the increase of the amount of nanoparticulate material indicates that bilirubin oxidase is adsorbed not only on the surface of the outermost

nanoparticles, but also present in the film. The promotion of mediatorless bioelectrocatalysis with BOx was earlier reported for carbon [497] and gold [498] nanoparticulate film. Therefore, it is difficult to say which type of nanoparticles more contribute to the bioelectrocatalytic activity of the electrode.

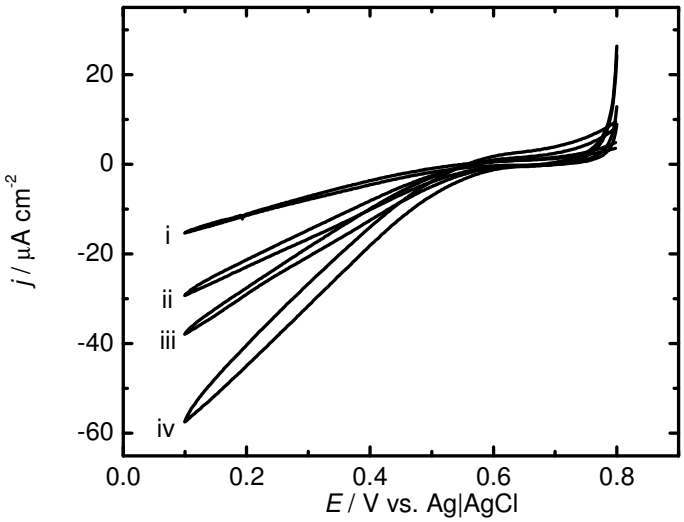

Fig. 129. CVs obtained in oxygen saturated 0.1 mol dm^{-3} phosphate buffer (pH = 4.8) at an electrode coated by one (i), three (ii), six (iii) and nine (iv) immersion and withdrawal steps to cationic AuNPs and anionic CNPs alternatively and modified with BOx. v = 1 mV s^{-1}.

10.4. Electrodes modified with positively and negatively charged gold nanoparticles.

The subsequent deposition of the particles of the opposite charges have been also employed to obtain gold nanoparticles deposit on ITO electrodes. The two types of gold nanoparticles have been used in these experiments: MIUSHCl modified nanoparticles ((+)AuNPs) and sodium 11-mercapto-1-undecane sulfonate modified nanoparticles ((-)AuNPs).

ITO slides have been cleaned as described before. There were immersed alternately into the (+)AuNPs suspension in methanol (5 mg cm^{-3}) and (-)AuNPs suspension in water (5 mg cm^{-3}) for 2 s. Every step was followed by drying and immersion in clean solvent for 2 s to remove weakly bonded particles (Fig. 130).

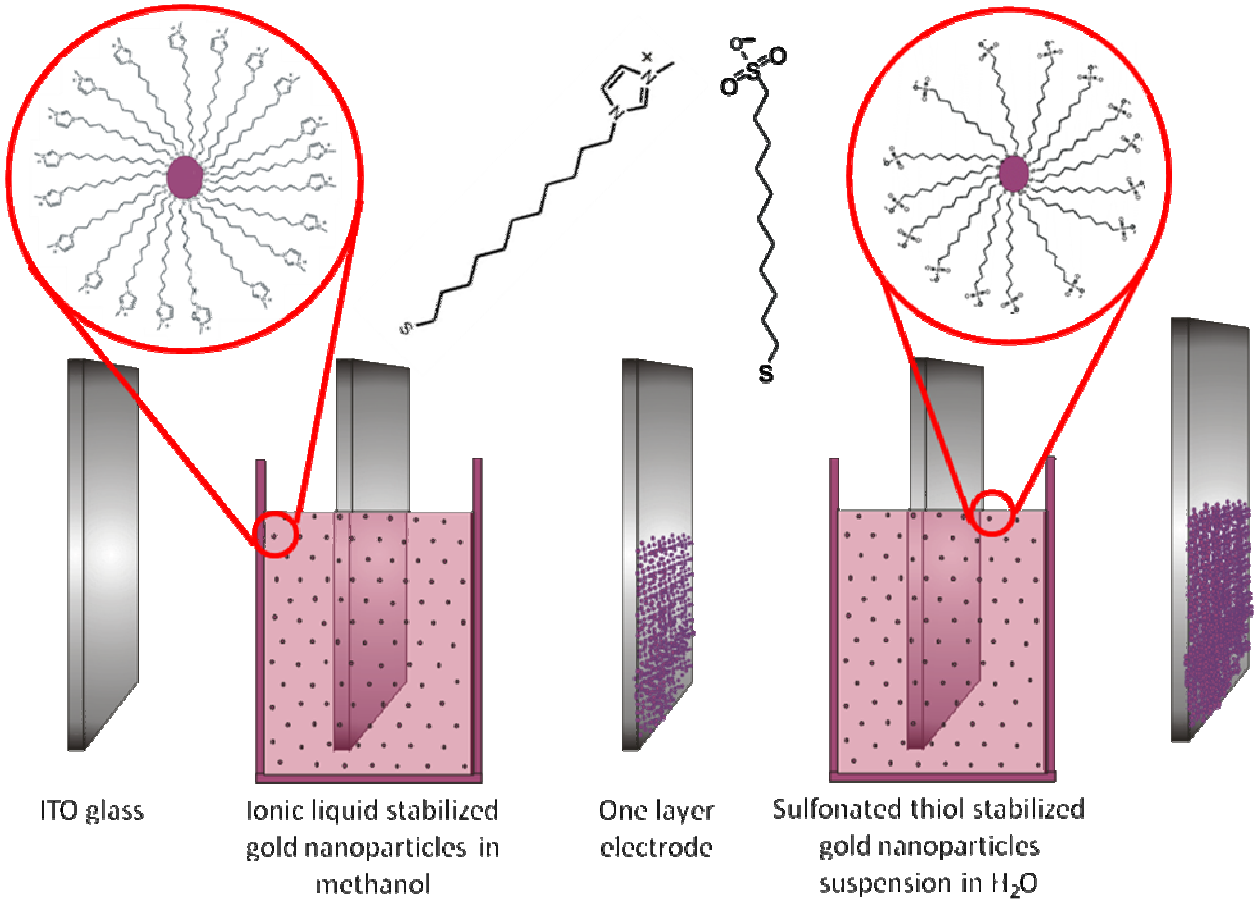

Fig. 130. Scheme of (+)AuNPs--CNPs electrode preparation by LbL method.

The nanoparticulate film formation have been observed with the naked eye. The more immersion steps have been done the darker the electrode was. The violet color of the electrodes was ascribed to the localized surface plasmon resonance of the AuCNPs. This observation have been confirmed with UV-Vis spectroscopy experiment (Fig. 131).

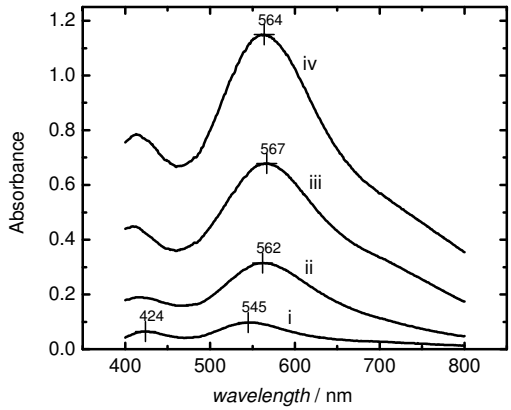

Fig. 131. Absorbance spectra obtained for the (+)AuNPs--CNPs electrodes obtained by one (i), three (ii), six (iii) and nine (iv) immersion and withdrawal steps to cationic (+)AuNPs and anionic (-)AuNPs alternatively.

The shift of the absorbance maximum peak (Fig. 131) connected with localized surface plasmon resonance is probably the effect of the nanoparticles aggregation. It was also observed with the naked eye that the more immersion and withdrawal steps is performed the more visible the metallic shine of the electrode is. This confirms the hypothesis that nanoparticles' aggregates of even gold thin film forms

10.4.1. SEM analysis

The SEM picture of (+)AuNPs-(-)AuNPs electrode shows that ITO electrode is tightly covered with nanoparticulate material. Film seems to be highly uniform however some bigger aggregates have been observed at the surface (Fig. 132).

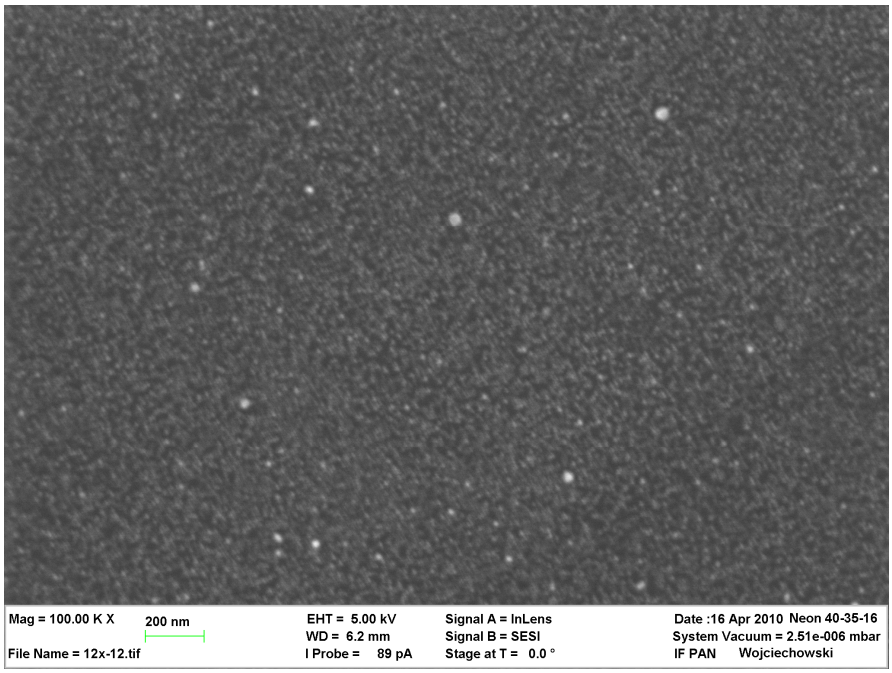

Fig. 132. The SEM image obtained for the 12 bilayers (+)AuNPs-(-)AuNPs electrode.

10.5. Electrochemical characterization of electrodes modified with positively and negatively charged gold nanoparticles.

The gold film growth have been also investigated by cyclic voltammetry. (+)AuNPs-(-)AuNPs electrodes obtained by one, three, six and nine immersion and withdrawal steps to cationic (+)AuNPs and anionic (-)AuNPs alternatively have been immersed to the deareated 0.1 M H_2SO_4 solution. CVs have been recorded (Fig. 133).

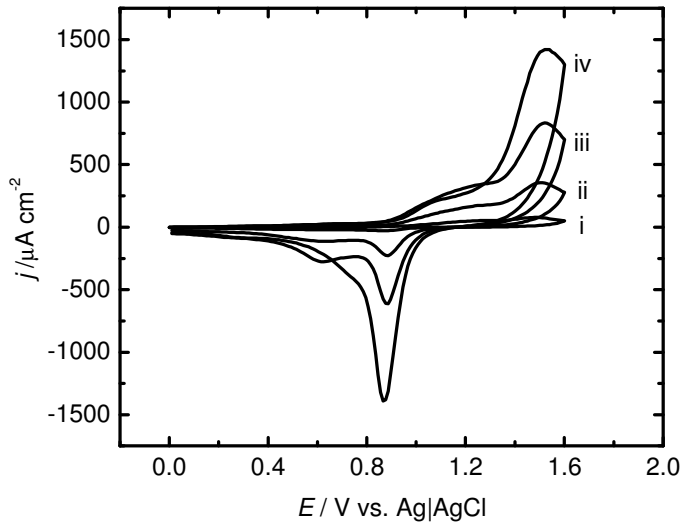

Fig. 133. CVs obtained for the (+)AuNPs-(-)AuNPs electrodes obtained by one (i), three (ii), six (iii) and nine (iv) immersion and withdrawal steps to cationic (+)AuNPs and anionic (-)AuNPs alternatively immersed in the deareated 0.1 M H_2SO_4 solution. v = 100 mV s^{-1}.

Characteristic gold voltammograms consisting peaks characteristic for gold oxide formation and its reduction [499] have been obtained for the (+)AuNPs-(-)AuNPs electrodes. The current increase with the number of immersion and withdrawal steps indicates clearly LbL mechanism of the film formation.

The method described above is an alternative approach of thin gold film deposition on the various substrates. The main advantage of the new method is possibility of film deposition on the substrates of the different shapes. The mild conditions (no vacuum nor high temperature was needed) of the film deposition can be important if working with biological or other fragile samples.

11. Conclusions

In this thesis the preparation and characterization of electrodes modified with materials functionalized with covalently bonded imidazolium type ionic liquids have been described. Two main strategies of IL immobilization on the solid substrates have been employed: immobilization in sol-gel silicate matrix and on gold surface with help of the S-Au bond.

1. The silicate based materials have been prepared in the form of thin films on the electrode surface and as submicrometer particles. In the latter case different methods of their immobilization on the electrode surface were developed. These hybrid particles have been immobilized in carbon paste electrodes, on the electrode surface by solvent evaporation technique and together with nanoparticles with the opposite charge by layer by layer method.

The ionic liquid appended film have been demonstrated to accumulate ions. This process have been significantly more effective than for the unconfined ionic liquid deposit. The accumulation process was shown to be dependent on the anion's charge. The less negative charge was the more effective the accumulation. Positively charged redox probes are repulsed from the film, however the electron transfer can be semi-reversibly turned on by anion exchange process. The film have been found as an suitable support for enzyme immobilization. After $ABTS^{2-}$ and laccase immobilization the film modified electrode exhibits bioelectrocatalytic properties towards ORR. The SCILF was demonstrated to promote t-$BuFc^{+}$ cation ejection from t-BuFc droplet on the electrode immersed into the water electrolyte solution. This is opposite behavior that the one observe for the bare ITO electrodes. Moreover this behavior is significantly different for confined and unconfined IL. Electroassisted generation of ordered, mesoporous, IL modified film on the electrode substrate was also attempted and some anion accumulation was observed.

IL modified mesoporous submicroparticles synthesized via modified Stober method have been first immobilized in carbon paste electrodes. These electrodes shows anion accumulation properties, however their stability is affected by the electrolyte penetration of the electrode material. This is not a problem when the particles have been immobilized at the electrode surface by solvent evaporation method. For this electrode the anion accumulation process have been observed as well as electrocatalytic NADH oxidation reaction. The silicate confined IL particles have been successfully applied as an element for building LbL deposits from the particles of opposite charges. Electrodes obtained from the silicate confined IL particles and CNPs have well developed surface, which can be controlled by number of immersion and withdrawal steps. They exhibit anion accumulation and have been successfully

applied in electrocatalytic NADH oxidation reaction. After laccase adsorption mediatorless bioelectrocatalytic ORR have been observed. The new material was found to facilitate the electron transfer between electrode and the laccase active center. Bioelectrocatalytic ORR was also observed for the silicate confined IL particles and CNPs electrodes further modified with $ABTS^{2-}$ and BOx. Obviously this material have been found suitable for enzymes immobilization.

2. The S-Au bond formation have been utilized to modify the flat gold disc electrodes with thiol functionalized IL. The same IL have been also used for AuNPs functionalization.

There is an ion rectification process observed on the gold disc electrodes modified with self assembled monolayers of thiol functionalized IL. However the IL functionalized AuNPs have been demonstrated as promising building blocks for LbL systems. Electrode prepared from gold and carbon nanoparticles was found to have catalytic activity towards ORR both in acidic and alkaline environment. This effect can be further enhanced by BOx immobilization. If the IL modified AuNPs have been deposited subsequently with carboxylic groups modified AuNPs the nanoparticulate gold film formation have been observed. It has to be emphasized that this process occurs in relatively mild conditions.

Both above mentioned strategies leads to connection of imidazolium type ionic liquids to the electrode. The most important properties of new electrodes are: ability to anion accumulation, enzymes immobilization, electrocatalysis and ion rectification. Sol-gel approach allows to immobilize more imidazolium groups on the electrode in comparison to the gold-sulfur bonding strategy. The latter is interesting because of the possibility to explore the unique properties of gold nanoparticles. It has to be emphasized that proposed method allows for nanoparticulate film formation in the absence of binder. It is very promising and can be potentially applied for various particles immobilization.

12. List of papers which have evolved from the experiments described in this thesis.

1. **A. Lesniewski, J. Niedziolka, B. Palys, C. Rizzi, L. Gaillon, M. Opallo**
   Electrode modified with ionic liquid covalently bonded to silicate matrix for accumulation of electroactive anions.
   Electrochem. Commun., **9,** 2580-2584 (2007).
2. **M. Opallo, A. Lesniewski, J. Niedziolka, E. Rozniecka, G. Shul**
   Ion transfer processes at ionic liquid modified electrodes.
   Review of Polarography, **54,** 21-30 (2008).
3. **A. Lesniewski, M. Jonsson-Niedziolka, J. Niedziolka-Jonsson, C. Rizzi, L. Gaillon, M. Opallo**
   The effect of ionic liquid covalent bonding to sol-gel processed film on ion accumulation and transfer.
   Electroanalysis, **21,** 701-706 (2009).
4. **A. Lesniewski, J. Niedziolka-Jonsson, J. Sirieix-Plenet, L. Gaillon, M. Opallo**
   Electrode modified with nanoporous silicate submicrometre particles with appended ionic liquid.
   Electrochem. Commun., **11**, 1305–1307 (2009).
5. **A. Lesniewski, J. Niedziolka-Jonsson, C. Rizzi, L. Gaillon, J. Rogalski, M. Opallo**
   Carbon ceramic nanoparticulate film electrode prepared from oppositely charged particles by layer-by-layer approach
   Electrochem. Commun., **12**, 83-85 (2010).
6. **A. Lesniewski, M. Paszewski, M. Opallo**
   Gold-carbon three dimensional film electrode prepared from oppositely charged conductive nanoparticles by layer-by-layer approach
   Electrochem. Commun., **12**, 435-437 (2010).
7. **M. Opallo, A. Lesniewski**
   A review on electrodes modified with ionic liquids
   Submitted to J Electroanal. Chem.

13. References

[1] Lane, R. F.; Hubbard, A. T. *J. Phys. Chem.* 1973, *77*, 1401-1410.
[2] Murray, R. W. *Acc. Chem. Res.* 1980, *13*, 135-141.
[3] Kissinger, P. T.; Heineman, W. R. *Laboratory techniques in electroanalytical chemistry*; Marcel Dekker, INC., 1996.
[4] Marken, F.; Webster, R. D.; Bull, S. D.; Davies, S. G. *J. Electroanal. Chem.* 1997, *437*, 209-218.
[5] Shi, C.; Anson, F. C. *Anal. Chem.* 1998, *70*, 3114-3118.
[6] Scholz, F.; Komorsky-Lovric, S.; Lovric, M. *Electrochem. Commun.* 2000, *2*, 112-118.
[7] Banks, C. E.; Davies, T. J.; Evans, R. G.; Hignett, G.; Wain, A. J.; Lawrence, N. S.; Wadhawan, J. D.; Marken, F.; Compton, R. G. *Phys. Chem. Chem. Phys.* 2003, *5*, 4053–4069.
[8] Scholz, F.; Gulaboski, R. *ChemPhysChem* 2005, *5*, 16-28.
[9] Wadhawan, J. D.; Schroder, U.; Neudeck, A.; Wilkins, S. J.; Compton, R. G.; Marken, F.; Consorti, C. S.; de Souza, R. F.; Dupont, J. *J. Electroanal. Chem.* 2000, *493*, 75–83.
[10] Samec, Z. *Pure Appl. Chem.* 2004, *76*, 2147-2180.
[11] Samec, Z.; Langmaier, J.; Kakiuchi, T. *Pure Appl. Chem.* 2009, *81*, 1473-1488.
[12] Adams, R. N. *Anal. Chem.* 1958, *30*, 1576.
[13] Svancara, I.; Vytras, K.; Kalcher, K.; Walcarius, A.; Wang, J. *Electroanalysis* 2009, *21*, 7 – 28.
[14] Švancara, I.; Walcarius, A.; Kalcher, K.; Vytřas, K. *Cent. Eur. J. Chem.* 2009, *7*.
[15] Kuwana, T.; French, W. G. *Analytical Chemistry* 1964, *36*, 241-242.
[16] Liu, H.; He, P.; Li, Z.; Sun, C.; Shi, L.; Liu, Y.; Zhu, G.; Li, J. *Electrochem. Commun.* 2005, *7*, 1357–1363.
[17] Buzzeo, M. C.; Evans, R. G.; Compton, R. G. *Chemphyschem* 2004, *5*, 1106-1120.
[18] Zhang, J.; Bond, A. M. *Analyst* 2005, *130*, 1132-1147.
[19] Hapiot, P.; Lagrost, C. *Chem. Rev.* 2008, *108*, 2238-2264.
[20] Wei, D.; Ivaska, A. *Anal. Chim. Acta* 2008, *607*, 126-135.
[21] Liu, H. T.; Liu, Y.; Li, J. H. *Phys. Chem. Chem. Phys.* 2010, *12*, 1685-1697.
[22] McCreery, R. L. *Chem. Rev.* 2008, *108*, 2646-2687.
[23] Opallo, M.; Lesniewski, A.; Niedziolka, J.; Rozniecka, E.; Shul, G. *Rev. Polarography* 2008, *54*, 21-35.
[24] Wang, Y. R.; Hu, P.; Liang, Q. L.; Luo, G. A.; Wang, Y. M. *Chin. J. Anal. Chem.* 2008, *36*, 1011-1016.
[25] Freemantle, M. *Introduction to Ionic Liquids*; Royal Society of Chemistry, 2009.
[26] Moniruzzaman, M.; Nakashima, K.; Kamiya, N.; Goto, M. *Biochem. Eng. J.* 2010, *48*, 295-314.
[27] Liu, Y.; Shi, L. H.; Wang, M. J.; Li, Z. Y.; Liu, H. T.; Li, J. H. *Green Chem.* 2005, *7*, 655-658.
[28] Ding, S.-F.; Wei, W.; Zhao, G.-C. *Electrochem. Commun.* 2007, *9*, 2202–2206.
[29] Galinski, M.; Lewandowski, A.; Stepniak, I. *Electrochim. Acta* 2006, *51*, 5567-5580.
[30] Rozniecka, E.; Niedziolka, J.; Sirieix-Plenet, J.; Gaillon, L.; Murphy, M. A.; Marken, F.; Opallo, M. *J. Electroanal. Chem.* 2006, *587*, 133-139.
[31] Zhao, F.; Wu, X.; Wang, M.; Liu, Y.; Gao, L.; Dong, S. *Anal. Chem.* 2004, *76*, 4960–4967.
[32] Liu, H. T.; He, P.; Li, Z. Y.; Sun, C. Y.; Shi, L. H.; Liu, Y.; Zhu, G. Y.; Li, J. H. *Electrochem. Commun.* 2005, *7*, 1357-1363.
[33] Schroder, U.; Wadhawan, J. D.; Compton, R. G.; Marken, F.; Suarez, P. A. Z.; Consorti, C. S.; de Souza, R. F.; Dupont, J. *New J. Chem.* 2000, *24*, 1009-1015.
[34] Blesic, M.; Marques, M. H.; Plechkova, N. V.; Seddon, K. R.; Rebelo, L. P. N.; Lopes, A. *Green Chem.* 2007, 481-490.
[35] Wang, M. D.; Deng, C. Y.; Nie, Z.; Xu, X. H.; Yao, S. Z. *Sci. China, Ser. B Chem.* 2009, *52*, 1991-1998.
[36] Wang, K.; Jian, F.; Zhuang, R. *Dalton Trans.* 2009, 4532–4537.
[37] Zhuang, R.; Jian, F.; Wang, K. *J. Organomet. Chem.* 2009, *694*, 3614–3618.
[38] Lee, B. S.; Chi, Y. S.; Lee, J. K.; Choi, I. S.; Song, C. E.; Namgoong, S. K.; Lee, S.-g. *J. Am. Chem. Soc.* 2004, *126*, 480-481.
[39] Chi, Y. S.; Hwang, S.; Lee, B. S.; Kwak, J.; Choi, I. S.; Lee, S.-g. *Langmuir* 2005, *21*, 4268-4271.
[40] Lesniewski, A.; Paszewski, M.; Opallo, M. *Electrochem. Commun.* 2010, *12*, 435-437.
[41] Rong, J. F.; Chi, Y. W.; Zhang, Y. J.; Chen, L. C.; Chen, G. N. *Electrochem. Commun.* 2010, *12*, 270-273.
[42] Wang, M.; Schneider, A.; Niedziolka-Jonsson, J.; Marcon, L.; Ghodbane, S.; Steinmuller-Nethl, D.; Li, M.; Boukherroub, R.; Szunerits, S. *Electrochim. Acta* 2010, *55*, 1582-1587.
[43] Lesniewski, A.; Niedziolka, J.; Palys, B.; Rizzi, C.; Gaillon, L.; Opallo, M. *Electrochem. Commun.* 2007, *9*, 2580–2584.
[44] Tanaka, K.; Nishi, N.; Kakiuchi, T. *Anal. Sci.* 2004, *20*, 1553-1557.

[45] Niedziolka, J.; Rozniecka, E.; Stafiej, J.; Sirieix-Plenet, J.; Gaillon, L.; di Caprio, D.; Opallo, M. *Chem. Commun.* 2005, 2954–2956.
[46] Safavi, A.; Movahedi, Z.; Mohajer, D.; Maleki, N. *Electroanalysis* 2006, *18*, 1227 – 1229.
[47] Yu, P.; Lin, Y.; Xiang, L.; Su, L.; Zhang, J.; Mao, L. *Langmuir* 2005, *21*, 9000-9006.
[48] Ding, S. F.; Zhao, G. C.; Wei, X. W. *Russ. J. Electrochem.* 2008, *44*, 338-342.
[49] Li, J. W.; Zhao, F. Q.; Xiao, P.; Zeng, B. Z. *Chin. J. Anal. Chem.* 2006, *34*, S5-S9.
[50] Shul, G.; Adamiak, W.; Opallo, M. *Electrochem. Commun.* 2008, *10*, 1201-1204.
[51] Lesniewski, A.; Jonsson-Niedziolka, M.; Niedziolka-Jonsson, J.; Rizzi, C.; Gaillon, L.; Opallo, M. *Electroanalysis* 2009, *21*, 701-706.
[52] Quentel, F.; Elleouet, C.; Mirceski, V.; Hernandez, V. A.; L'Her, M.; Lovric, M.; Komorsky-Lovric, S.; Scholz, F. *J. Electroanal. Chem.* 2007, *611*, 192–200.
[53] Hernandez, V. A.; Scholz, F. *Electrochem. Commun.* 2006, *8*, 967–972.
[54] Chen, P. Y. *Electrochim. Acta* 2007, *52*, 5484-5492.
[55] Toniolo, R.; Pizzariello, A.; Susmel, S.; Dossi, N.; Doherty, A. P.; Bontempelli, G. *Electroanalysis* 2007, *19*, 2141 – 2148.
[56] Shimojo, K.; Goto, M. *Anal. Chem.* 2004, *76*, 5039-5044.
[57] Buzzeo, M. C.; Hardacre, C.; Compton, R. G. *Anal. Chem.* 2004, *76*, 4583-4588.
[58] Zhang, J.; Bond, A. M. *J. Electroanal. Chem.* 2005, *574*, 299–309.
[59] Zhang, J.; Bond, A. M. *Anal. Chem.* 2003, *75*, 6938-6948.
[60] Lovrić, M.; Komorsky-Lovrić, Š.; Scholz, F. *Journal of Solid State Electrochemistry* 2007, *12*, 41-45.
[61] Ding, S. F.; Xu, M. Q.; Zhao, G. C.; Wei, X. W. *Electrochem. Commun.* 2007, *9*, 216-220.
[62] Yu, P.; Yan, J.; Zhang, J.; Mao, L. *Electrochem. Commun.* 2007, *9*, 1139–1144.
[63] Xiao, F.; Zhao, F. Q.; Deng, L. Z.; Zeng, B. Z. *Electrochem. Commun.* 2010, *12*, 620-623.
[64] Zhao, F. Q.; Xiao, F.; Zeng, B. Z. *Electrochem. Commun.* 2010, *12*, 168-171.
[65] Lin, X.; Xu, Y. *Electrochim. Acta* 2008, *53*, 4990–4997.
[66] Lin, X. Q.; Xu, Y. H. *Electrochim. Acta* 2008, *53*, 4990-4997.
[67] Zhang, L.; Song, Z.; Zhang, Q.; Jia, X.; Zhang, H.; Xin, S. *Electroanalysis* 2009, *21*, 1835 – 1841.
[68] Coll, C.; Labrador, R. H.; Manez, R. M.; Soto, J.; Sancenon, F.; Segui, M.-J.; Sanchez, E. *Chem. Commun.* 2005, 3033–3035.
[69] Kopytin, A. V.; Pyatova, E. N.; Zhukov, A. F.; Politov, Y. A.; German, K. E.; Tsivadze, A. Y. *J. Anal. Chem.* 2008, *63*, 888-890.
[70] Maminska, R.; Dybko, A.; Wroblewski, W. *Sens. Actuators, B* 2006, *115*, 552–557.
[71] Kakiuchi, T.; Yoshimatsu, T.; Nishi, N. *Anal. Chem.* 2007, *79*, 7187-7191.
[72] Wei, Z. L.; Li, Z. J.; Sun, X. L.; Fang, Y. J.; Liu, J. K. *Biosens. Bioelectron.* 2010, *25*, 1434-1438.
[73] Li, J.; Liu, L.; Yan, R.; Xiao, M.; Liu, L.; Zhao, F.; Zeng, B. *Electrochim. Acta* 2008, *53*, 4591–4598.
[74] Li, J. W.; Liu, L. H.; Xiao, F.; Gui, Z.; Yan, R.; Zhao, F. Q.; Hu, L.; Zeng, B. Z. *J. Electroanal. Chem.* 2008, *613*, 51-57.
[75] Liu, L. H.; Zhao, F. Q.; Liu, L. Q.; Li, J.; Zeng, B. Z. *Colloids Surf., B* 2009, *68*, 93-97.
[76] Mo, Z. R.; Zhang, Y. F.; Zhao, F. Q.; Xiao, F.; Guo, G. P.; Zeng, B. Z. *Food Chem.* 2010, *121*, 233-237.
[77] Li, G. P.; Du, L. W.; Chen, H. J.; Zhang, L. X.; Wang, E. K. *Electroanalysis* 2008, *20*, 2171-2176.
[78] Yang, L.; Wu, X. Q.; Wang, R.; Lu, Z. Q.; Hou, W. J.; Li, H. X. *Chin. Chem. Lett.* 2008, *19*, 1483–1486.
[79] Chen, H. J.; Wang, Y. L.; Liu, Y.; Wang, Y. Z.; Qi, L.; Dong, S. J. *Electrochem. Commun.* 2007, *9*, 469-474.
[80] Zhao, G. C.; Xu, M. Q.; Zhang, Q. *Electrochem. Commun.* 2008, *10*, 1924-1926.
[81] Safavi, A.; Farjami, F. *Anal. Biochem.* 2010, *402*, 20-25.
[82] Li, Z. J.; Wang, Z. Y.; Sun, X. L.; Fang, Y. J.; Chen, P. P. *Talanta* 2010, *80*, 1632-1637.
[83] Yu, J. J.; Zhao, T.; Zhao, F. Q.; Zeng, B. Z. *Electrochim. Acta* 2008, *53*, 5760-5765.
[84] Zhao, G.-C.; Xu, M.-Q.; Ma, J.; Wei, X.-W. *Electrochem. Commun.* 2007, *9*, 920–924.
[85] Dong, J. P.; Jin, C. L.; Xu, J. Q.; Yan, H. *Electroanalysis* 2009, *21*, 2597-2601.
[86] Pan, Z. Y.; Ma, R. N.; Li, J.; Liu, Y.; Zhao, Q.; Wang, G. T.; Wang, H. S. *Acta Chim. Sinica* 2009, *67*, 2721-2726.
[87] Dai, Z.; Xiao, Y.; Yu, X.; Mai, Z.; Zhao, X.; Zou, X. *Biosens. Bioelectron.* 2009, *24*, 1629–1634.
[88] Sun, H. *J. Porous Mater.* 2006, *13*, 393–397.
[89] Hong, S. *J. Porous Mater.* 2006, *13*, 393-397.
[90] Lu, X.; Hu, J.; Yao, X.; Wang, Z.; Li, J. *Biomacromolecules* 2006, *7*, 975-980.
[91] Lu, X.; Zhang, Q.; Zhang, L.; Li, J. *Electrochem. Commun.* 2006, *8*, 874–878.
[92] Zhang, Y.; Zheng, J. *Electrochim. Acta* 2008, *54*, 749–754.

[93] Long, J. S.; Silvester, D. S.; Wildgoose, G. G.; Surkus, A. E.; Flechsig, G. U.; Compton, R. G. *Bioelectrochemistry* 2008, *74*, 183-187.
[94] Xi, F. N.; Liu, L. J.; Wu, Q.; Lin, X. F. *Biosens. Bioelectron.* 2008, *24*, 29-34.
[95] Yan, R.; Zhao, F.; Li, J.; Xiao, F.; Fan, S.; Zeng, B. *Electrochim. Acta* 2007, *52*, 7425–7431.
[96] Gao, R.; Shangguan, X.; Qiao, G.; Zheng, J. *Electroanalysis* 2008, *20*, 2537 – 2542.
[97] Zhang, Y.; Zheng, J. B. *Electrochem. Commun.* 2008, *10*, 1400-1403.
[98] Wen, Y.; Yang, X.; Hu, G.; Chen, S.; Jia, N. *Electrochim. Acta* 2008, *54*, 744–748.
[99] Shangguan, X. D.; Zheng, J. B.; Sheng, Q. L. *Electroanalysis* 2009, *21*, 1469-1474.
[100] Fan, D. H.; Sun, J. Y.; Huang, K. J. *Colloids Surf., B* 2010, *76*, 44-49.
[101] Guo, C.; Song, Y.; Wei, H.; Li, P.; Wang, L.; Sun, L.; Sun, Y.; Li, Z. *Anal. Bioanal. Chem.* 2007, *389*, 527–532.
[102] Gao, R. F.; Zheng, J. B.; Qiao, L. F. *Electroanal.* 2010, *22*, 1084-1089.
[103] Xiang, C.; Zou, Y.; Sun, L.-X.; Xu, F. *Electrochem. Commun.* 2008, *10*, 38-41.
[104] Guo, G. P.; Zhao, F. Q.; Xiao, F.; Zeng, B. Z. *Int. J. Electrochem. Sci.* 2009, *4*, 1365-1372.
[105] Chen, J.; Yang, G.; Chen, M.; Li, W. *Russ. J. Electrochem.* 2009, *45*, 1287-1291.
[106] Haghighi, B.; Hamidi, H.; Gorton, L. *Electrochim. Acta* 2010, *55*, 4750-4757.
[107] Mo, Z. R.; Zhao, F. Q.; Xiao, F.; Zeng, B. Z. *Journal of Solid State Electrochemistry* 2010, *14*, 1615-1620.
[108] Rahimi, P.; Rafiee-Pour, H. A.; Ghourchian, H.; Norouzi, P.; Ganjali, M. R. *Biosens. Bioelectron.* 2010, *25*, 1301-1306.
[109] Zhang, X. Z.; Liu, S. F.; Jiao, K.; Hu, Y. W. *Electroanalysis* 2008, *20*, 1909-1916.
[110] Tu, W. W.; Lei, J. P.; Ju, H. X. *Chem. Eur. J.* 2009, *15*, 779-784.
[111] Zhang, X. Z.; Jiao, K.; Piao, G. Z.; Liu, S. F.; Li, S. X. *Synth. Met.* 2009, *159*, 419-423.
[112] Sheng, Q. L.; Zheng, J. B.; Shang-Guan, X. D.; Lin, W. H.; Li, Y. Y.; Liu, R. X. *Electrochim. Acta* 2010, *55*, 3185-3191.
[113] Yang, M. H.; Choi, B. G.; Park, H.; Hong, W. H.; Lee, S. Y.; Park, T. J. *Electroanal.* 2010, *22*, 1223-1228.
[114] Liu, K. P.; Zhang, J. J.; Yang, G. H.; Wang, C. M.; Zhu, J. J. *Electrochem. Commun.* 2010, *12*, 402-405.
[115] Xu, J.-S.; Zhao, G.-C. *Int. J. Electrochem. Sci.* 2008, *3*, 519 - 527.
[116] Chen, X. J.; Xuan, J.; Jiang, L. P.; Zhu, J. J. *Sci. China, Ser. B Chem.* 2009, *52*, 1999-2005.
[117] Lu, L. P.; Kang, T. F.; Cheng, S. Y.; Guo, X. R. *Appl. Surf. Sci.* 2009, *256*, 52-55.
[118] Zeng, X. D.; Li, X. F.; Xing, L.; Liu, X. Y.; Luo, S. L.; Wei, W. Z.; Kong, B.; Li, Y. H. *Biosens. Bioelectron.* 2009, *24*, 2898-2903.
[119] Hua, L. J.; Zhou, J. J.; Han, H. Y. *Electrochim. Acta* 2010, *55*, 1265-1271.
[120] Xiao, F.; Zhao, F. Q.; Li, J. W.; Liu, L. Q.; Zeng, B. Z. *Electrochim. Acta* 2008, *53*, 7781-7788.
[121] Zhu, H.; Lu, X. Q.; Li, M. X.; Shao, Y. H.; Zhu, Z. W. *Talanta* 2009, *79*, 1446-1453.
[122] Zhang, Y. F.; Guo, G. P.; Zhao, F. Q.; Mo, Z. R.; Xiao, F.; Zeng, B. Z. *Electroanal.* 2010, *22*, 223-228.
[123] Tsuda, T.; Yoshii, K.; Torimoto, T.; Kuwabata, S. *J. Power Sources* 2010, *195*, 5980-5985.
[124] Li, F. H.; Li, F.; Song, J. X.; Song, J. F.; Han, D. X.; Niu, L. *Electrochem. Commun.* 2009, *11*, 351-354.
[125] Xiao, F.; Zhao, F. Q.; Zhang, Y. F.; Guo, G. P.; Zeng, B. Z. *J. Phys. Chem. C* 2009, *113*, 849-855.
[126] Zhu, W. L.; Zhou, Y.; Zhang, J. R. *Talanta* 2009, *80*, 224-230.
[127] Sun, W.; Wang, D. D.; Zhong, J. H.; Jiao, K. *J. Solid State Electrochem.* 2008, *12*, 655-661.
[128] Lin, J. H.; He, C. Y.; Zhang, S. S. *Anal. Chim. Acta* 2009, *643*, 90-94.
[129] Wang, Q.; Tang, H.; Me, Q. J.; Tan, L.; Zhang, Y. Y.; Li, B.; Yao, S. Z. *Electrochim. Acta* 2007, *52*, 6630-6637.
[130] Wu, X.; Zhao, F.; Varcoe, J. R.; Thumser, A. E.; Avignone-Rossa, C.; Slade, R. C. T. *Biosens. Bioelectron.* 2009, *25*, 326-331.
[131] Yi, H. C.; Hu, L. L.; Mei, P. *Chem. Anal.* 2009, *54*, 19-29.
[132] Zhang, J.; Lei, J. P.; Liu, Y. Y.; Zhao, J. W.; Ju, H. X. *Biosens. Bioelectron.* 2009, *24*, 1858-1863.
[133] Zhu, J. W.; Qin, Y.; Zhang, Y. H. *Electrochem. Commun.* 2009, *11*, 1684-1687.
[134] Wan, J.; Yan, X.; Ding, J. J.; Ren, R. *Sens. Actuators, B* 2010, *146*, 221-225.
[135] Sun, W.; Gao, R. F.; Zhao, R. J.; Zhu, H. T.; Jiao, K. *J. Iran. Chem. Soc.* 2010, *7*, 470-477.
[136] Zhu, Z. H.; Li, X.; Wang, Y.; Zeng, Y.; Sun, W.; Huang, X. T. *Anal. Chim. Acta* 2010, *670*, 51-56.
[137] Li, J. W.; Zhao, F. Q.; Wang, G. Y.; Gui, Z.; Xiao, F.; Zeng, B. Z. *Electroanalysis* 2009, *21*, 150-156.
[138] Ragupathy, D.; Gopalan, A. Y.; Lee, K. P. *Electrochem. Commun.* 2009, *11*, 397-401.
[139] Xiao, F.; Zhao, F. Q.; Mei, D. P.; Mo, Z. R.; Zeng, B. Z. *Biosens. Bioelectron.* 2009, *24*, 3481-3486.
[140] Zhang, W.; Yang, T.; Zhuang, X. M.; Guo, Z. Y.; Jiao, K. *Biosens. Bioelectron.* 2009, *24*, 2417-2422.
[141] Tang, D. P.; Li, H.; Liao, J. Y. *Microfluid. Nanofluid.* 2009, *6*, 403-409.

[142] Marcilla, R.; Mecerreyes, D.; Odriozola, I.; Pomposo, J. A.; Rodriguez, J.; Zalakain, I.; Mondragon, I. *Nano* 2007, *2*, 169-173.
[143] Wang, Z. J.; Zhang, Q. X.; Kuehner, D.; Xu, X. Y.; Ivaska, A.; Niu, L. *Carbon* 2008, *46*, 1687-1692.
[144] Deepa, M.; Awadhia, A.; Bhandari, S. *Phys. Chem. Chem. Phys.* 2009, *11*, 5674-5685.
[145] Ren, R.; Leng, C. C.; Zhang, S. S. *Biosens. Bioelectron.* 2010, *25*, 2089-2094.
[146] Xiao, F.; Mo, Z.; Zhao, F.; Zeng, B. *Electrochem. Commun.* 2008, *10*, 1740–1743.
[147] Sun, W.; Li, X.; Jiao, K. *Electroanalysis* 2009, *21*, 959 – 964.
[148] Wei, W.; Jin, H.-H.; Zhao, G.-C. *Microchim. Acta* 2009, *164*, 167–171.
[149] Peng, Y.; Ji, Y.; Zheng, D.; Hu, S. *Sens. Actuators, B* 2009, *137*, 656–661.
[150] Xiao, F.; Zhao, F.; Li, J.; Yan, R.; Yu, J.; Zeng, B. *Anal. Chim. Acta* 2007, *596*, 79-85.
[151] Zhou, C.; Zheng, Y.; Li, Z.; Liu, Z.; Dong, Y.; Zhang, X. *Electrochim. Acta* 2009, *54*, 5909–5913.
[152] Liu, L.; Zhao, F.; Xiao, F.; Zeng, B. *Electroanalysis* 2008, *20*, 2148 – 2152.
[153] Qi, B.; Yang, X. *Mater. Lett.* 2008, *62*, 980–983.
[154] Gopalan, A. I.; Lee, K.-P.; Ragupathy, D. *Biosens. Bioelectron.* 2009, *24*, 2211–2217.
[155] Jia, J.; Cao, L.; Wang, Z.; Wang, T. *Electroanalysis* 2008, *20*, 542-549.
[156] Wang, Y.; Wu, J.; Zhan, T. R.; Sun, W.; Jiao, K. *Sens. Lett.* 2009, *7*, 1106-1112.
[157] Li, J.; Fan, C.; Xiao, F.; Yan, R.; Fan, S.; Zhao, F.; Zeng, B. *Electrochim. Acta* 2007, *52*, 6178–6185.
[158] Xiao, X. L.; Lu, W.; Yao, X. *Electroanalysis* 2008, *20*, 2247-2252.
[159] You, J.; Ding, W. P.; Ding, S. J.; Ju, H. X. *Electroanalysis* 2009, *21*, 190-195.
[160] Wang, D. D.; Liu, H. J.; Zhao, C. Z.; Hui, N.; Sun, W. *J. Chin. Chem. Soc.* 2010, *57*, 99-104.
[161] Zhang, Q.; Wei, W.; Zhao, G.-C. *Electroanalysis* 2008, *20*, 1002 – 1007.
[162] Li, J.; Yu, J.; Zhao, F.; Zeng, B. *Anal. Chim. Acta* 2007, *587*, 33-40.
[163] Gao, R.; Zheng, J. *Electrochem. Commun.* 2009, *11*, 608–611.
[164] Sun, W.; Gao, R.-f.; Jiao, K. *Electroanalysis* 2007, *19*, 1368 – 1374.
[165] Safavi, A.; Maleki, N.; Moradlou, O.; Tajabadi, F. *Anal. Biochem.* 2006, *359*, 224–229.
[166] Musameh, M.; Wang, J. *Anal. Chim. Acta* 2008, *606*, 45-49.
[167] Maleki, N.; Safavi, A.; Tajabadi, F. *Anal. Chem.* 2006, *78*, 3820-3826.
[168] Musameh, M. M.; Kachoosangi, R. T.; Xiao, L.; Russell, A.; Compton, R. G. *Biosens. Bioelectron.* 2008, *24*, 87-92
[169] Chernyshov, D. V.; Shuedene, N. V.; Antipova, E. R.; Pletnev, I. V. *Anal. Chim. Acta* 2008, *621*, 178-184.
[170] Kakiuchi, T. *Anal. Sci.* 2008, *24*, 1221-1230.
[171] Kachoosangi, R. T.; Wildgoose, G. G.; Compton, R. G. *Electroanalysis* 2007, *19*, 1483– 1489.
[172] Kachoosangi, R. T.; Musameh, M. M.; Abu-Yousef, I.; Yousef, J. M.; Kanan, S. M.; Xiao, L.; Davies, S. G.; Russell, A.; Compton, R. G. *Anal. Chem.* 2009, *81*, 435-442.
[173] Sun, W.; Yang, M.; Jiao, K. *Anal. Bioanal. Chem.* 2007, *389*, 1283–1291.
[174] Zhang, Y.; Zheng, J. B. *Electrochim. Acta* 2007, *52*, 7210–7216.
[175] Zheng, J.; Zhang, Y.; Yang, P. *Talanta* 2007, *73*, 920–925.
[176] Li, J.; Zhao, F.; Zeng, B. *Microchim. Acta* 2007, *157*, 27-33.
[177] Shangguan, X.; Zheng, J. *Electroanalysis* 2009, *21*, 881 – 886.
[178] Shangguan, X.; Zhang, H. F.; Zheng, J. B. *Electrochem. Commun.* 2008, *10*, 1140-1143.
[179] Sun, W.; Duan, Y.; Li, Y.; Gao, H.; Jiao, K. *Talanta* 2009, *78*, 695–699.
[180] Maleki, N.; Safavi, A.; Sedaghati, F.; Tajabadi, F. *Anal. Biochem.* 2007, *369*, 149–153.
[181] Sun, W.; Jiang, Q.; Xi, M.; Jiao, K. *Microchim. Acta* 2009, *166*, 343–348.
[182] Sun, W.; Li, Y.; Gao, H.; Jiao, K. *Microchim. Acta* 2009, *165*, 313–317.
[183] Sun, W.; Gao, R. F.; Bi, R. F.; Jiao, K. *Chin. J. Anal. Chem.* 2007, *35*, 567-570.
[184] Maleki, N.; Safavi, A.; Farjami, E.; Tajabadi, F. *Anal. Chim. Acta* 2008, *611*, 151-155.
[185] Safavi, A.; Maleki, N.; Momeni, S.; Tajabadi, F. *Anal. Chim. Acta* 2008, *625*, 8-12.
[186] Sun, W.; Jiang, Q.; Yang, M. X.; Jiao, K. *Bull. Korean Chem. Soc.* 2008, *29*, 915-920.
[187] Sun, W.; Li, Y. Z.; Duan, Y. Y.; Jiao, K. *Biosens. Bioelectron.* 2008, *24*, 988-993.
[188] Sun, W.; Li, Y. Z.; Yang, M. X.; Li, J.; Jiao, K. *Sens. Actuators, B* 2008, *133*, 387-392.
[189] Ding, C. F.; Zhao, F.; Ren, R.; Lin, J. M. *Talanta* 2009, *78*, 1148-1154.
[190] Li, Y. H.; Liu, X. Y.; Zeng, X. D.; Liu, Y.; Liu, X. T.; Wei, W. Z.; Luo, S. L. *Sens. Actuators, B* 2009, *139*, 604-610.
[191] Safavi, A.; Maleki, N.; Farjami, E.; Mahyari, F. A. *Anal. Chem.* 2009, *81*, 7538-7543.
[192] Safavi, A.; Maleki, N.; Farjami, F.; Farjami, E. *J. Electroanal. Chem.* 2009, *626*, 75-79.
[193] Sun, W.; Duan, Y. Y.; Li, Y. Z.; Zhan, T. R.; Jiao, K. *Electroanalysis* 2009, *21*, 2667-2673.
[194] Sun, W.; Jiang, Q.; Jiao, K. *J. Solid State Electrochem.* 2009, *13*, 1193-1199.
[195] Chen, Y. T.; Chen, X.; Lin, Z. Y.; Dai, H.; Qiu, B.; Sun, J. J.; Zhang, L.; Chen, G. N. *Electrochem. Commun.* 2009, *11*, 1142-1145.

[196] Sun, W.; Qin, P.; Gao, H. W.; Li, G. C.; Jiao, K. *Biosens. Bioelectron.* 2010, *25*, 1264-1270.
[197] Musameh, M. M.; Kachoosangi, R. T.; Compton, R. G. *Analyst* 2008, *133*, 133-138.
[198] Wang, S. F.; Xiong, H. Y.; Zeng, Q. X. *Electrochem. Commun.* 2007, *9*, 807–812.
[199] Sun, W.; Jiang, Q.; Wang, Y.; Jiao, K. *Sens. Actuators, B* 2009, *136*, 419–424.
[200] Sun, W.; Li, X.; Wang, Y.; Li, X.; Zhao, C.; Jiao, K. *Bioelectrochemistry* 2009, *75*, 170.
[201] Sun, W.; Li, X.; Wang, Y.; Zhao, R.; Jiao, K. *Electrochim. Acta* 2009, *54*, 4141–4148.
[202] Sun, W.; Li, Y.; Duan, Y.; Jiao, K. *Electrochim. Acta* 2009, *54*, 4105–4110.
[203] Sun, W.; Wang, Y.; Li, X.; Wu, J.; Zhan, T.; Jiao, K. *Electroanalysis* 2009, *21*, 2454-2460.
[204] Zheng, L.; Zhang, J.-q.; Song, J.-f. *Electrochim. Acta* 2009, *54*, 4559–4565.
[205] Brondani, D.; Scheeren, C. W.; Dupont, J.; Vieira, I. C. *Sens. Actuators, B* 2009, *140*, 252-259.
[206] Dai, H.; Xu, H. F.; Wu, X. P.; Chi, Y. W.; Chen, G. N. *Anal. Chim. Acta* 2009, *647*, 60-65.
[207] Franzoi, A. C.; Migowski, P.; Dupont, J.; Vieira, I. C. *Anal. Chim. Acta* 2009, *639*, 90-95.
[208] Franzoi, A. C.; Dupont, J.; Spinelli, A.; Vieira, I. C. *Talanta* 2009, *77*, 1322-1327.
[209] Franzoi, A. C.; Vieira, I. C.; Dupont, J.; Scheeren, C. W.; de Oliveira, L. F. *Analyst* 2009, *134*, 2320-2328.
[210] Zhu, Z. H.; Li, X.; Zeng, Y.; Sun, W. *Biosens. Bioelectron.* 2010, *25*, 2313-2317.
[211] Ganjali, M. R.; Khoshsafar, H.; Faridbod, F.; Shirzadmehr, A.; Javanbakht, M.; Norouzi, P. *Electroanalysis* 2009, *21*, 2175-2178.
[212] Ganjali, M. R.; Khoshsafar, H.; Shirzadmehr, A.; Javanbakht, M.; Faridbod, F. *Int. J. Electrochem. Sci.* 2009, *4*, 435-443.
[213] Faridbod, F.; Ganjali, M. R.; Larijani, B.; Norouzi, P. *Electrochim. Acta* 2009, *55*, 234-239.
[214] Sun, W.; Li, X.; Zhai, Z.; Jiao, K. *Electroanalysis* 2008, *20*, 2649 – 2654.
[215] Dai, H.; Wang, Y. M.; Wu, X. P.; Zhang, L.; Chen, G. N. *Biosens. Bioelectron.* 2009, *24*, 1230-1234.
[216] Zhang, X. Z.; Jiao, K.; Wang, X. L. *Electroanalysis* 2008, *20*, 1361-1366.
[217] Sun, W.; Guo, C. X.; Zhu, Z. H.; Li, C. M. *Electrochem. Commun.* 2009, *11*, 2105-2108.
[218] Brondani, D.; Vieira, I. C.; Piovezan, C.; da Silva, J. M. R.; Neves, A.; Dupont, J.; Scheeren, C. W. *Analyst* 2010, *135*, 1015-1022.
[219] Maleki, N.; Safavi, A.; Tajabadi, F. *Electroanalysis* 2007, *19*, 2247 – 2250.
[220] Safavi, A.; Maleki, N.; Honarasa, F.; Tajabadi, F.; Sedaghatpour, F. *Electroanalysis* 2007, *19*, 582 – 586.
[221] Safavi, A.; Maleki, N.; Tajabadi, F. *Analyst* 2007, *2007*, 54-58.
[222] Sun, W.; Yang, M.; Gao, R.; Jiao, K. *Electroanalysis* 2007, *19*, 1597 – 1602.
[223] Sun, W.; Li, Y.; Yang, M.; Liu, S.; Jiao, K. *Electrochem. Commun.* 2008, *10*, 298–301.
[224] Sun, W.; Yang, M.; Li, Y.; Jiang, Q.; Liu, S.; Jiao, K. *J. Pharm. Biomed. Anal.* 2008, *48*, 1326–1331.
[225] Sun, W.; Yang, M. X.; Jiang, Q.; Jiao, K. *Chin. Chem. Lett.* 2008, *19*, 1156–1158.
[226] Zhang, Y.; Zheng, J. *Talanta* 2008, *77*, 325–330.
[227] Sun, W.; Zhai, Z.; Wang, D.; Liu, S.; Jiao, K. *Bioelectrochemistry* 2009, *74*, 295–300.
[228] Zhang, Y.; Zheng, J. B. *Chin. J. Chem.* 2007, *25*, 1652-1657.
[229] Safavi, A.; Maleki, N.; Moradlou, O. *Electroanalysis* 2008, *20*, 2158-2162.
[230] ShangGuan, X. D.; Zhang, H. F.; Zheng, J. B. *Anal. Bioanal. Chem.* 2008, *391*, 1049-1055.
[231] Lin, Z. Y.; Chen, X. P.; Chen, H. Q.; Qiu, B.; Chen, G. N. *Electrochem. Commun.* 2009, *11*, 2056-2059.
[232] Wang, Y.; Xiong, H. Y.; Zhang, X. H.; Wang, S. F. *Microchim. Acta* 2010, *169*, 255-260.
[233] Jiang, P.; Yan, L.; Zhang, X. C.; Yuan, H. Y.; Xiao, D.; Choi, M. M. F. *Electroanalysis* 2010, *22*, 204-208.
[234] Sun, B.; Qi, H. L.; Ling, C.; Zhang, C. Q. *Chin. J. Anal. Chem.* 2009, *37*, 1601-1605.
[235] Shul, G.; Sirieix-Plenet, J.; Gaillon, L.; Opallo, M. *Electrochem. Commun.* 2006, *8*, 1111-1114.
[236] Haghighi, B.; Hamidi, H. *Electroanalysis* 2009, *21*, 1057 – 1065.
[237] Ji, H. M.; Zhu, L. D.; Liang, D. D.; Liu, Y.; Cai, L.; Zhang, S. W.; Liu, S. X. *Electrochim. Acta* 2009, *54*, 7429-7434.
[238] Sun, W.; Gao, R.; Li, X.; Wang, D.; Yang, M.; Jiao, K. *Electroanalysis* 2008, *20*, 1048 – 1054.
[239] Huang, K. J.; Sun, J. Y.; Niu, D. J.; Xie, W. Z.; Wang, W. *Colloids Surf., B* 2010, *78*, 69-74.
[240] Li, J.; Huang, M.; Liu, X.; Wei, H.; Xu, Y.; Xu, G.; Wang, E. *Analyst* 2007, *132*, 687–691.
[241] Li, Y. H.; Zeng, X. D.; Liu, X. Y.; Liu, X. S.; Wei, W. Z.; Luo, S. L. *Colloids Surf., B* 2010, *79*, 241-245.
[242] Safavi, A.; Maleki, N.; Farjami, E. *Biosens. Bioelectron.* 2009, *24*, 1655–1660.
[243] Safavi, A.; Maleki, N.; Tajabadi, F.; Farjami, E. *Electrochem. Commun.* 2007, *9*, 1963–1968.
[244] Sun, W.; Gao, R.; Jiao, K. *J. Phys. Chem. B* 2007, *111*, 4560-4567.
[245] Sun, W.; Wang, D. D.; Gao, R. F.; Jiao, K. *Electrochem. Commun.* 2007, *9*, 1159–1164.
[246] Safavi, A.; Maleki, N.; Moradlou, O.; Sorouri, M. *Electrochem. Commun.* 2008, *10*, 420–423.
[247] Zhao, R. J.; Jiang, Q.; Sun, W.; Jiao, K. *J. Chin. Chem. Soc.* 2009, *56*, 158-163.

[248] Safavi, A.; Maleki, N.; Farjami, E. *Electroanalysis* 2009, *21*, 1533-1538.
[249] Zhang, W.; Yang, T.; Li, X.; Wang, D. B.; Jiao, K. *Biosens. Bioelectron.* 2009, *25*, 428-434.
[250] Haghighi, B.; Nikzad, R. *Electroanalysis* 2009, *21*, 1862-1868.
[251] Gao, R. F.; Zheng, J. B. *Electrochem. Commun.* 2009, *11*, 1527-1529.
[252] Sun, W.; Wang, D.; Li, G.; Zhai, Z.; Zhao, R.; Jiao, K. *Electrochim. Acta* 2008, *53*, 8217–8221.
[253] Sun, W.; Wang, D.; Zhai, Z.; Gao, R.; Jiao, K. *J. Iran. Chem. Soc.* 2009, *6*, 412-419.
[254] Hui, N.; Gao, R. F.; Li, X. Q.; Sun, W.; Jiao, K. *J. Braz. Chem. Soc.* 2009, *20*, 252-258.
[255] Fan, S. S.; Xiao, F.; Liu, L. Q.; Zhao, F. Q.; Zeng, B. Z. *Sens. Actuators, B* 2008, *132*, 34-39.
[256] Yu, Q.; Liu, Y.; Liu, X. Y.; Zeng, X. D.; Luo, S. L.; Wei, W. Z. *Electroanal.* 2010, *22*, 1012-1018.
[257] Li, X. Q.; Wang, Y.; Sun, X. Y.; Zhan, T. R.; Sun, W. *J. Chem. Sci.* 2010, *122*, 271-278.
[258] Zhan, T. R.; Xi, M. Y.; Wang, Y.; Sun, W.; Hou, W. G. *J. Colloid Interface Sci.* 2010, *346*, 188-193.
[259] Li, Y. H.; Liu, X. Y.; Zeng, X. D.; Liu, Y.; Liu, X. S.; Wei, W. Z.; Luo, S. L. *Microchim. Acta* 2009, *165*, 393-398.
[260] Sun, W.; Wang, D. D.; Gao, R. F.; Sun, J.; Jiao, K. *Chin. Chem. Lett.* 2006, *17*, 1589-1591.
[261] Sun, W.; Gao, R. F.; Wang, D. D.; Jiao, K. *Acta Phys.-Chim. Sin.* 2007, *23*, 1247-1251.
[262] Sun, W.; Li, X. Q.; Liu, S. F.; Jiao, K. *Bull. Korean Chem. Soc.* 2009, *30*, 582-588.
[263] Sun, W.; Zhai, Z. Q.; Li, X. Q.; Qu, L. N.; Zhan, T. R.; Jiao, K. *Anal. Lett.* 2009, *42*, 2460-2473.
[264] Sun, W.; Qin, P.; Zhao, R. J.; Jiao, K. *Talanta* 2010, *80*, 2177-2181.
[265] Li, X. Q.; Zhao, R. J.; Wang, Y.; Sun, X. Y.; Sun, W.; Zhao, C. Z.; Jiao, K. *Electrochim. Acta* 2010, *55*, 2173-2178.
[266] Rozniecka, E.; Shul, G.; Sirieix-Plenet, J.; Gaillon, L.; Opallo, M. *Electrochem. Commun.* 2005, *7*, 299-304.
[267] Fukushima, T.; Kosaka, A.; Ishimura, Y.; Yamamoto, T.; Takigawa, T.; Ishii, N.; Aida, T. *Science* 2003, *300*, 2072-2074.
[268] Fukushima, T.; Kosaka, A.; Yamamoto, Y.; Aimiya, T.; Notazawa, S.; Takigawa, T.; Inabe, T.; Aida, T. *Small* 2006, *2*, 554-560.
[269] Tao, W. Y.; Pan, D. W.; Liu, Q.; Yao, S. Z.; Nie, Z.; Han, B. X. *Electroanalysis* 2006, *18*, 1681-1688.
[270] Xiao, F.; Zhao, F. Q.; Zeng, J. J.; Zeng, B. Z. *Electrochem. Commun.* 2009, *11*, 1550-1553.
[271] Choi, B. G.; Park, H.; Park, T. J.; Kim, D. H.; Lee, S. Y.; Hong, W. H. *Electrochem. Commun.* 2009, *11*, 672-675.
[272] Xiao, F.; Liu, L. Q.; Li, J.; Zeng, J. J.; Zeng, B. Z. *Electroanalysis* 2008, *20*, 2047-2054.
[273] Liu, X. H.; Ding, Z.; He, Y. H.; Xue, Z. H.; Zhao, X. P.; Lu, X. Q. *Colloids Surf., B* 2010, *79*, 27-32.
[274] Dong, J. P.; Hu, Y. Y.; Zhu, S. M.; Xu, J. Q.; Xu, Y. J. *Anal. Bioanal. Chem.* 2010, *396*, 1755-1762.
[275] Zhao, Y.; Gao, Y.; Zhan, D.; Liu, H.; Zhao, Q.; Kou, Y.; Shao, Y.; Li, M.; Zhuang, Q.; Zhu, Z. *Talanta* 2005, *66*, 51-57.
[276] Liu, Y.; Zou, X.; Dong, S. *Electrochem. Commun.* 2006, *8*, 1429–1434.
[277] Zhao, Y.; Ye, T.; Liu, H.; Kou, Y.; Li, M.; Shao, Y.; Zhu, Z.; Zhuang, Q. *Front. Biosci.* 2006, *11*, 2976 -2982.
[278] Sun, Y.; Fei, J.; Hou, J.; Zhang, Q.; Liu, Y.; Hu, B. *Microchim. Acta* 2009, *165*, 373–379.
[279] Zhao, F.; Liu, L.; Xiao, F.; Li, J.; Yan, R.; Fan, S.; Zeng, B. *Electroanalysis* 2007, *19*, 1387 – 1393.
[280] Zhang, X.-Z.; Jiao, K. *Acta Phys.-Chim. Sin.* 2008, *24*, 1439-1444.
[281] Yan, Q.; Zhao, F.; Li, G.; Zeng, B. *Electroanalysis* 2006, *18*, 1075 – 1080.
[282] Li, C. M.; Zang, J.; Zhan, D.; Chen, W.; Sun, C. Q.; Teo, A. L.; Chua, Y. T.; Lee, V. S.; Moochhala, S. M. *Electroanalysis* 2006, *18*, 713 - 718.
[283] Chailapakul, O.; Wonsawat, W.; Siangproh, W.; Grudpan, K.; Zhao, Y.; Zhu, Z. *Food Chem.* 2008, *109*, 876–882.
[284] Xiao, F.; Ruan, C.; Li, J.; Liu, L.; Zhao, F.; Zeng, B. *Electroanalysis* 2008, *20*, 361 – 366.
[285] Bao, X.; Tang, Y.; Yang, H.; Chen, X. *Chin. Chem. Lett.* 2009, *20*, 849–851.
[286] Tao, H.; Wei, W.; Zeng, X.; Liu, X.; Zhang, X.; Zhang, Y. *Microchim. Acta* 2009, *166*, 53–59.
[287] Xiao, F.; Ruan, C. P.; Liu, L. H.; Yan, R.; Zhao, F. Q.; Zeng, B. Z. *Sens. Actuators, B* 2008, *134*, 895-901.
[288] Du, P.; Liu, S.; Wu, P.; Cai, C. *Electrochim. Acta* 2007, *52*, 6534–6547.
[289] Zhao, Q.; Zhan, D. P.; Ma, H. Y.; Zhang, M. Q.; Zhao, Y. F.; Jing, P.; Zhu, Z. W.; Wan, X. H.; Shao, Y. H.; Zhuang, Q. K. *Front. Biosci.* 2005, *10*, 326-334.
[290] Liu, Y.; Huang, L.; Dong, S. *Biosens. Bioelectron.* 2007, *23*, 35-41.
[291] Zhang, Y.; Shen, Y.; Li, J.; Niu, L.; Dong, S.; Ivaska, A. *Langmuir* 2005, *21*, 4797-4800.
[292] Tani, Y.; Itoyama, Y.; Nishi, K.; Wada, C.; Shoda, Y.; Satomura, T.; Sakuraba, H.; Ohshima, T.; Hayashi, Y.; Yabutani, T.; Motonaka, J. *Anal. Sci.* 2009, *25*, 919-923.
[293] Yu, P.; Yan, J.; Zhao, H.; Su, L.; Zhang, J.; Mao, L. *J. Phys. Chem. C* 2008, *112*, 2177-2182.

[294] Shan, C. S.; Yang, H. F.; Han, D. X.; Zhang, Q. X.; Ivaska, A.; Niu, L. *Biosens. Bioelectron.* 2010, *25*, 1504-1508.
[295] Shen, Y.; Zhang, Y.; Zhang, Q.; Niu, L.; You, T.; Ivaska, A. *Chem. Commun.* 2005, 4193–4195.
[296] Han, D.; Qiu, X.; Shen, Y.; Guo, H.; Zhang, Y.; Niu, L. *J. Electroanal. Chem.* 2006, *596*, 33-37.
[297] Shen, Y.; Zhang, Y.; Qiu, X.; Guo, H.; Niu, L.; Ivaska, A. *Green Chem.* 2007, *9*, 746–753.
[298] Yang, F.; Jiao, L.; Shen, Y.; Xu, X.; Zhang, Y.; Niu, L. *J. Electroanal. Chem.* 2007, *608*, 78–83.
[299] Yu, B.; Zhou, F.; Hu, H.; Wang, C.; Liu, W. *Electrochim. Acta* 2007, *53*, 487-494.
[300] Szot, K.; Lesniewski, A.; Niedziolka, J.; Jonsson, M.; Rizzi, C.; Gaillon, L.; Marken, F.; Rogalski, J.; Opallo, M. *J. Electroanal. Chem.* 2008, *623*, 170-176.
[301] Zhang, Q.; Lv, X.; Qiao, Y.; Zhang, L.; Liu, D. L.; Zhang, W.; Han, G. X.; Song, X. M. *Electroanal.* 2010, *22*, 1000-1004.
[302] Li, F.; Shan, C.; Bu, X.; Shen, Y.; Yang, G.; Niu, L. *J. Electroanal. Chem.* 2008, *616*, 1-6.
[303] Sanchez-Paniagua Lopez, M.; Mecerreyes, D.; Lopez-Cabarcos, E.; Lopez-Ruiz, B. *Biosensors and Bioelectronics* 2006, *21*, 2320–2328.
[304] Chu, X. C.; Wu, B. H.; Xiao, C. H.; Zhang, X. H.; Chen, J. H. *Electrochim. Acta* 2010, *55*, 2848-2852.
[305] Xiao, C. H.; Chu, X. C.; Wu, B. H.; Pang, H. L.; Zhang, X. H.; Chen, J. H. *Talanta* 2010, *80*, 1719-1724.
[306] Kim, K. I.; Kang, H. Y.; Lee, J. C.; Choi, S. H. *Sensors* 2009, *9*, 6701-6714.
[307] Li, F. H.; Chai, J.; Yang, H. F.; Han, D. X.; Niu, L. *Talanta* 2010, *81*, 1063-1068.
[308] Wright, J. D.; Sommerdijk, N. A. J. M. *Sol-Gel Materials Chemistry and Applications*; Gordon and Breach Science Publishers, 2001.
[309] Hiemenz, P. C. *Principles of Colloid and Surface Chemistry*; Marcel Dekker: New York, 1977.
[310] Pierre, A. C. *Introduction to sol-gel processing*; Kluwer Academic Publishers, 1998.
[311] Brinker, C. J.; Scherer, G. W. *Sol-Gel Science The Physics and Chemistry of Sol-Gel Processing*; Academic Press, 1990.
[312] Shacham, R.; Avnir, D.; Mandler, D. *Adv. Mater.* 1999, *11*, 384-388.
[313] Walcarius, A.; Sibottier, E.; Etienne, M.; Ghanbaja, J. *Nat. Mater.* 2007, *6*, 602-608.
[314] Sayen, S.; Walcarius, A. *Electrochem. Commun.* 2003, *5*, 341-348.
[315] Etienne, M.; Goux, A.; Sibottier, E.; Walcarius, A. *J. Nanosci. Nanotechnol.* 2009, *21*, 731–741.
[316] Niedziolka, J.; Opallo, M. *Electrochem. Commun.* 2008, *10*, 1445-1447.
[317] Lautenschlager, K.-H.; Schroter, W.; Wanninger, A. *Nowoczesne kompendium chemii*; PWN: Warsaw, 2007.
[318] Rosen, M. J. *Surfactants and interfacial phenomena*; John Wiley & Sons, Inc.: Hoboken, New Jersey, 2004.
[319] Kresge, C. T.; Leonowicz, M. E.; Roth, W. J.; Vartuli, J. C.; Beck, J. S. *Nature* 1992, *359*, 710-712.
[320] Beck, J. S.; Vartuli, J. C.; Roth, W. J.; Leonowicz, M. E.; Kresge, C. T.; Schmitt, K. D.; Chu, C. T. D.; Olson, D. H.; Sheppard, E. W.; McCullen, S. B.; Higgins, J. B.; Schlenker, J. L. *J. Am. Chem. Soc.* 1992, *114*, 10834-10843.
[321] Corma, A. *Chem. Rev.* 1997, *97*, 2373-2419.
[322] Kickelbick, G. *Hybrid materials: synthesis, characterization, and applications*; Wiley-VCH: Weinheim, 2007.
[323] Wang, J. *Anal. Chim. Acta* 1999, *399*, 21-27.
[324] Feng, X.; Fryxell, G. E.; Wang, L.-Q.; Kim, A. Y.; Liu, J.; Kemner, K. M. *Science* 1997, *276*, 923-926.
[325] Nicole, L.; Boissiere, C.; Grosso, D.; Quach, A.; Sanchez, C. *J. Mater. Chem.* 2005, *15*, 3598-3627.
[326] Walcarius, A.; Sayen, S.; Gerardin, C.; Hamdoune, F.; Rodehuuser, L. *Colloids Surf., A* 2004, *234*, 145-151.
[327] Etienne, M.; Walcarius, A. *Electrochem. Commun.* 2005, *7*, 1449-1456.
[328] Sanchez, C.; Boissiere, C.; Grosso, D.; Laberty, C.; Nicole, L. *Chem. Mater.* 2008, *20*, 682-737.
[329] Goubert-Renaudin, S.; Etienne, M.; Brandes, S.; Meyer, M.; Denat, F.; Lebeau, B.; Walcarius, A. *Langmuir* 2009, *25*, 9804-9813.
[330] Klein, L. C. *Sol-Gel technology for thin films, fibers, preforms, electronics, and speciality shapes*; Noyes Publications: New Jesrey, 1988.
[331] Orgaz, F.; Rawson, H. *J. Non-Cryst. Solids* 1986, *82*, 378-390
[332] Brinker, C. J.; Harrington, M. S. *Sol. Energy Mater. Sol. Cells* 1981, *5*, 159-172
[333] Avellaneda, C. O.; Macedo, M. A.; Florentino, A. O.; Aegerter, M. A. In *13th Conference on Optical Materials Technology for Energy Efficiency and Solar Energy Conversion*; Wittwer, V., Granqvist, C. G., Lampert, C. M., Eds. 1994, p 38-51.
[334] Canva, M.; Lesaux, G.; Georges, P.; Brun, A.; Chaput, F.; Boilot, J. P. *Opt. Lett.* 1992, *17*, 218.
[335] Chen, L.-C.; Tsai, F.-R.; Fang, S.-H.; Ho, Y.-C. *Electrochim. Acta* 2009, *54*, 1304–1311.
[336] Kakihana, M. *J. Sol-Gel Sci. Technol.* 1996, *6*, 7-55.

[337] Huang, K.; Feng, M.; Goodenough, J. B. *J. Am. Ceram. Soc.* 2005, *79*, 1100 - 1104.
[338] Liu, C.; Zou, B.; Rondinone, A. J.; Zhang, Z. J. *J. Am. Chem. Soc.* 2001, *123*, 4344-4345.
[339] Guglielmi, M. *J. Sol-Gel Sci. Technol.* 1997, *8*, 443-449
[340] Cooney, T. G.; Francis, L. F. *J. Micromech. Microeng.* 1996, *6*, 291-300.
[341] Hwang, D. K.; Moon, J. H.; Shul, Y. G.; Jung, K. T.; Kim, D. H.; Lee, D. W. *J. Sol-Gel Sci. Technol.* 2003, *26*, 783-787.
[342] Holmesfarley, S. R.; Yanyo, L. C. *J. Adhes. Sci. Technol.* 1991, *5*, 131-151.
[343] Lin, J.; Brown, C. W. *TrAC, Trends Anal. Chem.* 1997, *16*, 200-211
[344] Haas-Santo, K.; Fichtner, M.; Schubert, K. *Appl. Catal., A* 2001, *220*, 79–92.
[345] Grant, S. A.; Glass, R. S. *Sens. Actuators, B* 1997, *45*, 35–42.
[346] Shinmou, K.; Nakama, K.; Koyama, T. *J. Sol-Gel Sci. Technol.* 2000, *19*, 267-269.
[347] Konishi, S.; Shingyouchi, K.; Makishima, A. *J. Non-Cryst. Solids* 1988, *100*, 511-513
[348] Hrubesh, L. W.; Pekala, R. W. *J. Mater. Res.* 1994, *9*, 731-738.
[349] Schimpf, S.; Lucas, M.; Mohra, C.; Rodemerck, U.; Brückner, A.; Radnik, J.; Hofmeister, H.; Claus, P. *Catal. Today* 2002, *72*, 63–78.
[350] Trudinger, U.; Muller, G.; Unger, K. K. *J. Chromatogr.* 1990, *535*, 111-125.
[351] Zhang, A.; Li, Z.; Li, Z.; Zhu, Y. *J. Sol-Gel Sci. Technol.* 2009, *49*, 6-11.
[352] Kursawe, M.; Glaubitt, W.; Thierauf, A. *J. Sol-Gel Sci. Technol.* 1998, *13*, 267-271.
[353] Gates, B.; Yin, Y.; Xia, Y. *Chem. Mater.* 1999, *11*, 2827-2836.
[354] Salimi, A.; Pourbeyram, S. *Talanta* 2003, *60*, 205-214.
[355] Aurobind, S. V.; Amirthalingam, K. P.; Gomathi, H. *Adv. Colloid Interface Sci.* 2006, *121*, 1-7.
[356] Braun, S.; Rappoport, S.; Zusman, R.; Avnir, D.; Ottolenghi, M. *Mater. Lett.* 1990, *10*, 1-5.
[357] Jonsson, M.; Szot, K.; Niedziolka, J.; Rogalski, J.; Karnicka, K.; Kulesza, P.; Opallo, M. *J. Nanosci. Nanotechnol.* 2009, *9*, 2346-2352.
[358] Zou, Y. J.; Xiang, C. L.; Sun, L. X.; Xu, F. *Biosens. Bioelectron.* 2008, *23*, 1010-1016.
[359] Tsionsky, M.; Gun, G.; Glezer, V.; Lev, O. *Anal. Chem.* 1994, *66*, 1747-1753.
[360] Salimi, A.; Pourbeyram, S.; Haddadzadeh, H. *J. Electroanal. Chem.* 2003, *542*, 39-49.
[361] Bharathi, S.; Lev, O. *Anal. Commum.* 1998, *35*, 29-31.
[362] Sampath, S.; Lev, O. *Anal. Chem.* 1996, *68*, 2015-2021.
[363] Lev, O.; Wu, Z.; Bharathi, S.; Glezer, V.; Modestov, A.; Gun, J.; Rabinovich, L.; Sampath, S. *Chem. Mater.* 1997, *9*, 2354-2375.
[364] Depre, L.; Ingram, M.; Poinsignon, C.; Popall, M. *Electrochim. Acta* 2000, *45*, 1377-1383.
[365] Perthuis, H.; Colomban, P. *Mater. Res. Bull.* 1984, *19*, 621-631.
[366] Nishio, K.; Tsuchiya, T. *Sol. Energy Mater. Sol. Cells* 2001, *68*, 295-306.
[367] Cheng, W.; Baudrin, E.; Dunn, B.; Zink, J. I. *J. Mater. Chem.* 2001, *11*, 92-97.
[368] Jain, V.; Khiterer, M.; Montazami, R.; Yochum, H. M.; Shea, K. J.; Heflin, J. R. *ACS Appl. Mater. Interfaces* 2009, *1*, 83-89.
[369] Collinson, M. M.; Martin, S. A. *Chem. Commun.* 1999, 899-900.
[370] Ozin, G. A.; Arsenault, A. C.; Cademartiri, L. *Nanochemistry, A chemical approach to nanomaterials* Cambridge, 2009.
[371] Binning, G.; Rohrer, H.; Gerber, C.; Weibel, E. *Phys. Rev. Lett.* 1982, *49*, 57-61.
[372] Binnig, G.; Quate, C. F.; Gerber, C. *Phys. Rev. Lett.* 1986, *56*, 930-933.
[373] Becker, R. S.; Golovchenko, J. A.; Swartzentruber, B. S. *Nature* 1987, *325*, 419-421.
[374] Lee, H. J.; Ho, W. *Science* 1999, *286*, 1719-1722.
[375] Kroto, H. W.; Heath, J. R.; Obrien, S. C.; Curl, R. F.; Smalley, R. E. *Nature* 1985, *318*, 162-163.
[376] Edelstein, A. S.; Cammarata, R. C. *Nanomaterials: synthesis, properties, and applications*; Taylor & Francis Group, LLC: New York, 1996.
[377] Welch, C. M.; Compton, R. G. *Anal. Bioanal. Chem.* 2006, *384*, 601-619.
[378] Nutzenadel, C.; Zuttell, A.; Chartouni, D.; Schmid, G.; Schlapbach, L. *Eur. Phys. J. D* 2000, *8*, 245-250.
[379] Guo, S. J.; Wang, E. K. *Anal. Chim. Acta* 2007, *598*, 181-192.
[380] Schmitt, J.; Decher, G.; Dressick, W. J.; Brandow, S. L.; Geer, R. E.; Shashidhar, R.; Calvert, J. M. *Adv. Mater.* 1997, *9*, 61-&.
[381] Musick, M. D.; Keating, C. D.; Keefe, M. H.; Natan, M. J. *Chem. Mater.* 1997, *9*, 1499-&.
[382] Wuelfing, W. P.; Zamborini, F. P.; Templeton, A. C.; Wen, X. G.; Yoon, H.; Murray, R. W. *Chem. Mater.* 2001, *13*, 87-95.
[383] Xiao, Y.; Patolsky, F.; Katz, E.; Hainfeld, J. F.; Willner, I. *Science* 2003, *299*, 1877-1881.
[384] Liang, R. P.; Qiu, H. D.; Cai, P. X. *Anal. Chim. Acta* 2005, *534*, 223-229.
[385] Macdonald, S. M.; Szot, K.; Niedziolka, J.; Marken, F.; Opallo, M. *J. Solid State Electrochem.* 2008, *12*, 287-293.

[386] Szot, K.; Nogala, W.; Niedziolka-Jonsson, J.; Jonsson-Niedziolka, M.; Marken, F.; Rogalski, J.; Kirchner, C. N.; Wittstock, G.; Opallo, M. *Electrochim. Acta* 2009, *54*, 4620-4625.
[387] Liu, S. Q.; Ju, H. X. *Electroanalysis* 2003, *15*, 1488-1493.
[388] Miscoria, S. A.; Barrera, G. D.; Rivas, G. A. *Electroanalysis* 2005, *17*, 1578-1582.
[389] Simm, A. O.; Banks, C. E.; Wilkins, S. J.; Karousos, N. G.; Davis, J.; Compton, R. G. *Anal. Bioanal. Chem.* 2005, *381*, 979-985.
[390] Dai, X.; Nekrassova, O.; Hyde, M. E.; Compton, R. G. *Anal. Chem.* 2004, *76*, 5924-5929.
[391] Sanz, V. C.; Mena, M. L.; Gonzalez-Cortes, A.; Yanez-Sedeno, P.; Pingarron, J. M. *Anal. Chim. Acta* 2005, *528*, 1-8.
[392] Welch, C. M.; Nekrassova, O.; Dai, X.; Hyde, M. E.; Compton, R. G. *ChemPhysChem* 2004, *5*, 1405-1410.
[393] Templeton, A. C.; Wuelfing, M. P.; Murray, R. W. *Acc. Chem. Res.* 2000, *33*, 27-36.
[394] Dai, X.; Compton, R. G. *Electroanalysis* 2005, *17*, 1325-1330.
[395] El-Deab, M. S.; Ohsaka, T. *Electrochim. Acta* 2002, *47*, 4255-4261.
[396] El-Deab, M. S.; Okajima, T.; Ohsaka, T. *J. Electrochem. Soc.* 2003, *150*, A851-A857.
[397] Shipway, A. N.; Katz, E.; Willner, I. *ChemPhysChem* 2000, *1*, 18-52.
[398] Raj, C. R.; Okajima, T.; Ohsaka, T. *J. Electroanal. Chem.* 2003, *543*, 127-133.
[399] Wang, L. Y.; Shi, X. J.; Kariuki, N. N.; Schadt, M.; Wang, G. R.; Rendeng, Q.; Choi, J.; Luo, J.; Lu, S.; Zhong, C. J. *J. Am. Chem. Soc.* 2007, *129*, 2161-2170.
[400] Wohltjen, H.; Snow, A. W. *Anal. Chem.* 1998, *70*, 2856-2859.
[401] Raguse, B.; Chow, E.; Barton, C. S.; Wieczorek, L. *Anal. Chem.* 2007, *79*, 7333-7339.
[402] Shipway, A. N.; Lahav, M.; Willner, I. *Adv. Mater.* 2000, *12*, 993-998.
[403] Janata, J. *Analyst* 1994, *119*, 2275-2278.
[404] Katz, E.; Willner, I.; Wang, J. *Electroanalysis* 2004, *16*, 19-44.
[405] Pingarron, J. M.; Yanez-Sedeno, P.; Gonzalez-Cortes, A. *Electrochim. Acta* 2008, *53*, 5848-5866.
[406] Zawisza, I.; Rogalski, J.; Opallo, M. *J. Electroanal. Chem.* 2006, *588*, 244-252.
[407] Schuhmann, W.; Ohara, T. J.; Schmidt, H. L.; Heller, A. *J. Am. Chem. Soc.* 1991, *113*, 1394-1397.
[408] Emr, S. A.; Yacynych, A. M. *Electroanalysis* 1995, *7*, 913-923.
[409] Lei, C. X.; Hu, S. Q.; Shen, G. L.; Yu, R. Q. *Talanta* 2003, *59*, 981-988.
[410] He, L.; Musick, M. D.; Nicewarner, S. R.; Salinas, F. G.; Benkovic, S. J.; Natan, M. J.; Keating, C. D. *J. Am. Chem. Soc.* 2000, *122*, 9071-9077.
[411] Englebienne, P.; Van Hoonacker, A.; Verhas, M. *Analyst* 2001, *126*, 1645-1651.
[412] Dequaire, M.; Degrand, C.; Limoges, B. *Anal. Chem.* 2000, *72*, 5521-5528.
[413] Luo, H. X.; Shi, Z. J.; Li, N. Q.; Gu, Z. N.; Zhuang, Q. K. *Anal. Chem.* 2001, *73*, 915-920.
[414] Sherigara, B. S.; Kutner, W.; D'Souza, F. *Electroanalysis* 2003, *15*, 753-772.
[415] Wang, Y.; Li, Y. M.; Tang, L. H.; Lu, J.; Li, J. H. *Electrochem. Commun.* 2009, *11*, 889-892.
[416] Huang, J. S.; Liu, Y.; You, T. Y. *Anal. Method.*, *2*, 202-211.
[417] Amiri, M.; Shahrokhian, S.; Marken, F. *Electroanalysis* 2007, *19*, 1032-1038.
[418] MacDonald, S. M.; Fletcher, P. D. I.; Cui, Z. G.; Opallo, M. C.; Chen, J. Y.; Marken, F. *Electrochim. Acta* 2007, *53*, 1175-1181.
[419] Amiri, M.; Shahrokhian, S.; Psillakis, E.; Marken, F. *Anal. Chim. Acta* 2007, *593*, 117-122.
[420] Rassaei, L.; Bonne, M. J.; Sillanpaa, M.; Marken, F. *New J. Chem.* 2008, *32*, 1253-1258.
[421] Rassaei, L.; Sillanpaa, M.; Marken, F. *Electrochim. Acta* 2008, *53*, 5732-5738.
[422] Watkins, J. D.; Lawrence, R.; Taylor, J. E.; Bull, S. D.; Nelson, G. W.; Foord, J. S.; Wolverson, D.; Rassaei, L.; Evans, N. D. M.; Gascon, S. A.; Marken, F. *Phys. Chem. Chem. Phys.* 2010, *12*, 4872-4878.
[423] Bok, S.; Lubguban, A. A.; Gao, Y. F.; Bhattacharya, S.; Korampally, V.; Hossain, M.; Thiruvengadathan, R.; Gillis, K. D.; Gangopadhyay, S. *J. Electrochem. Soc.* 2008, *155*, K91-K95.
[424] Yu, J. J.; Zhao, F. Q.; Zeng, B. Z. *J. Solid State Electrochem.* 2008, *12*, 1167-1172.
[425] Yuan, Y.; Jeon, Y.; Ahmed, J.; Park, W.; Kim, S. *J. Electrochem. Soc.* 2009, *156*, B1238-B1241.
[426] Wang, M. F.; Zhang, W.; Fang, B. *Chin. J. Anal. Chem.* 2010, *38*, 125-128.
[427] Rassaei, L.; Sillanpaa, M.; Edler, K. J.; Marken, F. *Electroanalysis* 2009, *21*, 261-266.
[428] Ghorbani-Bidkorbeh, F.; Shahrokhian, S.; Mohammadi, A.; Dinarvand, R. *Electrochim. Acta* 2010, *55*, 2752-2759.
[429] Ghorbani-Bidkorbeh, F.; Shahrokhian, S.; Mohammadi, A.; Dinarvand, R. *J. Electroanal. Chem.* 2010, *638*, 212-217.
[430] Vidal, L.; Chisvert, A.; Canals, A.; Psillakis, E.; Lapkin, A.; Acosta, F.; Edler, K. J.; Holdaway, J. A.; Marken, F. *Anal. Chim. Acta* 2008, *616*, 28-35.
[431] Iler, R. K. *J. Colloid Interface Sci.* 1966, *21*, 569-&.
[432] Decher, G. *Science* 1997, *277*, 1232-1237.

[433] Decher, G.; Hong, J. D. *Makromol. Chem. Macromol. Symp.* 1991, *46*, 321-327.
[434] Decher, G.; Hong, J. D. *Ber. Bunsen Phys. Chem.* 1991, *95*, 1430-1434.
[435] Decher, G.; Hong, J. D.; Schmitt, J. *Thin Solid Films* 1992, *210*, 831-835.
[436] Crespilho, F. N.; Zucolotto, V.; Oliveira Jr., O. N.; Nart, F. C. *Int. J. Electrochem. Sci.* 2006, *1*, 194-214.
[437] Siqueira, J. R.; Gasparotto, L. H. S.; Crespilho, F. N.; Carvalho, A. J. F.; Zucolotto, V.; Oliveira, O. N. *J. Phys. Chem. B* 2006, *110*, 22690-22694.
[438] Abdelrahman, A. I.; Mohammad, A. M.; Okajima, T.; Ohsaka, T. *J. Phys. Chem. B* 2006, *110*, 2798-2803.
[439] Zhang, H.; Hu, N. F. *J. Phys. Chem. B* 2007, *111*, 10583-10590.
[440] Wang, Y. D.; Joshi, P. P.; Hobbs, K. L.; Johnson, M. B.; Schmidtke, D. W. *Langmuir* 2006, *22*, 9776-9783.
[441] Deng, L.; Liu, Y.; Yang, G. C.; Shang, L.; Wen, D.; Wang, F.; Xu, Z.; Dong, S. J. *Biomacromolecules* 2007, *8*, 2063-2071.
[442] Deng, L.; Wang, F.; Chen, H. J.; Shang, L.; Wang, L.; Wang, T.; Dong, S. J. *Biosens. Bioelectron.* 2008, *24*, 329-333.
[443] Hao, E. C.; Yang, B.; Zhang, J. H.; Zhang, X.; Sun, J. Q.; Shen, S. C. *J. Mater. Chem.* 1998, *8*, 1327-1328.
[444] Kumar, A.; Mandale, A. B.; Sastry, M. *Langmuir* 2000, *16*, 6921-6926.
[445] Lee, D.; Rubner, M. F.; Cohen, R. E. *Nano Lett.* 2006, *6*, 2305-2312.
[446] Lee, D.; Gemici, Z.; Rubner, M. F.; Cohen, R. E. *Langmuir* 2007, *23*, 8833-8837.
[447] Lee, D.; Omolade, D.; Cohen, R. E.; Rubner, M. F. *Chem. Mater.* 2007, *19*, 1427-1433.
[448] Promnimit, S.; Cavelius, C.; Mathur, S.; Dutta, J. *Physica E* 2008, *41*, 285-291.
[449] Zhang, L. H.; Wang, F.; Dong, S. J. *Electrochim. Acta* 2008, *53*, 6423-6427.
[450] Shul, G.; McKenzie, K. J.; Niedziolka, J.; Rozniecka, E.; Palys, B.; Marken, F.; Hayman, C. M.; Buckley, B. R.; Page, P. C. B.; Opallo, M. *J. Electroanal. Chem.* 2005, *582*, 202-208.
[451] Freischlad, K. *Laser Focus World* 2010, *46*.
[452] Dutkiewicz, E. T. *Fizykochemia powierzchni*; Wydawnictwa Naukowo-Techniczne: Warszawa, 1998.
[453] Burevski, D. *Colloid. Polym. Sci.* 1982, *260*, 623-627.
[454] Reimer, L. *Scanning electron microscopy physics of image formation and microanalysis* Heidelberg, 1998.
[455] http://www.sv.vt.edu/classes/MSE2094_NoteBook/96ClassProj/experimental/electron.html
[456] Erni, R.; Rossell, M. D.; Kisielowski, C.; Dahmen, U. *Phys. Rev. Lett.* 2009, *102*, 096101.
[457] Parker, S. P.; The McGraw-Hill Companies, Inc.: 2003.
[458] Bard, A. J.; Faulkner, L. R. *Electrochemical Methods Fundamentals and Applications*; Wiley, 2001.
[459] Niedziolka, J.; Palys, B.; Nowakowski, R.; Opallo, M. *J. Electroanal. Chem.* 2005, *578*, 239-245.
[460] Zaharescu, M.; Jitianu, A.; Braileanu, A.; Madarasz, J.; Pokol, G. *J. Therm. Anal. Calorim.* 2001, *64*, 689-696.
[461] Trasferetti, B. C.; Davanzo, C. U.; de Moraes, M. A. B. *J. Phys. Chem. B* 2003, *107*, 10699-10708.
[462] Orel, B.; Vuk, A. S.; Jovanovski, V.; Jese, R.; Perse, L. S.; Hocevar, S. B.; Hutton, E. A.; Ogorevc, B.; Jesih, A. *Electrochem. Commun.* 2005, *7*, 692-696.
[463] WYKO Vision Help
[464] Davies, T. J.; Compton, R. G. *J. Electroanal. Chem.* 2005, *585*, 63-82.
[465] Niedziolka, J.; Szot, K.; Marken, F.; Opallo, M. *Electroanalysis* 2007, *19*, 155-160.
[466] Palmore, G. T. R.; Kim, H. H. *J. Electroanal. Chem.* 1999, *464*, 110-117.
[467] Niedziolka, J., PhD thesis, Institute of Physical Chemistry, PAS, 2006.
[468] Bullen, R. A.; Arnot, T. C.; Lakeman, J. B.; Walsh, F. C. *Biosens. Bioelectron.* 2006, *21*, 2015-2045.
[469] Katz, E.; Willner, I.; Kotlyar, A. B. *J. Electroanal. Chem.* 1999, *479*, 64-68.
[470] Mano, N.; Mao, F.; Heller, A. *ChemBioChem* 2004, *5*, 1703-1705.
[471] Szot, K.; Niedziolka, J.; Rogalski, J.; Marken, F.; Opallo, M. *J. Electroanal. Chem.* 2008, *612*, 1-8.
[472] Bilewicz, R.; Opallo, M. In *Fuel Cell Science: Theory, Fundamentals and Bio-Catalysis*; Wiley-VCH: Weinheim, 2009.
[473] Shul, G., 2006.
[474] Bond, A. M.; Marken, F. *J. Electroanal. Chem.* 1994, *372*, 125-135.
[475] Ryabov, A. D.; Amon, A.; Gorbatova, R. K.; Ryabova, E. S.; Gnedenko, B. B. *J. Phys. Chem.* 1995, *99*, 14072-14077.
[476] Simm, A. O.; Ward-Jones, S.; Banks, C. E.; Compton, R. G. *Anal. Sci.* 2005, *21*, 667-671.
[477] Stober, W.; Fink, A. *J. Colloid Interface Sci.* 1968, *26*, 62-69.
[478] Rouquerol, J.; Avnir, D.; Fairbridge, C. W.; Everett, D. H.; Haynes, J. H.; Pernicone, N.; Ramsay, J. D. F.; Sing, K. S. W.; Unger, K. K. *Pure Appl. Chem.* 1994, *66*, 1739-1758.

[479] Zhang, D.; Wang, K.; Sun, D. C.; Xia, X. H.; Chen, H.-Y. *Chem. Mater.* 2003, *15*, 4163-4165.
[480] Ellis, D.; Eckhoff, M.; Neff, V. D. *J. Phys. Chem.* 1981, *85*, 1225-1231.
[481] Shan, C.; Yang, H.; Han, D.; Zhang, Q.; Ivaska, A.; Niu, L. *Biosens. Bioelectron.* 2009, *25*, 1504-8.
[482] Klajn, R.; Bishop, K. J. M.; Fialkowski, M.; Paszewski, M.; Campbell, C. J.; Gray, T. P.; Grzybowski, B. A. *Science* 2007, *316*, 261-264.
[483] Servat, K.; Tingry, S.; Brunel, L.; Querelle, S.; Cretin, M.; Innocent, C.; Jolivalt, C.; Rolland, M. *J. Appl. Electrochem.* 2007, *37*, 121-127.
[484] Brunel, L.; Denele, J.; Servat, K.; Kokoh, K. B.; Jolivalt, C.; Innocent, C.; Cretin, M.; Rolland, M.; Tingry, S. *Electrochem. Commun.* 2007, *9*, 331-336.
[485] Karnicka, K.; Miecznikowski, K.; Kowalewska, B.; Skunik, M.; Opallo, M.; Rogalski, J.; Schuhmann, W.; Kulesza, P. J. *Anal. Chem.* 2008, *80*, 7643-7648.
[486] Nogala, W.; Szot, K.; Burchardt, M.; Jonsson-Niedziolka, M.; Rogalski, J.; Wittstock, G.; Opallo, M. *Bioelectrochemistry*, *79*, 101-107.
[487] Tsujimura, S.; Tatsumi, B.; Ogawa, J.; Shimizu, S.; Kano, K.; Ikeda, T. *J. Electroanal. Chem.* 2001, *496*, 69-75.
[488] Nogala, W.; Celebanska, A.; Szot, K.; Wittstock, G.; Opallo, M. *Electrochim. Acta*, *55*, 5719-5724.
[489] Nogala, W.; Rozniecka, E.; Zawisza, I.; Rogalski, J.; Opallo, M. *Electrochem. Commun.* 2006, *8*, 1850-1854.
[490] Lee, S. K.; George, S. D.; Antholine, W. E.; Hedman, B.; Hodgson, K. O.; Solomon, E. I. *J. Am. Chem. Soc.* 2002, *124*, 6180-6193.
[491] Johnson, D. L.; Thompson, J. L.; Brinkmann, S. M.; Schuller, K. A.; Martin, L. L. *Biochemistry* 2003, *42*, 10229-10237.
[492] Daniel, M.-C.; Astruc, D. *Chemical Review* 2004, *104*, 293–346.
[493] Hwang, S.; Chi, Y. S.; Lee, B. S.; Lee, S.-g.; Choi, I. S.; Kwak, J. *Chem. Commun.* 2006, 183–185.
[494] El-Deab, M. S.; Sotomura, T.; Ohsaka, T. *Electrochem. Commun.* 2005, *7*, 29-34.
[495] El-Deab, M. S.; Sotomura, T.; Ohsaka, T. *Electrochim. Acta* 2006, *52*, 1792-1798.
[496] Inasaki, T.; Kobayashi, S. *Electrochim. Acta* 2009, *54*, 4893-4897.
[497] Tsujimura, S.; Kamitaka, Y.; Kano, K. *Fuel Cells* 2007, *7*, 463-469.
[498] Murata, K.; Kajiya, K.; Nakamura, N.; Ohno, H. *Energy Environ. Sci.* 2009, *2*, 1280-1285.
[499] Burke, L. D.; Nugent, P. F. *Gold Bull.* 1997, *30*, 43-53.